THE UNIVERSITY OF WOLVERHAMPTON

School of Engineering and The Built Environment

Engineering Division

MULTIVARIATE TOOL CONDITION MONITORING IN A METAL CUTTING OPERATION USING NEURAL NETWORKS

By

Dimla E. Dimla Snr., M. Eng.(Hons.)

A Thesis submitted in part fulfillment of the requirements for a

Doctor of Philosophy Degree in Mechanical Engineering at the

University of Wolverhampton

June, 1998

DECLARATION

This work or any part thereof has not been previously presented in any form to the University or to any other body whether for assessment, publication or for other purpose (unless previously indicated). Save for any express acknowledgments, references and/or bibliographies cited in the work, I confirm that the intellectual content of the work is the result of my own efforts and of no other person.

The right of Dimla Eric Dimla Senior to be identified as author of this work is asserted in accordance with ss.77 and 78 of the Copyright, Designs and Patents Act 1988. At this date copyright is owned by the author.

Signature 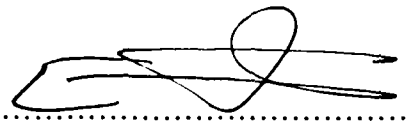

Date 17/07/98

TABLE OF CONTENT

ABBREVIATIONS AND SYMBOLS

AE	Acoustic Emission
ANN	Artificial Neural Networks
AR	Autoregressive
ARMA	Autoregressive Moving Average
ART	Adaptive Resonance Theory
BP	Back-propagation
BUE	Built-up Edge
CIM	Computer Integrated Manufacturing
CNNN	Condensed Nearest Neighbour Networks
DAC	Data Acquisition Card
DOC	Depth of Cut
FFT	Fast Fourier Transform
FMS	Flexible Manufacturing Systems
KFM	Kohonen Feature Maps
KSOM	Kohonen Self-Organising Maps
LVQ	Linear Vector Quantisation
MLP	Multiple Layer Perceptron
MMR	Metal Removal Rate
MSE	Mean Square Error
PCA	Principal Component Analysis
RBF	Radial Basis Function
RCE	Restricted Coulomb Energy
RMS	Root Mean Square

RTS	Remote Thermocouple Sensing
SLP	Single Layer Perceptron
SSE	Sum Square Error
STP	Sum Total Power
TCM	Tool Condition Monitoring
TCMS	Tool Condition Monitoring System

$\rightarrow$	Approach or converges to
a	The depth of cut value (mm)
a_x, a_y, a_z	Feed (Axial), Radial (Horizontal) and Tangential (Vertical) direction acceleration components (g) respectively. Also denoted as x-, y- and z-components of acceleration (g)
V	The surface cutting speed value (m/min)
s	The feed-rate value (mm/rev)
F_x, F_y, F_z	Feed (Axial), Radial (Horizontal) and Tangential or Cutting (Vertical) direction forces components (N) respectively.. Also denoted as x-, y- and z-components of Force (N)
$\bar{x}$	Mean value of the sampled data points
a:b:c	Feed-forward MLP with a inputs, b hidden neurons and c outputs.
a	Dimension of the input vector
b	Number of hidden neurons
c	Number of network outputs
α	Empirical constant in the integer-weight learning procedure
Δw^{t-1}	The previous weight modification
w^t	Current weight
δw	Smallest modification that can be made to weight

η	Learning rate constant
μ	Momentum term
t_j	Target/Desired value of the jth output layer neuron
o_j *or* y_j	Response of the jth output layer neuron
$f(.)$	Neuron activation function of the network
w_{ij}	Synapse connecting the ith input to the jth hidden neuron
w'_j	Synapse connecting the jth hidden neuron to the output neuron
W	Weight vector of a network
X	Network input vector
x_i	ith input to the network
EI	Flexural rigidity
K_Bmean	Mean flank wear length (mm)
K_Bmin	Minimum flank wear length (mm)
K_td	Crater wear depth (mm)

DEDICATION

This work is dedicated to **ALL** ***my family***, especially to my wife ***Maria Giovanna Lo Porto DIMLA*** and my son ***Dafydd Nyofi Toguem Dimla Junior DIMLA.***

"Le savant doit ordonner, on fait la science avec des faits comme une maison avec des pierres, mais une accumulation des faits n'est pas plus une science qu'un tas de pieres n'est une maison"

Henri Poincaré

"A scientist has to organise, science is made from facts like a house that is built from stones, but an accumulation of facts is no longer science just like a pile of stones is not a house"

Translation by ***Dimla E. Dimla Senior***.

ACKNOWLEDGEMENT

The author would like to thank the Research Support Unit (RSU) in the University of Wolverhampton for providing the funds, facility and support to carry out this study.

Dr. Paul Lister and Dr. Nigel Leighton are gratefully thanked for stimulating conversations, productive guidance, supervision and encouragement during the preparation and write-up of this thesis. Sincere thanks to Dr. Peter Musgrove for his advise on neural network matters.

Special thanks to my colleagues Dr. T. Sihra and Dr. T. Rafik of the University of Wales Institute Cardiff (UWIC) for their patience in having to endure with all my trials and tribulations and their forthright encouragement.

It was a pleasure working with Ilias Oraifige, Heru Susanto, David Turner, Yen Koo, Tero Kaipio, Kay Cattell, Jasbir Aujla, Shipping Yao, Tazmmal Husein, Drs. Ruth Pessu, S. T. Kometa, A. Akinsola, J. Gao, S. Gower and Leonid Smelov, who maintained an enjoyable working environment at occasionally difficult but interesting times. Technicians Jim Stamps, John Harris and John Pitt are thanked for their help on all machining matters.

This work is dedicated to my wife Maria Giovanna Lo Porto Dimla and baby Dafydd Nyofi Toguem Dimla Jnr. Dimla. Thanks Gio for enduring and sharing all my moments of near hysteria.

Very special thanks go to Mr. T. G. Dimla and Mme. Monica Manka for offering the author existence and uniqueness. The constant support of Dr. Ngong Beri Dimla, Ngwa Elisabeth Dimla, Love Shaw-Dimla, Dott. Giuseppe Lo Porto and Signora Palma Lo Porto are gratefully acknowledged.

Finally, sincere gratitude go to Mr. William Fru Mbafor and Mr. Dave Proverbs who took time off their own hard PhD work schedules to read and comment on an earlier draft of this thesis.

ABSTRACT

This thesis gives an account of an investigative study to develop a modular Tool Condition Monitoring System (TCMS) for metal cutting operations (turning in particular) through the application of multivariate process parameters and perceptron neural networks.

The initial phase of the work was concerned with a literature survey that was conducted to investigate the extent of applicability of neural networks to TCMS to-date. The survey showed that in spite of well over a decade of research in this direction, a truly universally applicable TCMS has not yet been developed.

A test bed to generate cutting data using a simple centred lathe onto which were attached the necessary sensors (a triaxial accelerometer and a triaxial dynamometer) was set-up. The instrumentation for the test bed comprised a personal computer fitted with a data acquisition card and connected to various peripheral signal conditioning instruments.

After validating the test rig against an existing result set, a number of limited cutting test cuts were carried out to assess the impact of cutting conditions on signal behaviour for both worn and sharp plane-faced tool inserts. The acquired cutting data was used to assess the ability of a neural network in tool wear diagnosis. The application of a linear neural network model in the form of a Single Layer Perceptron (SLP) could not satisfactorily classify the cutting data into the two tool state classes desired. The non-linear nature of the cutting data led to the application of Multi-Layer Perceptron (MLP) networks that were better at handling such non-linearity. However, when the MLP neural network was trained and tested on cutting data, the nature of the results lead to the conclusion that changes in chip form during machining resulted in false alarms. The propensity for such false alarms was reduced by using tool inserts with controlled tool-chip contact (i.e. chip breaker geometry). The success of an initial system

utilising flank wear only as the tool wear indicator to effect classification was extended. Nose wear and flank wear were used together but limiting the desired tool states to worn and sharp. This was further extended to include part worn, chipped and/or fractured tools. Finally, the developed model's range of application in a turning process was performed and its ability to recognise and distinguish tool wear from changes in the cutting conditions assessed. Though the developed modular TCMS model was capable of reasonable tool wear classification, it was incapable of detecting changes in the cutting conditions (particularly a reduction or an increase in the area of cut). A different classifier was developed to be used in parallel with the TCMS model in order for the system to be applicable over a broad range of cutting conditions.

CONTENT OF CHAPTERS

LIST OF FIGURES

LIST OF GRAPHS

LIST OF TABLES

CHAPTER 1

INTRODUCTION

1.0. Motivation

This chapter provides fundamental background on, and advances reasons for the need for a Tool Condition Monitoring System (TCMS). It outlines the basic characteristics and nature of TCMSs developed to-date. Some of the primary reasons for their non-ubiquitous implementation are recounted and ideas that one hope if properly implemented could lead to the development of a potential widely applicable TCMS are outlined. A brief synopsis of the mechanics of metal cutting and chip formation is also provided. The chapter ends with a brief recap of the objectives of the research work and an outline of the content of subsequent chapters of the thesis.

1.1. Subject Matter

The drive in manufacturing industries for cost saving, productivity improvement, the production of reliable and better quality products, has culminated over the years in the creation of minimally manned factories. Demand for better returns by investors and the quest for continued customer satisfaction through assured product quality, have been the main reasons for the rapid increase in factory automation in the last 20 years. In metal cutting operations, untended machining initially concentrated on automatic tool change procedures on-demand such as with Computer Numeric Control (CNC) machines. Recently, considerable research effort has focused on the feasibility of instituting automatic tool change due to tool wear/damage through implementation of adaptive tool inspection mechanisms (Dan and Mathew, 1990). The main difficulty in implementing total automation in the cutting process lies in determining the extent of tool wear or damage on a cutting tool in-situ. Traditionally, a tool might be changed to meet

new process requirements (e.g. differing tool geometry and material), or to suit the kind of cutting (roughing, finishing, profiling). To change a tool when worn however, requires on-line wear determination and this cannot be easily accomplished. The reason for this is primarily because tool wear is a complex phenomenon, which manifests itself in different and varied ways. The consequences of not changing worn tools when needed might lead to a deterioration of workpiece surface finish or excessive vibration levels on the machine set-up. Catastrophic tool failure could lead to machine tool damage and the production of scrapped workpieces, and therefore unnecessary costs.

A properly designed and implemented TCMS can be viewed as serving the following purposes:

i. Act as an advanced fault detection mechanism for both cutting and machine tool,

ii. Provide a means of checking and safeguarding machining process stability,

iii. Help keep machining tolerances on the workpiece to acceptable limits by providing a compensatory mechanism for tool wear offsets, and

iv. Act as a machine tool ***damage avoidance*** system.

The cost and implications of the lack of TCMS include amongst others the following:

a) Excessive power take-off,

b) Damage of workpiece (inaccurate tolerances, serrations and uneven surface finish on the workpiece)

c) Scrapped workpieces thus unnecessary costs

d) Can lead to machine tool and/or machine peripheral damage, and

e) Unstable cutting environment.

Much research has been carried out to develop reliable TCMS over the last decade, but none has yet found ubiquitous industrial use (Lister, 1993; Dan and Mathew, 1990; Lister and Barrow, 1986). Several factors have impeded advances in TCMS including inappropriate choice of sensor signals and their utilisation. One of the primary reason for the lack of industrial application of developed TCMS models is due to the fact that they have been largely developed based on mathematical models requiring huge amounts of empirical data. Another possible hindrance lies in the nature and characteristics of the utilised sensor signals in general, which tend to be stochastic and non-stationary, and therefore difficult to model. The random behaviour can be attributed to the large scale variation and inhomogeneities that exist in the workpiece (Ravinder *et al.*, 1993). There are difficulties involved in designing TCMS that take account of the noise sources. Typically, most metal cutting processes can be classified as having one or more of the following characteristics (Warnecke *et al.*, 1990):

i. complex to chaotic behaviour due to inhomogeneities in workpiece material

ii. sensitivity of the process parameters to cutting conditions

iii. non-linear relationship of the process parameters to tool wear.

Misleading information easily results as disturbances from either of the aforementioned sources pose a practical problem, limiting precision and control of the cutting process. A high degree of reliability for diagnosing the ensuing tool condition with a sufficient level of accuracy therefore becomes paramount (Novak and Wiklund, 1992). When unexpected disturbances occur, a TCMS ought to be capable of diagnosing, and identifying the fault and possibly isolate or respond with remedial action within a prescribed response time (Warnecke *et al.*, 1990).

Example based methods of process parameter correlation to tool wear have come to be viewed as a better method for TCMS development, commonly performed through the application of artificial neural networks (ANN) of both the supervised and unsupervised types. This has proven particularly popular and reliable because of the stochastic nature of the cutting process and its empirical non-dependency as it incorporates elements of intelligence to the process parameters (Rangwala and Dornfeld, 1987; Rangwala, 1988; Burke, 1989; Choi *et al.*, 1990; Dornfeld, 1990; Lui and Ko, 1990; Elanayar *et al.*, 1990; Emel, 1991; Tansel *et al.*, 1992; Kamarthi, 1994; Purushothaman and Srinivasa, 1994; Noori-Khajavi and Komanduri, 1995). Neural network algorithms and training methods are presented in Chapter 3, and a review of some of the key ANN based TCMS developed over the last decade are provided in Chapter 4.

Fundamentally, most of the methods presented attempt to classify and quantify tool wear states, assuming that tool wear states can be defined. It can be argued that this approach fails to accommodate the complex and diverse nature of the metal cutting operation, and may explain the failure of existing systems to achieve widespread industrial use. Ideas on conceptual and developmental perspectives have also been put forward and can be found in Moriwaki (1994).

Though ANNs are a fairly new technique, they have become extremely popular in industry and financial circles because of their classification and optimisation capabilities. Neural computing has its origins as far back as the early 1940s. A period of unpopularity in the 1960s and 1970s has been superseded by an upsurge in the late 1980s to the present. This renewal of interest in neural computing has largely been as a result of the discovery of new techniques and advanced developments in computer hardware technology such as VLSI, and the current reduction in computer prices. The most important characteristics and features that make ANN attractive in TCMS applications can be summarised as follow:

- Fault tolerance and adaptability

- Data driven nature
- Better noise suppression capabilities
- Limited success of statistical methods
- Learns relationships rather than make assumptions
- Handles a wide variety of problems- 'Generalises'
- Proven success in practical settings, and
- Performance exceeds human decision making.

An ANN has a mathematical background and theory, with its development stemming from basic mathematical principles modelled on biological neurons and the nervous system (Harvey, 1994). Neural networks can learn from examples, with the neurons performing their operations in parallel (distributed processing) by forming non-linear discriminants. They are robust, capable of non-linear modelling, associative storage of information, control of dynamic systems and classification of noisy or complicated data. Some of the most notable contributions have been from mathematics, biology, physiology, psychology, neuroscience and engineering (Fausett, 1994; Beale and Jackson, 1990; Lippman, 1987). Neural networks basically consist of several neurons called processing elements, grouped together to form a network, performing identical tasks with 'network' being the main point of concern. The structure and architecture of these networks generally vary according to the desired application. In this respect it is reasonable to suggest that there are almost as many ANN types as there are applications, but another school of thought classifies ANN types from an architectural point of view (Harvey, 1994).

The implementation of intelligent TCMS in a specified operation (drilling or turning) in a rapidly changing and unpredictable environment was considered paramount (Choi *et al.*, 1990). A major drawback though to the implementation

of the aforementioned system has been that development of an adequate sensor for on-line monitoring of the cutting process has not yet been accomplished (Lister, 1993; Burke, 1989; Rangwala, 1988). Historically, TCM has been performed by human operators, using a combination of sight and sound. It is impossible to develop sensors to mimic exactly the human operator, who is subjective and flexible but inaccurate. This problem has been circumvented by using descriptive parameters of the cutting process that show sensitivity to tool wear, thus precluding the need for a unique sensor. This in effect could be viewed as an extension of the traditional human operator TCMS process, and its main advantages are that, emerging and established sensor signal processing technologies can be employed on the tapped signals, making use of less complicated and widely available commercial sensors and instruments. Advanced sensor design permits information gathering of the cutting process enabling adequate measurements. Recent surveys of sensor application in TCMS can be found in Byrne *et al.* (1995), Martin (1994) and, Dan and Mathew (1990).

1.1.1. Fundamentals of Metal Cutting - A brief theoretical overview

Metal cutting broadly constitutes turning, boring, drilling, facing, forming and parting-off, milling and shaping/planning. Cutting tools generally can be classed into two categories: single point tools (turning, shaping, planning) which have one and only one cutting part and a shank, while multiple tool points (drilling, milling, broaching) have more than one cutting parts. Fig 1.1 shows the most commonly used terms and tool geometry definition of a typical metal cutting tooling system.

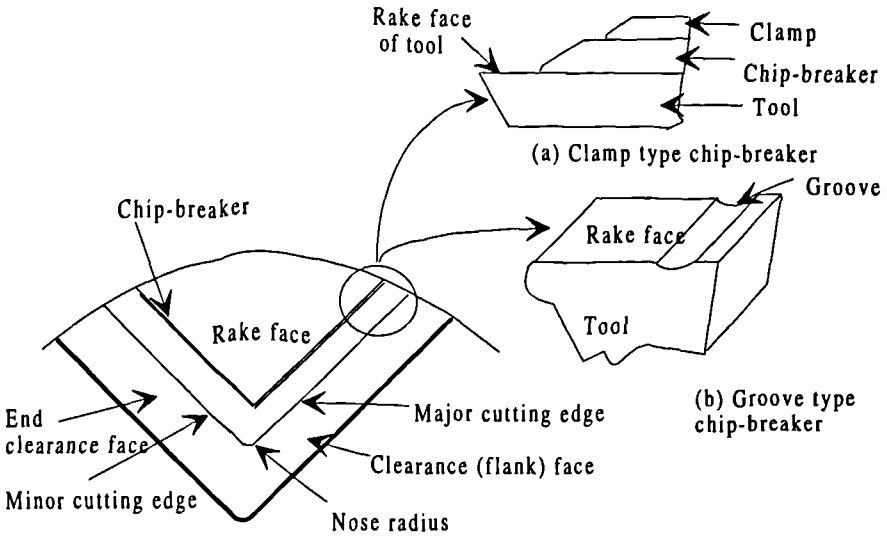

Figure 1.1. Cutting tool terminology

The main focus of this research centres on turning. Turning could be defined as a machining process for generating external surfaces by the action of a cutting tool on a rotating workpiece, usually carried out on a lathe. Two kinds of metal cutting operations in turning can usually be encountered; oblique and orthogonal cutting. Orthogonal cutting, could be argued, represents a reasonable approximation of cutting on the major cutting edges and, therefore is the most prevalent form of cutting (Shaw, 1984). In orthogonal cutting, the cutting tool approaches the workpiece at right angles to the direction of cutting, with the cutting edge parallel to the uncut surface. A typical orthogonal process, turning on a centre-lathe machine is shown in Fig. 1.2.

The rate at which the uncut surface of the workpiece passes the cutting edge of the tool is the cutting speed, V. In turning, the feed-rate (s) is the distance moved by the tool in an axial direction at each revolution of work. The depth of cut (a) is the thickness of metal removed from the bar, measured in radial direction. Principally, these three parameters determine how quick or slow the metal (swarf) is removed, and their product, the metal removal rate (MRR) measured as a volumetric quantity could be considered an efficiency indicator of the cutting operation (Trent, 1977).

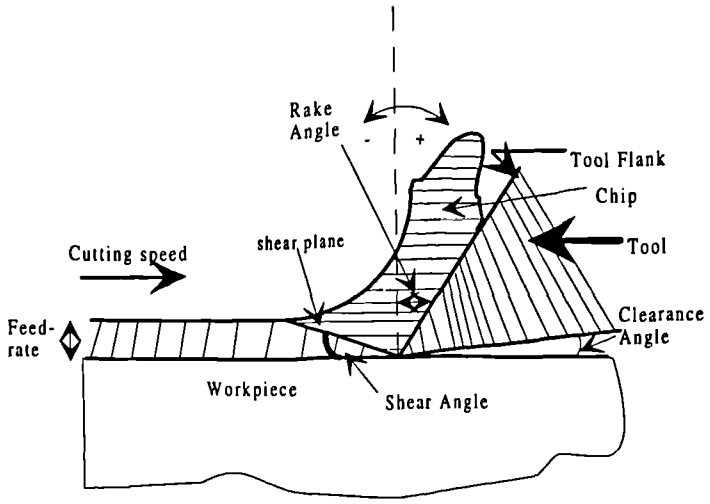

Figure 1.2: Schematic diagram of an orthogonal metal cutting process

Cutting parameters (depth of cut, feed-rate and speed) are chosen so as to be consistent with the strength of the part, chunk, power of machine and amount of stock to be removed. As depth of cut increases, the cutting force becomes larger, and must therefore be limited to the available power of the machine. Feed-rate depends on the finish desired, strength of machine and its rigidity. Finishing cuts require a light feed-rate whereas roughing cuts are often large with the cutting speeds dependent entirely on workpiece hardness. Several other machining processes can be performed in conjunction with turning, such as facing, reaming, boring, etc. although less frequently. The only restriction in turning seems to be the availability of equipment size, to hold and rotate the workpiece, with problems in holding and handling as size and weight increases.

During orthogonal cutting, a large amount of energy is required to form the chip creating two new surfaces by shearing: the new surface of the workpiece and the underside of the chip. Most of the energy in metal cutting is used to plastically deform and remove the chip, consequently this area has received considerable research efforts to understanding the phenomenon (Trent, 1977). A full understanding of the mechanics of the orthogonal cutting process is not intended to be discussed in this research as it is out of the scope of the work. It is however fair to assume that high stresses and strain rates developed as the cutting tool

ploughs through the workpiece give rise to complicated forces, high temperatures, and dynamic behaviour across a broad spectrum of frequencies. Possible explanations for the increased dynamic behaviour have been put forward by Piispenen, Merchant and Zlatin, and Drucker (Shaw. 1984). The cutting force (F) can be resolved into three mutually perpendicular force components: the Tangential Force F_t (vertical or z-axis component), the Feed Force F_f (axial or x-axis component) and the Radial Force F_r (y-axis component) as depicted in Fig. 1.3. These copmponents fluctuate and their excursions give rise to machine chattering (tool holder vibrations manifested on the workpiece by saw-tooth marks and serrations on the underside of chip).

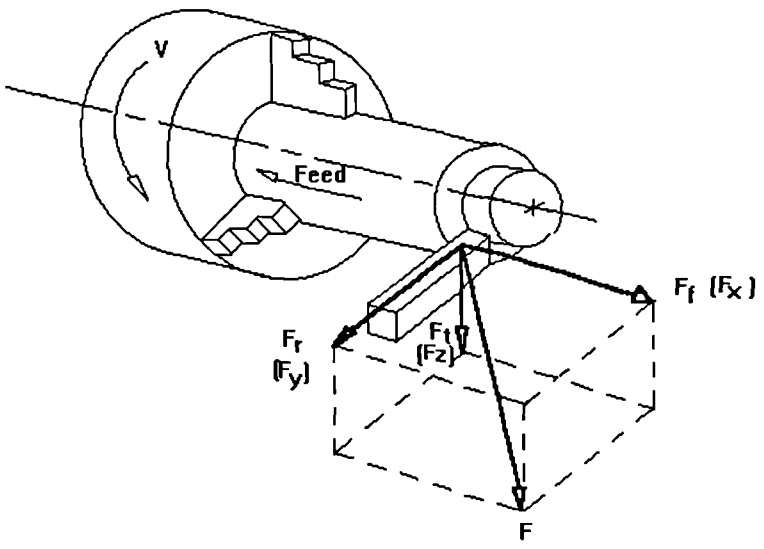

Figure 1.3: Forces acting on a cutting tool in orthogonal metal cutting

Orthogonal cutting generates considerable amounts of heat and energy at a rate proportional to both the cutting speed and the resultant tool force. Elastically deforming materials generate a small amount of energy and usually this energy is stored in the material as strain energy. Plastically deforming materials generate

large amounts of heat, as the material of the workpiece is subjected to high strain levels that is converted to heat energy at the zones of primary and secondary deformation (Fig. 1.4) (Boothroyd, 1975). Some heat also arises due to friction between the tool and the new workpiece surface.

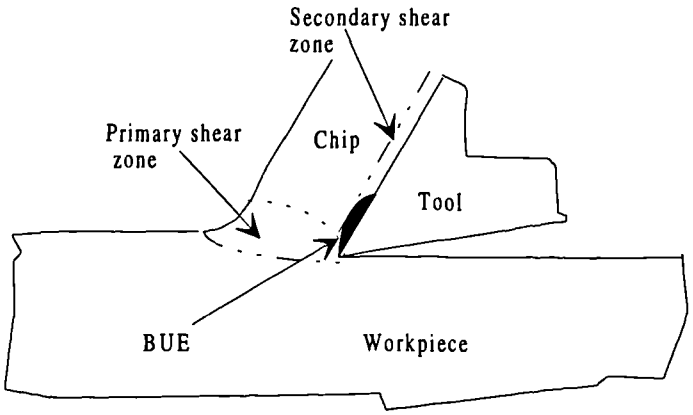

Figure 1.4: Metal cutting shear zones and BUE

Dynamic and static forces constitute the cutting forces in any metal cutting operation. The static force gives an indication of force magnitude levels, whereas the dynamic force represents the degree of fluctuation in the cutting force.

1.1.2. Chip Formation

Several mechanisms have been put forward in an attempt to explain the means by which a chip is formed during a metal cutting process (Moore and Kibbey; 1982). These mechanisms can be categorised into FOUR main groups as follows:

i. Postulations based on considering the cutting tool as a simple loading device (the classic chisel model),

ii. Models based on the proposition that the cutting forces are created by the ploughing action of the tool motion,

iii. Excessive stresses caused by material failure, and

iv. Models proposing chip formation as dependent on material and cutting conditions.

The latter model is based on the more generally accepted theories and is extensively covered by Merchant's, Lee and Shaffer's, and Christopherson, Oxley and Palmer's theories (Radford and Richardson; 1974).

Generally, two main classes of chips are produced from metal cutting: continuous and discontinuous, sometimes with built-up edge (BUE) and serration occurring between them (Kalpakjian, 1991). The two categories of chips formed are not so easily defined as both shades of gradation between the two types can be observed. Discontinuous chips are desirable as they are easy to clear from the working area and chip-breakers (Fig. 1.1 (a) and (b)), an integral groove in the rake face or a separate piece fastened to the tool used to cause the chip to break into short sections or curl. Continuous chips could become entangled in the machine tool posing a serious problem to the machine operator.

Continuous chip usually forms at a high cutting speed or high rake angle as the material deformation occurs principally in the primary shear zone. Discontinuous chip results from a combination of material property, low rake angle, very low or very high cutting speed and the secondary shear zone.

Movement of the chip and workpiece across the face of the cutting tool has in the past been inappropriately treated as classical friction situations, but detailed studies have shown this not to be the case (Trent, 1977). Under certain conditions (low cutting speeds and high feed-rates), the flow of chip from the cutting tool is such that it welds itself onto the cutting tool. This increases the friction on the cutting edge, leading to a building-up of more layers of chip material on the tool (Fig. 1.4) commonly referred to as BUE (Trent, 1977; Boothroyd, 1975; Radford and Richardson; 1974).

1.2. Forms of Tool Wear Encountered During Metal Cutting

Cutting tool wear can be classified into several types as follows:

i. Adhesive wear associated with shear plane deformation,

ii. Abrasive wear resulting from hard particles cutting action,

iii. Diffusion wear occurring at high temperatures, and

iv. Fracture wear such as chipping due to fatigue.

Tool wear processes generally occur in combination with the predominant wear mode, dependent upon the cutting conditions, workpiece and tooling material, and the tool insert geometry. For a given cutting tool and workpiece material combination, the tool wear form may depend exclusively on the cutting conditions, principally cutting speed V and the undeformed chip thickness t, and a combination of the aforementioned wear mechanisms. Ranges of cutting speed where each type of wear is predominant can be identified by considering the product of these values as Vt which is directly proportional to the cutting speed (Shaw, 1984). Sometimes, the tool life can be considerably reduced if the area of cut, the area swept by the cutting tool, is significantly increased (i.e. by increasing the DOC mainly). At low cutting speeds, the tool wears predominantly by a rounding-off of the cutting point and subsequently looses sharpness. As the cutting speed increases the wear-land pattern changes to accommodate the ensuing change with extremely high values leading to plastic flow at the tool point. Cratering on the other hand depends largely on the cutting temperature than on the cutting speed. The various forms of wear-land pattern and prevailing cutting speed in Fig. 1.5. The more predominantly occurring forms of cutting tool wear often identified as the principal types of tool wear in metal turning using single-point tools are nose, flank, notch and crater wear. Fig 1.6 shows how these wear features are usually measured.

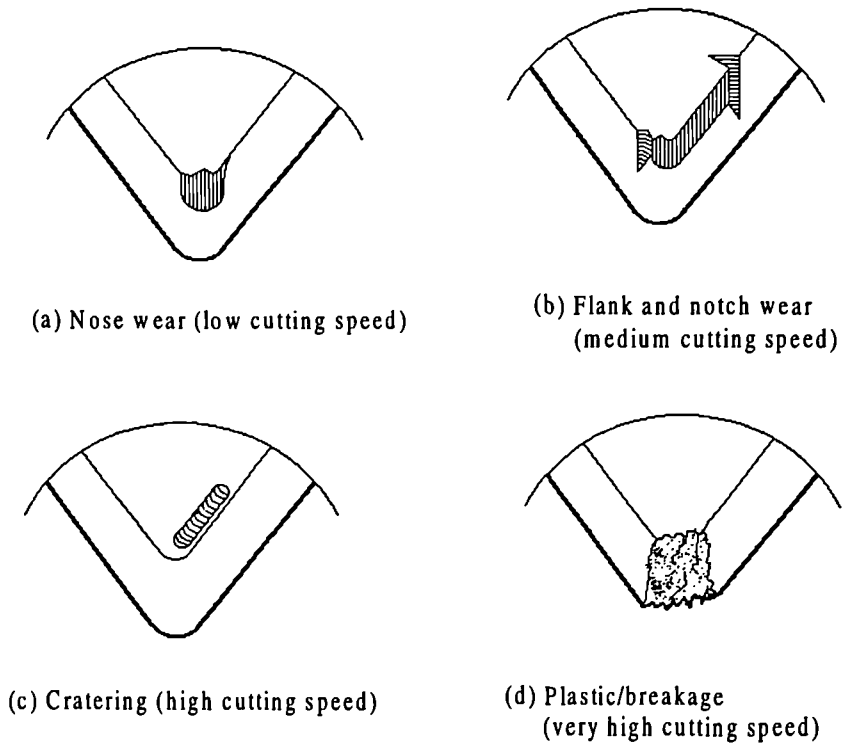

Figure 1.5: Cutting tool wear forms in orthogonal metal cutting

Nose Wear or edge rounding occurs predominantly through the abrasion wear mechanism on the cutting tool's major edges resulting in an increase in negative rake angle. Nose wear can be dependent entirely on the implemented cutting conditions with tool sharpness lost through plastic or elastic deformation. At high cutting speeds, the edge deforms plastically and may result in the lost of the entire nose, Fig. 1.5(a) and Fig. 6(b). Edge chipping and cracking occurs during periodic breaks of the BUE in interrupted cuts with brittle tool and thermal fatigue. Catastrophic failure may also occur if the nose is considerably worn or as a result of the utilisation of inappropriate machining conditions and brittle tools such as ceramics and cemented carbide (Schey, 1987).

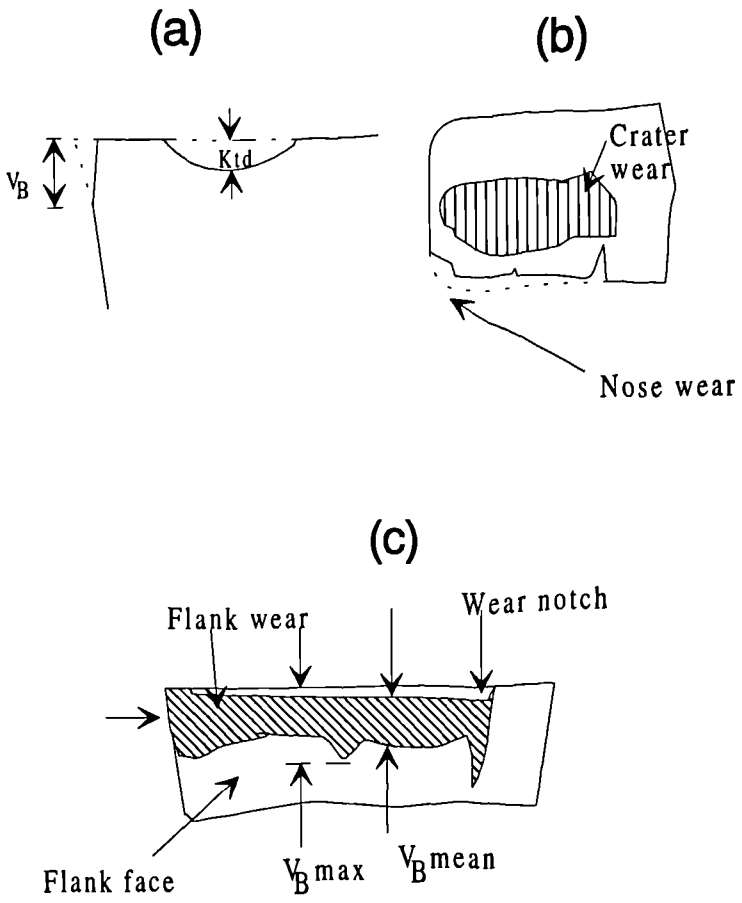

Figure 1.6: Conventional features of tool wear measurements

Nose Wear or edge rounding occurs predominantly through the abrasion wear mechanism on the cutting tool's major edges resulting in an increase in negative rake angle. Nose wear can be dependent entirely on the implemented cutting conditions with tool sharpness lost through plastic or elastic deformation. At high cutting speeds, the edge deforms plastically and may result in the lost of the entire nose, Fig. 1.5(a) and Fig. 6(b). Edge chipping and cracking occurs during periodic breaks of the BUE in interrupted cuts with brittle tool and thermal fatigue. Catastrophic failure may also occur if the nose is considerably worn or as a result of the utilisation of inappropriate machining conditions and brittle tools such as ceramics and cemented carbide (Schey, 1987).

Flank wear arises due to both adhesive and abrasive wear mechanisms from the intense rubbing action of the two surfaces in contact, i.e. the clearance face of the

cutting tool and the newly formed surface of the workpiece. Its rate of increase at the beginning of the tool life is rapid, settling down to a steady-state then accelerating rapidly again at the end of tool life (Fig. 3.1). Flank wear leads to a deterioration of surface quality, increased contact area and consequently to increased heat generation (Fig. 1.5 (b) and Fig. 6(c)).

Wear notch forms at the DOC line as the tool rubs against the shoulder of the workpiece (Fig 1.6(b) and 1.6(c). Wear notch can lead to abrasion setting by the surface layers accelerated by oxidation or chemical reactions, possibly leading to total tool failure.

Crater wear results from a combination of high cutting temperatures and high shear stresses creating a crater on the rake face some distance away from the tool edges, quantified by depth and cross-sectional area (Fig. 1.5(c)). Crater wear also arises due to a combination of wear mechanisms: adhesion, abrasion, diffusion or thermal softening, and plastic deformation. Severe depths of crater may trigger catastrophic collapse of the cutting point (Fig. 1.5(d) and Fig 1.6(d).

1.3 Monitoring Tool Wear in Unmanned Machining Operations

The type and nature of sensor signal presents an enormous hindrance to the development of a TCMS. The main drawback to the implementation of metal cutting TCMS lies in the fact that development of a sensor to replace the human operator exactly is impossible. Researchers have therefore carried out varied and extensive work on the various parameters related to tool wear in a cutting operation rather than attempt a direct replacement of the subjective human operator. This has been achieved through application of advanced sensor designs and signal processing technologies, that allow adequate measurements to be taken of the cutting process parameters, that accurately describe the cutting process.

Generally, techniques for on-line TCMS can be grouped into two main categories: ***direct sensing*** and ***indirect sensing*** techniques. While direct methods of wear

measurement have been attempted (Lister, 1993), the majority of methods have been indirect (Ko *et al.*, 1994; Purushothaman and Srinivasa, 1994; Lister, 1993; Tansel *et al.*, 1993; 1992; 1991; Masory, 1991; Rangwala and Dornfeld, 1987; 1990;).

Direct methods are of less benefit because the cutting area is largely inaccessible, and therefore monitoring can not be performed while the tool is actively engaged in in-process cutting. These methods include amongst others, touch trigger probes, optical, radioactive, proximity sensors and electrical resistance measurement techniques (Lister, 1993; Tansel *et al.*, 1992; Trent, 1977).

Indirect methods take measurements while the tool is actively engaged, since it involves recording a variable that can be correlated to tool wear (i.e. indirect methods measure factors that result as a consequence of tool wear). Commonly used methods include amongst others cutting forces, acoustic emission, temperature, vibration, spindle motor current, cutting conditions, torque and strain. These factors reflect far more than tool wear alone and parameters associated with tool wear must therefore be extracted from them and correlated to give a measure or extent of tool wear. The main practical drawback with this popular method is the need for calibration of the associated parameters in monitoring the cutting process. The cutting conditions (speed, feed-rate and depth of cut) are known to affect the sensor signals and a range of methods have been suggested for separating the effects of these conditions from those of wear on the measured parameter (Karmathi, 1994).

Methods for correlating the measured process parameters to tool wear, breakage or chipping fall primarily into three categories (Guinea *et al.*, 1991). The first class consists of methods that can be viewed as ***heuristic based rules*** with a priori knowledge only of the process parameters, and use as mathematical modelling and adaptive observers. The second category consists of methods that could be viewed as requiring formal knowledge of the process and these can be grouped

together as ***analytical based models*** such as time series analyses and Fast Fourier Transform (FFT) peak tracking. The last category is one of example based models with ***inductive learning capabilities*** such as pattern recognition, decision surfaces, mapping techniques, clustering and ANN.

1.3.1. Methods for Detecting Tool Wear

Most indirectly measured sensor signals are generally affected by workpiece material variation, geometry of the cutting tool and the cutting conditions (Lister, 1993; Choi *et al.* 1990). An on-line monitoring system designed to take the above factors into consideration, is extremely demanding. In many cases, the machining system does not need to have a global knowledge of the machining process, as it only requires knowledge about the machining operation in the neighbourhood of the optimum for the operating process (Byrne *et al.*, 1995). The cutting conditions cannot be neglected, as their variable parameters affect the sensor signals and therefore the cutting tool state.

The use of these indirect methods requires accurate predictive models that link the un-measurable parameter of interest (tool wear), with the indirectly detectable variables (Oraby and Hayhurst, 1991). The process of tapping useful signals or process parameters directly or indirectly from a cutting process constitutes what Burke (1989) symbolically terms, the ***detection level***. This level in any TCMS is primarily concerned with choosing the relevant sensory signal.

1.3.2. Identification of Tool Wear

The choice of a suitable sensor type and its point of application (sensor location) are inextricably linked, with a suitable location for any such sensor being where the specified signal has the highest concentration and best reproducibility. Certain limitations however do exist due to the structure of the machine. A school of thought has it that information from a variety of different sensors has to be collected and these signals of varying reliability integrated (fused). The primary

benefit of sensor fusion it would seem is the fact that it serves to enhance the richness of the underlying information (wear level) contained in each signal thereby increasing the reliability of the monitoring process (Dornfeld, 1990). The lack of an accurate model for wear prediction has thus led researchers resorting to other methods of sensor integration which do not rely on any theoretical or empirical process.

The fusion and subsequent correlation of sensor signal features to tool wear is viewed as constituting the identification of wear, thus the characteristic ***identification level*** (Burke, 1989). The utilisation of single sensor signals offers incomplete sensory information as to the wear state (condition) of an engaged cutting tool. This shortfall can be obviated by pursuance of a sensor fusion strategy (Lui and Ko, 1990). This method has proven highly successful as more reliable information on the tool state was extractable. In addition to pattern recognition techniques, hyperplane decision surfaces, mapping techniques, neural networks, clustering techniques and perceptron techniques are reported by Noori-Khajavi and Komanduri (1995) in their literature survey as other fusion techniques. Methods primarily based on neural networks have proven particularly popular because tool wear intrinsically is a non-linear process. Its representation via a neural network is viable, reliable and an attractive alternative to previously employed empirical methods (Elanayar *et al.*, 1990). Neural networks are robust and highly parallel processing devices, capable of non-linear modelling. Explicit problem description is not required, and they are capable of handling large amounts of data (information) out of which they build knowledge bases that are consulted during decision making (Yan *et al.*, 1995; Govekar and Grabec, 1994; Markos *et al.*, 1993).

1.4. Objectives

This research work is aimed at emulating the way a human operator perform TCM, by developing a modular TCMS that precludes the need for complex mathematical models and large amounts of empirical data. Such a system, it is hoped, would have a potential wide applicability and yield broad-based solutions.

The research set out to collect multivariate descriptive information (i.e. data from more than one sensor) of the cutting process in real-time, measuring the severity of the wear forms for subsequent analysis using the inductive learning capabilities of simple feed-forward perceptron neural networks. Initial work concentrated on the identification of signals and process parameters considered appropriate as inputs to a neural network to detect inception of tool unacceptable levels of wear. This necessitated a comprehensive literature survey on the applications of neural networks to date in TCMS, and the development of a fully instrumented test rig that was validated against an existing set of data. The identification of suitable process parameters from knowledge of existing practice and results of preliminary cutting tests was undertaken. It was apparent from the literature survey that TCMS that can cope with significant variations in the tooling/workpiece material and other specifications such as the cutting conditions (feed-rate, depth of cut and cutting speed) did not exist. The research work attempts to address these significant shortfalls, from which it is hoped to develop a system that would accommodate the complex and varied nature of the cutting process.

The development of the neural network model concentrated on training it on a range of cutting conditions from which its design was improved by optimisation and validation in the range of data investigated. The developed model was then tested for a range of significantly changed cutting conditions and the effect of changing tooling material also investigated, and its performance assessed.

This work was also partly motivated by the current lack of research and data based on chip breaker tool configurations. Currently, existing methods have been

mostly based on plane-faced tool geometry, with flank wear often the main mode of tool life measurement. The effects of utilising chip-breaker geometry inserts alters the mechanics of machining, and experimental verifications showed that flank wear alone was not the single most important factor that affected tool life.

1.5. Organisation of Thesis

This thesis is divided into 13 chapters. The next chapter outlines and formulates the TCM problem. Chapters 3, 4 and 5 documents the literature survey conducted to situate the research work. Chapter 3 presents a brief documentation of the various metal cutting process parameters that can be used as possible sensor signals. Chapter 4 follows on the same theme as chapter 3, but deals exclusively on theoretical, development and application issues of neural networks. Chapter 5 documents a literature survey that sought to outline trend and results achieved in the development of TCMS through the application of ANNs. The test rig set-up, its components (hardware, software and instrumentation configurations) are described in chapter 6. Chapter 7 outlines the results of the investigations of the impact of the cutting conditions on the chosen sensor signals for plane-faced tool geometry, followed by a preliminary application of neural networks in TCM on the acquired data in chapter 8. Chapter 9 describes the impact of the cutting conditions on measured parameters for chip-breaker geometry tool inserts. The investigation of the effects of progressive tool wear on the sensor signals is reported in chapter 10, and the implementation of neural networks for the tool state classification using chip breaker geometry tool data appears in chapter 11. In chapter 12, the final conclusions reached from the work carried out are presented, and some novel aspects of the research highlighted. Suggestions for future work appear in chapter 13.

CHAPTER 2

THE TOOL CONDITION MONITORING PROBLEM: AN OUTLINE

2.0. Overview

This chapter presents a philosophical outline of the fundamental requirements of a TCMS. Attention is paid to exploring the need for such devices, illustrating what could be termed the main reasons for the lack of a comprehensive TCMS. A synopsis of the problems encountered in the two main stages of development of a TCMS are listed and discussed, with a view on how best to achieve a comprehensive TCMS outlined.

2.1. Introduction

Research in metal cutting has been performed for well over a century now, but researchers are not yet significantly closer to quantitatively predicting certain aspects of the cutting process. For example, it is not yet possible to predict with any great accuracy the forces involved in an orthogonal metal cutting due to the complexity of the mechanics of the cutting process and the characteristic lack of geometrical constraint due to linkages and bearings.

In the later part of the 1800s, three review papers detailing the work done in this field that far were published respectively by Fennie, Cocquilhat and Hartig, and these publications set the current trend in metal cutting research (Boothroyd, 1975). It was not until 1906 that the most authoritative publication was made by Taylor. This publication remains to date the basis of many recent studies. In Taylor's paper, he is reputed to have made fundamental discoveries pertaining to machine economics, and one of his discoveries was concerned with cutting tool wear rate. He stated that,

studies he performed showed that the cutting tool edge temperature was solely responsible for tool wear rate. Subsequent studies have proven his prediction to be true though in conjunction with other process parameters such as cutting forces and the influence of the cutting conditions (Boothroyd, 1975).

A metal cutting operation generally can be viewed as consisting of a number of semi-independent (inter-linked) systems. The subsystem of interest in this study concerns the workpiece/cutting tool. A complex and dynamically varying system forms between the workpiece and the cutting tool, with the cutting forces, power requirements, vibrations, temperature and acoustic emission having a non-linear relationship with wear accruement on the cutting tool edges. For decades, cutting tool variables have been measured through the application of sensors, and their behaviour monitored to effect in predicting tool wear in order to distinguish a worn tool from a sharp one. The sole aim of such investigations has been to establish distinctive sensor signal characteristics whose trend could be monitored to distinguish each cutting tool phase.

When a cutting tool wears, the cutting tool edges become weakened. Increases in the amount of wear leads to a situation whereby the cutting tool is no longer able to support the cutting forces, the results of which can lead to catastrophic tool failure (Tanner and Loh, 1994). The rate of tool wear is not a point of primary concern in any cutting process, but factors such as the surface finish and dimensional integrity of the workpiece, and overall machine dynamics (vibrations) would normally be. Over the years, it has been established that these factors are affected by the amount of wear on the cutting tool edge rather than the rate at which it increases. A cutting tool is therefore considered to have 'softly' failed (i.e. become worn through progressive wear build-up), if it can no longer produce parts within its required specifications. These required specifications could be aspects of dimensional stability, a deterioration of surface finish quality (saw-tooth marks and serrations), excessive cutting forces or a combination of these factors (Tanner and Loh, 1994).

2.2. *Consequences of Tool Wear*

Often, subjective wear levels are set which translates on the workpiece as the maxima or minima permitted tolerances. If this value of wear is superseded, a costly consequence could be the rejection of the workpiece during quality control assessment and possibly an increase in scrapped components level.

Most aspects and occurrence of tool wear are eventually detrimental to the cutting tool/workpiece subsystem. Tool wear studies usually are interested in prevalent tool wear forms such as nose, crater, rake face (henceforth face) and flank wear. Retrospectively, different mechanisms are thought to be responsible for these failures, such as diffusion wear (flank and crater), thermal (chipping micro cracking), material build-up on the cutting edge, and plastic deformation of the tool. These mechanisms depend partly on a combination of the type of cutting required, the nature of tooling and workpiece materials and the cutting conditions.

As most manufacturing systems are increasingly converting into fully automated environments such as computer integrated manufacture (CIM) and flexible manufacturing systems (FMS), tool wear monitoring inevitably would become an automated aspect of such a manufacturing environment. A precautionary measure to expeditiously recognise a worn cutting tool and have it replaced as soon as possible becomes necessary. Failure might lead to a catastrophic tool breakage causing excessive power overloads and damage to the machine tool and the workpiece. In cases of high replacement costs, avoidance or limitation of such a failure becomes paramount.

2.3. *Earlier Attempts of TCM*

In view of the damage that tool failure can cause to a machine tool and its peripheral components, there has been a big drive to develop systems aimed at providing advanced warnings of imminent tool failure (Monostori, 1993; Warnecke *et al.*, 1990). These devices have taken the form of tool wear detection and identification

mechanisms, referred to in this thesis as TCMS. For such a system to be successfully developed and implemented, crucial tool wear information need to be harnessed from the cutting tool. These challenges have proven enormous. Firstly, a suitable means of detecting the signals mechanically, such as through sensors, as opposed to the human operator who uses his/her senses of sound, smell and sight to observe the cutting tool has to be devised. Secondly, the signals would have to be processed to identify any deviation in trend patterning to the ensuing tool state.

2.4. Problems Encountered

The use of auditory, olfactory or visual sensors to replace the human operator simply will be an expensive and futile undertaking (Burke, 1989). Direct methods such as those associated with measuring and correlating the volumetric loss of cutting tool material can be time consuming and misleading. Consequently, mechanically and physically based sensors have been developed in an attempt to tackle the wear detection problem. Amongst these sensors are touch trigger probes, optical, radioactive and electrical resistance measurement techniques, and a number of proximity sensors (Lister, 1993). The operation of such sensors and their development have tended to depend on the fact that they operate more like 'STOP - GO' devices requiring measurements to be taken only when the tool is out of cut, (i.e. off-line) necessitating the interruption of the cutting operation. Interruption of the cutting process increases both lead- and down-time, hence is an unwanted process that ought to be avoided.

The problems that off-line sensors posed, led to the development of sensors that could be mounted directly on the cutting tool holder or the workpiece, and these have proven to better serve the purpose of tool wear monitoring (Burke, 1989). The primary technologies behind these sensors lie in the indirect methods of tool wear detection, whereby factors or process changes which results as a consequence of tool wear were measured. A vast array of probable sensing technology and sensors exist. Amongst

these are sensors based either on the mechanical or physical property changes, static or dynamic changes.

The inception of indirect tool wear measurement introduces the complimentary and desirable technique of on-line analysis. Through the process of on-line monitoring, the optimum conditions to minimise tool wear could be selected simply by changing the various process parameters. This is possible because on-line tool wear monitoring could be viewed as a closed loop control system with feedback mechanisms. The consequences of process parameter changes can be instantaneously measured and analysed to yield the resulting effect on the tool behaviour through indirect sensing.

Clearly, tool wear monitoring presents a difficult problem and many attempts have been pursued in the quest to develop such a system. The detection level, as defined by Burke (1989), is concerned with choosing the relevant sensory signals i.e. how and what to detect, whilst identification deals primarily with observing a trend or implementing a plausibility check on the sensory data in order to assess the degree of tool wear and/or tool failure.

2.4.1. The Detection Level Problems

Several sensory parameters have been used in various attempts to develop a TCMS. Failure in the industrial implementation of such systems would seem to suggest that a sensor to cater for all machining scenarios, i.e. 'universal applicability', does not exist (Lister, 1993). This generally can be attributed to the existence of a variety of machining conditions and consequently wider application areas. Suitable sensors have been developed for particular applications, such as static and dynamic force measurement, acoustic emission and vibration, but their characteristics vary widely and are often sensitive to variations in the cutting conditions (Burke, 1989; Rangwala, 1988).

Another prime source of failure in the detection level can be labelled at the way the studies have been conducted. Present day studies have tended to use just one of the

variety of sensor signals available, rather than using combinations of two or more complimentary signals. Such a system fails to recognise the complex and diverse nature of the cutting process (Lister, 1993). A thorough attempt to correlate a single process parameter to the ensuing tool state would require complicated signal processing and analyses possibly leading to an overly designed TCMS and rendering it ineffectual because of its' sophistication. Sensor signal types and their correlation to tool wear and tool failure seem to determine the degree of success of any TCMS.

2.4.2. The Identification Level Problems

The secondary level of any TCMS essentially concerns signal processing and the correlation of characteristic sensor signal features to the prevailing tool wear levels. The prevailing lack of a comprehensive TCMS lies in the non-achievement of a 'smart' wear identification system. Accurate models for predicting wear are currently unavailable and laboratory research models are often less robust and unreliable either because they are solely based on empirical results or a set of relationship based rules. An example of such a rule is that which identifies a tool as worn when the cutting force signal's magnitude exceeds a certain fixed threshold. An integrated TCMS has to have the ability to recognise incipient, partial, total or catastrophic cutting tool wear situations. Some commercially available systems are not capable of this degree of distinction as they have been designed to rely on empirical results or a set of rules such as, if $A > A_{lim.}$, then...,. This assumes the system is continuous and non-changing (ideal) rather than an FMS or CIM. Such systems could be viewed as an initial step towards monitoring systems with the required performance level (Monostori, 1988).

A TCMS should not rely on aspects of repeatability and predictability, but encompass to an extent, the complex and diverse nature of the metal cutting process. Such a system, one hopes, can provide the operator with information on the tool condition, thus providing an indication as to when the tool should be changed without compromising workpiece surface finish, machine integrity and manufactured component tolerances.

2.5. Conclusions

From the elaborate TCM problem description outlined, it can be concluded that the complexity of the cutting process necessitates the utilisation of an 'intelligent' information observer such as neural networks. A cutting process does not stay the same but will continuously change. Therefore, a system that would use the variety of underlying effects occurring during such a cutting process is required to flexibly learn and/or observe. Through this process of continuous observation, dependence on fixed process parameters and/or a set of rules is eliminated. The use of multivariate process parameters rather than a single sensor parameter has to be properly explored. It is therefore imperative that any identification process (e.g. tool wear) involve both aspects of machining process i.e. monitoring and interpretation of the behaviour of static and dynamic characteristics.

CHAPTER 3

METAL CUTTING PROCESS PARAMETERS -POTENTIAL SENSOR SIGNALS

3.0. Introduction

The decision as to which sensor signal and how many to use in a TCMS is indeed a difficult one to make. One consideration is the cost of successfully tapping any chosen sensor signal. Another is how practical it would be to obtain the chosen signal. If these two questions can be answered, then choosing the sensor signals is made much easier. However, care and consideration must be taken to ensure that the measuring apparatus for the chosen sensor signal does not disturb or interfere with the machining process, and that the employed instrumentation is suitable for use in such an environment, i.e. adequate shielding. In case of interference with the machining processes, for example an exaggerated tool overhang, effects of such an exaggeration on the dynamic signals ought to be known. Most important of all, the chosen sensor signal should have been shown to be sensitive to tool wear and have a high signal to noise ratio.

3.1. Sensor Types

A variety of process parameters in the metal cutting operation have been sensed and subsequently fused to predict the cutting tool state. In these circumstances, a selective gathering of data to improve understanding of the process parameter changes as tool wear level increased has been paramount (Choi et al, 1990, Lee *et al*, 1989). A review of some typical application scenarios and their correlation to tool wear under experimental conditions is provided, to include:

- Acoustic emission,
- Tool temperature,
- Cutting forces (static and dynamic),
- Vibration signature (acceleration signals),
- Miscellaneous methods such as optical measurements, workpiece surface finish quality, workpiece dimensions, stress/strain analysis and spindle motor current, and
- Cutting conditions.

From the merit and demerits of each of the above parameters, utilising factors such as cost, ease of harnessing, robustness, reliability, applicability and repeatability, the decision as to which process parameters and cutting conditions to select for use in the experimental phase of this work will be made.

3.1.1. Acoustic Emission (AE)

During a metal cutting process, as the tool pushes through the workpiece, the workpiece undergoes considerable plastic deformation. Within the deformation zones (dislocation movements), strain energy is released as the bonds between the metal atoms are disturbed. This released energy is commonly referred to as acoustic emission (AE) and is a low intensity elastic signal propagated in all directions throughout the workpiece, machine tool and cutting tool. Sources of AE include phase transformations, friction mechanisms (tool-workpiece contact) and crack formation or extension fracture (accounting for well over 90% of the emitted AE).

Kakade *et al.* (1994) used AE analysis to predict tool wear and chip-form in a milling operation. Selected AE parameters (ring-down count, rise time, event duration, frequency and event rate) were recorded simultaneously and the

corresponding flank wear land length measured at the selected intervals. Analysis of the results concluded that AE signals could distinguish clearly the cutting actions of a sharp and worn or broken tool. As for continuous tool monitoring, no suggestions were made, presumably because the method was deemed unsuitable.

Dornfeld (1992 and 1994) presents compelling reviews of AE applications sensing techniques in manufacturing processes. Amongst the listed manufacturing processes, he alluded that AE could be applied in tool wear detection in machining. However, he was of the opinion that though AE was easy to measure, and correlates significantly well to tool wear, it required extensive signal processing techniques to extract such useful information.

Zheng *et al.* (1992) presented an intrinsic method of AE sensing based on an optic fibre sensor. The sensor consisted of two distinct parts: the sensing element and an interferometer. The sensing element principally was used to produce a shift of phase in the light transmitted through the optical fibre allowing the interferometer to detect and measure the photoelastic modulations in the light intensity. Preliminary tests were conducted (drilling and milling operations) and the AE signal measured using an optic fibre sensor and a commercially available PZT AE sensor. The obtained results were compared, and these showed a reasonable degree of agreement. However detailed experimental trials were not conducted.

König *et al.* (1992) performed studies to detect fracture and/or monitor the condition of small drills using AE features. They circumvented the time consuming and cost-intensive signal processing usually accompanying AE applications by employing simple process-adapted band pass filters, a rectifier and a low pass filter. The underlying principle, they asserted, was because the normally high frequency AE signal when converted to a low frequency signal, can be sampled at a low rate and subsequently digitised or digitally processed. Drilling operations were performed and a special ceramic knock detector sensor (designed for industrial application) used to measure the AE signals. The

recorded AE-RMS was plotted for the number of holes that each drill performed before it failed. Inspection of their plots showed that at the closing phase of tool life (i.e. tertiary phase of tool wear), the RMS value increased dramatically. The rise, one could argue, was a direct response to the fractured tool, hence König *et al.* used this as a prescribed threshold beyond which the RMS for normal operating drills should not reach. This method however was found to be sensitive to tool chipping.

Blum and Inasaki (1990) performed experimental test cuts to determine amongst other things, the influence of flank wear on the generation of AE signals. They proposed to use the AE mode, a parameter describing the 'whole' characteristics of the cutting process as the DC component of the measured signal. Experiments were conducted from which AE and the cutting forces were recorded simultaneously for pre-ground and sharp tool inserts. The result analysis involved studying the effects of the cutting conditions on the chosen AE features and tool flank wear. With knowledge of the former, it was possible for its influence in flank wear interpretation not to be misconstrued. Inspection of the obtained graphs for AE-mode/cutting forces and flank wear for various cutting speeds showed an indispensable correlation of AE-mode to flank wear. A not so good correlation was realised with the cutting forces, as its slopes were significantly smaller compared to the AE-mode ones that were almost linear. This was interpreted as the flank wear length being extremely sensitive to AE-mode. They, however, concluded that extraction of such information from the AE signal was difficult.

Moriwaki and Tobito (1990) proposed a method based on AE measurement and analysis for coated tool life estimation. The underlying principle behind their devised method for coated tool life estimation, was that during progressive tool wear, the tool material changes from one substrate layer to another and emit AE signals that could be monitored to determine tool life. An experimental test rig was set-up and tests were conducted on it. The AE and tool wear (flank and

crater) were measured together with the surface roughness. Typically, AE RMS values for the recorded AE signal and the wear values (initial, middle and tertiary stages of tool wear) were graphed on the same scale for comparison. Inspection of the presented plots indicated a strong correlation of AE RMS amplitude to tool wear, increasing with wear progression. Further analyses to extract statistical features (mean, variance and the coefficient of RMS) were performed and plots made for the complete cutting cycle. The variance clearly was the most sensitive to tool wear, as it had the largest amplitude in the final phase of tool life. The recorded data was applied to a pattern recognition system and it performed reasonably well. Thus, by measuring the AE emitted from specially treated coatings on a cutting tool, it was possible to identify and predict the ensuing tool life. The only drawback to the application of this method, it could be argued, was its limitation to the use of coated tool inserts only and therefore not universally applicable.

Emel and Kannatey-Asibu (1989) used AE supplemented by force signals via a pattern recognition analysis system to perform progressive tool wear monitoring and tool breakage detection. Jiaa and Dornfeld (1992) also used the same sensor combination but applied a gradient adaptive lattice analysis and pattern recognition.

Roget *et al.* (1988) carried out machining tests from which they used the sensed AE signals from the cutting operation to predict the state of the cutting tool. Their conclusion was that such task could only be successfully accomplished under specific and limited conditions. Using custom made AE sensors, machining test cuts (turning and milling) using normal grade and alloyed steels were carried out. Several parameters of the AE were recorded (i.e. RMS, mean and peak values). Further statistical features (variance, kurtosis, 3rd and 4th order moments and skew) were extracted from the recorded parameters. A comparison of the recorded AE and measured flank wear curves were carried out, and showed a remarkable similarity with the characteristic three distinct phases depicted on both

the wear-time and AE-time plots. There was a corresponding initial rise in both curves due to the grinding period of the tool after engagement in cutting. This was followed by a slowing down of the wear rate reciprocated on the AE signal curve by a much gentle slope. As soon as the flank wear began to increase to catastrophic levels, the AE signal reflected the increase and its undulations became more erratic. They extended their method to identifying tool breakages as well but using a milling operation instead of the test bed. Their final conclusions were that AE provided sufficient warning of the ensuing changes in both cutting conditions, tool breakage and tool wear.

Two types of acoustic emission waves can generally be encountered during the metal cutting process: continuous AE waves and the burst-type AE. Continuous AE results from the shear deformation of the workpiece. The sliding interaction between the cutting tool and the workpiece, tool and chips are the main regions of concentration of this AE type. On the other-hand, burst-type AE is an indictor of discrete events with its main source being tool and chip breakage. During metal cutting substantially little AE is thought to be generated compared to the larger amount accompanying tool breakage and fracture (Tansel and McLaughlin, 1991; Lee *et al.*, 1989). Therefore, AE is much dependent on the cutting material (work-piece) structure than on the cutting tool. Its signal reflects the behaviour of the response from the machine tool set-up rather than the cutting tool (Tansel and McLaughlin, 1991). As the emphasis on any TCMS would generally be on tool wear rather than tool fracture, AE is not a suitable tool wear indicator in monitoring applications, but could be used to good effect in detecting tool tip breakage on machining centres.

On another note, Lister (1993) pointed out that one of the most profound limiting factor in the application of AE to a TCMS does not lie on the sensing technology, but on the ensuing analysis. This void was due to a l ck of a suitable database of knowledge on AE, entailing that the user has to experiment and establish the necessary trigger responses to a variety of machining conditions thereby placing

considerable burden upon them. When compared to instances for example- where the concept of lowering and increasing the force limits might be understood, spectral analysis is not so easily comprehended. Hence instead of the system being an aid to the operator, it rather presents a real-time quandary.

Because AE might be sufficiently available on the entire machining area, choosing a suitable area to place the AE sensor as to trap sufficient AE signals becomes debatable as an understanding of the AE path has to be established. A drawback to the application of AE as an indicator of tool wear is the fact that its signals are more sensitive to variations in the cutting conditions and noise than of the tool condition itself, hence using AE on its own to monitor the state of a cutting tool is a difficult task (Yan *et al.*, 1995; Rangwala, 1988). AE is therefore only suitable as an additional sensing method for increased reliability. In this respect, AE is deemed to be an unsuitable tool wear indicator for the envisaged TCMS.

3.1.2. The Tool Tip/Cutting Edges Temperature

Metal cutting generates a significant amount of heat. The resultant high temperatures are generated in the region of the cutting tool edges and has a direct controlling influence on the rate and mode of cutting tool wear, and the friction between chip and cutting tool, tool and new surface. Because of these effects, Boothroyd (1975) suggested that this has been the main reason for the considerable attention paid to determining the characteristics and fluctuations of this temperature.

Frictional behaviour on the tool faces is thought to affect the geometry of the cutting process by some mechanism not completely understood (Boothroyd, 1975; Trent, 1977). Two metallic surfaces in sliding contact would normally experience dry friction commonly referred to as Coulomb friction. In metal cutting, the coefficient of friction is substantially independent of the sliding speeds and area of contact and force is therefore required for the continual shearing of the tips of the

aspirates or hills. This required force or load is proportional to the frictional force (in dry sliding), and the coefficient of friction between tool and chip vary considerably due to changes in cutting speed and rake angle, giving rise to high pressures. In the meantime, the real area of contact would approach unity thereby giving rise to high frictional forces that eventually lead to high temperatures and renders sliding at the interfaces almost impossible (Trent, 1977). Removal of the generated heat is either by the chip, workpiece and/or tool. As the temperature distribution is not uniform, knowing the exact amount of heat transferred via the tool is not straightforward. It is thought that the amount of heat removed or conducted via the tool chip is as high as 90% of the overall heat generated, implying that less than 10% of the heat is either absorbed or dispersed of through the tool and workpiece material.

Initial attempts at measuring the cutting edge temperature have proven difficult due to lack of direct access to the cutting zone. Boothroyd (1975) had earlier proposed the use of thermocouple techniques in the workpiece-tool interface. Through such techniques the generated EMF at the junction is considered to be a measure of the mean temperature in that region, but it does not give any indication of temperature distribution. Most currently available remote thermocouple sensor instruments can only allow either the cutting tool-workpiece interface or some other remote area temperature to that effect to be measured and not the tool tip temperature. This process parameter, though a suitable tool wear indicator, is useless in TCMS due to its inaccessibility to the cutting area. However, approximation methods have been pursued, sometimes with experimental verifications.

Sarwar *et al.* (1996) recently developed a thermal image system for metal cutting applications. This system essentially consisted of a mathematical model of the energy partition during metal cutting. Thermal imaging data obtained showed that it was practicable and modifiable to fulfil the requirement of orthogonal cutting. Further work was reportedly underway to extend the model to accommodate the

transient nature of the temperature field during dynamic cutting conditions.

Lin (1995) in his attempt to measure the cutting tool temperature on-line during a milling process devised an inverse approach for real time tool/workpiece interface temperature. Infrared pyrometry was employed to measure the actual temperature on the machined surface and a least square inverse method applied through an ellipsoidal mapping model of the heat conduction equation. Using a 1-D co-ordinate transformation of a moving heat source system, the measured temperature and heat dissipation to the workpiece was calculated inversely by FEA to predict the tool-workpiece interface temperature (considered the heat source). The designed model was tested by applying known heat flux input and verifying the inverse output. Plots of the actual temperature of heat source and that estimated by the proposed method showed very minute deviations. He proceeded to test the model further using flame heating to primarily verify the uncertainties in temperature measurement of a moving heat body. The final stage of Lin's work involved on-line temperature measurements of a milling process using his now tried and tested inverse estimation method. A good agreement between the inverse solutions of a quasi-steady interface temperature from measurements of two distinct measuring points were reported. He concluded that such agreement implied that his model produced accurate real-time temperature estimates and was therefore acceptable for tool-workpiece interface temperature estimation. Main drawbacks included the fact that measurements using this model were influenced by the thermal properties of the workpiece (and tooling material) and the employed pyrometer had a limited measurement range of only 0-500°C. Detailed knowledge of the thermal properties of the workpiece material (density, thermal diffusion and thermal conduction) was crucial to realising this method.

Radulescu and Kapoor (1994) designed and tested an analytical tool temperature field's prediction model during continuous and interrupted cutting. Their modelled tool-chip interface temperature was reported to agree well with

experimental tests.

Raman *et al.* (1992) proposed and developed a mathematical model for cutting tool temperature measurement based on the remote thermocouple sensing (RTS) principle. Differential quadrature modelling of the forward thermal behaviour of the insulated cutting tool was pursued. The credibility of the method lied in the fact that the tool chip interface temperature distribution had a unique characteristic relationship between the tool/chip temperature and the remote thermocouple temperature. Cutting process temperature change was then determined by observing the behaviour of the rest of tool temperature (sink response) to variations in the source of temperature (tool tip). Once the behaviour between sink and source temperatures had been established, it was possible to estimate 'on-line', the tool interface temperature based on the remote thermocouple response. The existence of large temperature gradients closer to the tool's cutting edge led to an initial modelling to achieve an accurate theoretical base for experimentation i.e. exact locations of the thermocouples. This was carried out by performing mathematical formulations of the physical behaviour of the tool system to obtain differential equations expressing the tool temperature distribution (which they referred to as the differential quadrature method). They concluded that the mathematical analysis performed was quite suitable for remote thermocouple sensing but more analysis was required to better their technique as it was still in its earlier phase of development.

Stephenson and Ali (1990) performed studies of tool temperature effects on interrupted metal cutting and reported theoretical and experimental results. The theoretical base of the work was principally to develop a tool temperature distribution model based on a series of infinite rectangular corners, heated by a time-varying heat flux with various spatial distributions. The experimental analysis involved using both infrared and tool-chip contact thermocouple temperature measurements. The measured temperatures for a series of machining conditions were found to be dependent upon two main factors:

- Length of cutting cycles, and
- Length of cooling interval between cycles.

Overall, the temperature measurements were found to be lower when the cutting was occasionally interrupted than for continuous cutting, under the same cutting conditions. They pointed out that it was difficult to instrument a thermocouple for tool-chip or tool-workpiece interface temperature sensing when the workpiece was not hollow. The best option was the use of a non-contact measurement technique such as infrared thermal imaging. Taking measurements required a detailed understanding of black body radiation. This technique was only capable of temperature measurements that might be considered at best averages rather than the true temperatures, and therefore tended to be dominated by chip images.

Strenkowski and Moon (1990) devised both a finite element analysis (FEA) method of chip geometry prediction and tool-workpiece interface temperature measurement and prediction. Their method essentially was based on a temperature modelling principle. The modelling of cutting temperature was presented as a single unidirectional tool involving a series of complicated mathematical relationships comprising elements of viscoplasticity, strain-stress rate distribution, and finally the interactive thermal solution. Experimental data to confirm model validity was collected from cutting tests, and they reported a good correlation of results, thus confirming the validity of their method.

Lin *et al.* (1987) carried out numerical FEA to predict the temperature distributions in both the workpiece, tool insert and chip during machining. Like Lin (1993), the thermal properties of the workpiece and tooling material details had to be taken into account. As a variant of the procedure outlined by Stephenson and Ali (1990), they identified the heat source as the cutting edges of the tool and proceeded to predict the heat flux in the primary and secondary plastic zones. They then concentrated on identifying the effects that different flank wear types had on the heat dissipation at various cutting speeds.

Experimental verification of the established FEA formulation was carried out. They concluded from the nature of the results obtained that the temperature of the cutting tool increased significantly when the cutting tool flank wear land length increased.

Chow and Wright (1988) were concerned with devising a suitable on-line method for tool-chip interface temperature measurement in a turning process. Principally, a standard thermocouple was inserted at the bottom of the tool insert. Measurements of the interface temperature were made and correlated to tool wear. Results from the experimental verifications were also compared to previously established metallographic techniques. Firstly, a suitable FEA method was devised which they envisaged correlated the thermocouple temperature to the cutting edge temperature. This necessitated a series of numerical analyses and ratio curve fitting. Experiments were then conducted from which practical cutting data were collected for comparison with the predicted interface temperatures obtained from the theoretically devised model. The test cuts involved dry machining performed on plain steel tube (AISI 1020) with controlled contact tool inserts (coated and un-coated). A comparison of the measured and predicted temperatures showed a reasonable agreement to within 5.4-13.1%. Analysis of both results obtained showed that an increase in the tool wear (or increased contact in the FEA approach) resulted in an increase in the cutting temperature in an undisclosed manner. Further analyses were carried-out to find exactly which component of the temperature: original heat source or tool wear source, changed during machining. They reported that the temperature increases were primarily due to tool wear which could be used to effect TCM during metal cutting.

Kitagawa *et al.* (1988) presented by far what could be regarded as the most interesting experimental approach and method of cutting tool edge temperature measurement. A special purpose thermocouple was constructed from first principles using two carbide tip parts and a quartz glass for insulation. By changing the exit position of the circuitry wire involved, they claim that it was

possible to measure the interface temperature anywhere on the flank face of the tool (i.e. the cutting edges). To validate this design, a series of test cuts were conducted using nominally sharp and artificially worn tool inserts. From the ensuing analysis and discussions, they were able to establish the dependency of temperature change rate on flank wear length for both interrupted and continuous cuttings. From the viewpoint of tool life estimation, they were of the opinion that their observations of wear characteristics were in agreement with the wear rate equation:

$$\frac{dW}{\sigma_t dL} Ce^{-\frac{\lambda}{\theta_t}} \qquad [3.1]$$

where C and λ are tooling and workpiece material constants; W and L are wear volume per unit length of the tool insert face and wear distance respectively; θ_t and σ_t are the absolute temperature and normal stress distribution respectively. However it is worthwhile mentioning that beyond designing the thermocouple, their aim was not to perform TCM but to establish the mechanisms principally responsible for flank wear rate.

Shaw (1988) cited the complexity involved in any attempt to predict the mean tool face temperature because it defied exact solutions. He proposed and evaluated an approximate solution based on the principle of moving heat source.

Yen and Wright (1986) devised a complex method using RTS for cutting tool/workpiece interface temperature measurements. The same method of ellipsoidal modelling as Lin (1993) was followed, but the boundary conditions in the ensuing mathematical FEA and numerical analyses were obtained through application of complex analyses. Computer simulation results for various model errors were carried out and the results showed a dependency upon the insert thickness. Best results of predicted tool-workpiece interface temperatures were obtained (simulations based only) when the insert thickness was of the order of the contact length, otherwise, correlation was poor. This method offered no

practical or realisable advantage over established RTS based methods and could be a real time quandary in application.

For practical applications such as in an on-line TCMS, FEA methods are not suitable. Remote thermocouple sensing would appear to be the only plausible method worth investigating, but this can only measure the workpiece-tool temperature with no indication of the tool-tip temperature distribution or rake face obtainable. Temperature is not considered to be an appropriate input for the TCMS at this stage as it is difficult to implement.

3.1.3. Cutting Forces

During cutting, the interface between tool and work material is largely inaccessible to observation, but indirect evidence concerning the forces and vibration between tool and work material has been contributed by many researchers. It has been widely established that variations in cutting force signals can be correlated to tool wear (Ko and Cho, 1994; Purushothaman and Srinivasa, 1994; Tarng *et al.*, 1994; Lister, 1993; Dornfeld, 1990; Lee *et al.*, 1989). In practice, application and interpretation of this parameter has been diverse with more effort concentrated on studying the dynamic characteristics of the cutting force signal and interpreting its relation to tool wear level. This can largely be attributed to the fact that this force becomes important in worn tool conditions as a result of the variations produced due to cutting tool flank friction and the workpiece (Ko and Cho, 1994; Dornfeld, 1990).

Existing force-based TCMS typically operate independently of absolute force levels, measuring the relative change of force that occurs as a new tool wears (Elanayar *et al.*, 1990; Gould, 1988). Experiments have shown that the three components of the cutting force respond differently to the various wear forms occurring on the tool, for example the feed force is insensitive to crater wear whereas the feed and thrust forces maybe much more influenced by tool wear than the main cutting force (Lister, 1993; Gould, 1988).

Lister (1993) analysed the power spectra of dynamic cutting forces and reported an increase in power level frequency bands as the tool wore. The results bore a strong indication of the dependency of dynamic force on cutting tool wear though not a general trend. As with many non-linear systems, modelling of the process is very often used in order to capture and gain an understanding of process behaviour.

Ravindra *et al.* (1993) developed a mathematical model for tool wear estimation based on cutting forces in a turning operation. Essentially, this involved carrying out experiments from which the wear progression was studied and these modelled by a multiple regression analysis method. Their experiments indicated that the wear trend propagated with increases in cutting speed, and the occurrence of inflections on the wear display curves indicated a predominately thermally controlled mechanism. An increase in the three force components' magnitude was evident as the wear on the used inserts increased. The wear-time and wear-force plots seemed to support their propositions, from which they concluded that their experiments had provided vital proof of evidence for a good correlation between flank wear, feed and radial forces.

Lee *et al.* (1992) in their quest for an on-line TCMS developed a PC based FFT software to track the dynamic cutting force signal. Intermittent test cuts were performed on a Colchester mascot lathe at 100 mm intervals using two work-pieces and a single tool insert type (P30). The cutting forces and wear levels were measured and recorded. Subsequent analyses of the obtained data showed that the feed and tangential dynamic force components bore a good relationship to flank wear trend.

Marques and Mesquita (1991) investigated the relationship between wear of sintered high speed steel cutting tools and the associated cutting forces. A wear-force model equation was established and experimentally verified. The theoretical models used considered the independent influence of the flank and

crater wear, and also that of the indentation force (the blunt tool effect). Experimental tests were conducted from which the forces were measured. The test types conducted consisted of short duration cuts to establish force-wear relationship and longer duration cuts to observe the progressive influence of wear on the forces. They reported a good correlation between experimental and theoretical results.

The modelling of dynamic cutting forces was performed by Kim and Lee (1991). Practical situation test data were collected from experiments and compared with the theoretical model predictions. Good agreement between the theoretical limits of stability and experimental data was reported. However, in the low cutting speed range, some deterioration was observed, a fact which they attributed to built-up edge effect. Similar modelling of the dynamic cutting force for chatter prediction have been performed by Grabec (1988) and Khraisheh *et al.* (1995).

Oraby and Hayhurst (1991) developed a model for tool wear analysis in a turning operation for force characteristics within the different phases of tool wear. Quantification of the developed model was performed by measurement of the variation of radial/vertical force component ratios, accomplished through force/wear-inter-relationship formulated on simple 2-D plots. The experimental data for these models were obtained from machining test cuts of an alloy steel using a Colchester mascot lathe and triple-coated carbide tool inserts. These tests were carried out following a central composite design (CCD) strategy composing of 24 tests at variable cutting speeds, feed-rate and depth of cut. For each test, the wear values (nose, flank and notch) were measured and recorded. Time displays of the forces and wear types were deduced. The wear displays confirmed theoretical predictions: a slow rise, then almost constant and a fast climb to failure. The force displays indicated a similar trend to the wear plots but exhibited a higher rate of change in the tertiary phase of the wear. The force displays were also reported to provide evidence on the nature of the relationship between force and wear, but was affected by cutting conditions. The radial force

component (F_z) was reported to be the most sensitive force to nose wear, with feed (F_x) and radial (F_z) components affected by flank wear. To establish a universal rather than a case-based example of individual characteristics, they proposed a mathematical method to quantitatively formulate the wear force and their inter-relation to the relevant parameters to achieve repeatability and reliability for practical applications. The equation formulated by Taylor:

$$T = a_0 V^{\alpha} f^{\beta} d^{\gamma} \qquad [3.2]$$

was used and a statistical method adopted in order to obtain the constants a_o, α, β and γ. Following the statistical and mathematical analysis, they concluded that their analysis showed that there existed a strong correlation between force variation and wear progression. However their model was only applicable when the tool insert was either in the primary or secondary phase of wear.

Yao *et al.* (1990) and, Yao and Fang (1992) investigated what they described as a comprehensive TCMS which included the measurement of major and minor flank, crater, and nose wear based on the analysis of dynamic cutting forces. Tool wear experiments were carried out on a Colchester lathe at varying cutting conditions using only one tool insert and work-piece type, and the three orthogonal pre-processed force components recorded. Eight parameters describing the desired wear features were selected. A dispersion analysis based on auto-regressive moving averages (ARMA) was performed. Two distinctive frequency bands were accomplished in all three axes associated with a wear rate mechanism of some sort: a low frequency band 0.5-1 Hz and a higher band 2.6-3.5 KHz. These trends were in agreement with the recorded wear values, thus, indispensable as a wear monitoring system.

Shi and Ramalingam (1990) performed machining tests to investigate the feasibility of using different force components for on-line TCM. Through their investigation, they were able to correlate the feed and cutting force components to flank wear length though it also transpired that these parameters were sensitive to

changes in the cutting conditions. Experimental observations of the feed force to cutting force ratio showed sensitivity to flank wear, but was insensitive to process changes (speed and depth of cut). By combining *a prior* fast tool fracture detection scheme with their developed flank wear sensing method, it was possible to develop a new TCM strategy.

Lee *et al.* (1989) cited that significant variation existed in the findings of various researchers who attempted to correlate static cutting forces to tool wear. Other limitations of the static force approach (such as disturbances caused by variation in workpiece material, depth of cut and tool edge geometry) were put forward as further evidence that appoaches based upon static forces had not made any significant gains. They proceeded to examine the nature and principal source of the dynamic force frequency and its correlation to flank wear. Experiments were carried out from which both the static and dynamic forces and the flank wear length were measured. A time display of the forces and flank wear showed the three features to vary differently: the static forces showed an initial rise as wear increased then a consistent fluctuation whereas the dynamic cutting forces exhibited a monotonic increase followed by a relatively sharp fall towards the end of tool life. Flank wear increased gradually in the earlier phase of cutting and before the tool failed, its value monotonically increased. The drop in dynamic force magnitude in the latter state of tool wear was attributed to the cutting edges and subsequent deformation. A kind of damping effect results, because the edges are collapsing under plastic deformation thereby causing greater damping of the tool oscillation, resulting in a decrease in the amplitude of the dynamic force. The rapid increase in crater wear and a corresponding rise in the working rate angle account for the drop in dynamic force.

An inter-relationship between the tangential, feed and normal components of the dynamic cutting forces has been established in Dan and Mathew (1990). In their review, the dynamic forces are reported to fluctuate with excursions to zero and then to higher magnitudes during cutting. A consequence of these excursions has

been the onset of tool holder vibration whereby, chattering at high magnitudes often results. As the cutting forces and vibration signatures are coupled, the decision on cutting forces would be deferred until the vibration signals have been discussed and a final decision made based on both the static and dynamic signals of the system because they together furnish information on vibration.

3.1.4. Vibration Signature (Acceleration Signals)

Vibrations are produced due to the cyclic variations in the dynamic components of the cutting forces. Usually, these vibrational motions start as small chatter, responsible for the serrations on the finished surface and chip thickness irregularities and progress to what has come to be commonly termed vibration. Mechanical vibrations generally result from periodic wave motions. In a metal cutting operation the generated vibrations are a blend of a free, forced, periodic and random types. Direct measurement of vibration is difficult to achieve because its determining characteristic feature, the vibration mode is frequency dependent. Hence, related parameters such as the rate at which dynamic forces change in unit time (acceleration) are measured and the characteristics of the vibration derived from obtained patterns.

Yao *et al.* (1991) investigated and reported detection and estimation of groove wear at the minor cutting edge of the tool by monitoring vibration signatures. A high precision lathe on to which was attached a miniature 3-D accelerometer was used to perform their test cuts. A single tool and material combination were used with variable (5) cutting conditions and tool geometry. Each cut was interrupted to take measurements of the wear mark values. A multivariate time series analysis was then carried out on the recorded vibration signals. Using a combination of autoregressive moving averages (ARMA) and some explicit functions, the vibration signals were analysed to obtain a dispersion of the signals' auto-covariance, decomposed into the various eigenvalues and normalised to within range -1 and 1. The dispersion analysis showed that he cutting and thrust

vibration components were sensitive to the length of groove wear with two peaks: one at a very low frequency <200 Hz and the other at a high frequency ≥ 10 KHz.

Dan and Mathew (1990) in their review paper mentioned data dependent system (DDS) discrete modelling methods which have been used to correlate vibrations to cutting tool wear. With this method, isolation of the vibration signals most sensitive to tool wear was possible. They obtained results that showed some variation in the amount of vibration energy within a specific frequency band. This phenomenon was observed consistently regardless of cutting parameter. The application of spectral analysis to the acceleration signals (of vibration) revealed a linear function of the cutting speed and cutting tool wear, hence, vibration signals could be regarded as showing sensitivity to tool wear.

Rotberg *et al.* (1987 and 1989) were interested in mechanical signature analysis (vibration) for tool state prediction during interrupted cutting. In Rotberg *et al.* (1987) the emphasis was on the milling tool entry and exit conditions. Face milling experiments were conducted and the ensuing flank and crater wear measured. Detailed signal processing of the recorded signals were carried out. Wear curves, average envelop at three points of tool life (sharp, half worn, worn) and spectral descriptions of the three wear phases were obtained. Inspection of the plots indicated that the vibration signal was a suitable indicator of tool wear, as it demonstrated considerable change during tool life. Rotberg *et al.* (1989) focused on tool wear monitoring using vibration as the principal signal. The analysis was performed using two basic models characterised by their signal features: low frequency and high frequency. Experiments were conducted to validate these models utilising recorded acceleration signal features. They concluded that their analysis showed certain peculiar and universally occurring features from the vibration signals that could be harness in developing a TCMS as it correlated well with tool wear.

Jiang *et al.* (1987) used purposely built test-rig to investigate the effects of vibration in the cutting and feed directions (z and x respectively) on a cutting tool. Using fixed cutting conditions, tests were conducted utilising plane-faced P10 tool inserts, with each cut lasting 10 minutes in a single pass. During the time of engagement, the wear on the tool gradually increased until it catastrophically failed. The recorded signal was post-processed and power spectra display (PSD) of the vibration signals produced. Three distinctive regions could be identified on the PSD which were divided into frequency ranges: up to 100 HZ, 117-510 Hz and 510-1 KHz. From these characteristics, Jiang *et al.* proposed and performed an in-process method of tool wear monitoring based on the frequency band energy analysis method. They concluded that their experimental investigations provided evidence that vibration signals were sensitive to tool wear states.

The inter-relationship between vibration signals and the cutting forces determines the dynamic nature of the cutting process. This postulation makes the utilisation of these process parameters attractive in the development of a TCMS. The static behaviour is governed solely by the cutting forces and momentum (or torsion of the tool holder). The dynamic behaviour on the other hand embodies vibration and certain aspects of the dynamic cutting force. Several independent studies have shown these parameters to be sensitive to tool wear. The combination of elements of the cutting forces and the vibration signal in developing a TCMS would proof indispensable, and these process parameters have been selected for further experimental investigations.

3.1.5. Miscellaneous Sensors and Methods

Generally speaking, other varieties of sensors have been employed in various attempts of tool wear prediction, monitoring or measurement in a metal cutting process. These methods fall principally into the follow categories:

- Optical methods,

- Stress/strain measurement,
- Methods based on measuring the work-piece dimension,
- Spindle motor current/torque/power, and
- Surface finish quality measurement.

3.1.5.1. Optical Methods

Martin *et al.* (1986) summarised in their review that amongst the optical methods to have been proposed for tool wear measurements were the following:

- Laser measurement of the surface finish,
- Photo diodes used in reflected light measurement from the cutting edge, and
- Fibre optic photocell for reflectance measurement of worn and unworn areas of the tool flank.

Clearly, none of these methods can be applicable in a TCMS scenario as in-process tool wear is more difficult to achieve. Other attempts based on optical techniques for tool wear sensing are listed in Lister (1993), and Lister and Barrow (1986).

Determining tool wear from processed images of the cutting tool has been pursued for over three decades now. Essentially, an image of the tool was captured and displayed on a TV screen, and then analysed to provide information in terms of wear pattern or quantity of wear accrued. A recent implementation of this method has been carried out by Du *et al.* (1993) and Oguamanam *et al.* (1994). In Oguamanam (1994) the vision machine system is used for monitoring purposes. For any given image, five features of the image were extracted and used in classifying the state of the tool (good, worn or broken). Extensive

computer image processing algorithms were developed to capture the image (off-line), segment it and then identify the tool state from the digitised image. Du *et al.* (1993) on the other hand, attempted to devise an on-line optical method utilising an 'off-the-shelf' optical tool condition sensor. This sensor was reputed to capture the image of the tool edges and these converted into pixels for computer processing. The captured tool profile could then be filtered and represented by an array of numbers for comparison to that of the master tool profile (i.e. captured when new and sharp). Experimental verifications showed that repeatability was a major threat to the success of the method, and at best, only average values of the measurements were obtainable. These techniques are expensive, inflexible and cannot truly be applied on-line. It has also been cited by Shiraishi (1988) to be riddled with high inaccuracies, and progress was not expected in the future.

3.1.5.2. Stress/Strain Measurements

Noori-Khajavi and Komanduri (1995b) used amongst other sensors, strain sensors in their study of the correlation of process parameters to drill wear. The recorded signals were analysed in both time and frequency domains, but meaningful correlation of the drill wear could only be achieved in the frequency domain. The area under the x-axis PSD for the strain sensor was found to correlate well to drill wear and they proceeded to base their study on this assumption.

Zhou *et al.* (1995b) proposed to monitor the stresses acting in a cutting edge during a machining process in order to predict tool spontaneous failure. However, because of the impracticalities of in-process measurement of the cutting tool stress, an on-line stress estimation based on in-process cutting forces, load functions and the cutting conditions were used instead. They designed and implemented a real-time TCMS based on VME computer system and real time kernel. This incorporated a fast data acquisition unit that analysed the stresses from force measurements. By monitoring the risk factor defined as a ratio of the

instantaneous stresses, they reported that it was possible to predict spontaneous failures.

Another method based on stress analysis of three-dimensional loading has been proposed by Lee *et al.* (1994). They combined FEA and detailed stress analysis of the cutting edges and tips of sharp and worn tools. They concluded that it was possible to predict the mode and location of tool failure.

3.1.5.3. Workpiece Dimension

El-Gomayel and Bregger (1986) proposed a method for tool wear monitoring based on measurements of workpiece deviation. They employed two electromagnetic probes on opposite sides of the workpiece such that electromagnetic waves could flow from the probe to the metal allowing accurate measurements of the workpiece diameter. Increases in the workpiece diameter were used as a tool wear criterion, but elaborate calibration procedures had to be undertaken before. An experimental verification of the method suggested a relationship between the accumulated flank wear length (manually measured) and accumulative voltage differences from the two differential probes. The results however were affected by several factors such as vibrations, deflections and misalignment. They concluded that though their model could measure minute tool wear, it could not quantify it (i.e. distinguish nose wear from flank wear).

Other sensors that have been used in the various attempts of tool wear monitoring and quantitative measurements of cutting tool wear include the measurement of spindle motor current in milling by Zhang *et al.* (1994), Dornfeld (1990) and, Constantinides and Bennett (1987) while magnetism has been employed by Jetley and Gollajesse (1994). The works of Dornfeld (1990) have already been extensively covered.

3.1.5.4. Electric Motor Current/Power Measurement

Zhang *et al.* (1994) used a hall effect sensor to measure the current supplied to the spindle motor drive of a vertical NC miller together with the cutting forces. They proceeded to develop a relation between the measured motor current and milling torque by relating the forces by modelling to the acquired motor current/torque relation. Computer algorithms were developed to track the waveforms, rate of peak change and the relative eccentricities of the modelled relation. They concluded that cutter breakages were reliably diagnosed with motor current measurements than force/torque measurements.

Constantinides and Bennett (1987) obtained the spindle motor power from a vertical milling machine and attempted to analyse features off it such as power spectral density, the moving average, running mean and the accumulative sum power to estimate tool wear. They concluded that spectral energy fluctuations of the spindle motor power was linearly related to the tool wear rate but was also affected by the cutting conditions and tool geometry.

It is worthwhile remembering that shaft power, cutting forces, torque and motor current are all related to each other, originating and depending entirely on one another. It suffices therefore to measure just one of these parameters as demonstrated by Rangwala and Dornfeld (1987, 1990) who dropped the electric current in preference to the cutting forces.

3.1.5.5. Magnetism

Jetley and Gollajesse (1994) proposed the magnetisation of tool inserts and then, monitor the magnetic field flux reduction as the tool wears. A preliminary investigative study involving the use of magnetised drills was devised and implemented in order to validate their methodology. They concluded that it was possible to accurately predict the end of tool life or fracture 'on-line' by observing

the magnetic flux, and the system was cost effective with potential for implementation in most metal cutting environments.

3.1.6. Cutting Conditions

Low wear levels would normally be considered acceptable so long as their effect on the work-piece dimensional integrity is not severe, but some kind of compensation must be made to provide for dimensional stability of the cutting system (Tanner and Lou, 1994). If a fresh cutting tool insert is engaged into cutting and its wear land measured until it fails and a plot of the wear levels against time made, three distinct regions can be identified on the plot (Fig. 3.1). As the tool begins to cut, it would normally wear very rapidly (high gradient) until a stable situation was reached. Then the wear level stabilises with little or no wear increments at all. Tool wear initially progresses in a linear manner but the rate of wear decreases soon after the tool had been engaged. The last region (i.e. just before the tool fractures) its wear level would rise dramatically. Catastrophic tool failure (fracture) is a very undesirable occurrence and the threat of such tool failure occurring forces the machine tool operator to use conservative feed rates and depths of cut, with the tool normally removed before its full life had elapsed.

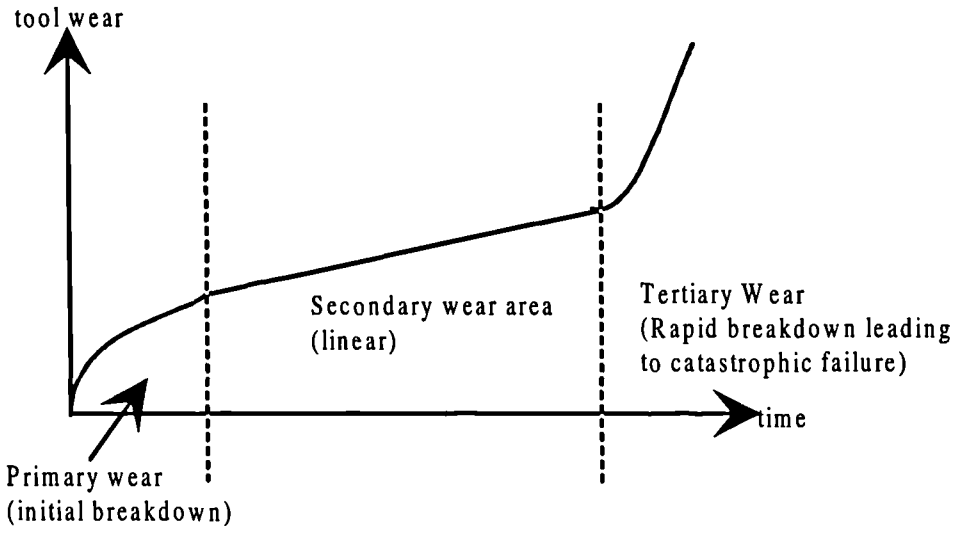

Figure 3.1: Generalised tool flank and nose wear progression

The effective tool life can very much depend on the nature of cutting conditions, but other factors are thought to be responsible as well. Amongst these are (Trent, 1977):

- Cratering of rake face
- Crumbling of the cutting edges
- Plastic Deformation
- Chipping and cracking
- Flank or clearance wear.

Cratering and crumbling emanate from utilisation of high and low cutting speeds respectively. High interface temperatures at high speeds account for tool deformation whereas chipping and cracking arise due to either steep thermal gradients or mechanical shock. The effect of the first five modes of tool failure could be drastically reduced by variation of the cutting conditions, but no matter how these parameters are set, flank wear, a progressive form of deterioration will always occur. Since flank wear is an unavoidable occurrence, the cutting conditions could be chosen so as to have the least effect on the wear rates on the cutting tool.

3.2. Final Decision on Static and Dynamic Signals

Finished workpiece accuracy is determined by deviations at the cutting point from the required working movements between the tool and workpiece. These deviations are caused primarily by static and dynamic force deformations (in addition to geometric and kinematics errors of machine frames, beds, spindles and slides). Present day instrumentation have made it possible for the behaviour of these process parameters to be monitored. In as much as force types are concerned, they can only be viewed as an approximation because there is a lack of

knowledge as to the damping and stiffness conditions of workpiece-tool area, joints and couplings (Weck, 1984).

Sensors selection for the envisaged TCMS had to take into consideration ***robustness***, ***reliability*** and ***applicability*** of the selected sensor signals. The cutting forces and vibration signature all satisfied reasonably well the following four criteria:

- They are easy to measure (dynamometer and accelerometer),
- They have a high signal to noise ratio, though could be improved through application of RC filters,
- They are robust and consistent in wear sensitivity, and
- Less peripheral instruments are required for their harnessing compared to AE and temperature for instance.

It is herein proposed that the following static and dynamic indicators of the cutting process will be experimentally investigated as possible inputs to the envisaged TCMS:

3.2.1. Static Forces

The degree of variability apparent in the cutting forces in metal cutting processes require that some estimation of the static cutting forces be known because accurate prediction is impossible. Estimates of the cutting forces are necessary to enable the surface cutting speed on the workpiece material kept within available power of the machine tool. Consequences of overloading the machine tool could lead to instances of excessive power take-off causing machining stalling or unacceptable deflections of workpiece and machine tool. Measurement of the deviation or fluctuations of the three static force components would provide information on the static behaviour of the cutting process.

3.2.2. Dynamic Forces

The nature of the cutting process is such that it can not be regarded as 'without deflections and instability'. The joints, couplings of the machine tool and minute changes in the cutting conditions lead to fluctuations in the value of the measured static forces. The cyclic variations of the static forces if not limited, leads to dimensional inaccuracy of the cutting operation as chatter results. It is difficult to predict the conditions under which it occurs or select cutting conditions necessary to correct this phenomenon. Therefore, to get an indication of the system fluctuations, the dynamic forces need to be known and can be calculated as the frequency dependent component of the measured static forces.

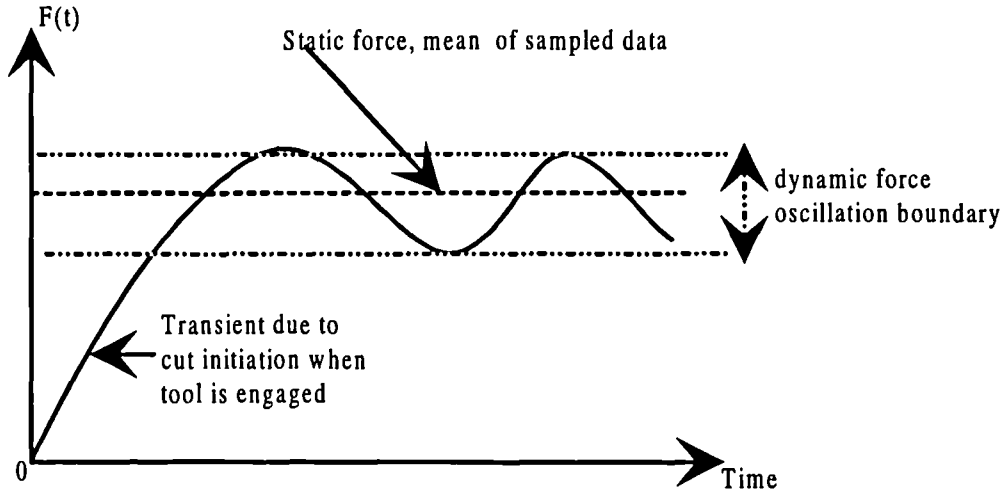

Figure 3.2: Force amplitude Vs. Time (fixed cutting conditions)

3.2.3. Vibration Signature

Cutting forces level are indicative only of cutting situations were the workpiece and tool contact point remains constant when the tool is engaged in cutting. The development of chatter and their subsequent progression to vibrations lead to a change in the work surface relative to the instantaneous cutting direction. It varies, often sinusoidally and alter the relationship between cutting forces and workpiece slope. These alterations are manifested as serrations or ripples on the

workpiece surface. Excessive vibrations can cause damage to the machine tool interfering with the required nominal motions (feed rate, cutting speed and depth of cut). Monitoring the relative rate at which the system is disturbed in all three planes would furnish the TCMS with adequate information as to the direction in which there exists a tendency to move, and hence, give an indication of that quantity and the acceleration signals in the three planes of cutting could be measured.

3.2.4. Incorporation of the Cutting Conditions

Different machining operations require varying cutting speed, while cutting may be continuous (several hours) or abrupt (few seconds). Poor cutting conditions give rise to increased forces, energies, tool temperature thus resulting in higher tool wear rate (Boothroyd, 1975). Cutting at high speeds and feed-rates causes an increase in temperature on the tool face resulting in increased crater wear. At low speeds, built up edges (BUE) are formed. The effects of the cutting conditions on the static and dynamic forces, and vibration signatures have a wide margin of variability. It is difficult to predict exactly what the magnitude of the cutting forces would be at specific cutting speeds, therefore, it is plausible to utilise the cutting conditions as significant variations in the sensor signals arise from changes in these parameters.

3.3. Sensor Fusion - Synergy of Signal Integration

Sensors for engineering process monitoring are generally designed to measure a desired parameter (e.g. accelerometers) and then correlated to the process of interest (e.g. vibration signatures). During measurement, the measurand is such that the determining principal signal component has distortion of some kind (noise). If the noise to signal ratio is high then the measurand yields no meaningful correlation to the desired quantity but if it is low the converse is true. A promising approach in engineering applications has been the utilisation of more than one sensor signal from different sources to detect the same parameter, and is

commonly termed ***sensor fusion***. Sensor fusion combines the noise dominant probably mediocre facets (similar or contradictory) of the individual signals to yield a better outcome (Holmbom *et al.*, 1989).

The implementation of sensory data fusion in theory, can be performed via traditional statistical methods such as Bayes rule, cluster, principal component, discriminant, linear and regression analyses. For practical application purposes, large errors unavoidably occur. Practical systems requiring multivariables therefore require alternative methods of data fusion to be applied (Bishop, 1994).

The choice of a suitable sensor type as well as the point of application (sensor location) are inextricably linked, with a suitable location being where the specified signal has the highest concentration and best reproducibility. However, certain limitations do exist due to the structure of the machine (i.e. bearings, lubrication and linkages). Information from a variety of different sensors therefore has to be collected and these signals of varying reliability integrated. Sensor fusion serves the following purposes:

- Enhances the richness of the underlying information (wear level) contained in each signal,
- Increases the reliability of the monitoring process as loss of sensitivity in one signal could be offset by that from another,
- Sensitivity of wear potentially increases x-times for y-number of sensors fused (Lister, 1993), and
- Previous efforts to find a unique signal forall tool wear monitoring applications have failed (Barschdorff *et al.*, 1993b).

The use of a single sensor signal in the development of a TCMS fails to recognise the complex and diverse nature of the cutting process and these TCM models often are less robust, unreliable and generally incapable of 'total' TCM (ability to

recognise incipient, partial, complete or catastrophic tool failure). The adoption of feature space dimensioning as a means of increasing the number of input signals by identifying and extracting more than one wear sensitive feature from a single signal, is debatable. Primarily, multi-feature extraction from a single signal does not constitute multi-sensing. In summary the following observations can be made on feature space dimensioning (Parra *et al.*, 1996):

- It involves the representation of statistically independent probability distributions in just a single signal, and
- Only minimal mutual information is acquired compared to features extracted from more than one signal.

Therefore, it is better to use the principal value or components of signals as they contain more information especially when used as inputs to an ANN.

When sensors are fused, the task requirements would normally determine the structure of the ensuing fused data. Tanner and Loh (1994) take the view that three possible outcomes could result from data fusion: ***competitive***, ***complementary***, and uniquely ***independent*** outputs. Competitive fusion is when each fused sensor data increases in value or repudiates with all other sensor data. The competitive method of data fusion would be beneficial in a multivariate TCMS because when the various sensor signals are fused, they either reinforce or contradict with each individual sensor signal. For example, if all the sensor signals are geared towards measuring the same parameter such as tool wear, then if several report a similar behaviour pattern as the tool wear level increases then an increase in confidence in the parameter of interest (wear) is developed. If the sensors report dissimilar values, a reason for the discrepancy has to be established. Independent data fusion is simply when one sensor is used to sense a particular feature. Clearly this represents a situation where the data is not fused at all, hence a degenerate method. Complementary sensor fusion extracts relative

differences from sensors to enhance the advantages, while covering the disadvantages of the individual sensors.

3.3. Conclusions

A review of the possible sensor parameters for the envisaged TCMS has been conducted. This involved evaluating their suitability and sensitivity to tool wear, and also their potential to meet the required input criteria for successful on-line TCM, i.e. ease of harnessing and reliability of each signal. Two of the reviewed parameters, cutting forces (static and dynamic) and vibration (acceleration) are considered worthy of further investigation, with due consideration of cutting conditions. Advances and increased sophistication in instrumentation technology employed for measuring these parameters make them viable, practical and cost effective. Furthermore, they are robust, easy to mount and have the quick response time needed to indicate changes for on-line monitoring.

CHAPTER 4

ANN ARCHITECTURES AND TRAINING METHODS

4.0. Overview

This chapter presents a brief tutorial on the various ANN types and training methods applied in the several attempts to develop a TCMS. A theoretical overview of each paradigm is presented, with attention paid to the constituent parts exploring either similarity or dissimilarity of the considered ANNs. Procedures and illustrative applications of the discussed ANN architectures for TCM are outlined.

4.1. Theoretical Preliminaries of ANN

4.1.1. ANN Fundamental Background

Simplistically, ANN are mathematical models and algorithms that emulate certain aspects of the information processing and knowledge gathering method of the human brain (Musgrove, 1995; Zupan and Gasteiger, 1993; White *et al.*, 1992; Winston, 1992; Dayhoff, 1990; Aleksander and Morton, 1990; Wasserman, 1989).

McCulloch and Pitts first proposed the concept of artificial neurons in 1943. Subsequent connection of artificial neurons into a network simulated on a conventional computer was carried out by Rosenblatt in 1962 and he called his systems ***perceptrons***. Progress on neural computing in general received a serious setback when Minsky and Papert published in 1969 the results of their research on the Single Layer Perceptron (SLP). They exposed weakness of perceptrons and SLP in particular as being limited to tackling tasks that are linearly separable. They used known insoluble examples (at least not capable of being solved by an

SLP) like the exclusive XOR problem to illustrate their findings. It became evident that more than one layer of perceptrons was required to solve this problem (i.e. super feature detectors) in the form of a hidden layer (Wasserman, 1989). At that time no known algorithm for training Multiple Layer Perceptron (MLP) existed. Research in ANN was severely curtailed as more attention turned towards conventional computing.

Major differences exist between neural computing and conventional computing, none more so than the idea of memory retention and representation. Neural computing being a series of highly parallel processes, its knowledge retention is said to be 'content addressable'. In conventional computers using the classic Von Neumann architecture, information storage is referred to as 'context addressable'. In terms of memory representation, neural computing is said to be 'distributed' whereas conventional computation is 'localised'. Conventional computing dominated computing research until the 1980s when Rumelhart *et al.* in 1985 (though it is widely believed that it had been independently developed earlier by Werbos in 1974, Parker in 1985 and Le Cun in 1985) devised a suitable training algorithm for the MLP, the back-propagation of error method (Hertz *et al.*, 1994; Hecht-Nielsen, 1990; Lippman, 1987). Thus an upsurge in neural computing has been witnessed and this trend has continued.

4.1.2. Types and Structures of ANN

ANN generally consists of several neurons called processing elements grouped together to form a network, performing identical tasks with the network being the main point of concern. The structure and architecture of these networks generally vary according to desired application. Zupan and Gasteiger (1993) list the following as their categories of ANNs:

- Auto and hetero-associative networks,
- Classification networks,

- Transformation networks, and
- Modelling networks.

The aforementioned categories fall short of a complete ANN listing as no mention of prediction networks is made. The list also makes no allusion to their mutual non-exclusiveness i.e. a classifier network could be modelling as it tries to classify in the same process. In this respect it is reasonable to suggest that there are almost as many ANNs as there are applications. Another school of thought classes ANNs from an architectural point of view: perceptron, associative memory and biological models (Harvey, 1994).

ANNs take as their 'inspiration' the human brain and as such are viewed as 'mere' models of the human brain. The basic information processing system of the brain is the neuron consisting of a cell body and the central nucleus. Connected to the cell body are several dendrites which receive information from other neurons and an axon through which the cell dispatches information to other neurons. Synaptic connection between neurons is either excitatory or inhibitory, depending upon whether it is connected by a positive or negative weight. Signal transmission, be it excitatory or inhibitory, is electrical in nature in the form of ions. Learning and memory retention occurs when modifications are made to the coupling between these neurons. It is this basic operating principle that is simulated on a conventional computer (Musgrove, 1995; Hertz *et al.*, 1994) to form an ANN.

An artificial neuron is the basic processing element of any ANN which when simulated on conventional computers are an 'abstraction' of the human biological neuron. ANNs generally consist of sensor inputs, multiplicative weights, a bias (an arbitrary number), a summer and the threshold mechanism with non-linearity playing an essential role in ANN neuron behaviour (Lisboa, 1992). A typical diagram of an artificial neuron is shown in Fig. 4.1.

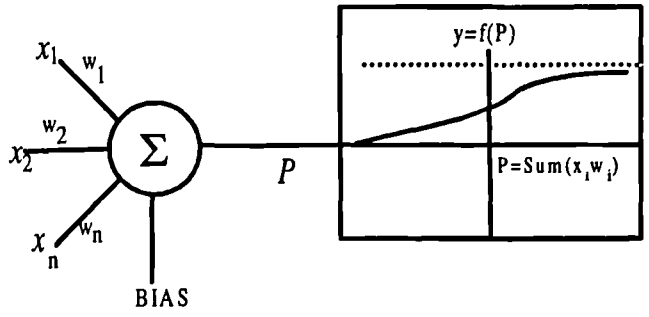

Fig. 4.1: Typical diagram of an artificial neuron

Considerable diversity is exhibited in ANNs and several variations come into effect as a result of this basic theme and are designed problem specific: adaptive controllers or processors, models of biological nervous systems or data analysis tools (Sarle, 1994). In these structures the neurons are either fully connected, recurrent or arranged in layers. In view of the importance of architectural configuration an attempt will be made to describe the various classes of ANN in some detail, starting with the smallest network types and progress to the more complex layered structures.

4.2. ANN Architectures

4.2.1. The Perceptron

A perceptron is a kind of ANN commonly viewed in its simplest form as consisting of just one neuron. A more complicated version would consist of many neurons in a 'single' layer. Its multiplicative weights and biases are trainable to produce a correct target when presented with a corresponding input. A perceptron neuron or single layer perceptron network has a hard limit transfer function, an adder and a threshold function trained with the perceptron learning rule. The perceptron learning rule will train any neuron or single layered hard limit network. A simple perceptron may be represented as shown in Fig. 4.2.

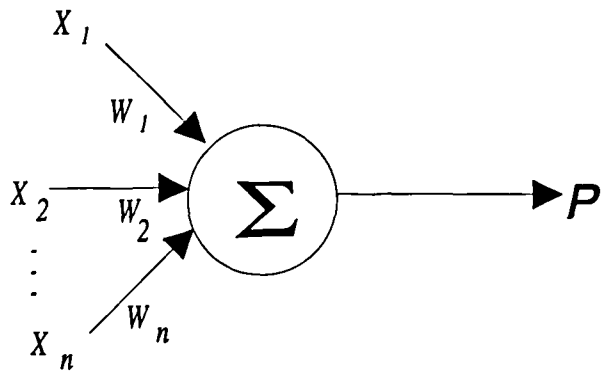

Figure 4.2: Generalised perceptron

In mathematical notation a perceptron consists of a number of neurons on a single layer. For example, if the ith weight is w_i with threshold T and its input in logical sequence x_i, then the output of the entire perceptron P is given as summarised in equation [4.1].

$$P = \begin{cases} 1 & \text{if } \sum_{i=1}^{n} x_i w_i > T \\ 0 & \text{otherwise} \end{cases} \qquad [4.1]$$

The threshold T can be replaced by a carefully chosen mapping function, the activation function such that its bounded range (0, 1) is as given by equation [4.1]. Typically there exist many such functions. Examples of the most popular ones are provided in Section 4.4. The state of the output signal is solely determined according to the summation and/or transformation of inputs x_i, multiplied by associated weights w_i. Positive and negative weights correspond respectively to excitatory and inhibitory connections and the performing function. A typical diagram of an SLP is shown in Fig. 4.3.

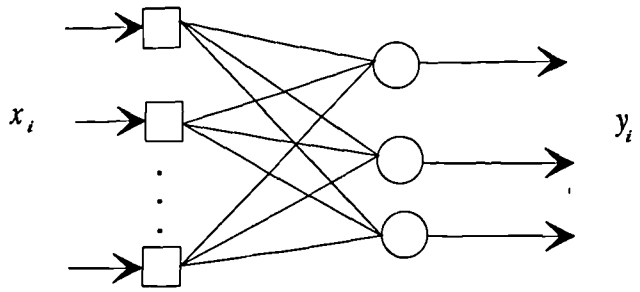

Figure 4.3: A simplified diagram of a Single Layer Perceptron

Groups of more than one layer of perceptron form what is popularly known as the Multiple Layer Perceptron.

4.2.2. The Multiple Layer Perceptron (MLP)

An MLP consists of at least three layers; an input layer, the hidden layer(s) and an output layer. The input layer links the inputs to the first hidden layer and the output layer connects the subsequent hidden layer. When data flows in one direction only (i.e. input to output) the networks are referred to as feed-forward networks (Gomm *et al.*, 1993; Carling, 1992; Myers *et al.*, 1992). Feed-forward networks therefore have a layered structure arranged such that each layer only receives inputs from the previous layers. The complexity of feed-forward MLP can be varied by increasing the number of hidden layers and nodes i.e. from simple parametric models (no hidden layer such as SLP) to more complex yet flexible non-parametric models with more than one hidden layer (Sarle, 94). MLPs generally have transfer functions which perform global changes to decision surfaces (Musgrove, 1995).

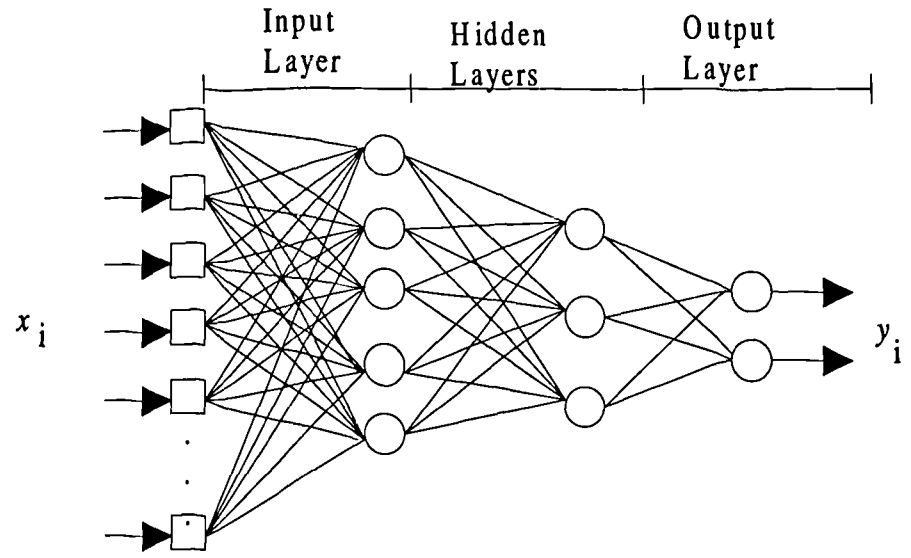

Figure 4.4: Diagram of a Typical Feed-forward MLP

When data flow is not in one direction only, the resulting networks are called recurrent networks. In these types of networks, a closed loop exists where part of a neuron output is fed-back to its inputs thus creating recurrence. Typical examples include Kohonen and Adaptive Resonance Theory (ART) for which a brief discussion follows.

4.2.3. Kohonen Networks

Kohonen neural networks are most commonly referred to as feature maps because of their self-organising and adaptive mechanisms of operation. These networks were originally developed by Teuvo Kohonen of the Helsinki University of Technology, and are constructed from fully connected arrays of neurons. They require no output data for training as the underlying information provided in the input patterns is used to form clusters or classes, and a numeric measure of the magnitude of the mapping error not used (Rojas, 1996). Kohonen networks have a pre-defined topology arranged in a grid, and learning mainly involves finding a way to distribute the grid into the input space thus creating a map of the input pattern in a self-organising manner.

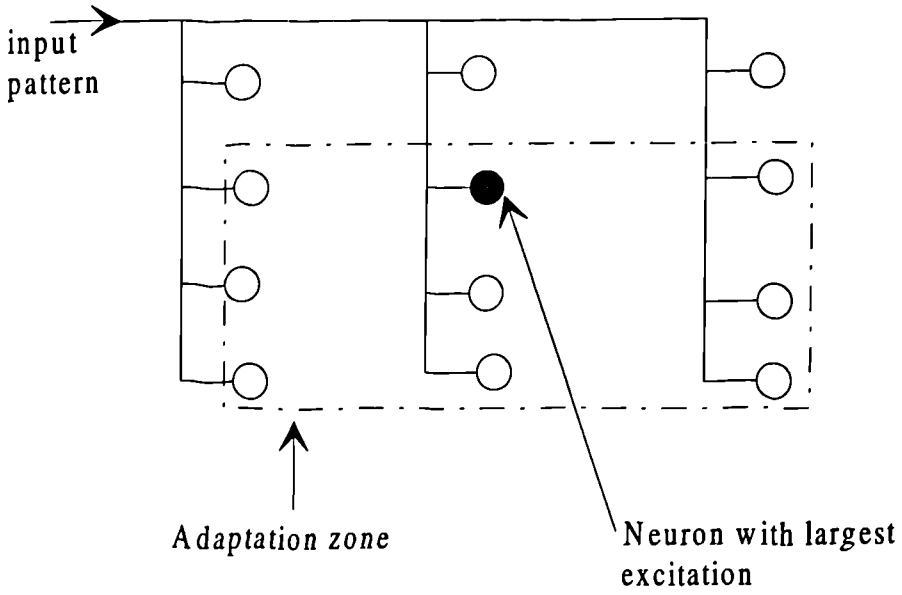

Figure 4.5: Typical Kohonen feature map

4.2.4. Adaptive Resonance Theory (ART) Neural Networks

These networks are based on the same operating principle of self-organisation as Kohonen nets, but are much more adaptable. They were developed to model massively parallel architectures by Grossberg and Carpenter (1987a, b) to address the problem that most neural networks are not able to learn new information on top of old information- referred to as the stability-plasticity dilemma. An ART network has the ability to switch modes from plastic i.e. the learning state where internal parameters are modifiable, to the stable (fixed classification set) without detriment to previous learning.

4.2.5. Radial Basis Functions (RBF) Neural Networks

These networks are similar to MLP in structure (Fig. 4.4) being three layer structured but differ in functionality. Typically an RBF may be regarded as a form of linear non-parametric model as shown in equation [4.2] with an N-dimensional response. Herein, RBF nodes represent changes to decision surfaces that are local compared to MLP nodes that perform global changes.

$$y_i = \sum_{i=1}^{N} W_{ij}\, h_i(x_{ij}) \qquad [4.2]$$

where $h_i(x_{ij})$ is the basis function.

RBF outputs are dependent upon a linear superposition of the basis functions on inputs computing radial distances to the Euclidean centres (weights vectors). The most commonly used function is Gaussian since it is capable of approximating and smoothing any arbitrary continuous function.

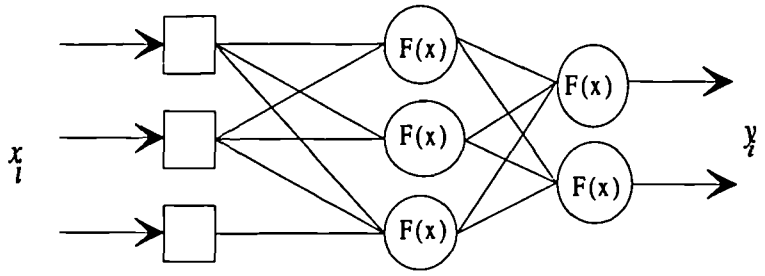

Figure 4.6: Typical Radial Basis Function neural network

Two further network types worth mentioning that have recently featured in the TCMS scene include restricted Coulomb Energy (RCE) and Condensed Nearest Neighbour Networks (CNNN).

RCE neural networks are parallel networks modelled on human learning and structured much like MLP, but their arrangement allows the classification of feed forward signal in real time without special hardware. During training the hidden nodes are connected to the output nodes selectively and correspond to different pattern classes. These connections are made such that a correct output cell will be fired when an appropriate pattern class is given to the system. CNNN are self-organising neural networks developed based on condensed clustering. Their training speeds are relatively faster than MLPs and can describe complex cluster problems. Just like MLP, they have three structured layers, but differs in that their nodes in the middle layer are problem fitted having none when untrained.

Many other neural network types exist that are both popular to implement and easy to understand. These include Propagation, Counter Propagation, Adaline, and Bi-directional networks. These networks are specialist types for which a comprehensive review and applications can be found in Myers *et al.* (1992).

When more than one neural network type is combined serially or in parallel the resulting networks are called hybrid neural networks.

4.3. Learning in ANN

In ANN, learning is the process by which weights and biases are adjusted to achieve some desired network behaviour. Principally there are two kinds of learning methods: Supervised learning and Unsupervised learning. A third kind of learning known as reinforcement learning is viewed as a half-way house of the former two methods.

4.3.1. Supervised Learning

This is generally referred to as Hebbian learning and was the first proposed learning algorithm derived for artificial neurons. Hebbian learning in principle operates by adjusting weights proportional to the product of the outputs of pre- and post-weight neurons. Supervised learning generally involves changes in a network's weights and biases and a parameter constant η (defined as the learning rate) controls the extent of weight and bias changes during learning. This is accomplished by comparing the network's current output against the desired target output as specified by the tutor, resulting in a measure of the current error with the primary aim being to minimise the error.

4.3.1.1. Perceptron Learning Rule

It is a learning rule used to train a SLP and can be summarised mathematically as follows (Hertz *et al.*, 1994):

For all i and all j,

$$W^{t}_{(i,j)} = W^{t-1}_{(i,j)} + \eta(T_i - A_i)P_{ij}$$

$$B^{t}_{i} = B^{t-1}_{i} + \eta(T_i - A_i) \qquad [4.3]$$

Where: P, A and T are the input, output and target vectors respectively; W and B are the weight and bias matrices respectively; and η is the learning rate parameter.

The presence of hidden layers introduces additional complexity and non-linearity which this method cannot adequately deal with. Due to such occurrences it is possible to implement higher order algorithms than illustrated by equation [4.3] to train multiple layer networks. One of such algorithms to have been devised is the delta learning rule.

4.3.1.2. The Delta learning Rule

This method consists of making small changes to the weights by increasing or decreasing them. Every time they are increased or decreased by a fractional amount controlled by the learning parameter as defined by the following equations:

$$\Delta W^{t}_{ij} = \eta \delta X_{ij}$$

$$W^{t}_{ij} = W^{t-1}_{ij} + \Delta W^{t}_{ij} \qquad [4.4]$$

where: δ = Correction norm of vector X; X_{ij} = input; W_{ij} = weight matrix.

A network undergoing delta learning performs a gradient descent search for an appropriate set of weights. Gradient descent is a mathematical method used for determining an extreme point in a curve. It requires taking repeated steps through the multi-dimensional space to the minimum. On each iteration the direction in which the gradient vector is decreasing fastest is identified and the procedure

repeated in that direction until the minimum is reached. The delta rule generalised extends to what has come to be called the back-propagation learning rule.

4.3.1.3. The Back-propagation (BP) Learning Rule

This is a learning rule in which weights and biases are adjusted by error derivative or delta vectors, back propagated through the network. Most often BP is applied only to feed-forward multi-layer networks (Musgrove, 1995; White *et al.*, 1992; Winston, 1992; Aleksander and Morton, 1990; Wasserman, 1989) for reasons outlined in Section 4.2.2. BP is the most popular training algorithm to have been devised. It is based on gradient descent learning being achieved as the error is affixed by propagating the output error backward through the connections to the previous layer and repeated until the input layer reached. A necessary condition is that error derivatives are obtainable, in effect, a continuous and bounded transfer function is desired as it satisfies the differentiability requirement.

Considering equation [4.3], in order to minimise the error, $(T_i\text{-}A_i)$, the weights need to be modified as defined by equation [4.4]. This requires the calculation of the partial derivatives of the multi-layered network (Hecht-Nielsen, 1990) thus backwardly propagating the error of the outputs. Equation [4.4] modified to reflect this change and condition leads to equation [4.5].

$$\Delta W_{\cdot} = \eta \frac{\partial E}{\partial W_{\cdot}}$$

$$W_{\cdot}' = W_{\cdot}' - \eta \frac{\partial E}{\partial W_{\cdot}} \qquad [4.5]$$

where $E = \frac{1}{2}\sum_{i}(T_i - A_i)^2$, called the Sum-Error-Square (Least Square) derived from the following cost function:

$$E_0 = \left(\sum_{j=1}^{J} |T_j - O_j|^P \right)^{\frac{1}{P}} \quad P \in N$$

for which when P=2, simplifies to the commonly called Least Square method.

Back-propagation is generally slow in operation. Methods have been devised to speed it up. The most prominent of these methods has been the addition of a momentum term μ and variation of the learning parameter η as shown by equation [4.6] (Minai and Williams, 1990).

$$\Delta W_{ij}^{t} = \eta \frac{\partial E}{\partial W_{ij}} - \mu \Delta W_{ij}^{t-1}$$

$$W_{ij}^{t} = W_{ij}^{t-1} - \eta \frac{\partial E}{\partial W_{ij}} - \mu \Delta W_{ij}^{t-1} \qquad [4.6]$$

The momentum term technique serves to make it less likely for the BP network to be caught in a shallow minimum during learning. More recently faster learning methods for MLP have been introduced such as conjugate gradient and quasi-Newton- thought to be superior in performance to BP (Bishop, 1994). However there are still limitations in the success of these techniques, and the learning methods are not guaranteed to find the best connection weights.

4.3.2. Unsupervised Learning

This is a direct opposite of the supervised learning method. Changes in the network's weights and biases are not due to an externally determined target. This is typical of recurrent networks where changes are a function of the current network input and output vectors, with previous weights and biases. This method could be viewed as autonomous, where the networks use their presented data to embark on finding out some underlying properties in the presented data and uses these as the basis for their classifications and/or modelling.

The first unsupervised learning method was suggested by Kohonen in 1984, an embodiment of ideas put forward earlier by Hebb, von der Marlburg and Rosenblatt (Rojas, 1996; Aleksander and Morton, 1990). In Hebbian learning networks weights are increased according to the product of the excitation levels of the source and destination neurons. The exact properties that unsupervised nets learn to recognise would depend on the network model and therefore the implemented learning method. Amongst the most prominently used methods in TCMS development are Kohonen learning and ART learning, both variants of competitive learning.

4.3.2.1. Kohonen Learning

Proposed in the mid 1980s based on the principle of self-organisation and adaptation. In summary, the learning rule for a 1-D chain of n nodes on an m-dimensional space starts by initialising the weight (randomly) from ith input node, x_i, to the jth node, x_j, in time t, $W_{ij}(t)$, for $0 \leq i \leq n-1$. Next the initial radius of the neighbourhood around node j, $N_j(0)$, is set large (maximum Euclidean distance over input space). Presentation of the input pattern computes the distance d_j between input and output node j using the following equation:

$$d_j = \sum_i \left(x_i(t) - W_{ij}(t)\right)^2 \qquad [4.7]$$

In the mean time the weights are updated and the calculated node minimum distance d_j, is designated J. The new updated weights defined in the new neighbourhood size $N_J(t)$ are then given by the following equation:

$$W_{ij}(t+1) = \eta(t) W_{ij}(t)\left(x_i(t) - W_{ij}(t)\right) \qquad [4.8]$$

where $\eta(t)$ *is gain,* $0 < \eta(t) < 1$.

In effect $N_j(t)$ decreases to the minimal Euclidean distance as t $\rightarrow \infty$ thus localising the area of maximum activity (Beale and Jackson, 1994) as shown in Fig. 4.5.

4.3.2.2. Competitive learning

In this learning method individual neurons learn to become feature detectors, and can be viewed as k-means clustering systems with cluster centroids as prototype vectors for some fixed number k of m group (Hertz at al., 1994).

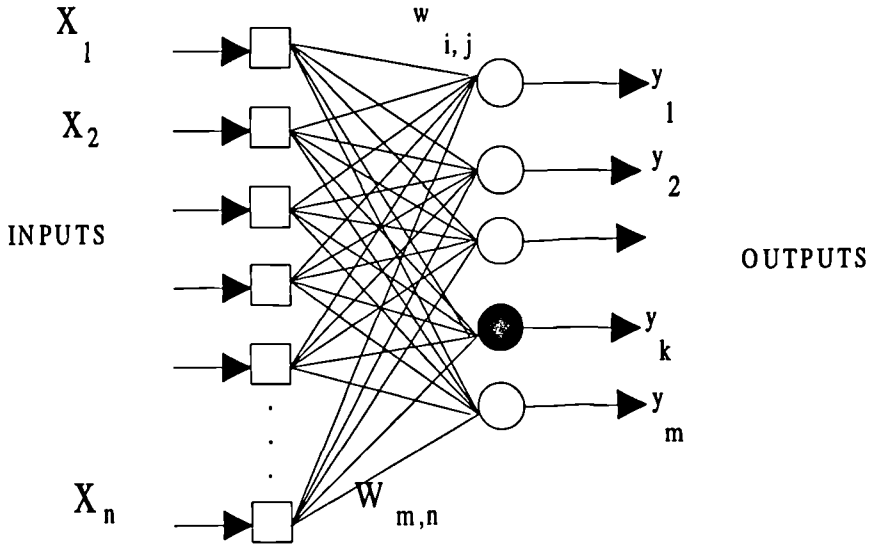

Fig. 4.7: Diagram illustrating competitive learning in ANNs

Input patterns are trained to associate to a cluster of patterns, creating outputs with an indication of membership of the input pattern with similar characteristics. Competitive learning generally exhibits a 'winner-takes-all' and the node with the largest total input claims the input pattern thus the right to respond to the input pattern, i.e. $y_k = 1$ (Fig. 4.7). As the adaptation process continues output node k establishes a competitive edge over the rest. It will tend to claim the net input thus the right to respond once more, by applying the rule of thumb 'learn-only-if-you-can-win' or by virtue of it having won before. After a few cycles of adaptation the only node responding to the input pattern is v_k and this means that

y_k dominates the network output. In the ensuing context no node can compete with y_k as it would always win. A state is reached when the amount of input information flow into the system is equal to that which y_k outputs thus indicating that a fully stable and trained system has been attained (Carpenter and Grossberg, 1987a, 1987b; Grossberg, 1987; Rumelhart and Zipser, 1985).

Two class types of competitive learning have been developed: linear and differential competitive learning.

Linear competitive learning obtain output clusters from the output nodes competing with each other for the right to respond to the input signal, with an output of '1' indicative of success while a '0' failure, represented mathematically as:

$$y_i = \begin{cases} 1 \text{ if } \sum w_i x_i = Max_{\dots} \left(\sum w_i x_i \right) \\ 0 \qquad \text{otherwise} \end{cases} \qquad [4.9]$$

A node is only allowed to learn if it can win, i.e. 'learn-only-if-you-win' or 'keep-your-distance', expressed mathematically by equation [4.10].

$$\frac{dw_i}{dt} = y\left(x_i - W_i\right) \qquad [4.10]$$

Differential Competitive learning aims at stabilising the neural network system by implementing a modified version of the linear learning rule as shown in equation [4.11].

$$\frac{dw_i}{dt} = \frac{dy_i}{dt}\left(x_i - W_i\right) \qquad [4.11]$$

4.3.2.3. Adaptive Resonance Theory Learning

The introduction of a wholly new pattern to the fully trained and stable aforementioned system may result in the adapted weights being changed hence, it

would no longer identify correctly previous patterns- the so called plasticity-stability dilemma. The plastic mode corresponds to the state when the network's weights can adapt (learn) whereas the stable state is when it would otherwise classify. If the network cannot realise when to switch modes then the output will be erroneous. So far the most successful technique aimed at making the networks sensitive to novelty was devised by Carpenter and Grossberg (1987a, b) called the Adaptive Resonance Theory (ART). ART networks consists of ART-1, ART-2, ART-3 and more recently fuzzy-ART, and suggest that some deal with binary values while others deal only with real values. ART network layers perform different functions, some possibly linked to external mechanisms with top-down and bottom-up mechanisms forming an anatomical attention-orienting system as highlighted by the basic ART-1 figure shown in Fig 4.8 (Carpenter and Grossberg, 1987a, b). Modified weights continually pass forwards or backwards thus cyclically resonating between the layers.

In principle ART learning rate is adjusted according to an algorithm during training to minimise training time, and employs the stability criterion for choosing winning processing elements through vigilance implementation. The ART training algorithm can be divided into four stages of implementation: the initialisation, recognition, comparison and search phase.

4.3.3. Reinforcement Learning

Considerable differences exist between the two aforementioned learning classes in ANNs that, to an extent, can be viewed as the two extreme points on the spectrum of training possibilities. In practice the network is most likely to be trained via a method that employs techniques from both methods. For systems that have feedback provided (regarding performance), but the feedback considerably weaker than should be if the training algorithm was supervised, a reinforcement learning system is instituted rather than specific target outputs (Hertz *et al.*, 1994). Reinforcement learning schemes are enforced on a system by modifying

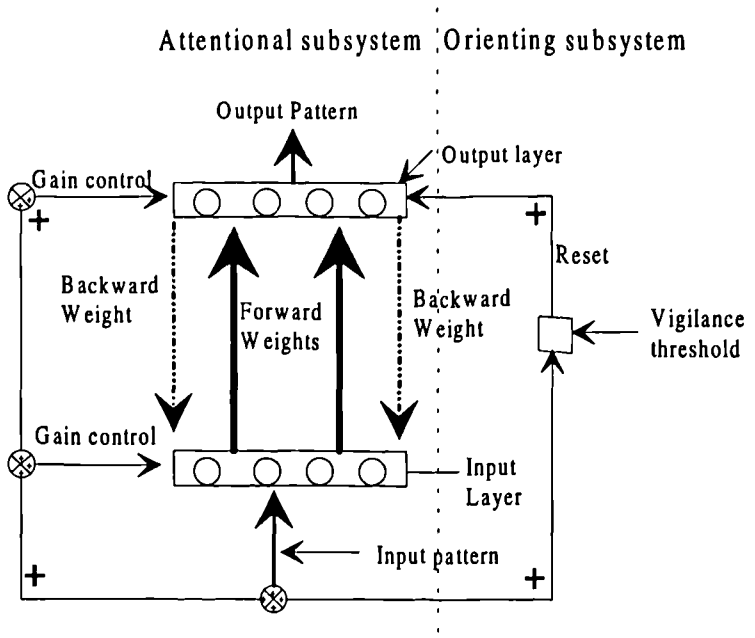

Figure 4.8. Simplified diagram of ART

according to a single scalar evaluation of the system's output. Bressloff (1995) uses the classical example of stochastic learning automaton to illustrate reinforcement learning. The automaton learns and adapts by selecting from a finite set of actions in discrete time steps and the environment responds by transmitting a failure or success binary signal to the automaton. Each action response leads to the modification of the automaton state with learning effected in increased likelihood of success. The optimum conditions or best response from the automaton occurs when the likelihood probability of success is largest.

This method lacks the generalisation vital in ANNs and consequently has found little or no success in terms of practical application. A successful case worth noting is Radial Basis Function neural network which, because of its Gaussian function implication (radial symmetry property), attracts local generalisation; thereby containing both elements of supervised and unsupervised learning methods.

4.4. Typical ANN Transfer Functions (Cost Functions)

Two distinct steps are normally involved in obtaining a neuron output: evaluation of the linear inputs (summation) and their transformation to give a non-linear output (by some function). These non-linear transformations are achieved through application of functions with the option of choosing them as desired according to required operation as illustrated by equation [4.12].

$$y = f(x) \qquad [4.12]$$

The function f(...) is called the transfer function. The primary reasons for such modifications have been on grounds of physical limitations on size and frequency of network output being non-negative and continuous but confined to a specified interval. There are several types of transfer functions, and some of the popular ones are discussed.

4.4.1. Hard-limiter (Step) Function

The function output is usually binary (0 and 1) such as that shown in equation [4.1]. A point exists called the threshold ϑ and the value of the function depends on where it is set as it decides whether neuron fires or not. For computational efficiency, scientists do not want an ON or OFF (TRUE/FALSE) situation as it tells very little for their applications. Equation [4.1] can be modified to give a bipolar function as in equation [4.13] that is necessary for certain control transfer function but does not tell anything more because it is a linear transformer.

$$y = f(x,\vartheta) = \begin{cases} 1 & \text{if } x_i w_i \geq \vartheta \\ -1 & \text{if } x_i w_i < \vartheta \end{cases} \qquad [4.13]$$

A graphical representation of this function is given in Fig 4.9.

4.4.2. The Threshold Logic Function

The threshold logic function is similar to the hard-limiter function but has an additional swap interval or ramp as illustrated in Fig 4.10. Within this interval the output is directly proportional (linearly) to x. A parameter constant, α, the 'reciprocal width of swap interval' defines the width of the said interval and starts at ϑ with a width of $1/\alpha$. Derivation of this threshold logic function using the defined conditions leads to equation [4.14].

The threshold logic is mostly used where a linear output is desired over the entire output range but may also contain singularities.

$$y = f(x,\alpha,\vartheta) = \begin{cases} 0 & x \le \vartheta \\ \alpha(x-\vartheta) & \vartheta < x < \vartheta + \dfrac{1}{\alpha} \\ 1 & x > \vartheta + \dfrac{1}{\alpha} \end{cases} \qquad [4.14]$$

4.4.3. The Logistic Sigmoid Transfer Function

This is the most widely used transfer function in neural network architectures, though it is slow in numerical calculations (cf. tan, tanh, sine and Gaussian). Its defining equation is given as follows:

$$y = f(x,\alpha,\vartheta) = \frac{1}{\left\{1 + e^{-(\alpha x + \vartheta)}\right\}} \qquad [4.15]$$

For convenience the exponential function in equation [4.15] can be replaced by an arbitrary function and a constant with threshold fixed, and thus can be re-written as follows:

$$y = \frac{1}{\left\{1 + e^{-\alpha x}\right\}} \qquad [4.16]$$

where $x = \sum w_i x_i$

Typically, sigmoidal transfer functions exhibit non-linear behaviour and the non-linearity tends to make neural networks flexible in adjusting to the many different learning situations they encounter with the constant α determining the slope of the curve as shown in Fig 4.11.

4.4.4. Tanh Function

Trigonometric functions (sine, tangent) are widely used but the hyperbolic function tanh(x) is used the most. The tanh function operates as shown in Fig 4.12 when described by the following equation:

$$y = \tanh(x) = \frac{e^{x} - e^{-x}}{e^{x} + e^{-x}} \qquad [4.17]$$

4.4.5. The Gaussian Function

The most commonly used function is as described in equation [4.18] and Fig 4.13 which minimises the error distribution to within 1% of patterns only. Its use in RBF networks are extremely desirable where local change in decision surface lead to more accurate models.

$$y = \frac{1}{\sqrt{2\pi\sigma}} e^{-\frac{1}{2}\frac{(x-\mu)^2}{\sigma^2}} \qquad [4.18]$$

When the mean, $\mu=0$ and the standard deviation, $\sigma=1$, equation [4.18] reduces to the following:

$$y = e^{-x^2/2} \qquad [4.19]$$

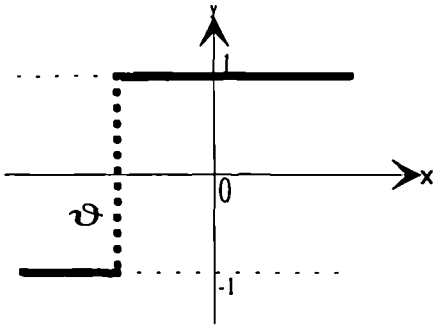

Figure 4.9: The Step Function

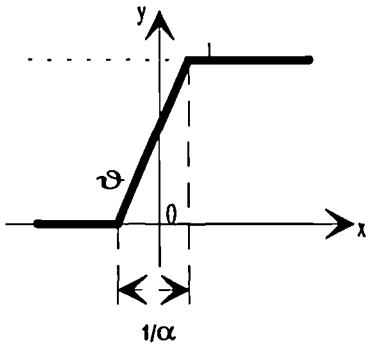

Figure 4.10: Threshold Logic Function

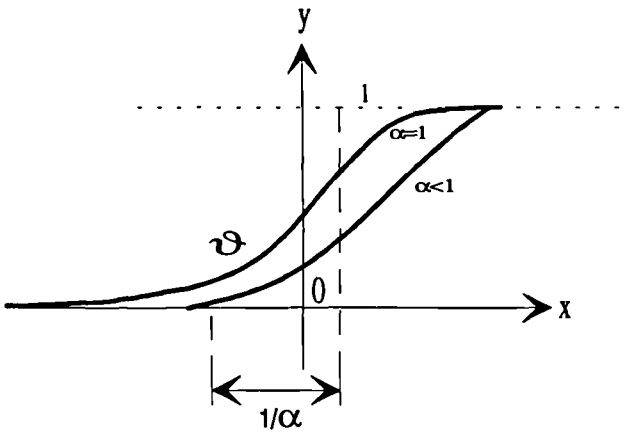

Figure 4.11: Sigmoidal Transfer Function

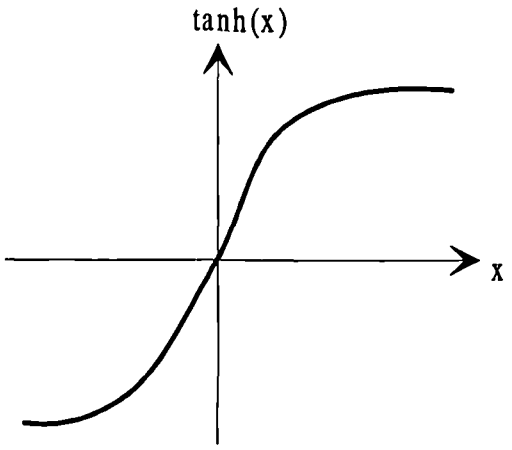

Figure 4.12: The tanh(x) Transfer Function

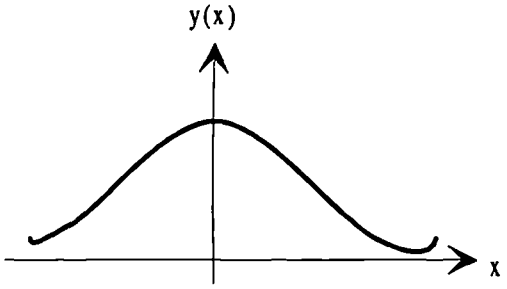

Figure 4.13: The Gaussian Transfer Function

4.5. Typical Engineering Application Scenarios

Applications are many and diverse. Some of the highly acclaimed applications include NETtalk which learns to pronounce English text; the Airline Marketing Tactician (AMT), a two stage procedure that assists airlines to forecast seat demand (first stage) and allocate airline resources to meet the projected demand (second stage); and the Electro-Cardiograph (ECG) noise filter (ACOST, 1992). Aircraft and target identification from sonar traces are some of the military applications (Burke, 1989). Closer to home British Rail has developed a vision system to assist in monitoring level crossings while British Telecommunications are involved in the application of ANN for speech processing, recognition and synthesis (ACOST, 1992; Myers *et al.*, 1992). Industrial applications include sensor validation and detection of tool wear, the subject of this study, and shaft imbalance; control systems, authentication and quality control, automatic image analysis and on-line plant monitoring.

4.6. The Merits of ANNs Utilisation in TCMSs

The merits of neural networks in TCM applications can be summarised as follows:

- Fault tolerance and adaptability: A combination of tool wear non-linearity, complexity of the cutting process and variation of cutting conditions lead to an inaccurate and unavoidably noisy cutting environment. For on-line monitoring purposes a device with adaptive and fault tolerant capability can reduce the error apparent in the sensor signal and concentrate on recognising tool wear levels.

- Neural networks, generally, are data driven devices not program driven as in conventional computers. Typically the amount of data that streams off a cutting process is very large and neural networks can successfully cope with this amount of data.

- Random variations in the workpiece material and the complex to chaotic nature of the cutting process requires for monitoring processes an information system capable of handling the subsequent profusion of signal states satisfactorily. Untended fully automated systems utilising conventional pattern recognition techniques such as Bayesian classifiers, Nearest neighbour or Stochastic approximators, have largely had limited success. The limit in success can partly be attributed to the wide range of signals, noise and distortions which made conventional techniques unsatisfactorily. Neural networks can satisfactorily handle noisy data or solve problems with complicated relationships that are poorly understood.

4.7. ANN Application in TCMS

Tool wear identification tasks usually involve at its preliminary stage, data pre-processing and recording (sampling) followed by signal analysis, commonly through application of the forward Fast Fourier Transforms (FFT), wavelet transforms or statistical analysis (mean, kurtosis, skews, RMS, AR, ARMA). The last stage involves a decision surface or classifier using as input the processed data to reach a decision on the ensuing tool state. A classic illustration of this process can be represented as shown in Fig 4.14.

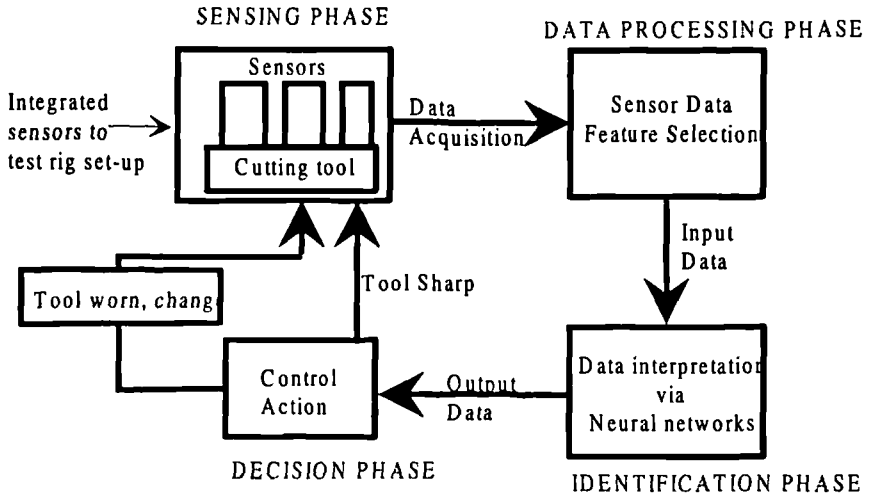

Figure 4.14: Classic diagram of an ANN TCMS

TCM methods based on neural networks are becoming increasingly popular because tool wear is a non-linear process and its representation by neural network, an attractive alternative to previously employed mathematical methods (Elanayar *et al.*, 1990). Amongst the neural networks paradigms to have been applied in TCM the most popular choice has been the MLP neural network. Experimentation with other types of neural networks of supervised and unsupervised nature have been pursued including less well known algorithms such as RCE network and CNNN.

Table 4.1 summarises the types of ANN that have been used in the development of TCMSs. The table shows that a wide range of ANNs (supervised and unsupervised types) have been used. According to this survey, well over 60% of researchers used the MLP neural network type, trained via BP. In several cases, using different MLP configurations in the same experiment, some researchers have been able to verify the most appropriate number of hidden nodes required for optimum system performance. The next most popular category seem to be ART and KSOM, used at equal proportions.

4.8. Conclusions

ANNs, though a fairly new field, have matured as they have gain wider applicability. They are increasingly being applied in manufacturing processes because of their intelligent capability, and may revolutionise the way monitoring (condition and processes), maintenance, and possibly non-destructive engineering testing are performed.

The review can be summarised as follows:

- ANNs are capable of learning from examples and generalise on unseen data, and

- ANNs can be regarded as universal approximators particularly suited for pattern recognition tasks.

ANNs' diversed range of applications include amongst others prediction of stocks and currency fluctuation in the financial markets, military target identification, vision systems, and speech processing. Industrial applications have been slow but recent areas of implementation include sensor validation and detection of tool wear, control systems and quality control, and on-line plant monitoring.

Neural networks are uniquely suitable for TCM tasks because they can learn non-linear relationships. Therefore, parameter estimation between sensor based information and the actual feature of interest can be estimated better using neural networks than with stochastic approximation techniques.

MLP neural networks are suggested for further investigation in the envisaged research. They are capable of modelling non-linear mappings and their recognition thereafter, of characteristic features of the phenomena of chaotic processes and incomplete sensory data. With sufficient training and optimal parameters, they are able to relate previously unseen problem data to a solution thereby providing a viable resolution to a brand new problem. Since the tool state identification level is one of pattern recognition and therefore, of classification, the classifier needs advanced knowledge on the various tool states (degree of wear) and corresponding descriptive data on the cutting process parameters.

TABLE 4.1: List of neural networks surveyed

AUTHOR(s)	MLP	*KSOM*	RCE	ART	RBF	SCBC	CNNN
Noori-Khajavi & Komanduri (1995)	√	√		√			
Zhou et al (1995)	√						
Govekar & Grabec (1994)		√					
Tarng *et al.* (1994)	√						
Lui & Anantharaman (1994)	√						
Ko & Cho (1994)	√						
Purushothaman & Srinivasa (1994)	√						
Barschdorff *et al.* (1993b)	√						√
Tansel *et al.* (1993)				√			
Yao & Fang (1993)	√						
Ruiz *et al.* (1993)	√						
Burke (1993)				√			
Markos *et al.* (1993)	√						
Jammu *et al.* (1993)		√		√		√	
Teshima *et al.* (1993)	√						
Monostori (1993)	√						
Moriwaki & Mori (1993)	√						
Tansel & McLaughling (1993)			√	√			
Tansel *et al.* (1993)				√			
Tansel *et al.* (1992)			√				
Burke (1992)	√			√			
Guillot & El Ouafi (1991)	√						
Masory (1991)	√						
Tansel *et al.* (1991)	√						
Emel (1991)	√						
Elanayar & Shin (1991)					√		
Kamarthi *et al.* (1991)		√					
Govekar *et al.* (1991)		√					
Choi *et al.* (1991)	√	√					
Dornfeld (1990)	√						
Rangwala & Dornfeld (1990)	√						
Elanayar & Shin (1990)	√						
Choi et al (1990)	√						
Liu & Ko (1990)	√						
Burke (1989)	√						
Rangwala (1988)				√			
Chryssolouris & Domroese (1988, 1989)	√						

CHAPTER 5

A CRITICAL REVIEW OF NEURAL NETWORK SOLUTIONS TO THE TOOL CONDITION MONITORING PROBLEM IN METAL CUTTING

5.0. Overview

Having reviewed the various neural network architectures in the previous chapter, this chapter covers a general literature review of the use of ANNs in TCM. This includes a critical analysis of the range of cutting tool monitoring techniques implemented through the application of neural networks and the trend in the results obtained is also presented. The sole aim of this review was to illustrate the extent of application of neural networks and highlight the need for multiple source sensor signals in TCMS. An attempt is also made to outline the fundamental shortfall of the developed systems.

5.1. Introduction

Previous efforts to develop TCMSs have focused mainly on the development of mathematical models of the cutting process which were dependent upon large amounts of experimental data (Lister, 1993). These methods did not take into account the complex and diverse nature of the metal cutting operation. It would seem that the lack of an accurate model for wear prediction led researchers to resort to other methods of sensor integration. Recently, it has been widely acknowledged that a better solution to previous theoretical and empirically based on-line TCMSs lies in an 'intelligent' discriminator (Rangwala and Dornfeld, 1990, Monostori, 1993). These systems could, without human assistance and/or

interruption, recognise most or all forms of tool abnormalities during metal cutting. The quest for such systems led to the introduction and use of neural networks to fuse sensor data, and has continued with vigorous diversity to date.

Methods based on neural networks have proven popular because intrinsically, tool wear is a highly non-linear process; its representation via a neural network is a viable, reliable and attractive alternative to previously employed methods (Elanayar *et al.*, 1990). Neural networks are robust and highly parallel processing devices, capable of non-linear modelling. Explicit problem description is not required, and they are capable of handling large amounts of data out of which they build knowledge bases that are consulted during decision making (Govekar and Grabec, 1994; Markos *et al.*, 1993; DTI, 1993).

5.2. Earliest Attempts of TCMS Development Using ANNs

Earlier methods of sensor fusion in machining which largely suffered from time consuming training, were particularly tedious and mostly inefficient for use in real time TCM. As an alternative approach, Dornfeld (1990) fused signals of acoustic emission (AE), cutting forces and spindle motor current, and used the output from this fusion as inputs to an MLP neural network. The sensor signals were first pre-processed to eliminate noise. The FFT of these sensor signals were then passed through a feature extraction block to select features most sensitive to tool wear. The extracted features were fed into an MLP that had been trained off-line via back-propagation. Dornfeld's choice of input parameters (cutting forces, AE and spindle motor current) were reportedly justified by his earlier findings which suggested that at certain frequencies, AE showed good sensitivity to tool wear over a wide range of machining conditions. Cutting forces and spindle motor current could be used individually as indicators of tool wear with some success. However, in subsequent works with Rangwala (1987, 1990), the spindle motor current was dropped in preference to the two other input parameters. This could be attributed to the fact that variations in spindle motor current are from

accountable sources such as bearing friction and lubrication oil type.

Following the pioneering work of Dornfeld, numerous attempts at TCM with various kinds of neural networks have been carried out, some more successful than others.

The use of ANNs in TCM, was carried one step further by Rangwala (1988) and Burke (1989). Rangwala concentrated principally on using cutting forces and AE, as Dornfeld had proposed earlier via a supervised MLP. Burke on the other hand, used Rangwala's experimental results and experience to employ a new and different kind of discriminator technique- the unsupervised neural network (Burke, 1989). Unsupervised neural networks are autonomous in that the network uses the presented data to embark on finding some underlying properties in the data. This is then used as the basis for its future classification. Rangwala's method, Burke asserts, requires expensive training and most importantly, was non-adaptive to the cutting conditions (Burke, 1993). To clarify their standpoints as far as the neural network classification successes were concerned, Burke and Rangwala together assessed the advantages of using an unsupervised method compared to a supervised one (Burke and Rangwala, 1991). Comparisons on output success, accuracy of classification and implementation speed were made. They concluded that both methods achieved nearly the same level of output success and accuracy of classification rate when tested. Burke's preferred method (unsupervised) was more adaptive to the cutting conditions (Burke, 1989, 1992, 1993; Burke and Rangwala, 1991) and achieved comparable success rates, (around 95%) whilst being faster to implement than a supervised method.

Incorporation of additional patterns into the system's memory without due training was cited as the main advantage of using unsupervised networks. Unsupervised networks, to an extent, could be viewed as not being entirely unsupervised, as they still required partially labelled samples or signals for training or implementation. However, the fact that they required only partially

labelled samples gave unsupervised ANNs a competitive edge over MLP (a typical supervised network that required completely labelled samples for training). In terms of cost, implementing Burke's method was cheaper and more cost effective as it was performed on-line, compared to MLP which required training to be performed off-line.

Work carried out to-date on the development of TCMSs have been tackled from different and diverse perspectives. While some researchers have concentrated on sensor signal processing, others have experimented on various neural network types. In order to present the extent of diversity in TCMS research, the intention is to critically review some of the key research in TCMS that have been implemented through application of ANNs. A comparison of results, and test percentage success scored, is outlined.

For any given TCMS, the investigator has at his/her disposal a variety of probable sensor signal inputs. Unfortunately he or she might be denied the means of utilising some of these signal inputs because of limited resources. Alternatively, the obstacle could be that the investigator can not gain access to the source of the intended sensor signal. A typical example of this is the tool tip temperature. A variety of sensor signals have been used as inputs to ANNs in the various attempts to develop a neural network based TCMS. A summary of these sensor signal inputs is provided in Table 5.1.

Sensor signal inputs on their own do not tell us a great deal about the state of the cutting tool. Some investigators have incorporated the cutting variables (e.g. cutting speed, feed rate and depth of cut) as further inputs to the network to enhance classification performance. For example, increasing the depth of cut during a cutting process leads to a proportional increase in the cutting forces. These could be confused with increased forces due to tool wear in the system. To achieve a widely applicable system, it is necessary that the effects of the cutting parameters, possible different workpiece material, and various tool insert types on

the sensor signals be properly understood.

From Table 5.1, it can be seen that sensor signal inputs have either been applied on their own, or in combination with others (multi-sensor approach), but a majority of the surveyed papers utilised single sensor. Table 5.1 also shows that cutting forces and AE have been the most widely researched sensor inputs for TCM according to this survey.

5.3. Single Sensor Inputs

Lee *et al.* (1996) proposed and implemented a neural network model for one-step ahead tool wear prediction using cutting force signals. Turning tests were conducted on a NC lathe and the necessary data collected and corresponding flank wear measured. Several tests were initially conducted i.e. different workpieces, different approach angles (1, 15 and 45) at a variety of cutting conditions. From these tests, the force component least sensitive to process parameter change but most sensitive to wear were identified. An MLP with 4 inputs (the resultant cutting force, feed-rate, chip breaker type and workpiece material), 4 nodes and a single output, was used to perform TCM. Obtained results showed close correlation between actual data and the estimated values. With varying cutting speed and depth of cut, an error estimate of 6-9.5% was reported for constant feed-rate, chip breaker and workpiece data.

Colbaugh and Glass (1995) implemented a TCMS through the application of both an ANN and a linear observer. The neural network consisted of a recurrent algorithm which modelled the tool wear dynamics. Its output was fed into the observer system that estimated tool wear from the model using cutting force measurements. The overall system was trained using simulated data and then experimental data was used to evaluate its performance. No quantification of the system was provided but Colbaugh and Glass subsequently concluded that their method provided wear estimates which were in close agreement with experimental results.

Elanayar and Shin (1995) proposed a unified method of cutting tool flank and crater wear estimation using Radial Basis Functions (RBF) neural network with components of the cutting forces used as inputs to the network. In the first part of their investigation, they found it necessary to initially train and test the chosen RBF network on purely simulated data, contaminated with white noise to reflect some similarity with experimental data. In the implementation stage of their method, data from experiments performed on a vertical lathe were used. The experiments involved recording the pre-processed (low-pass filtering) 3-components of the cutting forces from two sets of tests conducted. For the first set of tests, they used coated carbide inserts and carried out the tests at low cutting speeds. The second set of tests used ceramic inserts and was carried out at higher speeds. The same workpiece material, feed-rate and depth of cut were utilised in both test sets. Force-wear relationships, partly based on the same principle as reported in Purushothaman and Srinivasa (1994) and Elayanar *et al.* (1990) were employed to select the input coefficients for training the network. Test and verification of the trained network showed it to be capable of close flank wear estimation but poor crater wear estimation. Overall, the proposed method demonstrated an ability to estimate tool wear closely, over a wide range of cutting conditions but lacked vital accuracy. The inaccuracies could be attributed to poor input coefficient estimation, which were treated as linear (i.e. they related the cutting forces to tool wear with linear equations). This assumption of linearity somewhat precluded the optimisation and performance of the network, as the true variation between cutting forces and tool wear was rather non-linear. High inaccuracy could also be attributed to the fact that simulated data does not suffer from variation and distortion due to effects of the cutting parameters, as real or experimental data does. It is therefore misleading to contemplate combining the two data types and expect unanimity.

Zhou *et al.* (1995), Rahman *et al.* (1995b) and Hong *et al.* (1996) performed cutting tests from which they recorded the dynamic cutting force signature. A dimensional space features selection process was carried out, and the obtained

features used as input to an MLP neural network, and three different implementations carried out. In Zhou *et al.* (1995), they used a wavelet technique to extract such features from the convoluted force signal. Nine features in total were selected, each from 26 groups of tool data to train and test a 9-4-1 network, with output representing fresh or worn tool state only. Results obtained showed inaccuracies due to changed chip shape as a result of tool state change. To alleviate this, the network output was broadened to 3 nodes representing levels of tool wear, chip breakage and chatter vibration. The main reason for this, they claimed, was the fact that in any cutting process more than two classes of cutting states actually existed, and a network with just one output can only recognise two of them. Thus, the final classification results would not be entirely correct. In Rahman *et al.* (1995b), 5 features were extracted from the dynamic force signal and used as input to a 5-8-3 network, whose outputs were exactly the same as those reported in Zhou *et al.* (1995). Initially, during network training, the extracted features were used in combinations of 1, 2, 3, 4 and 5. Successful training was only accomplished with the 4 and 5 combinations, with testing achieving a 95% success rate. In Hong *et al.* (1996), the number of extracted features were reduced further to 2, again through application of wavelet transforms in the decomposition of the dynamic cutting force signal. The extracted features were scaled to form a 9 dimensions feature vector, and used as input to a 9-18-1 MLP network architecture, whose output provided the predicted level of tool wear. In the experiments, tool inserts with and without chip breaker geometry of known state, were used. Final prediction results showed that up to a 92.1% success rate was achievable with the best results obtained whilst cutting was performed with chip breaker tool geometry inserts.

Barschdorff and Femmer (1994) performed turning tests using a CNC-lathe machine and measured the acceleration (vibration) signals on the tool holder. An extensive feature selection process utilising the sequential forward selection algorithm with respect to clustering properties was carried. Several networks were utilised by Barschdorff and Femmer as to their suitability for tool state

classification and modelling of the tool wear process. They compared the performance of MLP, LVQ and CNNN. With regards to a two-class problem (worn, sharp) no classification errors were reportedly obtained for both the networks. Increasing the wear state to a four class problem with clearly defined wear mark values, due to the continuous nature of the wear values, considerable overlap of classes occurred leading to some error in the classification. Training success rates of 100%, 86% and 98% respectively for CNNN, LVQ and MLP were reported for approximately 20 data each in the four subclasses. Testing using exactly the same number of data gave success rate of 86%, 78% and 86%. They concluded that their study suggested that the main drawback in the application of CNNN and LVQ was their large size. On the other hand, MLP implementation was favoured for the estimation of wear values.

Govekar and Grabec (1994) used cutting force signals applied as components namely cutting momentum, and feed forces. The sensor input signals were pre-processed to obtain 33 components, three of which represented the drill wear states. Their results showed that the percentage error in the adapted cases were at least four times lower than the non-adapted cases. Nonetheless, success rate for tool wear classification was in the same range as those achieved by Dornfeld (1990), Rangwala (1988) and Burke (1989), however Govekar and Grabec (1994) achieved a faster convergence in the adaptation process than did Burke.

Purushothaman and Srinivasa (1994), Yao and Fang (1993), Elanayar *et al.* (1990) and, Elanayar and Shin (1990, 1991), also used the cutting force signal as input to an ANN, but implemented their TCM via different neural network architectures. Concentrating on the findings reported in Purushothaman and Srinivasa (1994), and Elanayar and Shin (1990), which employed the same sensor signal inputs, it was possible to explore their differences. Elanayar *et al.* (1990) used force ratios (F_X/F_Y and F_Z/F_Y) as inputs to an initial neural net (MLP). The output from this net depicting the severity of tool wear (flank, crater and tip) was then used as input to a second network (another MLP), together with the F_Z component of the

cutting force. The net output gave an indication of the product surface finish established earlier as representative of the in-situ tool state. Effectively, Elanayar *et al.* (1990) used this experiment to relate tool wear, surface finish, and cutting forces via neural network application and reported a high but un-quantified achievement rate. Purushothaman and Srinivasa's (1994) approach and methodology was similar to that of Dornfeld and Rangwala (1987), but differed in terms of sensor signal inputs, data processing, number of training patterns used, and employed MLP topology (number of nodes at the input, output and hidden layers). Purushothaman and Srinivasa saw no need to use dimensionally selected features, instead, they used the amplified components of the cutting force signal 'as sampled', together with the three cutting parameters (cf. Dornfeld (1990), Rangwala and Dornfeld (1987, 1990)). These input signals were normalised to give values of between 0-1, with expected outputs grouped into two classes and three neural network architectures investigated. The trained networks were tested using 6 fresh patterns, and for some *unexplained reason, their focus shifted from* TCM to identification of best performing MLP network topology. No quantification of their results was given.

Ly and Choi (1994) used ART-1 to identify a drilling tool as either sharp-still-useable or dull-change. Tests were conducted and the vibration signals collected. These were then processed though a short term Fourier Transform. Isolated regions of the obtained spectrogram were then used as the input feature to the network. The work was reportedly still underway at the time of this review.

Tarng *et al.* (1994) utilised the cutting forces as their sensor signal inputs with an additional component depicting the occurrence and none occurrence of tool breakage to monitor the cutting process. They incorporated the cutting condition parameters (cutting speed, radial and axial depth of cut) to their chosen sensor signals and workpiece material. Results obtained suggested that ANN could be successfully used to monitor the condition of a cutting tool. No quantification of results were provided.

Weis (1994) devised a direct method of tool wear monitoring based on framed images of the cutting tool utilising a sensor system for optical tool wear monitoring comprising a camera and infra-red flash light. The set-up was such that an external trigger system synchronised the signals for the camera with the spindle of the machine. The captured image underwent a series of image processing from which features of the image synchronous with tool wear were selected. These were then used to train and test a neural network. Fifty pictures were used for training and 22 for testing. Unusually, a two hidden layer MLP with 4 inputs, 12 nodes each in the two hidden layers and a single output was used. A 100% training success was reported for flank wear evaluation. During testing 95.5% success for flank wear accuracy of up to 0.1 mm was reported.

Jai *et al.* (1993), in their development of a TCMS fused four components of AE: 1st and 2nd enveloping signal, the differential signal, and the ring count signal. A 7-12-12-1 multi-layered perceptron neural network was used in the fusion stage, with the cutting conditions used as additional inputs. The single output represented the tool wear value. Their trained network was tested and validated 'on-line'. They reported a 96% accuracy rate under varying machining conditions.

Faced with unpredictable tool life in micro-drilling operations, Tansel and Rodriguez (1992) proposed a new approach to detect such failure. They performed drilling operations using micro-drills of 0.39 mm diameter and recorded the thrust force. From the recorded data four consecutive averages and four standard deviations were calculated. These calculated values were used as inputs to an ART-2 neural network architecture to estimate the ensuing tool condition. The presented data was classified into categories according to similarity of each set (i.e. normal-sharp or breakage-worn). The network was reported to have correctly categorised well over 95% of the presented data. Tansel and Rodriguez extended their investigation further by attempting to use either of only the 4 consecutive averages, or the standard deviations only. A

smaller number of categories were created, but with errors nearly twice as high compared to using both features simultaneously.

Wang and Dornfeld (1992), inspired by previous successful works by Dornfeld and others, proposed and investigated an in-process method of TCM. This method principally involved monitoring the progressive increase of flank wear during a turning operation by means of MLP neural networks. Cuttings tests were conducted using a 1000 Tree Lathe from which 300 samples of the raw RMS AE signals were recorded at three seconds intervals. From the recorded RMS AE, four dimensional features were each extracted viz.: mean, integral (energy), skew and kurtosis distribution, and the auto-regressive coefficients. The extracted values were used to train and test an MLP. Training involved using, within the inputs, an extra linearly interpolated feature and 30 AE samples, selected at 30 second interval. The inputs were scaled in the range -5 to +5 while the output were within 0.2 to 0.8 range. Initially, using only 5 nodes in the hidden layer, the inputs were varied from 6 to 2 features. The topology with 6 input features converged the quickest. Using the remaining unused data to test the network, it was reported to have accurately predicted progressive tool flank wear to within 10 % error with six hidden nodes.

Emel (1991), collected and processed data using a worn and sharp cutting tool at defined conditions (depth of cut, speed, feed rate, material hardness and tool wear levels). The processed results were to train three separate MLPs with 1, 2 and 3 layers respectively. Labelled and pre-identifiable samples were used to test each network and the classification rate per class noted. Better success rates were reported for the 3 layer MLP, which identified more correct classes of the labelled samples than either of those with one or two layers. Thus, Emel having done most of his initial TCMS based on pattern recognition techniques and recently implementing ANN, supported the postulation by other neural network based TCMS experts that ANN classify sharp-worn tools better than any other method (such as pattern recognition). In terms of percentage classification no such

quantification however was provided.

Guillot and El Ouafi (1991) used a milling machine to perform four test categories from which the cutting forces were recorded. The recorded forces were used in conjunction with the cutting parameters as inputs to an MLP neural network. The four cases investigated varied according to final signal inputs fed to the neural network. In the first instance, two cutting parameters (feed velocity and depth of cut) were fused with the 'most recently' sampled sensor signal. In case 2, only the most recent samples were used. In case 3, the normalised inputs of the most recently sampled signals were used whilst in case 4, the first derivatives of the sampled signals were used. Each case was conducted as a separate investigation, requiring training and testing. Results obtained showed cases 1, 2 and 4 performed better than case 3. Overall, using a limited range of patterns, correct interpretation of the tool condition was confirmed by application of simulated data. No quantification however of the system was provided to support this claim.

Making use of a single sensor input has been the approach followed by Tansel *et al.* (1991) who sought to predict chatter development. The proposed system was successfully used, and it identified 98% of the harmonic signals with over 90% accuracy (±5% error margin from short data sequences of 11 sampled points). Machine chatter is generated by forced or self-excited vibration and it degrades surface finish while reducing tool life. Tansel *et al.* set out to implement the sensed chatter by presenting typical chatter signals to two MLP based neural network architectures. One identified the system harmonics whereas the other was used to estimate its frequency, i.e. they analysed acceleration signals to predict chatter. When the two separate procedures were combined, an algorithm for identifying chatter and its frequency was obtained. A detailed discussion of this algorithm is provided in Tansel *et al.* (1991). Testing of this set-up was conducted, first based on digitised signals generated by a function generator. It was then tested on-line in a turning operation where it vas intended to detect

unstable vibrations. Accurate chatter development prediction was reported to have been achieved, hence substantially saving tool life. However, no percentage accuracy of this system was cited.

Moriwaki and Hino (1991), in their quest to develop a new method for the automatic detection of cutting tool wear and life in turning operations proposed an approach based on sensing the AE signals from carbide inserts and making use of its characteristic features for worn and sharp states. A 6-10-3 MLP network was employed to fuse the extracted features of the AE signals (mean, variance and moments). Results obtained confirmed that tool wear and life were correctly identified. However, no qualification of their findings were provided.

Tansel and McLaughlin (1991), interested in the detection of tool breakage in drilling operations, performed experiments from which the cutting force signals were measured. Experimental data was recorded together with simulated data and independently used as inputs to an ART2 network paradigm. A classification success rate of 97.2% was reported on the experimental data and 99.9% on the simulated data. Extending this method by carrying out a wavelet transformation on the sampled signals, Tansel *et al.* (1993) could detect severe tool damage just before complete tip breakage occurred in micro-drills. Of the 61 cases studied, direct classification was reported to have been reliably achieved, but no quantification provided. In further work, Tansel and McLaughlin (1993) proposed to compare the relative success rates of tool breakage detection by the ART2 method and the predominantly used supervised MLP architecture. Sighting inaccuracies and deficiencies in the MLP paradigm of unreliable decisions on the insufficiency of previous training, they decided to elaborate their work as reported in Tansel and McLaughlin (1991) to include an alternative supervised neural network paradigm instead. The Restricted Coulomb Energy (RCE) network was chosen and used to implement TCM. Obtained results showed that the supervised RCE paradigm was capable of 98% successful classification accuracy on presented data.

5.4. *Drawbacks to Single Sensor based TCMS*

The use of a single sensor signal in the development of a TCMS fails to recognise the complex and diverse nature of the cutting process (Lister, 1993). Such models are often less robust, unreliable and are generally not capable of 'total' TCM (ability to recognise incipient, partial, complete or catastrophic tool failure). The adoption of feature space dimensioning as a means of increasing input dimension whereby, various wear sensitive features are identified and extracted from a single signal, is debatable. This is because multi-feature extraction from a single signal does not constitute multi-sensing. Feature space dimensioning involves the representation of statistically independent probability distribution in just a single signal with minimal mutual information acquired compared to features extracted from more than one signal (Para *et al.*, 1996). Therefore, it is better to use more than one different source signals, as they contain more information, especially when used as inputs to an ANN.

5.5. *Multiple Sensor Inputs*

A single operational measurement can not satisfactorily describe the underlying effects of a cutting operation. Sufficient description by traditional mathematical models however is not achievable. Conversely, concentration on the non-linear principles and foundations of orthogonal cutting (used only as an illustrative example), would be futile, as the TCMS could become exhaustively sophisticated. Therefore, as an alternative to single-sensor based TCMS, the integration of several sensors has been investigated, complementing what has commonly been termed multiple sensor TCMS (Liu and Anantharaman, 1994; Dornfeld, 1990; Rangwala and Dornfeld, 1987).

A process such as orthogonal metal cutting involves a high level of noise coupled with the often changing cutting variables. If the noise level in a sensor signal completely suppresses its tool wear sensitivity feature, then without the presence of other sensor signals, its tool wear sensitivity is lost. If multiple sensors were in

place, the loss of sensitivity information from one sensor could be off-set and replaced if reliable information can be obtained from the other sensor(s) i.e. superior and better performance of such a system could be expected.

Barschdorff et al (1993a) mainly concentrated on the difficulties associated with varying the cutting conditions for tool state identification using force and vibration features (sequential forward search method) fused through an MLP neural network. Their interest was in identifying whether or not the ensuing tool state was either worn or sharp. The investigations began by attempting to class data whilst machining was conducted under constant cutting conditions. The main drawback from this investigation was its limited validity over a broader range of process parameters. They proceeded to train the network under varying cutting conditions. Testing showed that results varied depending on which features (force or vibration) was used. Overall, investigations utilising force features were better and in their next investigation, they used only force features but incorporated the cutting conditions as inputs. The results obtained were promising, scoring between 96.5 and 98% correct classification.

Barschdorff *et al.* (1993b) extended Monostori's work by carrying out turning experiments from which the cutting forces and AE signals were recorded under varying cutting conditions. They proceeded to extract 100 features from all the measured force and AE signals and these were used as inputs to a conventional MLP (reported in Barschdorff *et al.*, 1993b) and a novel self-organising ANN - the Condensed Nearest Neighbour Network (CNNN). The CNNN is a three layer network based on condensed clustering. Unlike MLP, CNNN does not have a fixed number of hidden neurons (specified by user/designer), but the number of its hidden layer neurons are problem driven and fitted during training. The performance of the two types of networks were compared for constant, varying, and complete inclusion of the process parameters in the input vectors. In all three cases, classification success rates of ≥95% and 97% were achieved by the MLP and CNNN paradigms respectively, with the most promising results obtained

when the cutting conditions were completely incorporated into the input vectors.

Chryssolouris and Domroese (1989, 1988) proposed four techniques and strategies for integrating multiple sensor signals from a cutting process amongst which were neural networks. Test cuts were carried out, from which the cutting forces, temperature, and acoustic emission were recorded for known tool states. A set of the recorded data were used to train the selected integrators. The learned parameters were used to provide an integrated estimate of tool state in the application phase. The neural network type used was a typical MLP with inputs being the wear and wear rate estimates from the process parameters. Two sets of tests and applications were conducted: constant feed rate; and variable feed rate tests, using the same test set-up periphery and materials. They concluded from subsequent analysis that neural networks provided lower mean square errors compared with the other three methods (i.e. they had the most promising and feasible approach to the development of the module). No quantitative values for the performances were provided.

Chryssolouris *et al.* (1992) proposed, investigated, and compared the performances of two approaches in the synthesising of multi-sensor information from a metal cutting operation. These approaches involved the fusion of multiple source sensor signals through ANN and compared the results with those obtained from methods based on statistical analysis (multiple least squares regression and group method of data handling or GMDH). Focus herein, is on the neural networks part of their implementation. This in essence was an extension of the work reported in Chryssolouris and Domroese (1989, 1988). Test cuts were conducted using a Daewoo Puma 10 CNC lathe, and the cutting forces (vertical and horizontal), tool-workpiece interface temperature, and AE signals recorded for known values of tool flank wear. The recorded signals were processed through a combination of methods, details of which are beyond the scope of this review. Initially, four sets of tests were conducted at constant feed-rate, depth of cut and cutting speed. Each set consisted of several machining experiments, with

each experiment in turn consisting of a specified machining time interval. Additionally, three further test sets were conducted at varying feed-rate and constant cutting speed. Using the obtained data the mean square error (MSE) of the trained neural network was evaluated. Overall, two neural network architectures were trained: a three layer network with 4 nodes in the hidden layer; and a four layered MLP network with 8 nodes each in the hidden layers. Results obtained during the training showed that high MSE values were achieved when wear estimation was based on single sensors only. With multiple sensors, the neural networks provided lower MSE values for both test condition categories. Overall, lowest MSE (0.003 mm) were realised when the architecture with two hidden layers were used. The trained networks were verified by application of a series of simulated tests and 95% certainty in tool state identification was reported.

Chung *et al.* (1993), cited tool wear levels as being solely responsible for the level of chattering on a machine tool. To investigate this, they performed test cuts on a conventional centre lathe using carbide tool inserts, and existing records of the AE and acceleration (vibration) signals. Time displays of the recorded signals clearly showed the coupling between chatter and tool wear with the surface profile becoming rougher as the AE and acceleration signals undulated. For better visualisation, they applied time series models and calculated the average band energy (frequency dependent) on the data and used the extracted features as inputs to a neural network. The auto-regressive (AR) time series analysis of the two data types yielded four features each. The neural network implementation was performed by first using the four time series features of each signal on its own, then as a combination, and finally as the band energy. Success rates of 70-90%, using time series parameters and 80-100%, using frequency band energy levels were quoted. However, these figures were applicable only on the investigated cutting parameter range.

Jammu *et al.* (1993) using a proposed unsupervised neural network algorithm

(Single Category-Based Classifier (SCBC), in conjunction with *KSOM* and ART2), performed extensive cutting tests in order to investigate tool breakage detection and compared success rates achieved via these methods on a vertical lathe. The sensor signal inputs used comprised of the fusion of vibration, ultrasonic energy (same source as AE), and current inputs to the carriage drive motors. In addition to these signals the feed-rates in x- and z-directions, and the spindle speed were utilised as further inputs. Data containing the breakage signatures were recorded as cutting progressed until a breakage occurred, at which point, a total of 6 such outcomes were achieved. The recorded signals were then analysed through application of a selective time windowing, i.e. block averaging, to reduce the data size. Using four processed measurements from each test the relative effectiveness of each method was evaluated. On-line test results showed that whereas the two traditional unsupervised classifiers (*KSOM* and ART2) produced false alarms and some undetected faults, SCBC detected all failures without producing any false alarms. However, no quantification of the test results was provided to substantiate this claim.

Javed *et al.* (1996) devised and tested on-line, what they claimed was a demonstrator system for flank wear and chipping identification. The system was described as capable of distinguishing discretely three levels of flank wear and two levels of chipping. The parameters of interest were encoded in three-bit form with the inputs comprising of components of cutting forces, vibration and acoustic emission. A BP trained neural network was used and testing achieved 100% success off-line. It is also reported that the demonstrator system was tested on-line and 100% success achieved. The reference however lacks sufficient detail, especially with regard to training and test conditions.

Kakade *et al.* (1995) utilised a decision based neural network to integrate cutting forces and AE signals in their studies of the influence of flank wear on the respective signals. Machining test cuts were conducted from which the cutting forces and the AE signals were recorded. Features from the parameters were used

to train and test the designed network. Different input parameter combinations were used in training and testing, i.e. training with either cutting forces and AE only, or combination of both. They concluded that by combining different source signals for tool wear identification, classification success rate considerably improved the performance of the system.

Kamarthi *et al.* (1991), using vibration signals fused with cutting force signals, trained and implemented their TCMS via a Kohonen self-organising map. They collected labelled samples (known wear depth on cutting tool) which were then analysed through their FFTs to obtain labelled patterns. These labelled patterns were used to train the *KSOM*. Seventy patterns were collected for each of the three cases and used in training the *KSOMs*. The trained *KSOMs* were identical in all respects (same training conditions) except for the differences exhibited in the 70 input patterns (wear degree). On-line implementation achieved satisfactory and reliable results - close to 95% accuracy prediction, which was similar to that obtained by Burke (1989) who used a similar neural network method (ART).

Ko and Cho (1994), fused vibration and cutting force signals from a milling process to obtain a feature vector which was fed through a neural network to yield the tool wear state. A success level of over 97% was claimed to have been achieved.

Liu and Anartharaman (1994) utilised the thrust and torque signals from a drilling experiment to predict tool state and flank wear measurement. Drilling tests were conducted using fresh and worn-out drills, and a feature extraction process carried out on the two recorded signals, obtaining eight indices. These eight indices were used, together with a ninth feature representing the drilling condition as the inputs to an MLP neural network. Various architectures of MLP (variable hidden layers) were trained on 46 data sets (comprising experimental and interpolated data) and tested with a further 50 data sets recorded at different drilling conditions. Reported results showed that, when the trained networks were cross-validated for

on-line drill wear classification, 100% accuracy was achieved by all the trained network architectures. Liu and Anantharaman further extended the research work to include the utilisation of experimental results in the measurement of drill wear. The same neural network architectures as described above were employed, except that the output was principally the measured flank wear. Forty five data sets were used to train the networks. Test results obtained using 49 data sets, sampled at a different drilling conditions from the training sets, showed a minimum on-line error measurement of 0.4%, a maximum of 19% and a mean error of 7.73%.

Liu et al. (1991, 1990) were concerned with the lack of research towards the condition monitoring of tapping tools. In view of the importance of tapping operations in general, they proposed and investigated the use of ANN in tapping tool diagnostics and one of the tool features investigated was tap wear. In Liu et al. (1990), they recorded the torque alone; and proceeded to perform a feature selection process on the recorded values. From these, 3 indices were extracted, namely: the average peak-to-peak torque, the modified RMS torque, and prediction errors of the torque signals. The wear conditions were categorised into 4 classes - fresh, slight, medium and severe wears. An MLP network with 2 hidden layers of 12 and 7 nodes respectively was used, i.e. 3-12-2-4, and trained using 16 data samples. Testing involved using two separate data samples collected when tapping a steel and composite material respectively with training performed only on one data set. Testing yielded a 95.8% success rate for the same workpiece train/test data and 100% for the composite material. The virtual non-detection of any misjudgement in the latter case could be partly attributed to the fact that dissimilar data categories have been compared. The results could well have been a 100% misjudgement and therefore this conclusion bears no meaningful significance.

In Liu *et al.* (1991), thrust, torque and lateral forces recorded from a tapping operation were used as inputs to the neural network. Artificial tap wear was generated by accelerated grinding of the clearance surface In total, 16 tests were

carried out for wear monitoring purposes. A feature selection (mainly statistical) was carried out, extracting 10 features from each single cut. These were normalised and used to train/test the designed network. The ANN was a 10-12-2-5 MLP, the 5 outputs representing the 5 investigated tap features (wear, misalignment, bore over/under sizing, normal). Testing the trained network resulted in only one misclassification out of the 40 tapping data used (eight from each category), yielding a relatively high successful rate of 97.5%.

Implementation of mapping technique via pattern recognition of tool wear/failure using neural network algorithms has been employed by Noori-Khajavi and Komanduri (1995; 1993). They were interested in predicting the wear land and tool condition, from acquired thrust and torque signals, and their respective subclass numbers (i.e. 1, 2, ...N) after training. The degree of tool wear or sharpness together with its associated sensor signals constituted a subclass. With classifications using BP trained MLP requiring three outputs (sharp, worn and failed tool respectively), they represented these tool states as their respective classes. Implementing these on-line via a trained network, it was reported that tool state was correctly classified. In effect, three methods (clustering, mapping and decision surfaces) were employed and tested via an MLP. Noori-Khajavi and Komanduri concluded that the integration of noisy sensor signals via neural networks actually led to a deterioration of drill wear estimation. They were of the opinion that TCMS, if effectively designed, would be simple, and therefore unnecessary to implement two or more sensor signals when one was adequate. Apparently, that contradicted the earlier findings of Rangwala and Dornfeld (1987), who found it useful to utilise extracted features to supplement other sensors rather than on their own. Noori-Khajavi and Komanduri argued that such extracted features were still noisy. However, the degree of accuracy of their TCMS was not reported.

Markos *et al.* (1993), also used cutting forces, vibration and cutting condition parameters on a milling machine and were mainly concerned with the

identification of tool breakage. Forty input patterns were used to train the network, comprising of the calculated and normalised parameters from resultant cutting forces, and a breakage/no breakage flag output. Breakages were reportedly predicted with 100% accuracy. Tool wear rates were also measured but, tool wear being a non-linear process, was difficult to measure compared with definitive breakage. They reported that a more complex network architecture was required to accurately predict tool wear and did not proceed any further.

Masory (1991), performed single point cutting test experiments, measured and recorded the tool tip temperature, the true root mean squared value (RMS) of the AE signal, and the three components of the cutting forces. Five sensor signal pattern vectors and two binary inputs representing tool types were presented to an MLP network. Three neural network architectures were trained and based on results obtained, the best one was selected. The desired output sought by Masory was estimated values of flank and crater wear. He reportedly achieved very accurate wear estimations but no quantification of the results was provided.

Monostori (1993) used the vibration and cutting forces from both turning and milling tests and an MLP neural network technique to perform tool state classification, continuous estimation of tool wear and the inverse modelling of the cutting process. Herein, focus would mainly be on the reported achievements in tool state classification. Monostori's experiments involved carrying out milling and turning test cuts utilising both fresh and worn inserts, recording the cutting forces, and vibration components from each cut. Using the measured signals, statistical and spectral features were computed, followed by performance of a sequential forward search or feature selection process using the same selection criteria as Dornfeld (1990), Dornfeld and Rangwala (1990; 1987) and Rangwala (1988). Monostori used the force data to perform classification tests using an MLP neural network comprising 6 inputs, 6 hidden nodes and 2 outputs. The first set of tests involved training and classification using only the processed signal features, i.e. at constant cutting conditions. Obtained results showed a 100%

recognition ability for all the patterns tested. Monostori then progressed to include in the next set of tests, limited cutting conditions to the input signal features (i.e. altered the cutting conditions by factors of 0.33 and 1.5). The results deteriorated to between 90-95% success rate for worn tool recognition but stayed the same (100%) for sharp tools. To eliminate any ambiguities complete incorporation of process parameters as inputs was performed. Once more a 100% recognition of the tool state was reportedly achieved. Monostori concluded that the results were dependent upon network topology, and a classification performance of between 96.5% and 98% was generally the norm.

Moriwaki and Mori (1993a, b) proposed a method for tool state recognition based on sensor fusion via neural networks, and used their system to detect the onset of chatter, chip tangling and tool wear (at the initial, middle, final stage). These features were reported to have been successfully recognised using as inputs to a 6-10-5 MLP neural network, time domain values of the cutting force, and AE. They began their investigation by first embarking on finding a suitable neural network structure and an improved learning procedure from conventional techniques that were then common. Using data from their experimental investigation and the proposed MLP neural network structure which was trained using their improved learning method, a success rate of 96.1% was reported.

Rahman *et al.* (1995a) continued their TCMS development by attempting a different neural network framework. Two features (mean and variance) of the dynamic cutting force signal were extracted through application of a wavelet decomposition technique. Further decompositions were performed to obtain a nine dimension input vector from the mean, variance and coherence coefficient of the original signal. These were used as inputs to a Kohonen feature map (*KSOM*) with 9 input nodes corresponding to the number of input features and 4 output ones. In total, 147 samples of input data were collected from experiments of varied cutting conditions and tool geometry. An additional window was used in the output nodes to restrict its values to 0 and 1. The final diagnostic results

showed that for two types of training samples implemented (fresh and worn, fresh) the success rates in both cases were marginally higher than 90%. They concluded that though the *KSOM* required no labelling of data, the occurrence of any new phenomenon would warrant an external interpretation of the new class, an observation that Burke had earlier suggested.

Ruiz *et al.* (1993) and Choi *et al.* (1990; 1991) used three sensor signals. Choi *et al.*'s approach, methodology and results were similar to Dornfeld's (1990) but unlike Dornfeld, they developed their system for applications in a shop environment. Ruiz *et al.*'s methodology however could be viewed as similar to Dornfeld's, except that it interchanged Dornfeld's cutting forces with temperature. Ruiz *et al.*, also introduced a second transformation in the feature extraction block and the extracted features were fed via four separate MLP neural net architectures. Wear recognition results for the four networks tested were presented and success rates higher than 90% achieved. Generally, high success rates were obtained as a result of increasing the number of input signals and hidden nodes in the MLP.

Teshima *et al.* (1993), interested in the estimation of cutting tool life and wear type accrued, performed tool condition monitoring in order to achieve their goal. They began by proposing to synthesise on-line tool information and cutting parameters by an image processing method of the cutting tool in post-process monitoring, so as to apply it to predict the next cutting process that could take place under different cutting conditions. Using an experimental set-up consisting of a camera, video tape recorder, colour data control device and display, a PC and an image processing board, 80 pattern data sets (input-output pairs) were collected for training their network. These patterns broadly consisted of data representing the tool state and the cutting conditions, used as inputs, with outputs being rest of tool life and wear type. Tool life was judged on the basis of observable (subjective) factors such as chip form, colour and roughness of the cutting surface. For the neural network, an MLP algorithm comprising 253 inputs (tool image data and cutting conditions), one hidden layer of 65 units, and an output

comprising 6 units provided information on wear type and tool life. The 80 pattern data sets obtained during their experimental investigation were divided into 3 groups: a training set, comprising 35 data patterns; an on-line evaluation set of 35 pattern sets; and the remaining 10 pattern sets for cross-validation of the trained net. The training was performed and evaluated and an optimum point for the sum-squared errors found. Although the optimum obtained was somewhat high, Teshima *et al.* were much more interested in finding an appropriate network configuration, and were therefore satisfied with such an outcome. Testing the trained network involved using the remaining 10 validation pattern sets from which they achieved standard deviations averaging <0.09 from the output results. Test results obtained confirmed the developed system as being capable of accurate measurements of tool life and wear type with maximum errors of 16% and 24% respectively.

Contradictory views will inevitably occur in past, present and future research as the drive for better TCMS continue. The primary sources of these controversies it would seem, stems from the fact that researchers are exposed to a variety of neural network types and architectures. This fact is compounded by the numerous sets of rules on the definition of a standard network architecture or topology. A second point to note is the method of sensor tapping from the various sensor signals potentially available. Reaching a decision on which sensor signal to use is difficult and this is made worse by the subjective arbitrary nature of the selection of processing techniques. The same results generally would not be expected but a trend would be indicative of an appropriate approach. These descripances, one could argue, could be attributed partly to the novelty of neural networks, the complex and diverse nature of metal cutting processes, and/or the complexity of the tool wear process itself (Lister, 1993).

5.6. ANN Architecture Driven TCMS

5.6.1. Utilisation of Feed-Forward MLP

Chen and Du (1996) introduced a new method of ANN architecture selection based on a proposed training method. In order to test the selected network architecture, they used, amongst other practical engineering monitoring and diagnoses examples, TCM in turning. Principally, Chen and Du demonstrated that the best method to select an ANN structure was to train many architectures, then that with nearest similarity to the training data will yield optimum solution. They provided elaborate mathematical background to substantiate their proposal, which can be summarised as attempting to minimise the total similarity in the ANN mapping of training samples. Thus, optimum architecture is that which realises this goal. They demonstrated the applicability of this hypothesis by varying the number of hidden nodes in an MLP of single hidden layer, from 7 to 12 nodes in single increments. Data representing eight different tool conditions, were collected based on a combination of eleven indices calculated from cutting forces, vibrations and cutting power. In total, 360 data (180 training and 180 testing, similarly distinguished) samples were collected at variable cutting conditions, tool inserts (coated and un-coated) and workpiece materials (steel and Al alloy steel). During training and testing the similarity measure and success rate was recorded. As predicted, the best success was scored by the network with least similarity measure, that with 9 hidden nodes (1201 and 69.49 respectively). This represented an increase in the success rate of nearly 3% over the other networks, and they concluded that its potential applicability as demonstrated was very efficient.

Noori-Khajavi and Komanduri (1995) proposed and used an MLP as a classifier to predict drilling tool state when data from a worn, sharp and fractured drill were introduced to the system in a block. This method can be viewed to be different from aforementioned methods involving straight forward MLP applications, as it

classified complicated surfaces and regions using decision surfaces or boundaries introduced as class members of either a worn, sharp or a fractured tool. Their proposed network had three outputs corresponding to the three possible predictable states of the tool. They found that in real time the surface boundaries of worn, sharp and fractured tools could not linearly be separated. Members of either class encroached the boundary where it clearly did not belong and so concluded that their method was not suitable for drill wear classification.

Yao and Fang (1993) carried out turning experiments from which they recorded the cutting forces at different cutting conditions. This data was used to train MLPs with different number of neurons in the hidden layer containing different transfer functions. Firstly they trained their neural networks with different topology and obtained the RMS errors for each function as the number of neurons in the hidden node was varied. They plotted a graph of RMS errors versus number of hidden neurons for the three selected transfer functions. Results obtained clearly showed that beginning with 7 neurons in all three topologies the RMS error decreased and reached an optimum at a hidden node number of 12. Beyond this number there was a dramatic increase in RMS error. They stated that their results were inconclusive. Clearly the number of neurons in the hidden layer(s) was a crucial and complicated issue. Nonetheless, their investigation clearly showed that it is misleading to suggest that the more the number of neurons in the hidden layer the more powerful the network.

Guillot and El Ouafi (1991) using AE, cutting forces and acceleration data from a milling operation employed three MLP network types both having the same number of input and output nodes but a different number of hidden nodes (20, 10 and 5) to identify tool breakage. The gain and momentum of the two network topologies were set to the same values and trained. Test results showed that the best convergence was achieved with the network architecture having the least number of neurons in its hidden layer as it had the smallest percentage error and number of passes considered.

Liu and Ko (1990) using MLP structures embarked on a similar study as Yao and Fang (1993) but did not limit their study to only three neural network architectures. They investigated six MLP structures with two input nodes and a single output node, varying the hidden nodes from 7 to 12. After training their networks a success rate chart was made listing the percentage scored by each in identifying the tool state when the same data sets were used for the various configurations. Those with <9 nodes scored up to 83.3% whereas those with >10 nodes achieved 86.6%. Liu and Ko's results when compared to the likes of Rangwala and Dornfeld (1987, 1990) and Yao and Fang (1993) who used the same neural network architecture but not the same topology and theirs achieved fractionally lower success accuracy. The reduction in the percentage success could be attributed to the fact that Liu and Ko did not pre-process the input signals as the latter did, otherwise no apparent reasons exist.

5.6.2. Radial Basis Functions (RBF) Networks

Elanayar and Shin (1995) while tackling the tool wear non-linearity problem on turning experiments data by the application of neural networks based on approximation theory called Radial Basis Functions (RBF). These types of ANN are underlined by the use of a linear combination of translated functions to smoothen and approximate continuous functions. They investigated 3 different basis functions to aid in the tool wear identification process. Flank and crater wear prediction results from simulated data for the three basis functions were reported as satisfactory achieving the same success rate in each case. When test data was applied an un-quantified accuracy rate was reported which was noted to be lower compared to that obtained using the simulated data.

5.6.3. Kohonen Self-Organising Maps (KSOM)

These networks have been utilised by amongst others Kamarthi *et al.* (1991), Govekar and Grabec (1994), Noori-Khajavi and Komanduri (1995) and Govekar *et al.* (1991). *KSOM* are based on competitive learning and constructed from fully

connected arrays of neurons requiring no output data for training. Usually the *KSOM* is such that it possesses two sets of weights: an adaptable and a fixed set. When a pattern is presented to the system, the adaptive weights are computed followed by a series of adaptation processes whereby the self-organising map attempts to match the unknown pattern according to the Kohonen rule (Govekar and Grabec, 1994). Kamarthi *et al.* (1991) used a 20x20 grid (i.e. 400 output nodes) chosen arbitrarily. Govekar and Grabec (1994) proposed that their results could be improved if they further trained their network using a different Kohonen training method, the Linear Vector Quantisation (LVQ) which is a supervised form of *KSOM*. This they performed and reported in Govekar *et al.* (1991) where a significant improvement in the results was reported.

5.6.4. Adaptive Resonance Theory (ART) Networks

Adaptive Resonance Theory (ART) has been used by, amongst others, Burke (1989) and Tansel *et al.* (1993). Burke (1989) mainly concentrated on extending the works of Rangwala and Dornfeld (1987, 1990) to use ART-2 and other unsupervised algorithms such as k-nearest neighbour and clustering techniques. Tansel *et al.* (1993) used the sampled cutting forces from a milling operation and applied a wavelet means of transformation on them. The transformed data was then implemented through an ART-2 type neural network. Tansel *et al.* obtained results through their implementation which suggested that ART-2 was capable of detecting tool failure but did not quantify their success.

Li *et al.* (1996) used AE inputs to a multi-ART2 neural network for detection of tool condition. Principally, three similar ART-2 architectures were connected in parallel and fed the same input features. Each was trained to predict only one each of severe tool wear, tool breakage and tool chipping. The performance of the devised TCMS was evaluated by conducting experimental test cuts for various conditions, from which the recorded data was digitised, processed and fed to the net. Obtained results seem to suggest that the integrated multi-ART2 achieved a

93.75% reliability (correct categorisation) under varying cutting conditions.

Kumudha *et al.* (1994) used an ART neural network to monitor the condition of a cutting tool off-line. Sixty input pattern vectors consisting of the cutting conditions and 3-components cutting forces were used and, they sought to categorise this based on the level of tool wear. The input data consisted of three classes (varying flank wear length) normalised to lie between 0 and 1. Thirty were reserved for testing and the remainder used for training. They reported that the trained network correctly categorised 90% of the presented data correctly.

Choi *et al.* (1991) performed TCM using both MLP and ART-2 networks (cf. Burke and Rangwala, 1991). In the first part they experimented with AE and cutting force data from a turning operation using a 3 layered MLP with variable number of neurons in the hidden node. Above 6 nodes in the hidden layer they reported a deterioration in the correct recognition rate, scoring most successes with 4 and 6 nodes (96%). For efficiency sake they decided to choose the 4 hidden node architecture (cf. Yao and Fang, 1993), and embarked upon choosing a suitable range of cutting conditions under which the monitoring system could be successfully implemented. They concluded that the system worked well for a wide range of cutting conditions provided the same cutting conditions were used off-line for training and on-line during implementation. Effectively their system was rendered specifically applicable as it was restricted to the defined cutting conditions where it was expected to perform well. For their ART-2 application they presented two groups of data to the system. Each group consisted of eight data representing worn and sharp tools. They reported that their network correctly distinguished between sharp and worn tools but did not specify the extent of reliability of categorisation.

ART remains adaptive after training, and in terms of classification accuracy, achieves virtually the same score as BP. If during implementation a previously unknown pattern is introduced, ART alerts the system by devising a new category

cluster for it and can shift into the training mode simply by external interpretation of the new category (Burke and Rangwala, 1991).

5.6.5. Restricted Coulomb Energy (RCE) Networks

Tansel *et al.* (1992) used RCE to predict the tool life of a micro-drill. In their experiments they measured the micro drill thrust force which was encoded and then proceeded to calculate four consecutive averages and standard deviations during each drilling operation cycle lasting between 4 and 7 seconds. They used the encoded and calculated averages from 61 different drill cycles and an RCE neural network with eight inputs and two outputs to evaluate their proposed system. Initially 31 from the 61 encoded samples were used to train the network and the remaining 30 used to evaluate the trained network. The RCE network was reported to have correctly recognised 90% of the normal and tool failure cases.

5.6.6. Condensed Nearest Neighbour Networks (CNNN)

Barschdorff *et al.* (1993b) used two kinds of ANNs in their classification experiments of cutting tool state in a turning operation: the familiar MLP and a relatively new unsupervised paradigm, CNNN. As inputs to the designated CNNN Barschdorff *et al.* used the J-dimension feature space (patterns) of the cutting forces and AE signals. Training was performed by presentation of patterns containing two desired classes (worn and sharp). During testing if a presented pattern could be matched exactly to an existing (trained) cluster its nearest subclass was sought and the pattern attached to that. Obtained results showed that this newly proposed algorithm performed better than the MLP in terms of percentage success, had a high convergence rate and self supervising ability.

5.6.7. Serial Combination of Networks

Ghasempoor *et al.* (1996) presented a method for flank wear estimation from simulated cutting force signal using a serial combination of MLPs. The second

MLP (NN2) used the cutting conditions and estimated wear length to predict the cutting forces. The first model (NN1) estimated the next value of flank wear from the cutting conditions and past values of flank wear estimates and cutting force. While NN2 was trained off-line NN1 was trained on-line. They concluded that studies conducted that far using simulated data showed that their TCMS model was capable of accurate flank wear estimation. They proposed to attempt to implement experimental data.

Venkatesh *et al.* (1994) used two types of ANN to perform TCM: standard MLP (no memory) and two recurrent types (with one and two phase memory). The inputs to these networks consisted of the cutting conditions (feed and speed), the cutting force signal, and real time. The devised TCMS was such that by flicking a switch, the system could be retrained or accuracy improved while the TCMS operated on-line. Training utilised simulated data, meanwhile testing was evaluated for four cases. The first three cases corresponded to utilising simulated data while the last involved actual experimental data. Obtained results were poor at diagnosing tool wear with the ANN without memory performing better. No quantification however was provided.

Kamarthi (1994) devised a novel fault-tolerant neural network model for flank wear estimation in turning by combining three types of neural networks. The first level which received the sensor signal inputs consisted of *KSOM*, whose n-outputs were fed into corresponding RBF networks. In the final stage a recurrent network used the RBF outputs as its inputs from which flank wear was estimated. In essence Kamarthi sought to develop a neural network structure that combined both supervised and unsupervised learning, and the hybrid network reputedly offered a shorter error convergence time than the popular MLP. Turning cuts were performed and the AE, two components of vibration and three components of the cutting force were recorded. In total 3 groups of data sets were collected: the first set was used for training whereas the remainder was used to evaluate the trained networks. Eight networks of exactly the same topology were designed. The first

seven were trained using uni-variate ARMA AE, force and vibration combinations and the eighth trained using only force and vibration combination. By computing the network output results' mean, standard deviation and RMS, it was concluded that their low estimation of error offered an attractive real-world application. The networks with only force and vibration used as inputs were noted to have performed better.

Leem and Dreyfus (1992) developed a hybrid ANN architecture for on-line tool wear monitoring in metal turning, by combining *KSOM* and a newly developed supervised feed-forward Input Feature Scaling (IFS) algorithm. Turning tests were conducted on a tree lathe and the cutting forces and AE recorded and digitised for three tool types at different cutting conditions. Using the recorded values of the acquired parameters (AE and cutting forces) 32 points each were deduced from which four statistical features (mean, variance, skewness and kurtosis) were obtained as final input features. Using the designed network with sequential feed from *KSOM* to IFS, the designated input data was used. The hybrid network's task was to classify the tool data into three classes; fresh, medium worn and worn. Test results showed successful classification of the tool states of $\approx$ 92%, when IFS was used. Furthermore, a blind two class segregation system (worn/fresh) yielded 94%. They concluded that their method dispenses off-line feature selection procedures and was a superior practical system compared to implementation of straight forward MLP or ART.

5.7. Signal Processing Methods

The noisy nature of sensor signals from a metal cutting process implied that the useful components of the signal had to be extracted from the contaminated signal. During signal processing, features were generated and selected by a heuristic trial and error approach based on certain physical considerations (Ruiz *et al.*, 1993). This approach often employed a systematic generation of possible parameters to evaluate the state descriptors. Usually, the first transformations were obtained

through application of the FFT or wavelet transforms. Others, however, have found it necessary due to the high dimension of the measurement vector to reduce the transformed vector by implementation of a features selection process. These features normally consisted of components of the data string that showed maximum sensitivity to tool wear. The approach could be structured on a plan consisting of several levels as summarised in Fig 5.1

The transformation on each level was arbitrarily chosen, with the only restriction being the time required to compute the features required to describe wear from the sensor signals. The structure shown in Figure 5.1 for tool wear identification features, proposes that only the subset of features with the best discerning capabilities need be considered from the sensor signals. Since the

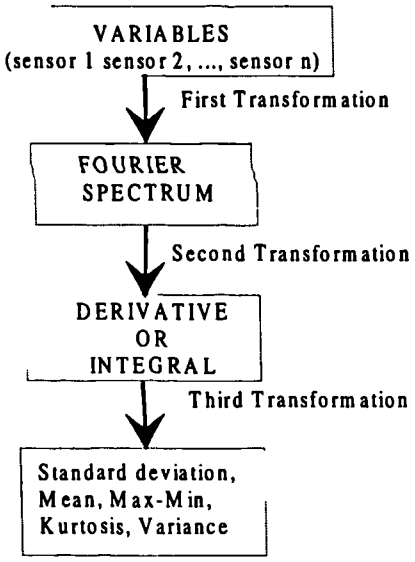

Figure 5.1: Feature generation plan and signal processing

selected features are identification method driven, their selection for neural network applications would depend on the topology of the network, i.e. a perceptron can cope well with mean values of forces whereas an ART whose inputs consists of the kurtosis (4th central moment of a Gaussian distribution) other than the mean values, would yield better results. Generally, signal processing has involved examining and extracting time and frequency domain

features for each of the chosen sensor signals, with a large interclass (mutual) variance and a small intraclass (within) variance. A summary of the signal processing methods and pursuance of a feature selection process are provided in Table 5.1.

5.8. Summary of reviewed methods

It is evident that ANNs have the potential of replacing the human operator, who is subjective and relatively inaccurate in deciding whether a cutting tool is performing well or not (Chryssolouris and Guillot, 1990). Classification and prediction of tool state for a TCMS with single and multiple sensor signal inputs have been reviewed, and from these it becomes evident that superior performance via neural nets could be achieved when information from multiple sensors are fused.

Neural networks generally suppress noise better because loss of sensitivity on one sensor domain can be offset by that from the other(s), provided the signals were sensitive to tool wear. In the same respect, the maximum amount of information on the tool state is potentially better achieved through multi-sensor signal inputs whereby each input contributes to a varying degree thereby increasing the accuracy of prediction or detection of the system, thus covering a broader range of the operating conditions. Neural networks are particularly suitable for TCMS because they can learn non-linear relationships. Parameter estimates from sensor based information and the actual parameters are better when done by neural networks than most statistically based methods such as linear regression, with greater sensitivity to deterministic errors in the sensed information (Kamarthi *et al.*, 1991).

There generally seems to be widespread agreement on the postulation that frequency spectra analysis reveals more on the cutting tool state via the determination of wear sensitive frequencies. However, Kamarthi *et al.* (1991) are of the opinion that a postulation based on the assumption of a number of hidden

classes in a pattern with clearly defined membership, preclude that its validity over a wide range of application is questionable.

Overall, neural network implemented TCMS could be viewed as a two level problem consisting of an initial training phase, and an implementation (application) phase (Chryssolouris and Guillot, 1990).

5.9. Conclusions

The literature survey shows first and foremost that both supervised and unsupervised neural network architectures have been applied in the TCM problem with fairly similar results being achieved. This could be partly attributed to the fact that supervised and unsupervised neural network paradigms represent rather extreme ends of a spectrum, and researchers using neural networks often design architectures that incorporate facets of each.

From this review it is evident that the most widely applied neural network architecture has been MLP which would appear to be associated with acceptable error prediction levels, and its rate of convergence adequate for TCM applications. The differences in MLP architecture in terms of its topology have been widely investigated and this showed that depending on inputs and outputs, an optimum number of hidden nodes exist for maximum performance. The benefits of using MLP include: its ability to perform a wide variety of learning; ability to deal with input environments containing outliers; and its ability to be able to classify without imposing assumptions. Multi-layer perceptrons are particularly suitable for high speed real-time application tasks such as TCM where the amount of data entering a typical three sensors' based system per second exceeds a gigabyte.

Further conclusions can be summarised as follows:

- The need for multi-sensor inputs in TCMS has largely been tackled, but in most cases insufficiently so. Mostly, a feature space dimensions selection

procedure was carried out where more than one feature was extracted from a single sensor, and this does not constitute a multi-sensor approach.

- There is need for additional machining operations to be investigated, apart from turning and drilling operations, such as boring and grinding, and multiple tools geometry used to extend and generalise the application of obtained systems. Also, more understanding of the various machining processes - wear and failure mechanisms is required.

- Generally, the majority of developed TCMS based on MLPs require retraining should a new decision class be encountered in operation either during testing or real-time application. There is therefore the need to address the issue of a multi-level system capable of unprocessed data handling. A truly realisable TCMS ought to aim for on-line applications with bulky data handling capability.

- The literature survey found little evidence in support of the proposition that networks were sensitive to changes in the cutting parameters, although the issue has not been adequately explored. In most instances the networks were trained with data sampled using only one set of cutting conditions, or only those conditions that were available from the machine controller were used. Using a wide range of the cutting conditions rather than a limited number of specific values might be more appropriate.

A better TCMS needs to accommodate the complex and diverse nature of the metal cutting operation. The main objective of the study outlined in this thesis therefore can be summarised in a sentence as ***"perform TCM by identifying and classifying tool states using acquired multivariate process parameters of the cutting operation and MLP ANNs"***.

The survey carried seem to suggest that most of the surveyed TCMS have not been successful implemented primarily because inadequate sensor information

and machining process models have been utilised, which did not satisfactorily reflect the process complexity. The outlined study involves the utilisation of not only one sensor signal, but also a multitude of sensor signals. Since it is difficult to emulate the human operator who is subjective and inaccurate in order to develop a TCMS, it is sufficient to develop a system that can be employed in the systematic monitoring and diagnosis of cutting tool conditions (wear levels, chipping and/or fracture), by learning and identifying tool states from experience, thus recognise and localise tool failure scenarios.

A process such as orthogonal metal cutting involves a high level of noise coupled with the often changing cutting variables. If the noise level in a sensor signal completely suppresses its tool wear sensitivity feature, then without the presence of one sensor signals, its tool wear sensitivity cannot be utilised as it is lost. Had multiple sensors been in place, the loss of sensitivity in information from that sensor could be off-set and replaced if reliable information can be obtained from the other sensors.

A schematic diagram showing the various parts of the anticipated TCMS is shown on Fig. 5.2.

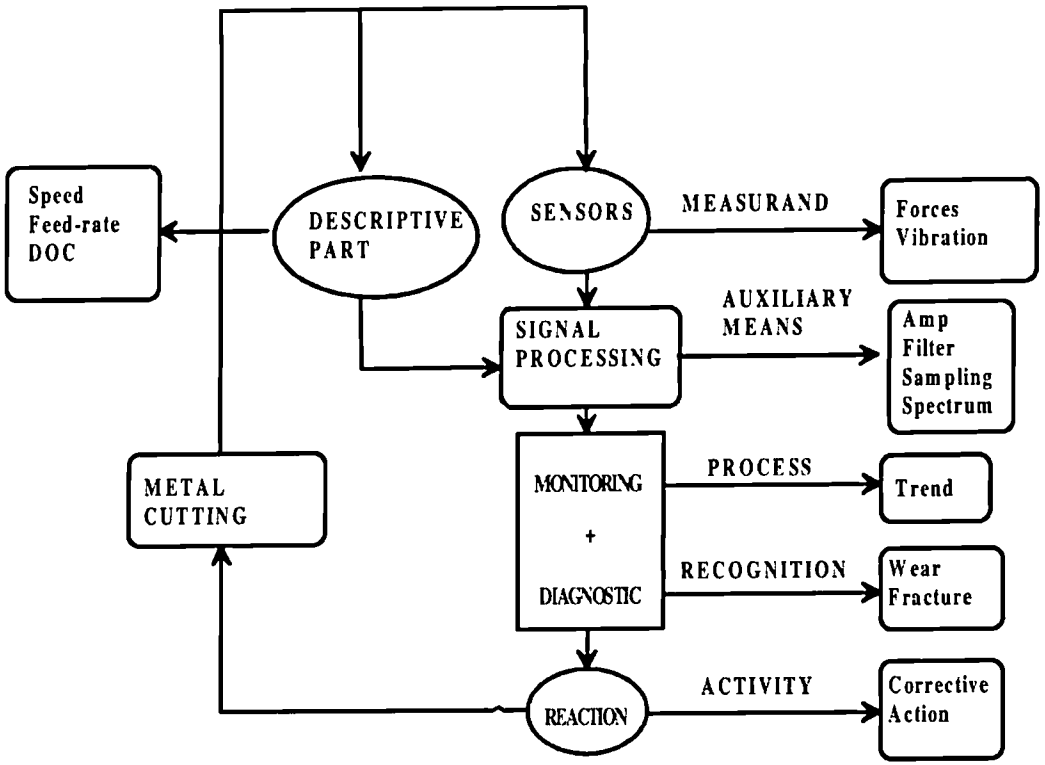

Figure 5.2: Schematic Diagram of Envisaged TCMS

TABLE 5.1: Sensor Signal Inputs Types

Author(s)	CF	AE	T	VC	SMC	FR	DC	CS	TO	IM	S
Noori-Khajavi & Komanduri (1995)	√								√		√
Zhou et al (1995)	√										
Govekar & Grabec (1994)	√										
Tarng *et al.* (1994)	√										
Lui & Anantharaman (1994)	√								√		
Ko & Cho (1994)	√			√							
Purushotharnan & Srinivasa (1994)	√					√	√	√			
Tansel & McLaughlin (1993)	√										
Tansel *et al.* (1993)	√										
Yao & Fang (1993)	√					√		√			
Ruiz *et al.* (1993)		√	√		√						
Markos *et al.* (1993)	√			√		√	√	√			
Jammu *et al* (1993)				√	√			√			
Teshima *et al* (1993)						√	√	√		√	
Monostori (1993)	√			√							
Moriwaki & Mori (1993)	√	√									
Barschdorff *et al* (1993)	√	√									
Tansel *et al.* (1992)	√										
Burke (1991, 1992,1993)	√	√				√	√	√			
Guillot & El Ouafi (1991)	√										
Masory (1991)	√	√	√								
Tansel *et al* (1991)				√							
Emel (1991)		√				√		√			
Elanayar & Shin (1991)	√										
Kamarthi *et al* (1991)	√			√							
Govekar *et al.* (1991)	√										
Choi *et al.* (1991)	√	√									
Dornfeld (1990)	√	√			√						
Rangwala & Dornfeld (1990)	√	√				√	√	√			
Elanayar & Shin (1990)	√										
Choi et al (1990)	√	√			√						
Liu & Ko (1990)	√			√							
Burke (1989)	√	√				√	√	√			
Rangwala (1988)	√	√				√	√	√			
Chryssolouris & Domroese (1988, 1989)	√	√	√								

KEY: CT = cutting force, AE = acoustic emission, T = temperature, VC = vibration/chatter, SMC = spindle motor current, FR = feed rate, DC = depth of cut, CS = cutting speed, TO = torque, S = strain and IM =image

TABLE 5.2: Summary of Methods

AUTHOR(s)	% Success	Signal Processing Method	Feature Space
Zhou et al (1995)	>92	TDS	YES
Govekar & Grabec (1994)	-	RMS, FFT	YES
Tarng *et al.* (1994)	-	Moving Average	YES
Lui & Anantharaman (1994)	92	TDS	YES
Ko & Cho (1994)	97	ARV	YES
Purushothaman & Srinivasa (1994)	-	TDS	NO
Tansel *et al.* (1993)	-	Wavelet Transform	NO
Yao & Fang (1993)	-	ARV	YES
Ruiz *et al.* (1993)	90	FFT	YES
Burke (1993)	95	FFT	YES
Markos *et al.* (1993)	-	TDS	NO
Jammu *et al.* (1993)	-	BLOCK AVERAGING	NO
Teshima *et al.* (1993)	-	-	No
Monostori (1993)	>96	TDS	YES
Moriwaki & Mori (1993)	100	TDS	NO
Tansel & McLaughling (1993)	>99	AVERAGES	NO
Tansel *et al.* (1993)	≈100	WAVELET TRANSFORM	NO
Barschdorff *et al.* (1993)	95-97	FFT	YES
Tansel *et al.* (1992)	90	TDS	YES
Burke (1992)	95	FFT	YES
Guillot and El Ouafi (1991)	-	TDS	NO
Masory (1991)	-	TDS	NO
Tansel *et al.* (1991)	90	ARV	NO
Emel (1991)	>77 (mean)	FFT	YES
Kamarthi *et al.* (1991)	95	TDS	NO
Govekar *et al.* (1991)	-	FFT, RMS	YES
Choi *et al.* (1991)	96	ARV	YES
Dornfeld (1990)	-	ARV, FFT	YES
Rangwala & Dornfeld (1990)	95	FFT	YES
Elanayar & Shin (1990)	-	Ratios of TDS	NO
Choi et al (1990)	>90?	FFT, ARV	YES
Liu & Ko (1990)	>85?	TDS	NO
Burke (1989)	95	FFT	YES
Rangwala (1988)	95	FFT	YES
Chryssolouris & Domroese (1988, 1989)	-	MEAN	NO

ARV = Autoregressive Time Series Vector
TDS = Time Domain Samples

CHAPTER 6

TEST RIG SET-UP AND INSTRUMENTATION VALIDATION

6.0. Overview

This chapter outlines the fundamental components of the experimental test rig platform and peripheral instruments, providing a detailed description of the hardware and software used in the study.

6.1. Experimental Requirements

In order to develop a TCMS, it is necessary to undertake cutting tests from which the chosen process parameters can be measured and their trend used n accessing their true indication of on-line tool wear. As indicated in Chapter 3, the chosen process parameters to be monitored are the cutting forces (three axes) and vibration signatures (three axes). The type of metal cutting envisaged will be semi-orthogonal turning on a lathe as it is the most common and versatile form of metal cutting process. Like any other metal removal equipment, the ultimate economic performance of a lathe depends on the cutting tool that actually takes the chips off the workpiece. Economy and productivity have made indexable inserts the primary tooling method for lathes. The cutting tools will be grades of 'throw-away' indexable inserts of plane cemented carbide and coated carbide with an integral chip-breaker geometry, held in place by a negative rake toolholder. As the metal removal rate is a direct reflection of the cutting speed, feed-rate and depth of cut, an increase in any one leads to a proportional increase in chip volume and possibly the acceleration of tool life. The nature and degree of constraints on the feed-rate, depth of cut and cutting speed vary widely i.e. the user is limited to pre-set feed-rate values whilst the cut ing speed is dependent on

the lathe driver motors and depth of cut dependent entirely on machine capability. For the anticipated test cuts, the tooling/workpiece combination and the power limitations of the cutting machine necessitate that the cuts will be carried out exclusively within the following ranges (minimum-maximum) to incorporate various tool wear modes (AB Sandvik, 1995):

- Feed-rates: 0.1mm/rev - 0.4mm/rev
- Cutting speed: 80m/min - 350 m/min
- Depth of cut: 0.5mm - 4mm

These cutting conditions are deemed appropriate for the realisation of the prevalent tool wear modes and forms of tool wear. As the the cutting speed is primarily responsible for the various wear modes being a direct function of temperature, the chosen speed range will help realise this. The chosen DOC range on the other hand will help to minimize notch wear, while the feed-rates are pre-set on the machine.

The selection of these parameters for any particular turning operation requires a complex assortment of considerations involving the interactions of workpiece, machine tool and tooling as a system (Hatschek, 1978). The workpiece material will be low carbon alloy steel of the EN8 (hard) and EN24 (harder) types, free of forging scale and hard skin. The harder steel is needed to accelerate the tool wear at the experience of a shorter tool life.

The sensors for the cutting forces and vibration would be:

- Accelerometers for acceleration signal (vibration) measurement
- Dynamometers for cutting force measurement

The recording instrumentation will be a computer fitted with a data acquisition card with the signals from the sensors passed through a signal conditioning unit

such as a charge amplifier. The interpretation of the data will be through ANNs built through an interactive scientific and engineering software called MATLAB (Mathworks, 1994).

MATLAB is an interactive program for numeric computation and data visualisation. Fundamentally, MATLAB is built upon a foundation of sophisticated matrix software for analysing linear systems of equations. The tools springing from these numerical foundations have proven to be extraordinarily versatile and capable in their ability to solve problems in applied math, physics, chemistry, engineering, finance - almost any application area that deals with complex numerical calculations.

6.2. Hardware Description

The hardware component of the instrumentation set-up comprised: three miniature accelerometers, a tri-axial tool-post dynamometer, the centre lathe, a PC with an internal data acquisition card, a charge amplifier and a coupler/power supply.

6.2.1. Tri-axial accelerometer (Kistler, type 8730)

The operation of this accelerometer is based on the principle of reversible piezoelectric effect (Section 6.1.2). Since force can be related to acceleration by Newton's Second law (a=F/m), mounting a known mass on a disk of piezoelectric material enables the measurement of acceleration. The indication rate emitted as an electrical charge can be passed on to a charge amplifier for amplification. The sensitivity of the transducer is expressed in terms of the ratio of the electrical output to the applied acceleration i.e. mV/g, with a range of $\pm$ 500g and, an average sensitivity at 100 kHz of approximately 10 mV/g before amplification. The mounted resonant frequency is 76 kHz. Other calibration parameters such as bias voltage, transverse sensitivity and the time constant are provided on the certificate of calibration (Kistler, 1994).

The accelerometer is also known as the K-shear® self-generating accelerometer because of its built-in piezoelectric element - the piezotron[1], and an impedance converter for converting the accelerometer output into a low impedance output. With such a low impedance device no charge amplifier or special cabling is required to carry the signal from the accelerometer. Signal transmission over long lines is also possible with little or no noise pick-up (Bruel and Kjaer, 1987). A simplified diagram is shown in Figure 6.1.

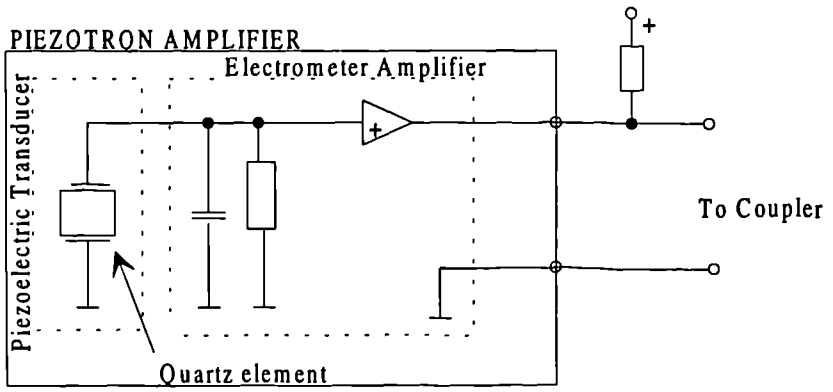

Figure 6.1: Simplified diagram of a K-shear accelerometer

6.2.2. Tri-axial tool post dynamometer (Kistler, type 9263)

This multi-component dynamometer provides dynamic and quasi-static measurements of the three orthogonal components of force acting from any direction on the tool holder (when attached onto the top plate of the platform device). With the aid of optional evaluation devices, the 3 moments (M_x, M_y and M_z) can be measured as well. It has a high rigidity with a high natural frequency. The high resolution enables very small dynamic changes to be measured as large

---

[1] A piezotron® device is a Kistler patented generic name for the piezo-electronic circuit in their low impedance devices such as the K-shear low impedance accelerometer. The main advantages of using a shear mode configuration in the K-shear configuration include amongst others the fact that the quartz elements produce excellent thermal stability and negligible low base strain sensitivity (Bruel and Kjaer, 1987). They also offer a wide frequency bandwidth while maintaining their calibration over years.

forces. The dynamometer is such that it measures the active cutting forces regardless of its point of application. The force to be measured is introduced in the top plate and distributed between four 3-components force sensors arranged between the base and top plates. Each of the sensors has three pairs of quartz plates, sensitive to pressure in the Z, X and Y-directions. Measurement is virtually without displacement and the introduced force is resolved into three components which are individually led away in the connecting cable. Depending on the direction of the force, +ve and -ve charges occur at the connections: -ve charges give +ve voltages and vice versa (Kistler, 1990).

The functional principle of the dynamometer is based on the piezoelectric effect. When piezoelectric crystals (the load cells) are stressed mechanically, they emit a charge proportional to the force applied. This electrical charge, because of the presence of very high resistance in the sensor elements and connecting cable, is a high impedance charge (a comparison of high and low impedance devices is made later) and therefore has to be passed onto a charge amplifier which converts the charge to a proportional voltage which can either be displayed, recorded or processed.

The dynamometer platform has a resolution of 0.01 N and a mounted resonance frequency of ≈2.5 kHz in both x and y directions and 3.5 kHz in the z-direction. Its natural frequency is 4 kHz, with an average sensitivity of -7.5 pC/N in the x- and y-directions, and -3.5 pC/N in the z-direction. The maximum applicable force within about 25 mm above the top surface of the platform is -5 to 5 kN.

6.2.3. Data Acquisition Card (DAC)

It is a full size high accuracy analogue and digital input/output board for IBM compatible PCs. It can be plugged into any existing PC motherboard slot. It features software programmable gain (1, 2, 4 or 8) on its analogue input channels, it is also compatible with and supports boards in the PC-30 range. Its main key specifications can be summarised as follows:

- A 12 bits A/D resolution
- A non-linearity of ≤ 0.75 LSB
- An A/D full scale input range of 0V to +10V or a bipolar of -5V to +5V
- single ended A/D inputs or 8 differential, and
- An A/D throughput rate of 200 kHz.

6.2.4. Charge Amplifier (Kistler, type 5006)

The charge amplifier converts the electrical charge from the high impedance dynamometer into a proportional voltage indicating the amount of cutting force on the tool point. The amplifier essentially consists of an operational amplifier with high input impedance and a high open loop gain with arrangement of capacitors and resistors that yield a proportional voltage from the charge input. It has a measuring range of between ±10 to ±500000 pC. It is fitted with slot-in cut-off filters that range from 10 Hz -180 kHz. The amplifier is incorporated with a long, medium and short time constant switch, and a voltage output of ±10 V/mA. The time constant switch allows measurement of both dynamic and stationary parameters.

6.2.5. Power supply/coupler (Kistler, type 5134)

It is a low impedance piezoelectric signal conditioner, housed in a standard 14 E, 3 U high Eurocassette, with isolated RS-232C serial interface. It is controlled by an internal micro-controller which allows inclusion of a self-test and LCD features. This set-up makes allowance for the use of a conventional coaxial cable between the transducer and the remotely located power supply. In essence, its main function is to supply the necessary constant current excitation to the accelerometer and decouple the signals from it to the DAC. Its configuartion

incorporates gain functions (2, 5, 10, 20, 50, 100) and pre-programmed cut-off frequency range of 10Hz, 100Hz, 1000Hz and 10Khz.

6.2.6. Lang Centre Lathe (type J6, Swing I6)

The lathe is fitted with an infinitely variable speed control, enabling cutting speeds to be selected which would not be practically possible with a conventional mechanical gearbox. This enables a constant cutting speed to be achieved as workpiece diameter decreases during cutting. Feed-rate can be chosen from fixed values by selecting appropriate gear levers.

6.2.7. PC Type

An IBM compatible, Tandon 386 SX/20 SL II PC, with a 387 maths processor, clock speed of 20 MHz, 4 MB Random Access Memory, 100 MB hard disk drive space and VGA colour monitor. The operating system on the PC was DOS 6.22.

6.3. Instrumentation Configuration

6.3.1. Acceleration measurement

The acceleration signals were measured through the application of accelerometers. The accelerometer was connected via a coaxial cable directly to a coupler from where its gain, bias and filter type is selected for pre-processing. The output signal was then relayed to a printout device i.e. through the DAC to the PC for storage (intermittent sampling) or real-time display.

6.3.2. Quasi-static and dynamic forces:

The cutting forces were measured using the three component dynamometer. The transducer device, a high impedance dynamometer was connected via a low noise coaxial cable to a charge amplifier. The measured impedance (pC/N) was cabled to a readout device for analysis or storage. Theoretically, it was possible to measure both the dynamic and static forces using only ne device, by switching

the time base setting as required. However, the time base can only be switched to one position at any given instance. It was therefore not possible to simultaneously measure both the static and dynamic forces as outlined. Splitting the charge so that two separate amplifiers could be used for each component was not viable as it would lead to distortion of the signal. A decision was made to sample the cutting forces whilst the time base was set to the long mode, then mathematically determine dynamic and static components from a single signal. This meant sacrificing some high frequency dynamic force measurements for ease of measurement.

6.3.3. Charge amplifier operation

The charge amplifier was primarily based on an operational amplifier (op-amp) input stage. The op-amp with capacitor of capacitance C_f, in feedback loop operates as an integration network and integrates the input current, I, to I_c. This input current is the result of charge developed across the high impedance piezoelectric device (dynamometer), Q_a. The amplifier works to nullify this current and in doing so, produces an output voltage, Vo, proportional to the charge (Figure 6.2).

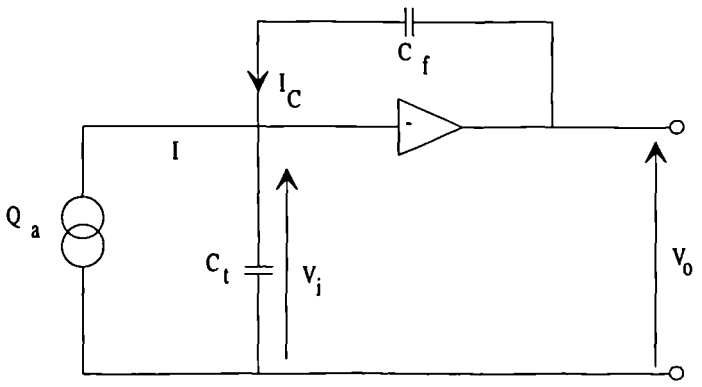

Figure 6.2: Schematic diagram of the charge amplifier

C_t = Combine resistance from the dynamometer, cable and amplifier

I_i & V_i = Current from C_t and constant voltage respectively.

6.3.4. Coupler Operation

The coupler simplistically consisted of three main components: a Polarity Protection Diode (PPD), a Constant Current Diode (CCD) connected in series, and the combination connected in parallel to a decoupling capacitor. This set-up achieves a high dynamic resistance and low DC resistance i.e. provides a constant current source (Figure 6.3)

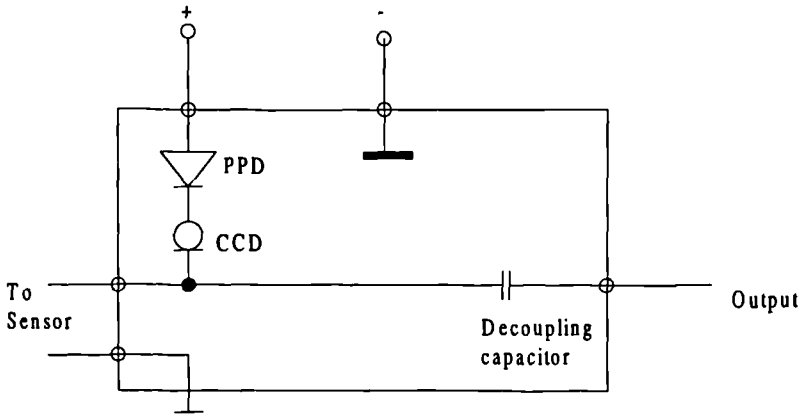

Figure 6.3: Schematic diagram of a simple coupler

6.3.5. Low Impedance Vs High Impedance devices

Contained within the low impedance accelerometer (K-shear) housing is a miniature electronic circuit, the piezotron. This circuit converts the high impedance charge signal generated by the piezoelectric element into a low impedance voltage output. Since the output impedance is typically below 100 Ω the transducer device requires an external power source, hence the utilisation of the power supply/coupler. A two wire cable is used to connect the accelerometer and the coupler. The signal and coupler share a common line, with the coupler providing a constant current source to the accelerometer and decoupling the DC bias from the measuring instrument (Figure 6.4).

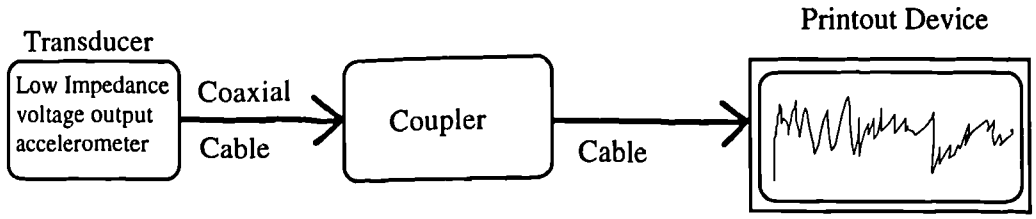

Figure 6.4: Low impedance device connection

On the other hand, sensors with a high impedance output such as the dynamometer do not have an integrated impedance converter. As such, the converted charge has to be externally amplified via a charge amplifier. This requires low noise and high impedance ($10^{14}\Omega$) cabling between the sensor and amplifier. These devices are highly suitable for very low frequency measurement or quasi-static stimuli.

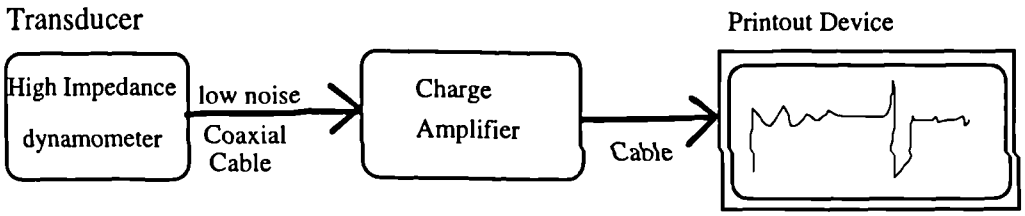

Figure 6.5: High impedance device configuration

6.4. Verification of Manufacturer Calibration of Transducers

It was necessary to ensure that during test cut investigation, the recorded signal values from both the dynamometer and accelerometers reflected accurately beyond any doubts, the variation of the underlying process parameters. A procedure to verify the manufacturer's calibration of the dynamometer and accelerometer was carried out and the summary of the investigation is outlined.

6.4.1. Verification of Accelerometer Response

An oscilloscope was set to DC mode at 1V/division setting and connected to the coupler output of the chosen accelerometer channel. The tool holder with the accelerometers attached onto it was held upright with respect to the designated accelerometer. The oscilloscope (dc line) was zeroed and then the tool holder flicked upside down (in relation to the accelerometer concerned) and the voltage change noted on the oscilloscope. This was repeated for the other two. A voltage change per accelerometer of 1.92 V was registered.

Flicking the accelerometer upside down caused a change of the gravitational pull from +g to -g, thus an overall change of 2g. Manufacturer supplied calibration for each of the accelerometers was 10 mV/g and the gain on the coupler was set to 100. This gave a calibrated sensitivity of 1 V/g (i.e. 2g corresponded to 2V on the oscilloscope). Voltage registered on the oscilloscope corresponding to a 2g acceleration was 1.92V, an error of 0.08V (< -4%). This was attributed to experimental error, and since error was marginal and therefore negligible, it could be concluded that the accelerometers responded accurately as manufacturer calibrations specified.

6.4.2. Verification of Dynamometer Response

As the dynamometer measured the active force regardless of point of application, its calibration, it was thought could best be verified by loading it with dead weights in all three directions. However, in the x- and y-directions, the weights had to be applied via a pulley owing to lack of suitable manoeuvring area.

The charge amplifier for the designated channel was set to 10 N/V, and an oscilloscope used to monitor the load on-line (not in dc mode). Placing two separate dead weights of 2 kg and 5 kg at a time on the top face of the platform, the oscilloscope reading was noted. The weights of 2 kg (20N) and 5 kg (50 N) each registered 2V and 5V respectively which when compared to the expected

output from the charge amplifier (load divided by amplification factor) were exactly the same, thus the z-axis calibration was as specified by the manufacturer.

The x- and y-directions required a horizontal loading compared to placing dead weights vertically. Unfortunately, there virtually existed no manoeuvring area from where to suspend the dead weights. A simply constructed pulley platform was used in the manner shown in Figure 6.6.

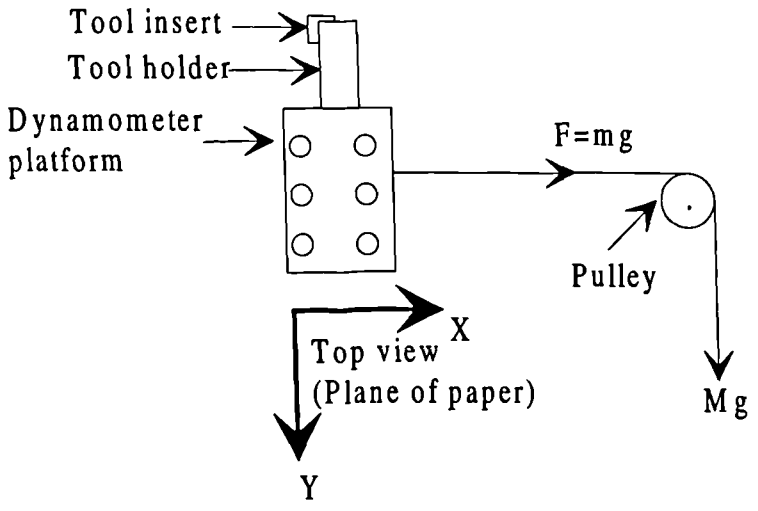

Figure 6.6: Apparatus for dynamometer calibration verification

Using this set-up the procedure outlined for the z-axis force measurement was repeated. Results obtained using known dead weights showed that the obtained voltages had approximately ±10% error. The error was viewed as arising from a combination of the following two factors:

- Stretching of the pulley line, and
- Friction in the pulley.

6.5. Software Description

The software used in this study comprised three distinct components: an off-the-shelf piece of software was used for the data acquisition while purposely

developed software in the MATLAB environment were employed in the analyses of the captured data and their interpretation. The software could therefore be viewed as a three phase process: the data acquisition phase, the data processing phase and finally, the interpretation and neural network implementation phase. A discussion of the main algorithms and their specific features follows.

6.5.1. Data Acquisition/Sampling Software

The software utilised for this process, Waveview for DOS 1.24 ©1996, Multiboard(3) version, was supplied together with the data acquisition card. Its main use was to capture the signal and either store, export, display the time varying nature of captured signal (amplitude variation) or perform an FFT analysis on it (frequency distribution).

The employed version of Waveview generally ran on any machine from an old XT to the much more advanced 50 MHz 486 or Pentium types. In fact, this software would support all data acquisition boards in the PC-30 range. It contains an advanced digital oscilloscope with pre-, mid- and post-triggering. Included in the same package was a spectrum analyser and logger. Parallel streaming from 3 boards simultaneously with unlimited number of samples was provided. It could support up to 4 sets of data in memory with direct streaming unto the hard disk possible. Waveview could also calculate and display graphs of the power spectra with provision made for the data to be exported (both sampled and calculated) in ASCII text for further analysis in other domains. The sampling software also had a full menu driven user interface with comprehensive on-line help.

6.5.2. Signal Processing

The noisy nature of the captured sensor signals required an active selection or mapping of useful features from the sampled sensor signals. This could yield useful features that might be sensitive to tool wear but not sensitive to other parameters. Features can either be generated or selected by a heuristic trial and

error approach based on certain physical considerations (Ruiz et al., 1993).

The sampled data files were converted and exported as ASCII readable text files, which could be analysed out of the sampling environment i.e. using MATLAB. Codes were developed to extract the static forces, dynamic forces and vibration signals, and the latter two further processed through application of a fast Forward Fourier Transform (FFT).

The signal processing paradigm consisted of five distinct stages. In the first stage, the data was loaded into MATLAB environment memory and the static force components of the cutting force calculated as the mean of the complete sampled cutting force signal. In the second stage, the dynamic force was calculated by using the previously obtained mean by subtracting the mean value of force from each sampled data point. The next stage was to obtain the FFT of the dynamic signals (dynamic force and vibration). The dynamic force data was first windowed through application of a Hanning window before its FFT calculated for repeatability of the record length throughout (Appendix I). The obtained FFT data was then smoothed using a seventh order factor to enhance the quality of any visual plots (spectra and contour plots).

6.5.3. Algorithm Description

1. The data whose FFT was required was multiplied by $\cos^2(t)$ - the Hanning window function which essentially was a bell-shaped function spanning $-\pi/2$ to $\pi/2$ in order to reduce signal leakage that otherwise would mask small frequencies.

2. The FFT of each data point was calculated and its negative component was taken into account by considering the RMS value corresponding to each frequency, and this was calculated and normalised (dividing by N). i.e.

$$P_{RMS}(f_k) = \frac{1}{N}\sqrt{2R_k^2}$$

3. Since only the power or energy distribution in certain frequency band was of interest, it was not necessary to obtain the complete energy distribution in the entire frequency range. Therefore, the total power in the FFT spectrum from f_k = 0 to f_k=N/2 was considered i.e.

$$P_{Total}(f_{\frac{N}{2}}) = \sum_{k=1}^{\frac{N}{2}+1} \frac{1}{N}\sqrt{2R_k^2}$$

The k=0 value corresponded to the dynamic force DC value in the FFT range, and since it was not affected by the transformation, it was neglected.

When spectra plots were required for visual confirmation of features, a smoothening filter was used to enhance and smoothen the curve. This simply replaced the concerned point with its mean i.e. for a 7th order filter, the smoothening began at the 4th data point, replacing it with the mean of first three ahead and three previous data points.

6.5.4. The Neural Network Paradigm

The basic structure of the paradigm is shown in Appendix III(b). The algorithm begins by initiating the desired size of the input nodes, the number of hidden layers and nodes, and the number of output nodes are set together with the method of weights initiation. The training parameters (i.e. number of epochs or training cycles, desired error goal, momentum coefficient, the learning rate and its increment and decrement) are then set. The training algorithm is then called (usually BP) and the network attempts to minimise the error output between the calculated and desired values. The last phase of the neural network algorithm concerned presenting the final network parameters (weights and biases) when either the number of specified epochs had been exhausted or the target error goal had been reached. When the network converges on the desired values before the number of training cycles that has been set is reached, then the number of training cycles and the converged error are also printed.

6.6. *Conclusions*

The necessary hardware and software for the envisaged study have been put together, and the manufacturer calibration specifications verified. The calibration verification procedure followed showed that the acceleration and dynamometer were adequately calibrated. The main components of the hardware have been connected and the software to capture and analyse the data developed.

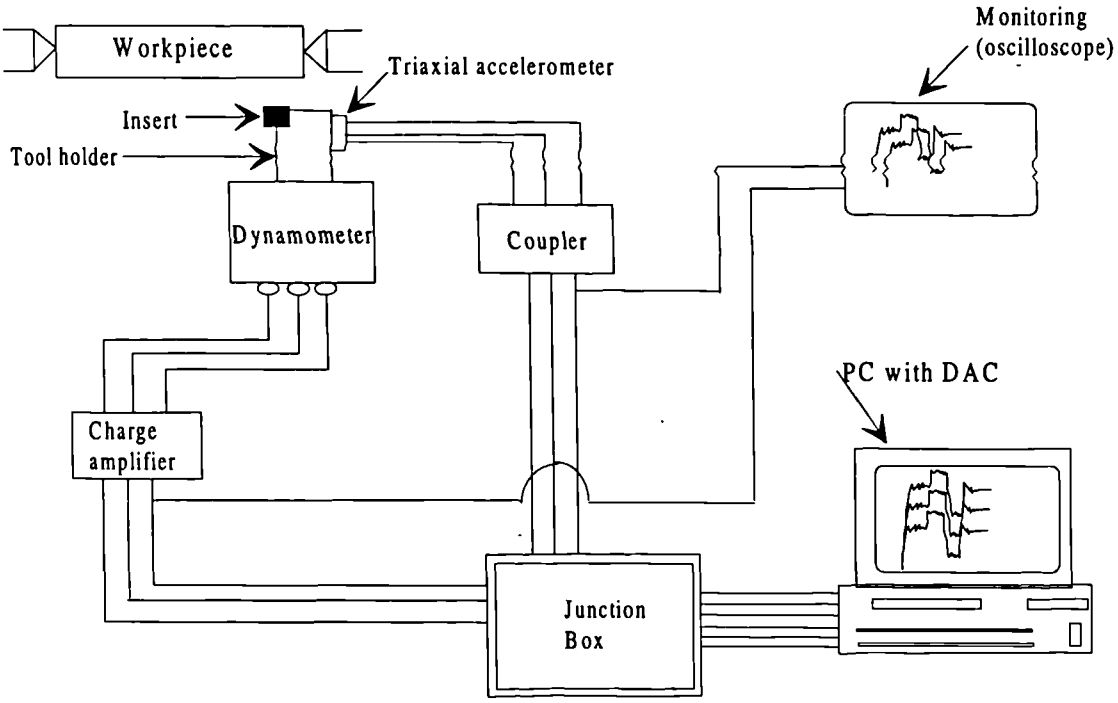

Figure 6.7: The Experimental set-up

CHAPTER 7

IMPACT OF CUTTING CONDITIONS ON SENSOR SIGNALS- PLANE FACED GEOMETRY

7.0. Overview

The results of the test rig validation are presented in this chapter and were aimed at evaluating the behaviour of the chosen sensor (cutting forces and vibration) signals in terms of reproducibility and repeatability.

7.1. Test Run Procedure

A hand held digital tachometer was used to adjust the cutting speed (V m/min) on the surface of the workpiece. The required feed-rate (s, mm/rev) was chosen from the lathe pre-set values and the cutting tool wound to the uncut diameter until it just touched the workpiece producing very fine chips at the tool point. This point was taken as the datum from which the desired depth of cut was to be applied. Resetting the charge amplifiers to discard any residual charge, data was then recorded after the tool had been engaged in cutting and sufficient time allowed for a steady state to be attained. Before any experimental data were recorded, the optimum sampling parameters (frequency, number of data samples and the sampling time) were determined. The procedure followed is presented in Appendix I. The recorded data consisted of the three components of acceleration and cutting forces with sampling performed at a frequency of 20 kHz, while recording 1024 data samples per channel. In later experiments, the sampling rate was increased due to anticipated increase in chip segmentation frequency when inserts with a chip breaker configuration were used.

The flank and crater wear on the tool faces were measured before and after the experiments. Crater wear was measured with the aid of a dial test indicator, whilst flank wear length was measured using a tool maker's microscope. The tool inserts used in this part of the study had plain faced geometry were uncoated and had an approach angle of 5°. Details of the cutting tests, cutting conditions, tool material and workpiece material are listed in Table 7.1.

A typical record of the sampled cutting force signal for a sharp and worn tool inserts for cut 1 (z-axis only) are shown in Figures 7.1 and 7.2 respectively while Figure 7.3 shows the sampled signal in the z-direction (vertical) for the acceleration signal when cutting with a sharp tool insert (V=200m/min, f=0.163rev/mm & a=2mm). On these time domain plots, it can be observed that the acceleration signal oscillated with a mean of zero. The vertical force signal for cut 1 unlike the acceleration plot, oscillated around a value that corresponded to the static cutting force in that direction. A force has to exist for cutting to take place. Its oscillatory component was an indication of the nature and extend of such dynamic movements.

Clearly Figures 7.1 - 7.3 offer no indication of the variation of chosen cutting process parameters apart from a magnitude change due to the tool being engaged in cutting. For each cutting test pass performed, a value of static force can be calculated from the sampled cutting force, together with an indication of the dynamic force variation.

7.2. ANALYSES

7.2.1. Static Force

The sensor signal processing performed was aimed at extracting features that best described the characteristics of the process conditions. Signals from the metal cutting process generally are non-stationary (Fig. 7.1 and 7.2) due to the non-linearity of the cutting process and workpiece inhomogineities. However, in this

part of the study, it has been assumed that the cutting static force signal is stationary and independent of time. Therefore, it suffices to characterise it using either Power Density Function (PDF), statistical mean (averaging) or time domain indices. The statistical mean of the sampled cutting force was chosen to describe the nature of the static force behaviour since the signal was assumed to be stationary, and its mean therefore remained constant throughout a cutting pass (details in Appendix I).

For each test cut, the static force component, $\overline{F}$, was calculated as the mean value of the sampled data. The mean value was necessarily taken because the data points continuously varied, thus had no effective value. Therefore, by taking the mean value its statistical variation was inclusive in the ensuing analysis, and was thus justified by the experimentation procedure i.e.

$$\overline{F} = \frac{1}{N}\sum_{i=1}^{N} F_i(t_i) \qquad [7.1]$$

7.2.2. Dynamic Force and Acceleration (Vibration Signal)

With the static force known for each cutting pass, the dynamic or time varying force component for each data point could also be determined.

If $F_{d(i)}$ represents the dynamic force for the *i*th data point and the sampled force is F_i, then $F_{d(i)}$ can be found as follows:

$$F_{d(i)} = F_i - \overline{F} \qquad [7.2]$$

Clearly the dynamic forces and acceleration signals vary as cutting time progresses, but this is not particularly evident on a time domain plot. In the time domain, smaller frequency components are masked by bigger ones, but in the frequency domain, the whole spectra could be viewed. It was also evident that in the time domain, the signals exhibited dynamic characteristics and behave in an apparently random manner. The dynamic data (dynamic force and acceleration)

were transformed from the time to the frequency domain through implementation of an FFT algorithm. The FFT reduces the size of the sampled data and alleviates collinearity among the dynamic signal components.

The static cutting force, Sum Total Power (STP) in the dynamic force and acceleration signals, were calculated and the plots are shown in Figures 7.4 - 7.15 for the sharp tool and in Figures 7.34 - 7.45 for the worn tool.

The power spectra for both acceleration signals and the dynamic forces were also obtained for both cutting conditions for the two tool states. A sample of these waterfall diagrams are shown in Figures 7.16 - 7.33 for the dynamic forces, and vibration spectra for the sharp tool, while spectra for the worn tool appear in Figures 7.46 - 7.63.

The implementation of spectral analysis involve a two step process: obtaining the transforms and interpretation of the obtained spectra. The implementation of the conventional FFT based spectral analysis is well noted as having several deficiencies. Some of the restraints are its frequency resolution (sampling frequency interval) and spectrum leakage. The number of data points sampled (2^{10}) was thought to be sufficient for the attainment of a moderate frequency resolution (see Appendix I). Results appear on Tables 7.3 - 7.6.

7.3. Discussion of Static Force Results

7.3.1. Effects of Cutting Speed

Inspection of Fig. 7.4 for the sharp tool shows that the mean static forces generally decreases as the cutting speed is increased. Since the feed-rate and depth of cut were fixed for each cut, the area of cut, a function of these entities remained constant. However, as the cutting speed increased the Metal Removal Rate (MRR) increased resulting in an increase in temperature. Increased cutting temperature caused the workpiece material to deform and flow easily, hence less cutting force was required to shear and remove the swarf.

The increase in cutting temperature was attributed to a decrease in the contact area caused by a drop in the shear strength in the flow zone. Usually with carbon steels, an initial increase in cutting forces shown in Fig. 7.4 peaking at V = 130 m/min is to be expected due to the phenomenon of Built-Up Edge (BUE). A BUE causes cutting forces to initially rise, due to restriction of the contact area and then begin to fall gently at medium speeds. The vertical cutting force is usually the major cutting force as it is in this direction that the workpiece impinges on the cutting tool. Beyond a cutting speed of 250 m/min., the cutting forces began to rise. This was attributed to the on-set of tertiary tool wear. At this stage, the cutting tool has been engaged in cutting such that its cutting edges had began to crumble from plastic deformation, thus increasing the area of contact. Inspection of the chips formed showed that they were thinner as a result of the decrease in clearance angle that causing an increase in the clearance contact area. This therefore meant that more force was required to shear the workpiece as the workpiece material does not flow that easily.

Observation of the worn tool plots in Fig. 7.34 showed a similarity in behaviour pattern. An initial decrease in the cutting forces was followed by a steep rise before it gradually fell, reflecting the formation and disappearance of BUE. The magnitudes were notably higher than those in the sharp tool. A comparison of the two curves showed that, in the worn tool state, BUE effects were much more pronounced and occurred in the same cutting speed region in both cases.

7.3.2. Effects of Feed-Rate

Fig. 7.4 showed that the forces generally increased as the feed-rate was increased. This was attributed to the fact that the area of cut substantially increased per cycle of cut, hence more shearing had to be done which required more force. For the worn tool state, Fig. 7.34 showed an initial decrease, then a gradual climb as was the case in Fig 7.5. However, the curves in Fig 7.34 were not as linear as those for the sharp tool state. This is attributed to progressive wear during the test.

7.3.3. Effects of Depth of Cut (DOC)

Plots of the curves for the worn tool are shown in Fig 7.36 and those for the sharp tool appear in Fig 7.6. Increasing the DOC generally resulted in a proportional increase in the cutting forces. The sharp tool cutting forces increased linearly whereas those for the worn tool were less linear and erratic but still showed an upward trend.

7.3.4. Summary of Observation

The static force could be viewed as exhibiting a linear relationship with the cutting conditions, increasing when DOC and feed-rate were increased. When cutting was performed using a worn tool, generally higher force magnitudes were required to shear the workpiece. Though the behaviour of the static cutting forces with DOC and feed-rate were linear, the same principle did not apply to the relationship with the cutting speed.

Another way of examining the effects of cutting conditions on the forces was to observe the power required to shear the metal in unit time. The effects of cutting speed, feed-rate and DOC on the power are depicted in Figures 7.13 -7.15 respectively for the sharp tool and in Fig. 7.43 - 7.45 for the worn tool. A linear increase was observed for the sharp tool and a general rise for the worn tool. Although the cutting forces actually decreased as the cutting speed increased, increases in cutting speed were much more pronounced when both cutting parameters were varied. More shearing was done per unit increase in cutting speed, and therefore more work done per second (power: J/s = watt) accounting for the power increase. On the other hand, increases in power as feed-rate and DOC increased were as a result of more material being removed, hence more work was done per second. The power required to shear is therefore proportional to the metal removal rate.

7.4. Discussion of Dynamic Components

The prominence of a consistent peak and several smaller harmonic frequencies were the principal observable features on the spectra plots of either the dynamic cutting forces or the vibration signals. Clearly, these prominent peaks can be expected to correspond to the natural frequency of the tool holder and vibrations due to the chip formation process.

Since it was not logical to attribute the prominent peak frequencies without careful thought and reason to either the resonant frequency of the tool holder or chip formation, it was necessary to investigate and establish the nature and origin of the observed peak frequencies. These prominent frequencies could only have one source: first mode resonant frequency of the cutting tool holder or chip formation frequency. In order to analyse the tool holder frequency, it was necessary to represent it as a fixed end cantilever with a rectangular cross-section and an end point load, and its natural frequency of vibration found from the equation below (Lee *et al.*, 1989):

$$f_n = (k_n l)^2 \sqrt{\frac{EI}{ml^4}} \qquad [7.1]$$

where k_n = parameter depending on end conditions ($k_n l$ = 1.875 for the 1st mode); l is the tool holder overhang from the clamping end, EI = Flexural rigidity of the tool holder shank cross-section, and m = mass of shank cross-section per unit length.

Using approximate values of these parameters the 1st mode vibration frequency was found to be ≈ 26 kHz. This value is notably higher than the expected mounted natural frequency of the dynamometer platform which is approximately 4 kHz, but less than that of the accelerometers (76 kHz). The discrepancy in the obtained and calculated values of the resonant frequency required an investigation of the effect of tool holder overhang length on the dynamic signals. Using a

conservative feed-rate of 0.163 mm/rev, DOC of 1.5 mm, cutting speed of 200 m/min while sampling 1024 samples at 20 kHz, results shown in Table 7.2 were obtained.

The experiment showed that as the overhang length was increased, the resonant frequency decreased. Calculations showed this to be the prevailing trend. The flexural rigidity (EI) and mass per unit length (m) of the shank are cross-sectional area properties and therefore remain constant regardless of the shank length (Gere and Timoshenko, 1991). Then since $f_n \alpha (1/l)^4$, as $l \rightarrow \infty$, $f_n \rightarrow 0$, i.e. increases in the overhang length lead to a decrease in the resonant frequency. Inspection of the chips formed (curl and segmentation) suggested that their formation frequencies were far less than the observed prominent peak frequencies depicted on the spectra plots. Having performed a verification of the chip formation frequency and the tool holder resonant frequency, it was concluded that the observed peak frequency was due mainly to the natural frequency of oscillation of the tool holder.

7.4.1. Acceleration Signals

7.4.1.1. Effects of Cutting Speed

Figures 7.19 -7.21 depict the effects of cutting speed on the power spectra for the sharp tool. These spectra show a relatively high concentration of energy spectra around the resonant frequency covering a wide bandwidth that stretches from 4.5 - 6.5 kHz with a relative large magnitude for low cutting speeds, but dispersed and becoming more evenly spread in the lower frequency quartile as the cutting speed is increased. The occurrence of this high peak consistent in all three directions at low cutting speed was attributed to the effects of BUE. The decline in magnitude thereafter and then rising again was associated to the fact that the BUE is a dynamic characteristic appearing and disappearing.

Meanwhile, observation of the individual acceleration signal power spectra in the x-, y- and z-direction, showed that the magnitudes were higher for the z-axis signals and least for the x-axis. This could be explained as having arisen from the fact that more movement occurred in the z-axis, the direction of cutting where the tool impinged onto the workpiece. Another observable feature on the y-axis graph was a significantly small but consistent frequency peak at around 600-800 Hz, which could be attributed to the chip formation frequency since it was lower than the resonant frequency of the tool holder. Fig. 7.20 also showed a smaller but consistent peak frequency at 8 kHz, whose peak initially was sharp, but declined as more energy was dispersed in the region before and after this frequency. This frequency suggested a harmonic of the tool holder peak frequency.

The worn tool spectra tended to be identical in behaviour in all three planes and exhibited the same characteristics as those for the sharp tool. The resonant peak frequency increased as speed was increased and then remained the same from and beyond cut 23. Notably on the vertical plot, Fig 7.51 (to a lesser extent in the x- and the y- axes), a low frequency harmonic occurred in cut 20, 21 and 22. This disappeared just before the main resonant frequency became predominant. The harmonic then appeared again together with the peak frequency but had a lower frequency and a wider bandwidth. These were attributed to harmonics of the chip formation frequencies.

Comparison of the sharp and worn tool spectra showed that the acceleration amplitudes were higher in the worn tool state. Energy dispersion seemed to occur more in cut 27 and 28 than the rest of the cuts. Such an occurrence was completely absent in the acceleration spectra. The discrepancy in worn tool spectra could be attributed to anyone or combination of the following:

- crater wear depth increase,
- tool-chip contact length alteration, and

- BUE effects at low cutting speeds.

7.4.1.2. Effects of Feed-rate

Plots of power spectra for feed-rate variations in the three axes are shown in Fig. 7.25 -7.27 respectively for x-, y- and z-directions. The main observable feature from these curves were the difference in magnitude along the three axes. In line with speed changes, the x-axis spectra were the least and the z- the largest. As the feed-rate was increased, both curves showed that the peak frequency increased in line with that increment, peaking at s = 0.264 mm/rev. The energy dispersion for the first feed-rate was initially uniform and moderately low, with its peak frequency magnitude below ≈ 5 g. As the feed increased to 0.163 mm/rev, no noticeable change occurred. A further increase to 0.264 mm/rev resulted in the peak frequency's magnitude rising above ≈ 10g with its energy concentrated in the frequency region f_k=0 to the resonance (peak) frequency (6 kHz).

The worn tool spectra shown in Fig. 7.55- 7.57 had an identical appearance, but had comparatively higher magnitudes. It was uniformly smooth, with a sharp and consistent resonant peak frequency.

7.4.1.3. Effects of DOC

The sharp tool spectra appear in Figures 7.31 - 7.33, while those depicting the worn tool behaviour appear in Figures 7.61 - 7.63. The sharp tool plots show that a peak frequency occur at ≈ 5 - 6 kHz and its height affected by changes in the DOC. Overall, the spectra are rather dispersed and spread from 0 - 6 kHz. The worn tool spectra are distinguishably different with only one main resonant frequency at ≈ 5 kHz. Its magnitude also increases as DOC is increased. On the y- and z-direction, a very small peak at 3.5 - 4 kHz is visible.

Generally, for the worn tool state, the spectra distribution concentrated at the peak frequency while the sharp tool spectra tended to be rather dispersed with a range of small peaks.

7.4.2. Dynamic Force Signals

7.4.2.1. Effects of Cutting Speed

For the sharp tool, the power spectra are shown in Figures 7.16 - 7.18. Magnitude wise, the y- and z-axis amplitudes were higher and the x-axis the smallest. Peak frequencies are apparent in a band extending from around 4 - 6 kHz in all three components, but extending slightly to 8 kHz in the x-axis. It was also observed that as the cutting speed increased, the amplitudes of the resonant frequency initially increased, peaking in cut 5 (V=200 m/min.) with a decrease thereafter. A chip formation frequency component around 600-800 Hz was visible in the y-axis plot.

The STP dynamic force for the worn tool increased in the y- and x-directions while remaining constant in the z-axis for cutting speed increments. Inspection of the dynamic force spectra at varying cutting speed for the worn tool showed no prominent peak frequency for the first three cuts (cut 20-22) for the x-component, but a small peak appears in the y- and z-axes around 3.5 kHz. As cutting progressed beyond cut 23, a single prominent peak frequency appears on both axes and progressively decreased (damped) as cutting continued. The power required to shear increased as the cutting speed was increased as depicted in Fig. 7.43.

7.4.2.2. Effects of Feed-Rate

The effects of feed-rate variation on the dynamic force signal for the sharp tool are shown in Fig. 7.22-7.24. The overall resonant frequency band extended from 6 - 8 kHz for both directions, with little noticeable change occurring in the x-axis. The peaks become prominent in the y- and z-direction (6 kHz) as the feed-rate is increased with energy dispersion on the spectra immediately after the resonant frequency.

For the worn tool, Fig. 7.52 - 7.54 show that there was also a single prominent resonant frequency 4.5 kHz, but as the feed-rate was increased to a higher value, the spectra becomes rather dispersed especially the z-axis plot. Inspection of the power plot showed an upward erratic trend. Further inspection of the z-axis spectra showed that there was some energy dispersion around 3.5 kHz, and the band progressively increased as the feed-rate increased and becomes very noticeable in cut 34 and 35.

7.4.2.3. Effects of DOC

As the DOC increases, so does the z- and y-STP dynamic force components, while the x-axis component remains constant (Fig. 7.7). The worn tool plot tended to increase linearly as the DOC increased. Inspection of the dynamic force spectra (Fig 7.28 - 7.30) for the sharp tool show the spectra to concentrate around a wider band of about 2.5 - 4.5 kHz. The magnitude of this resonant frequency peak increased with an increase in the DOC. With the trend again in the x-direction. The spectra plots also show that the peak frequency's magnitude and band width increased. The worn tool spectra were sharper and concentrated on the resonant frequency (≈5 kHz). The x- and y-direction peaks increased as DOC increased, with the y-direction being more pronounced. The z-direction's response is the least (smallest peak) though of the same behaviour and trend.

7.5. Summary of Observation and Conclusions

The relationship between the static cutting forces, dynamic cutting forces, power required to shear, and the acceleration signals with varying cutting conditions (cutting speed, feed-rate and DOC) has been investigated. The results obtained showed that the cutting forces (static and dynamic) and the power required to shear generally increased as the tool wore. As the tool enters the tertiary wear phase the dynamic force amplitude is damped. The effect of overhang length on the peak frequency was found to be length dependent.

In terms of wear monitoring through the observed feature parameters, there is potential for the monotonic increase in the static cutting forces' magnitude being employed as tool wear sensitivity parameters. The increase in magnitude of the static force during the onset of rapid tool wear has been noted and validated by observation of energy dispersion in the dynamic force signal spectra. Worn tool spectra were observed to contain more energy (dense concentration of spectra lines) than those for sharp tools.

Wear progression was demonstrated by the obtained spectra from the acceleration signals. In line with theoretical and other reported research verifications (Lee et al., 1989) the tool point vibrations rose rapidly (cut 1 to cut 4) during the primary wear phase but only steadily afterwards beyond cut 5 (secondary wear phase). Its oscillations could be seen to significantly become damped, thus a reduction in the amplitude of the spectra of dynamic forces and vibration signals. Cutting was not carried out long enough for the inception of the tertiary wear phase.

A detailed microscopic observation of the sharp tool insert before and after the cutting process was carried out. This showed that at the end of the cutting, the sharp tool insert had moderately worn, and significant flank and crater wear appeared on the tool faces. On the worn tool insert, crater and flank wear were deemed to have progressed significantly and catastrophic failure imminent. Inspection of the workpiece surface finish and the chips formed suggested that, for worn tools, the surface was serrated, the actual cut was less than the DOC and the chips were coiled. Features from the sharp tool test cuts showed that the surface finish was relatively smooth, the cut was equal to the DOC, and the chips were regular.

Increases in the cutting conditions caused the power spectra of both the dynamic forces and acceleration signals to converge in the region $f_k=0$ to the peak frequency, especially with cutting speed increments. Observations from the obtained spectra were consistent and in agreement with results from other

investigations (Lister, 1993; Lee *et al.*, 1989). The resonant frequency was unaffected by variations in the cutting conditions. On the dynamic force spectra, it was noticed that worn tools had a uniform distribution of energy in the peak frequency region.

These tests have confirmed the appropriateness of the instrumentation set-up. The trend of obtained results are in agreement with those obtained by other researchers, and this is considered to confirm the validity of the set-up, and the appropriateness of the chosen sensor signals as suitable tool wear indicators. The sensor signals investigated have been shown to be affected by variations in the cutting conditions, with the effects of cutting speed and feed-rate more complex compared to a linear increment in DOC change. For monitoring purposes, it is necessary to be able to distinguish changes in the signal arising from changes in the cutting conditions from those that are wear borne. Neural networks as outlined earlier, possess inductive properties that could be explored in other to distinguish a worn tool from a sharp one.

TABLE 7.1: Details of the cutting tests

Machine Tool:	Lang Swing J6	
Workpiece:		
	Work material	EN8 BS 970
	Hardness	Brinell 170
	Composition	0.35%C, 0.05% Si, 0.6% Mg
Tooling material:		
	Tool holder	Kennametal KSBPR 2525 M12
	Tool type	SPUN 12 03 08
	tool material	Sandvik Coromant S1P P10 2361
	overhang /mm	45
Cutting conditions:		
	Cutting speed (m/min)	100 - 300 @30 intervals
	Feed-rate (mm/rev)	0.081 0.0882 0.106 0.163
		0.265 0.326 0.706
	depth of cut (mm)	0.5 1 1.5 2 2.5 3
Cutting Fluid:	None	

Table 7.2: Effects of tool holder overhang on resonant frequency

	Frequency /kHz	
Overhang length /mm	Experimental	Calculated
25	7.9	207.2
35	5.2	105.6
45	3.8	63.9
55	3.2	42.5
65	2.5	30.6
75	1.8	23

TABLE 7.3: Experimental results utilising sharp tool insert

Cut	Speed	Feed	DOC	Static Force (N)			R	STP Dynamic Force (N)			STP Acceleration (g)		
				X	Y	Z	R	X	Y	Z	X	Y	Z
1	100	0.102	1 5	311	115	392	514	127	151	143	4.89	2.32	5.25
2	130	0.102	1.5	339	164	459	594	156	202	212	4.45	2.49	5.4
3	150	0.102	1.5	338	162	462	595	127	177	159	4.41	2.47	5.33
4	180	0.102	1.5	318	154	438	563	124	173	153	4.08	2.36	5.22
5	200	0.102	1.5	308	147	440	557	127	168	148	4.41	2.64	5.11
6	230	0.102	1.5	298	146	436	548	111	145	129	5.15	2.63	4.32
7	250	0.102	1.5	286	136	424	529	113	132	122	4.71	2.58	3.86
8	280	0.102	1.5	291	138	431	538	104	120	113	5.08	2.9	3.54
9	300	0.102	1.5	339	164	459	594	169	153	148	5.08	3.07	3.39
10	200	0.102	1.5	308	147	176	384	127	168	148	4.41	2.64	5.11
11	200	0.178	1.5	348	180	241	460	160	208	181	4.93	3.17	5.92
12	200	0.254	1.5	422	276	357	618	290	563	494	8.61	6.76	9.18
13	200	0.338	1.5	427	294	415	664	367	674	754	8.91	7.61	10.54
14	200	0.102	0.5	436	382	875	1050	651	701	497	18.87	13.59	20.89
15	200	0.102	1	846	506	1605	1884	616	790	670	17.28	13.67	21.22
16	200	0.102	1.5	1068	186	1850	2144	619	894	714	17.42	18.2	22.3
17	200	0.102	2	1406	458	2265	2705	637	1508	1017	22.6	20.4	26.8
18	200	0.102	2.5	1880	546	2955	3545	570	1134	887	18.5	18.9	28.1
19	200	0.102	3	2758	1118	4700	5563	560	1459	1078	20.2	21.2	29.9

TABLE 7.4: Power required to shear using sharp tool insert

Cut No.	Speed (m/min)	Feed (mm/rev)	DOC (mm)	Static Force (N)			Power Required (kW)		
				X	Y	Z	X	Y	Z
1	100	0 1016	1.5	311	115	392	1868	691	2351
2	130	0 1016	1.5	339	164	459	2645	1277	3584
3	150	0.1016	1.5	338	162	462	3040	1458	4159
4	180	0.1016	1.5	318	154	438	3437	1668	4728
5	200	0.1016	1.5	308	147	440	3694	1759	5286
6	230	0.1016	1.5	298	146	436	4118	2017	6015
7	250	0 1016	1.5	286	136	424	4292	2033	6354
8	280	0.1016	1.5	291	138	431	4882	2319	7249
9	300	0.1016	1.5	339	164	459	6105	2946	8270
10	200	0 1016	1.5	308	147	176	3694	1759	2114
11	200	0.1778	1.5	348	180	241	4178	2155	2891
12	200	0.254	1 5	422	276	357	5064	3311	4282
13	200	0.3378	1.5	427	294	415	5120	3529	4976
14	200	0.1016	0.5	436	382	875	4584	10500	55008
15	200	0.1016	1	846	506	1605	6072	19260	72864
16	200	0.1016	1.5	1068	186	1850	2232	22200	26784
17	200	0.1016	2	1406	458	2265	5496	27180	65952
18	200	0.1016	2.5	1880	546	2955	6552	35460	78624
19	200	0.1016	3	2758	1118	4700	13416	56400	160992

TABLE 7.5: Experimental results utilising worn tool insert

Cut	Speed	Feed	DOC	Static Force (N)				STP Dynamic Force (N)			STP Acceleration (g)		
No.	m/min	mm/rev	mm	X	Y	Z	R	X	Y	Z	X	Y	Z
20	80	0.163	2	796	384	960	1305	340	529	544	10.6	9	20.7
21	100	0.163	2	948	78	195	971	390	844	306	11.74	11.73	26.04
22	120	0.163	2	982	150	375	1062	413	975	379	14.13	13.03	26.66
23	150	0.163	2	1188	1072	2680	3121	1280	2453	381	11.6	13.3	11.3
24	180	0.163	2	1200	1114	2785	3231	1377	2570	925	14.7	11.9	10.1
25	200	0.163	2	1118	992	2480	2896	1236	2269	365	19.2	13.9	10.8
26	220	0.163	2	702	910	2275	2549	1227	2830	373	20.8	12.5	12
27	250	0.163	2	478	684	1710	1903	1292	1866	402	30.6	15.7	14.7
28	265	0.163	2	1032	778	1945	2335	1183	2443	390	24.9	17.3	13.7
29	200	0.08	2	1128	972	2430	2850	1210	2570	1118	16.3	13.8	10.9
30	200	0.0882	2	852	520	1300	1639	622	805	671	17.29	13.67	21.23
31	200	0.106	2	1178	1108	2770	3208	1204	2437	923	15.5	12.2	10.9
32	200	0.163	2	1242	1072	2680	3142	1682	3101	1402	18.2	12.3	10.2
33	200	0.265	2	1242	1072	2680	3142	1682	3101	1402	18.2	12.3	10.2
34	200	0.3256	2	1838	1314	3285	3987	1838	3009	1756	24.5	15.8	12.3
35	200	0.7056	2	1524	1612	4030	4600	2445	4322	3485	44.8	35.5	41.5
36	200	0.163	0.5	342	310	775	902	418	787	643	15.04	17.03	22.34
37	200	0.163	1	638	400	1000	1252	860	1321	823	18.1	16.3	12.3
38	200	0.163	1.5	1080	920	2300	2702	1088	2083	960	17.5	15.4	10.9
39	200	0.163	2	1210	1058	2645	3095	1401	2897	116	17.2	15	11.1
40	200	0.163	2.5	752	1260	3150	3475	2495	3626	1649	17.1	15.8	11.7
41	200	0.163	3	2352	1640	4100	5003	1814	3549	1552	20.6	17.7	13.5

TABLE 7.6: Power required to shear with worn tool insert

Cut No.	Speed	Feed	DOC	Static Force (N)			Power Required (kW)		
				X	Y	Z	X	Y	Z
20	80	0.163	2	796	384	960	4776	2304	5760
21	100	0.163	2	948	78	195	7394.4	608.4	1521
22	120	0.163	2	982	150	375	8838	1350	3375
23	150	0.163	2	1188	1072	2680	12830.4	11577.6	28944
24	180	0.163	2	1200	1114	2785	14400	13368	33420
25	200	0.163	2	1118	992	2480	15428.4	13689.6	34224
26	220	0.163	2	702	910	2275	10530	13650	34125
27	250	0.163	2	478	684	1710	8030.4	11491.2	28728
28	265	0.163	2	1032	778	1945	18576	14004	35010
29	200	0.08	2	1128	972	2430	13536	11664	29160
30	200	0.0882	2	852	520	1300	10224	6240	15600
31	200	0.106	2	1178	1108	2770	14136	13296	33240
32	200	0.163	2	1242	1072	2680	14904	12864	32160
33	200	0.265	2	1242	1072	2680	14904	12864	32160
34	200	0.3256	2	1838	1314	3285	22056	15768	39420
35	200	0.7056	2	1524	1612	4030	18288	19344	48360
36	200	0.163	0.5	342	310	775	4104	3720	9300
37	200	0.163	1	638	400	1000	7656	4800	12000
38	200	0.163	1.5	1080	920	2300	12960	11040	27600
39	200	0.163	2	1210	1058	2645	14520	12696	31740
40	200	0.163	2.5	752	1260	3150	9024	15120	37800
41	200	0.163	3	2352	1640	4100	28224	19680	49200

P10 FIGURES

(SHARP)

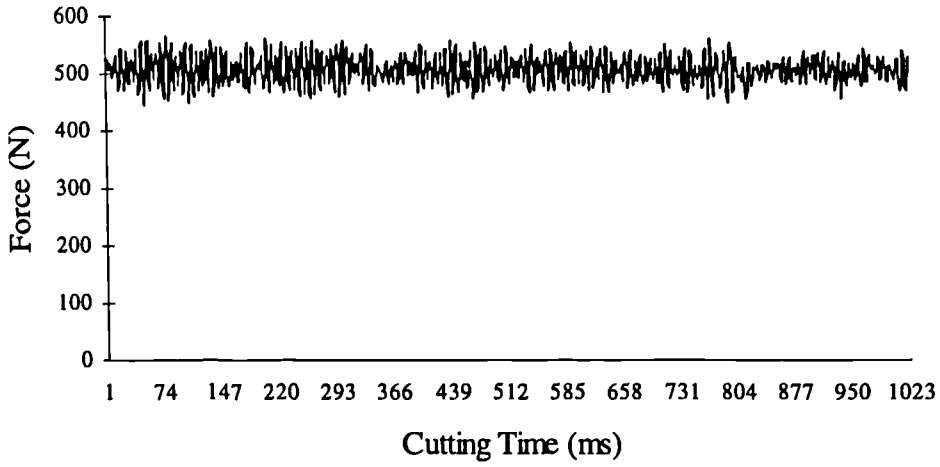

Fig. 7.1: Z-axis time display for the cutting force signal - sharp tool (V=200m/min., f=0.2mm/rev & a=2mm)

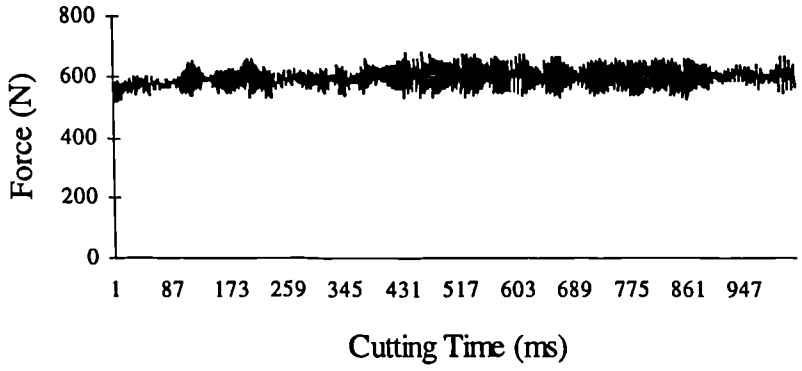

Fig. 7.2: Z-axis time display for the cutting force signal - worn tool (V=200m/min, f=0.2mm/rev & a=2 ım)

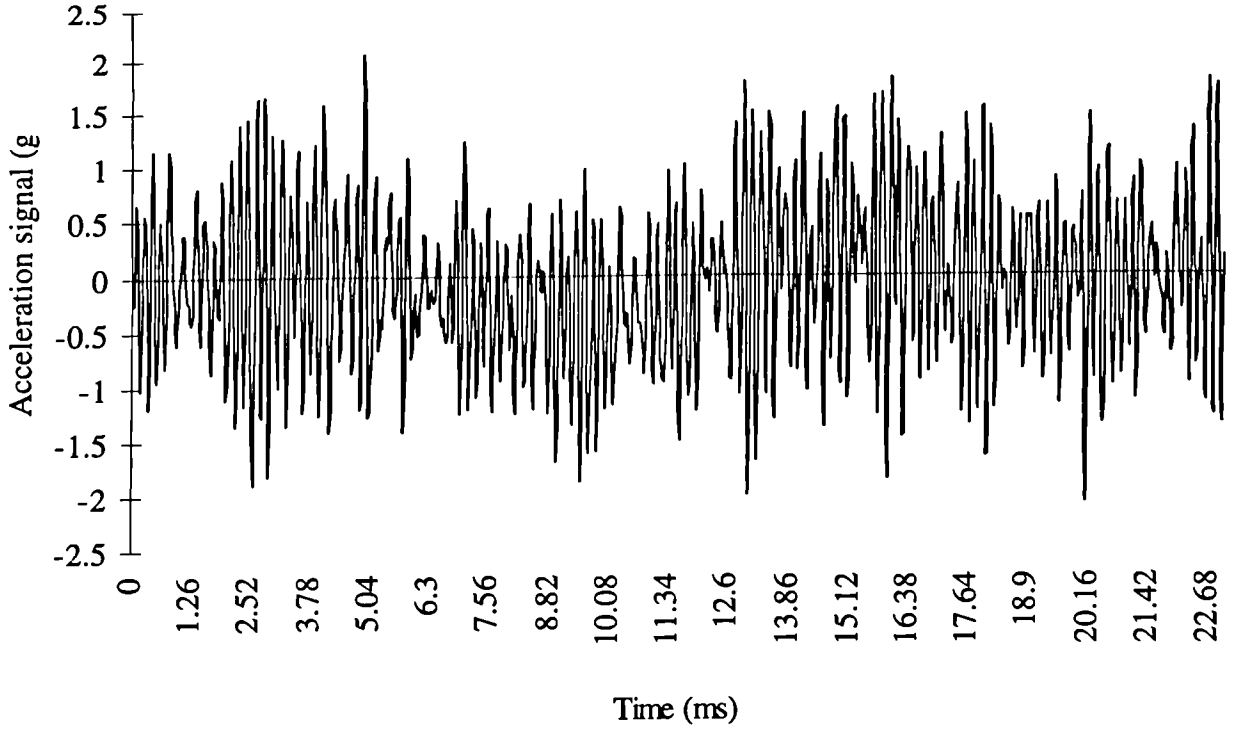

Fig. 7.3: Typical time display z-axis acceleration signal (V=200m/min., f=0.2mm/rev. & a=2mm)

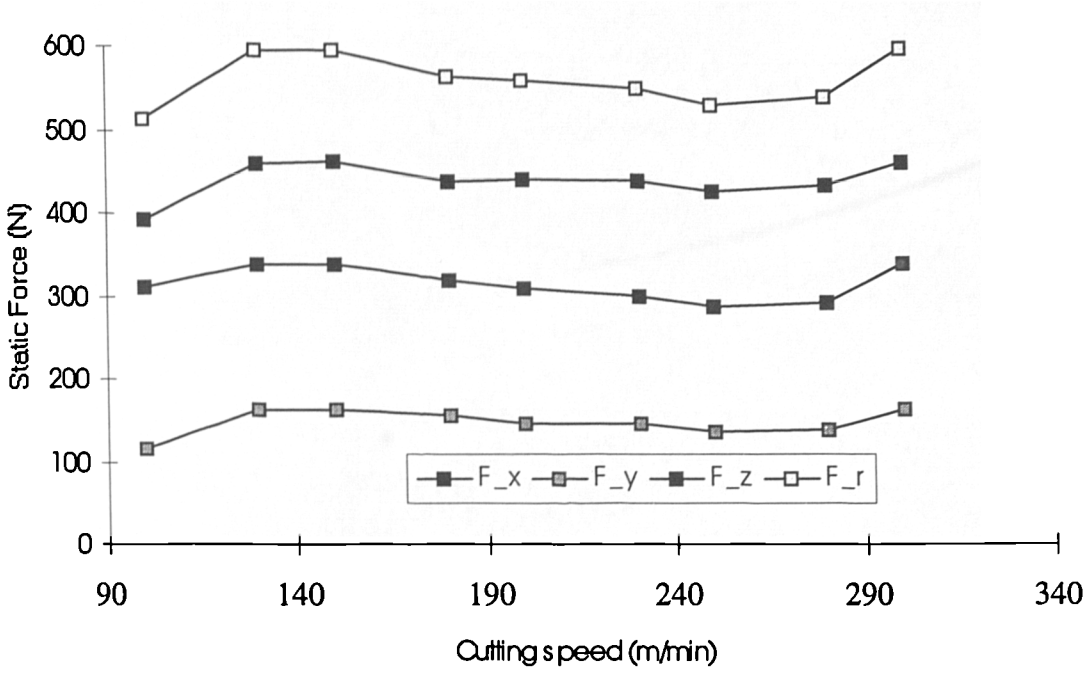

Figure 7.4: Static Force Vs. Cutting speed (f=0.1mm/rev & a=1.5mm)

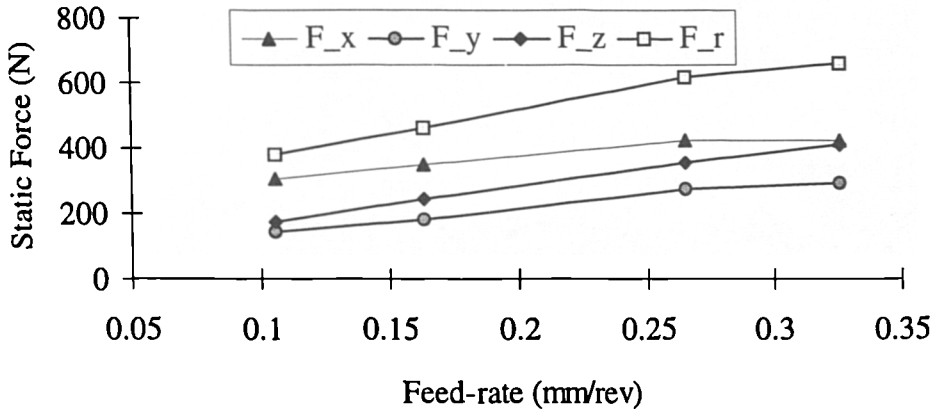

Figure 7.5: Static Force Vs. Feed-rate (V=200m/min & a=1.5mm)

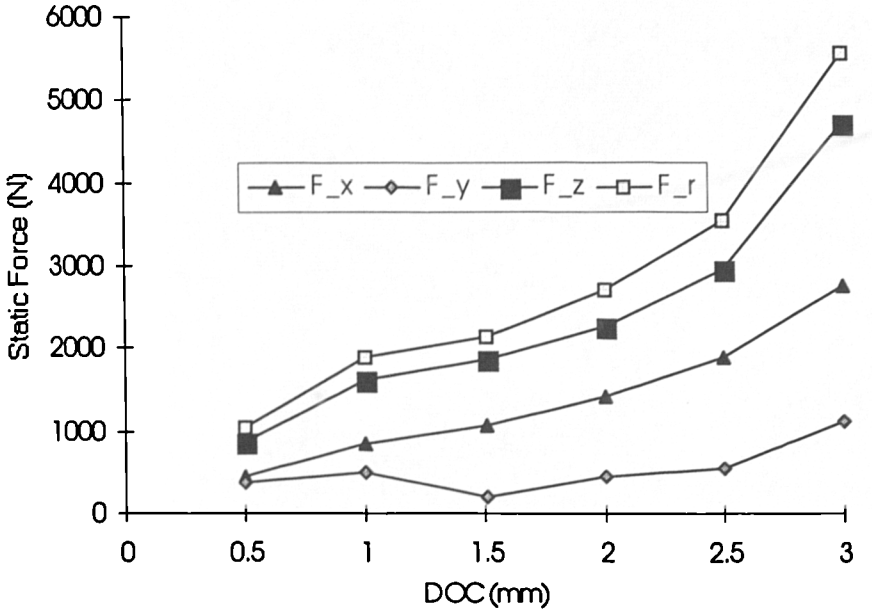

Figure 7.6: Static Force Vs. DOC (V=200m/min. &f=0.1mm/rev.)

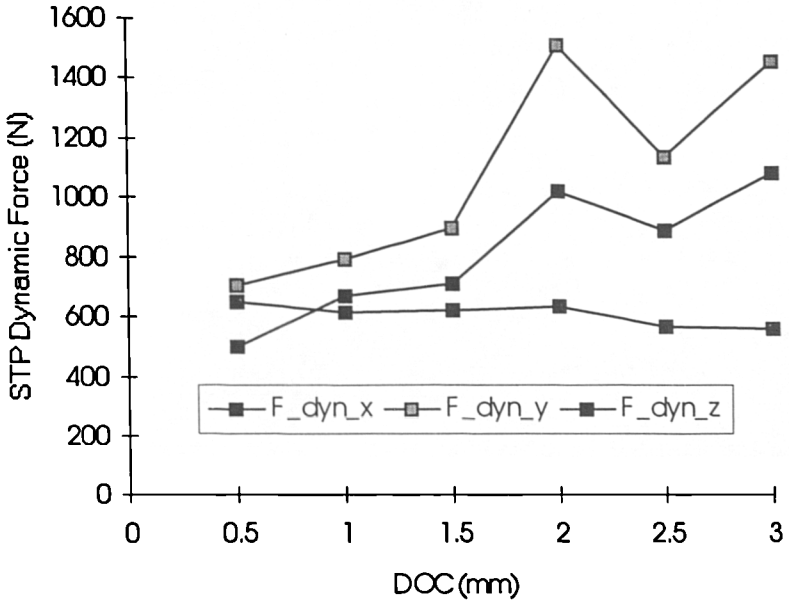

Figure 7.7: STP in Dynamic Force Vs. DOC (V=200m/min. & f=1.5mm/rev.)

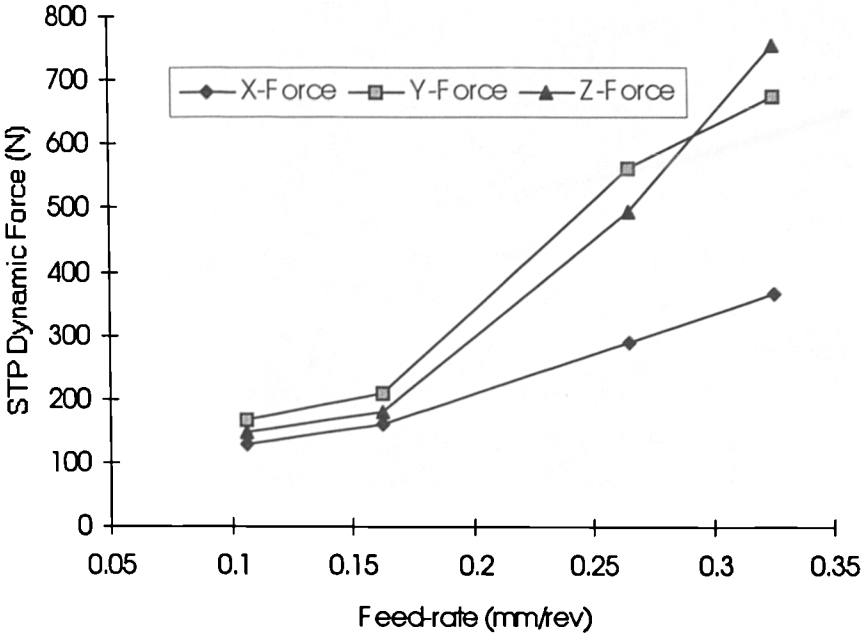

Figure 7.8: STP in Dynamic Force spectra Vs. Feed-rate (V=200m/min. & a=1.5mm/rev.)

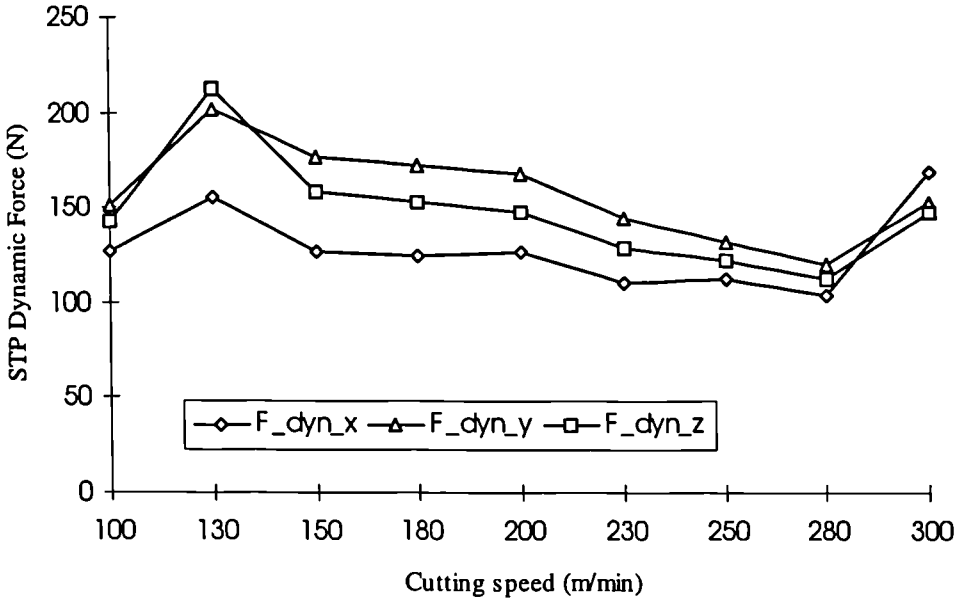

Figure 7.9: STP in Dynamic Force spectra Vs. Cutting speed (f=0.1mm/rev. & a=1.5mm)

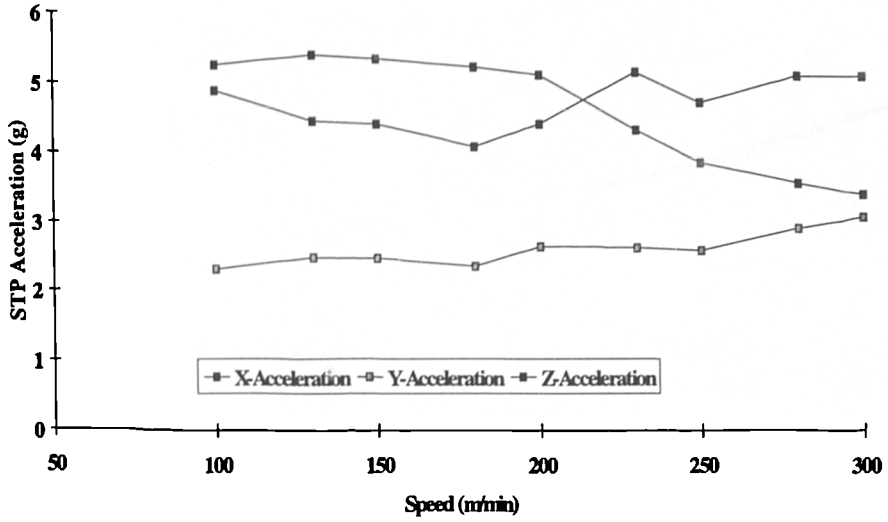

Figure 7.10: STP in Acceleration signal Vs. Cutting speed (f=0.1mm/rev. & a=1.5mm)

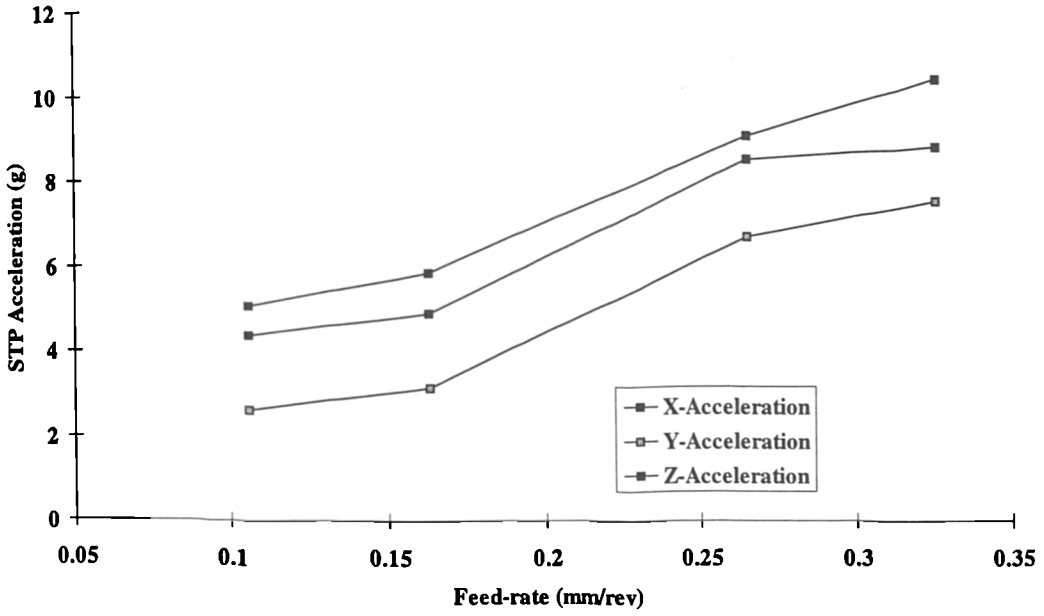

Figure 7.11: STP in Acceleration Signal Vs. Feed-rate (V=200m/min. & a=1.5mm)

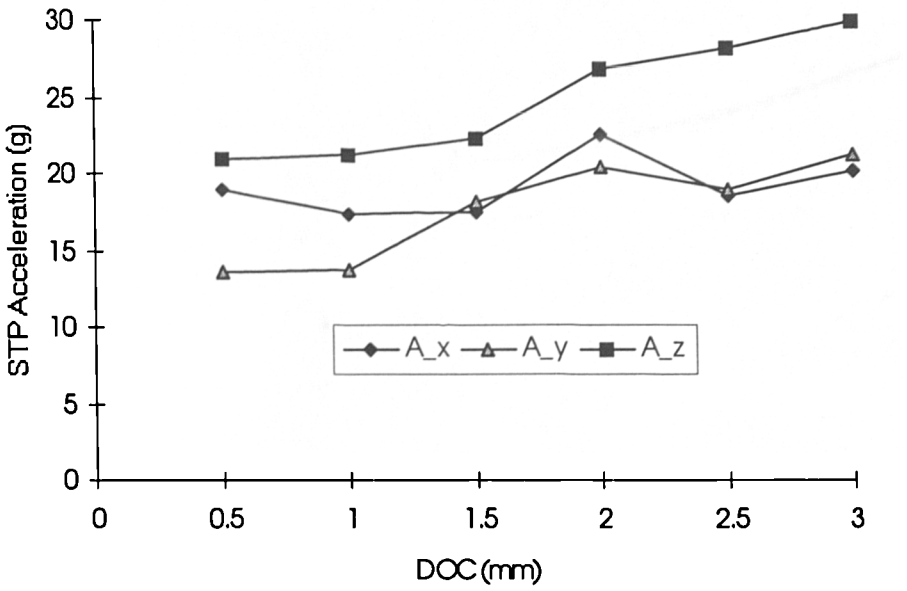

Figure 7.12: STP in Acceleration Signal Vs. DOC (V=200m/min. & f=0.1mm/rev.)

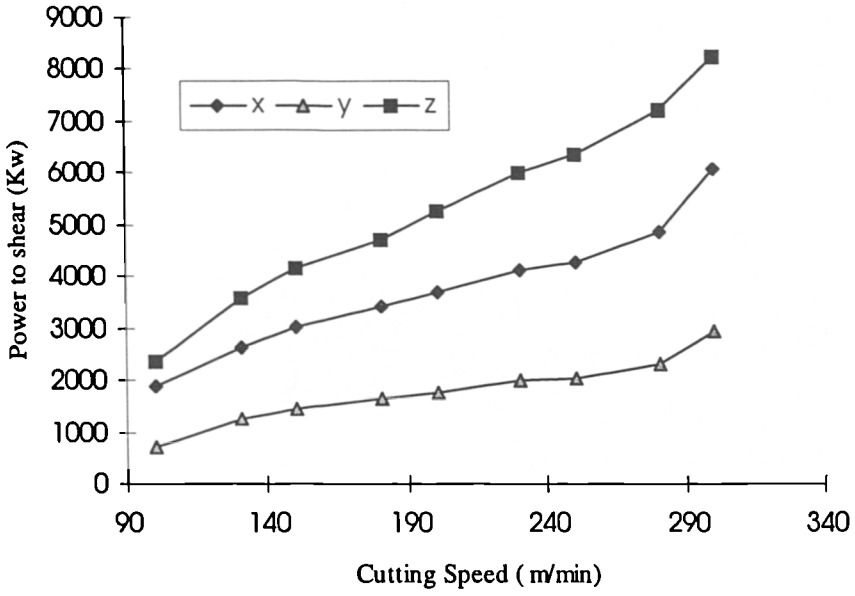

Figure 7.13: Cutting Power Vs. Cutting speed (f=0.1mm/rev. & a=1.5mm)

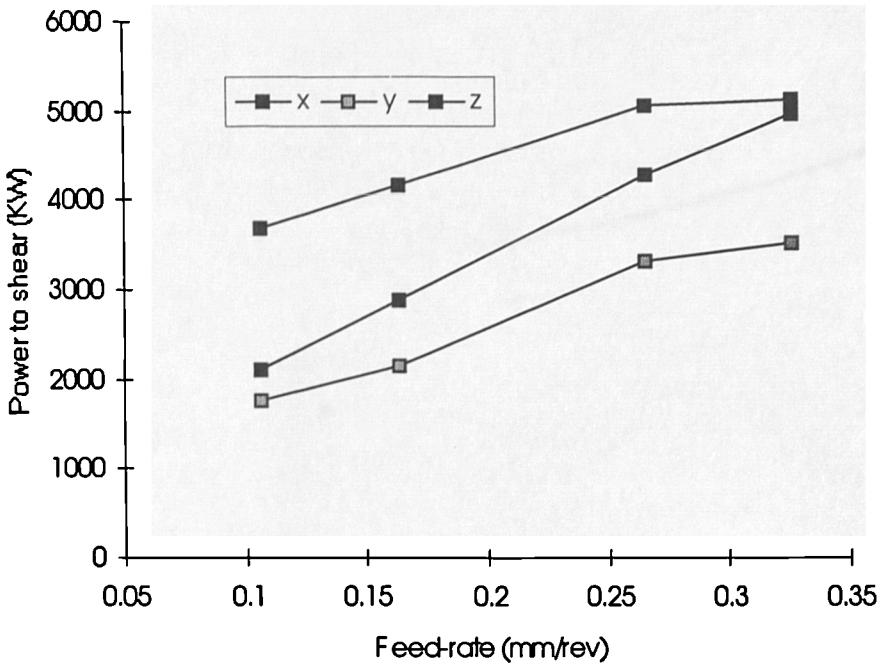

Figure 7.14: Cutting Power Vs. Feed-rate (V=200m/min. & a=1.5mm)

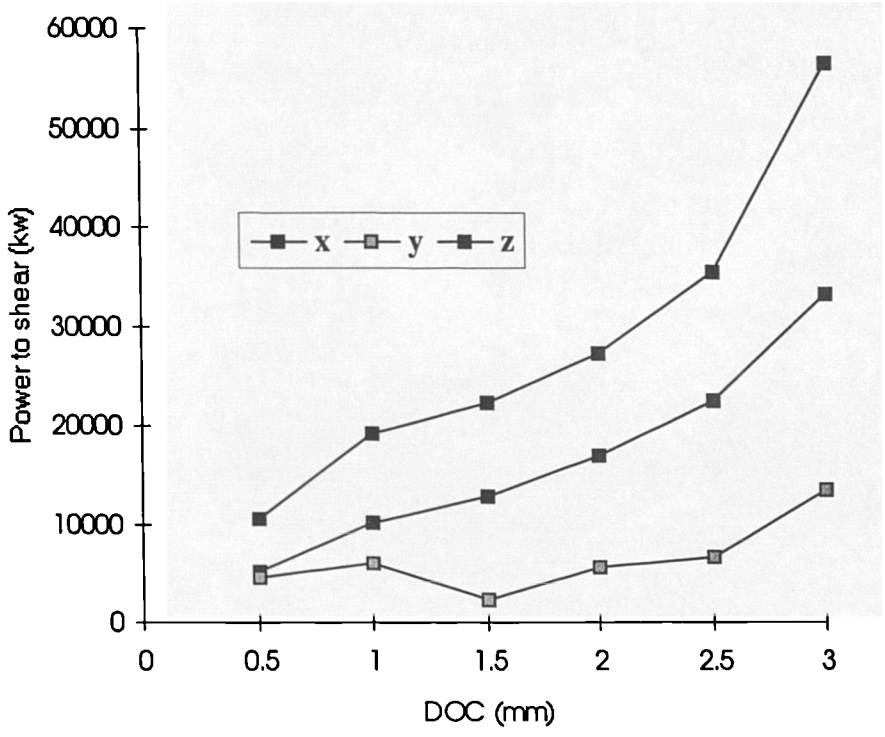

Figure 7.15: Cutting Power Vs. DOC (V=200m/min. & f=0.1mm/rev.)

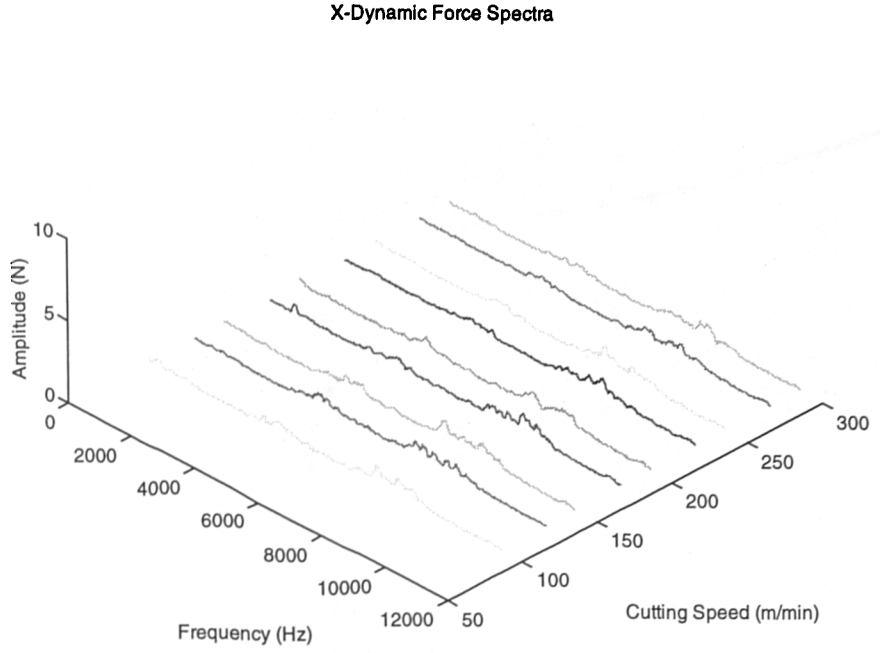

Figure 7.16: Horizontal (X) Dynamic Force Spectra Vs. Cutting Speed (f=0.1mm/rev. & a=1.5mm)

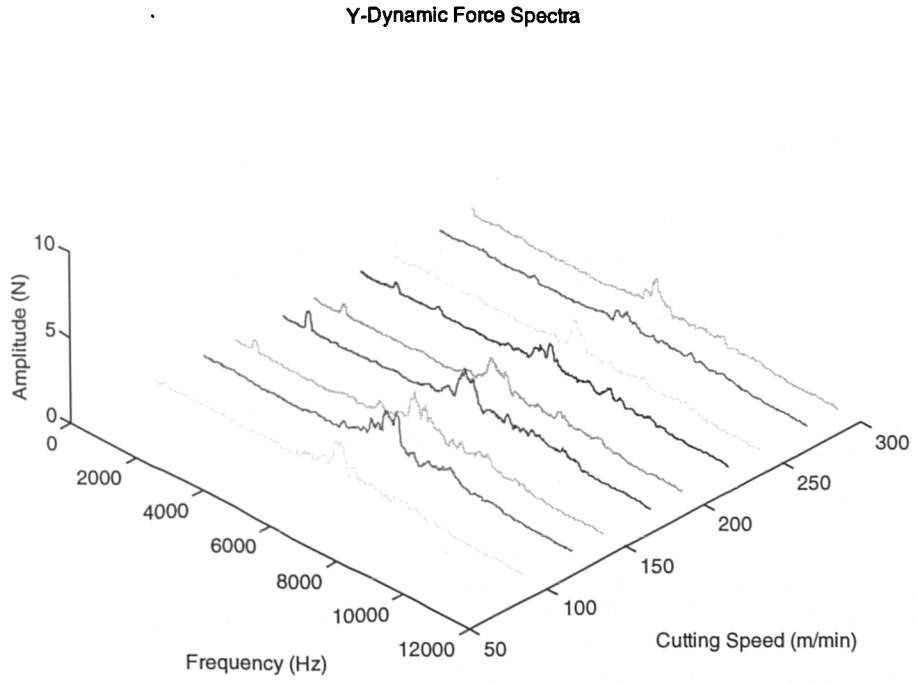

Figure 7.17: Horizontal (Y) Dynamic Force Spectra Vs. Cutting Speed (f=0.1mm/rev. & a=1.5mm)

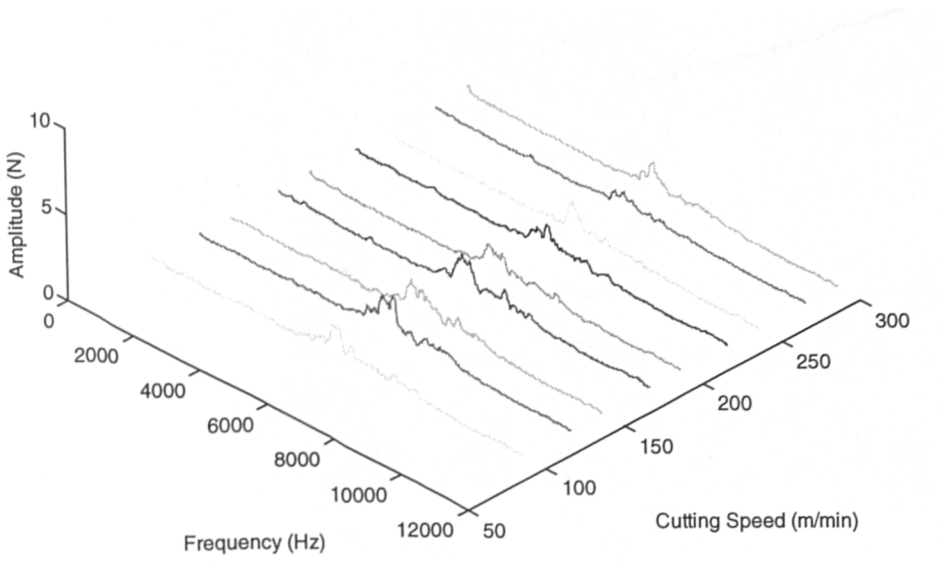

Figure 7.18: Vertical (Z) Dynamic Force Spectra Vs. Cutting Speed (f=0.1mm/rev. & a=1.5mm)

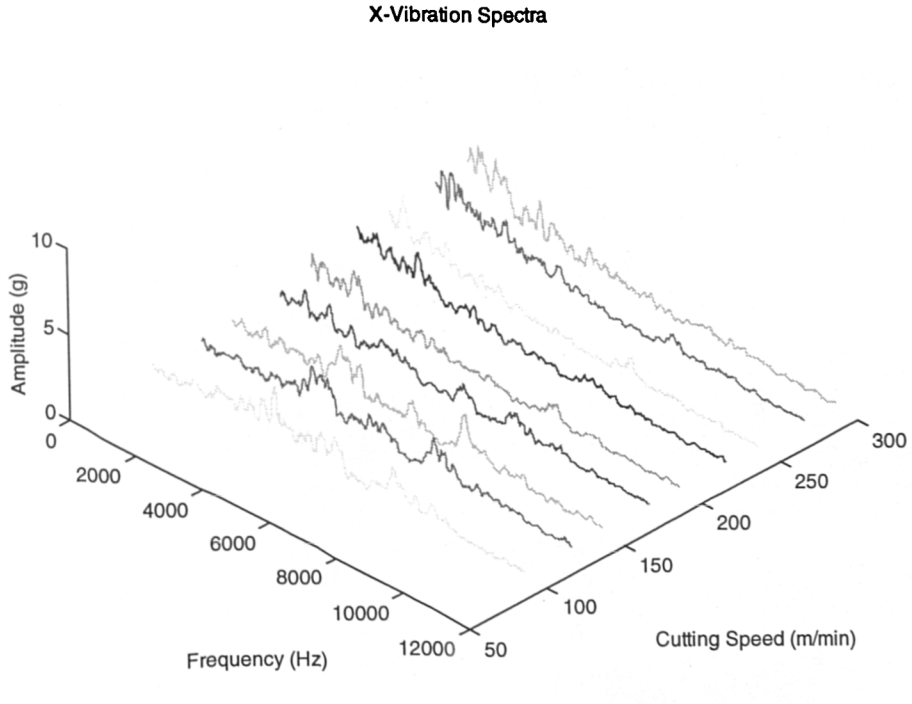

Figure 7.19: Horizontal (X) Vibration Spectra Vs. Cutting Speed (f=0.1mm/rev. & a=1.5mm)

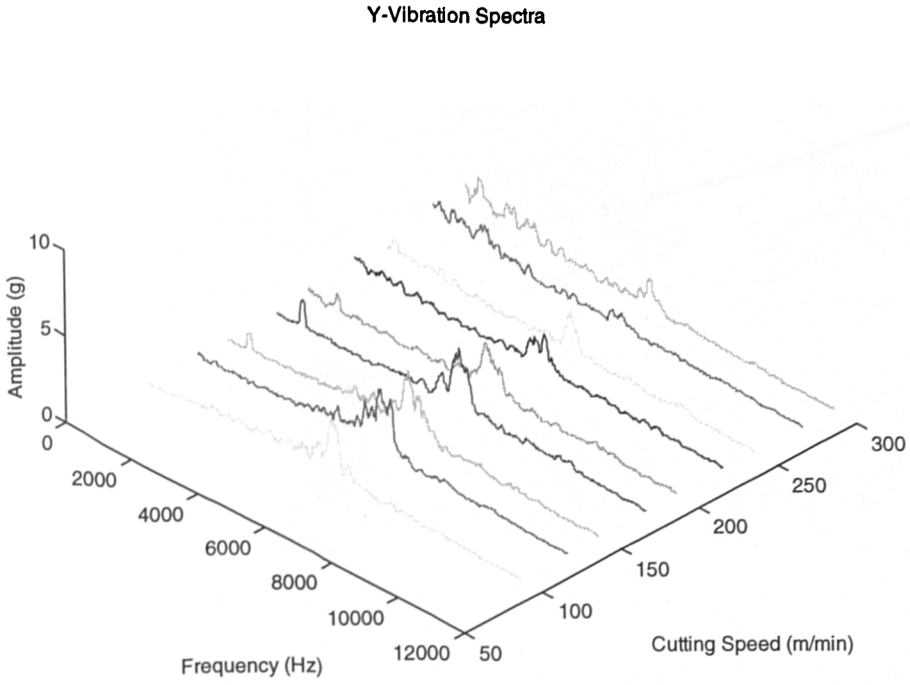

Figure 7.20: Horizontal (Y) Vibration Spectra Vs. Cutting Speed (f=0.1mm/rev. & a=1.5mm)

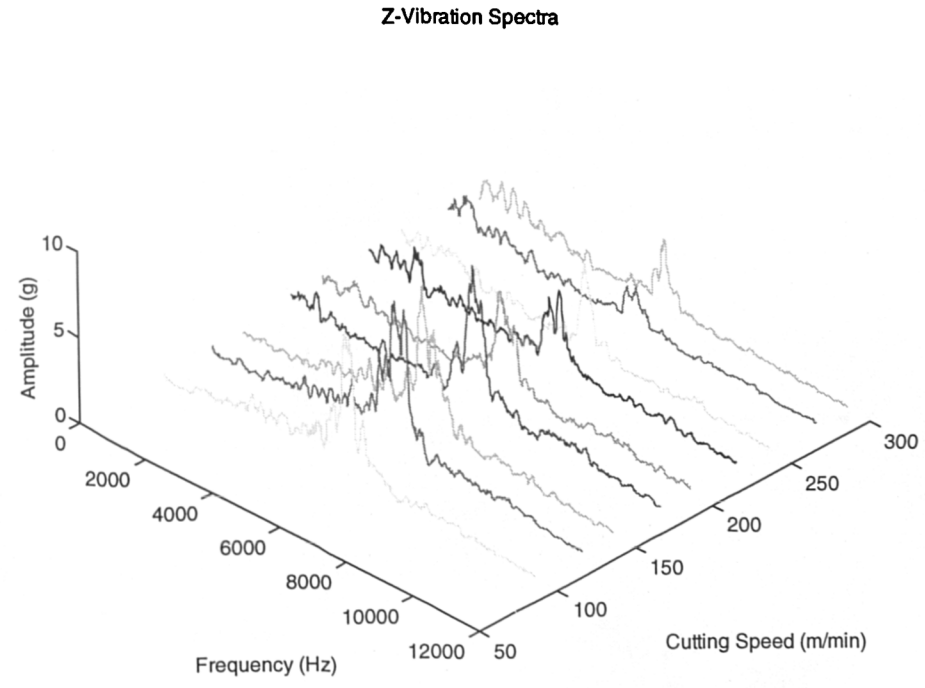

Figure 7.21: Vertical (Z) Vibration Spectra Vs. Cutting Speed (f=0.1mm/rev. & a=1.5mm)

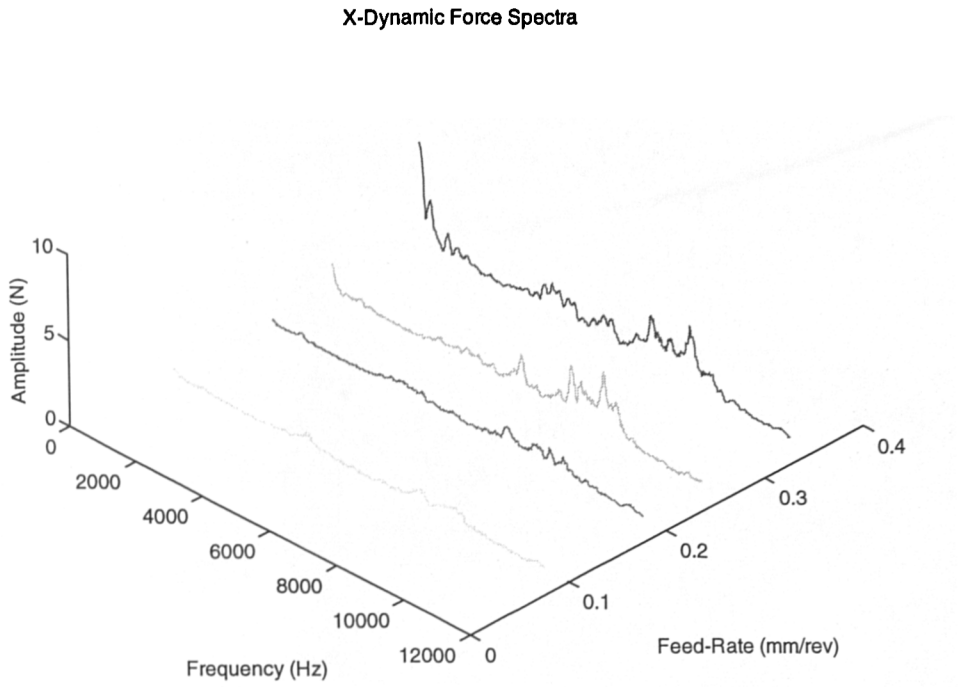

Figure 7.22: Horizontal (X) Dynamic Force Spectra Vs. Feed-Rate (V=200m/min. & a=1.5mm)

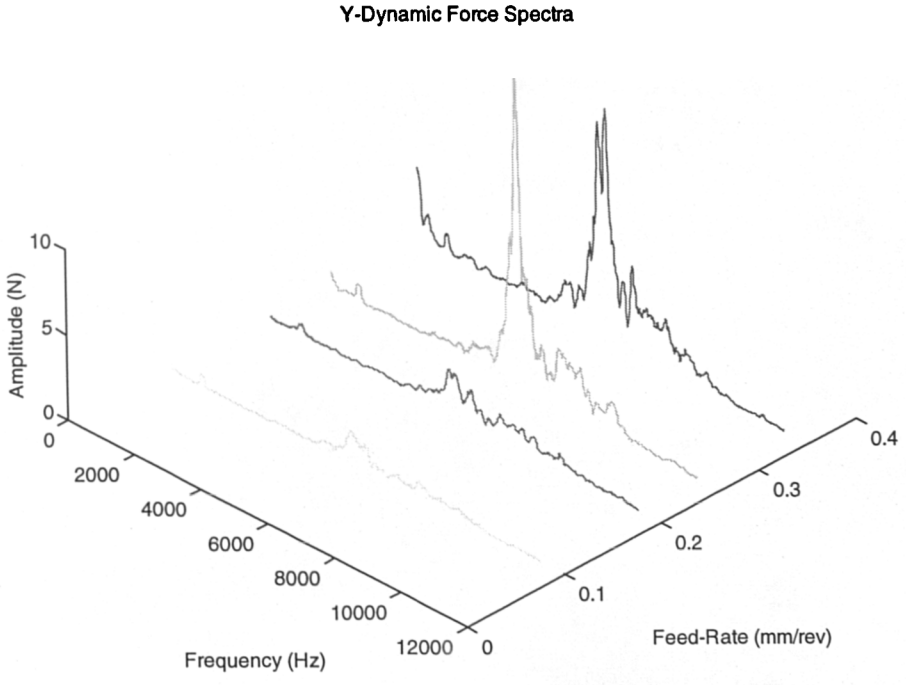

Figure 7.23: Horizontal (Y) Dynamic Force Spectra Vs. Feed-Rate (V=200m/min. & a=1.5mm)

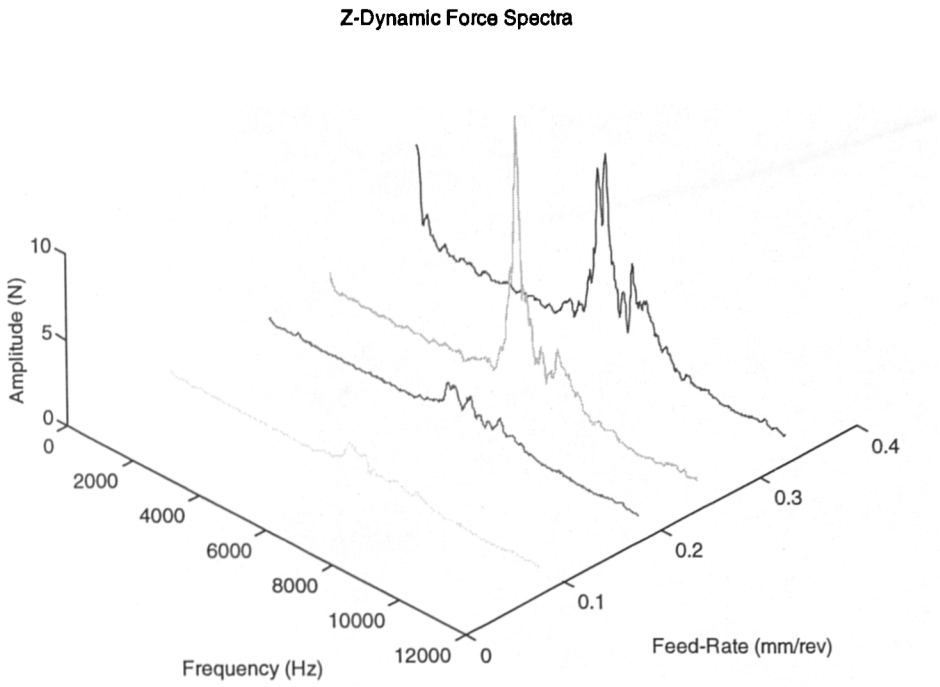

Figure 7.24: Vertical (Z) Dynamic Force Spectra Vs. Feed-Rate (V=200m/min. & a=1.5mm)

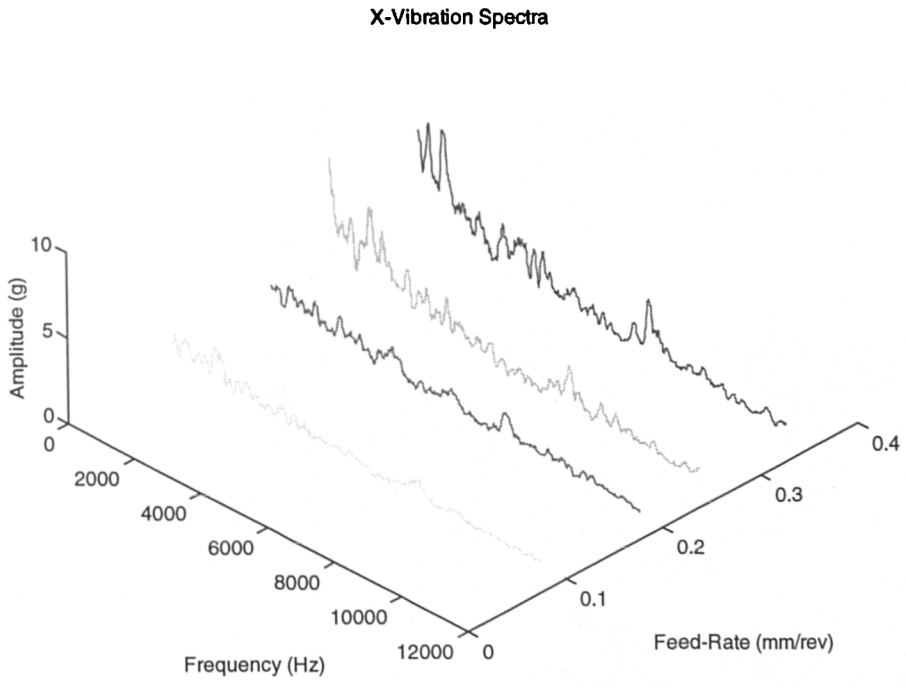

Figure 7.25: Horizontal (X) Vibration Spectra Vs. Feed-Rate (V=200m/min. & a=1.5mm)

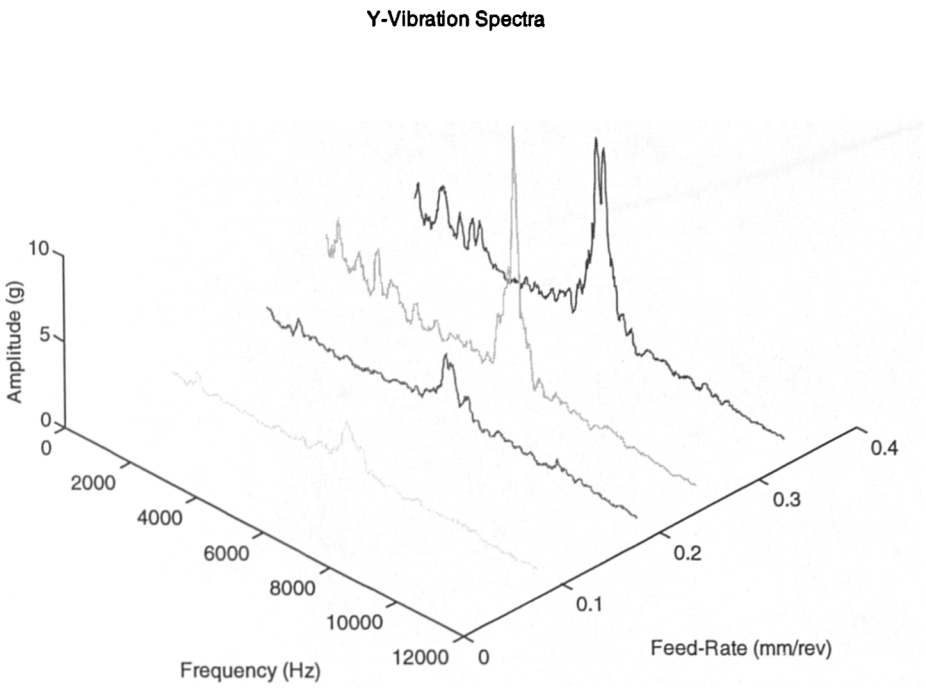

Figure 7.26: Horizontal (Y) Vibration Spectra Vs. Feed-Rate (V=200m/min. & a=1.5mm)

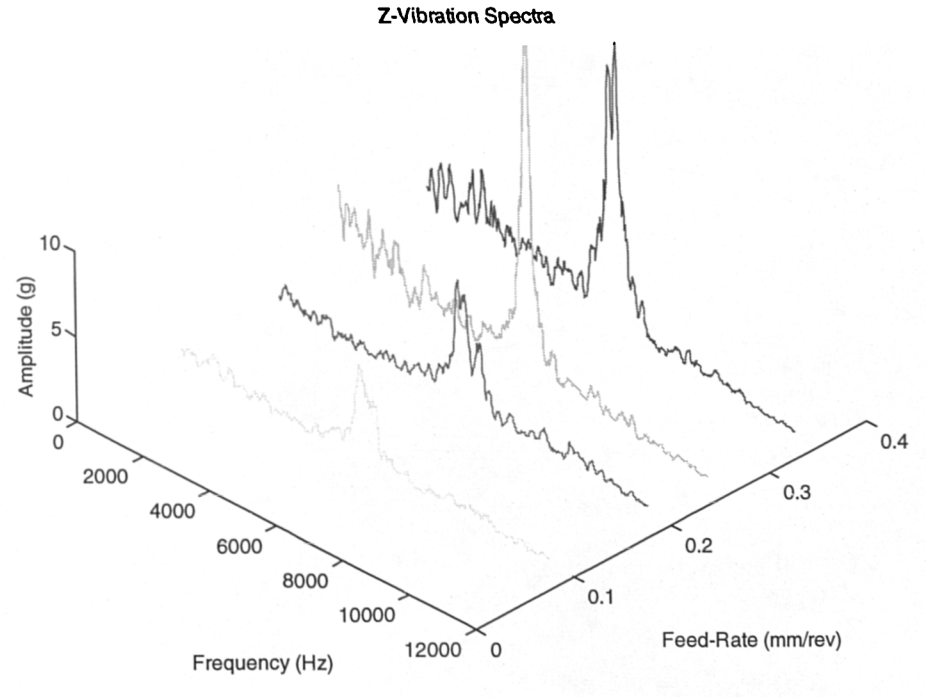

Figure 7.27: Vertical (Z) Vibration Spectra Vs. Feed-Rate

(V=200m/min. & a=1.5mm)

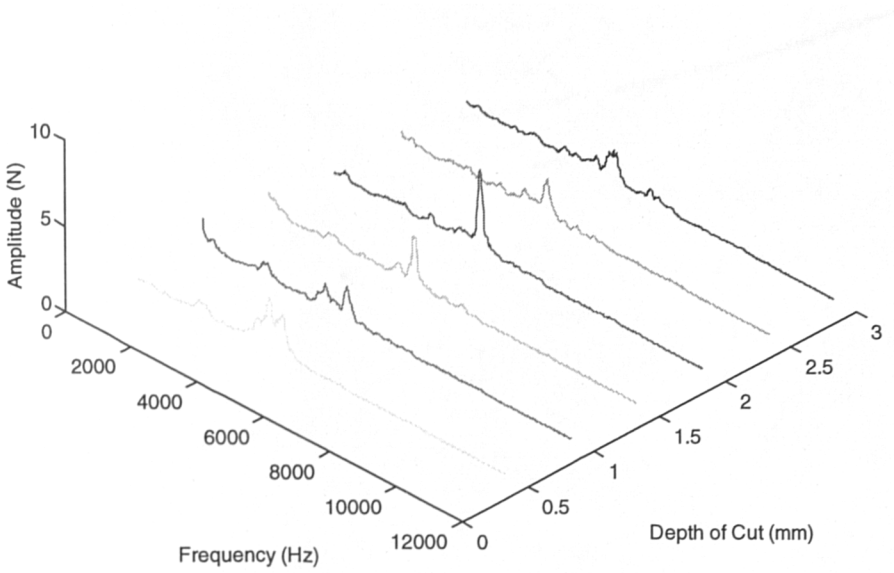

Figure 7.28: Horizontal (X) Dynamic Force Spectra Vs. DOC (V=200m/min. & f=0.1mm/rev.)

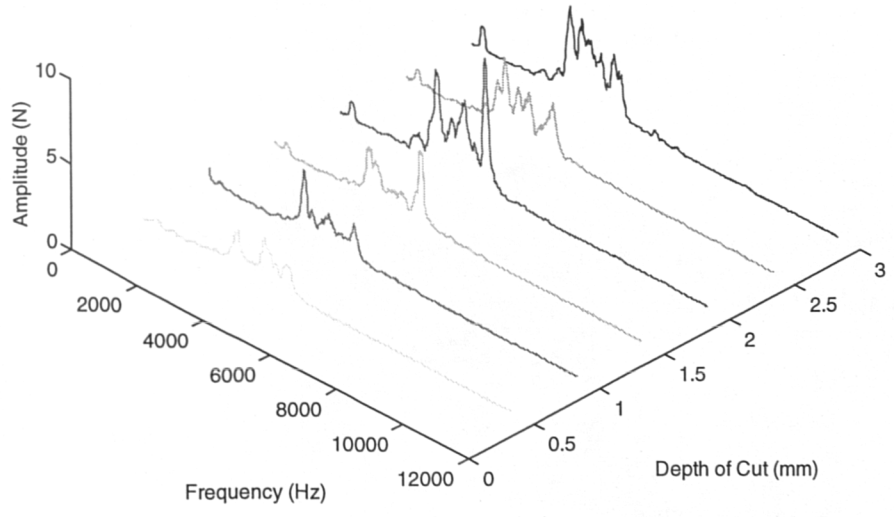

Figure 7.29: Horizontal (Y) Dynamic Force Spectra Vs. DOC (V=200m/min. & f=0.1mm/rev.)

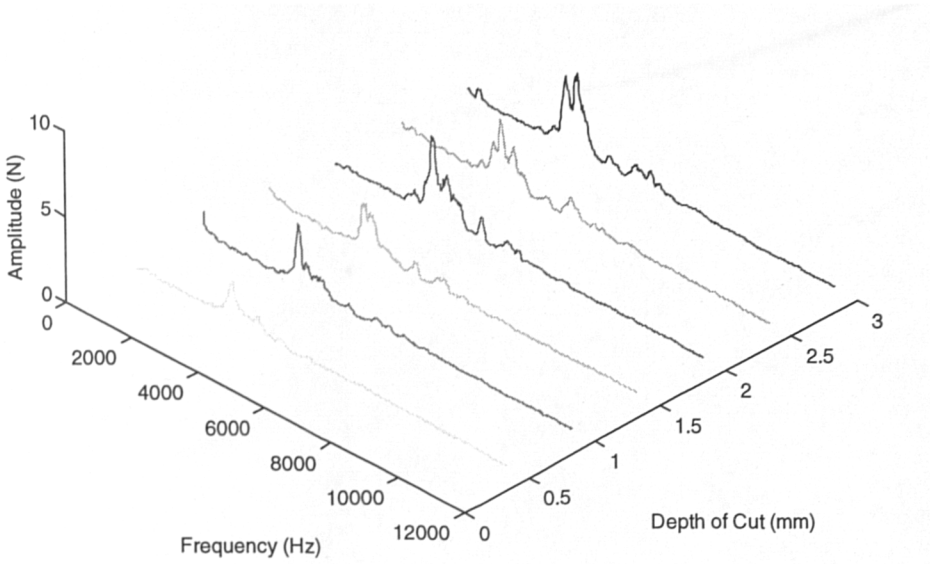

Figure 7.30: Vertical (Z) Dynamic Force Spectra Vs. DOC

(V=200m/min. & f=0.1mm/rev.)

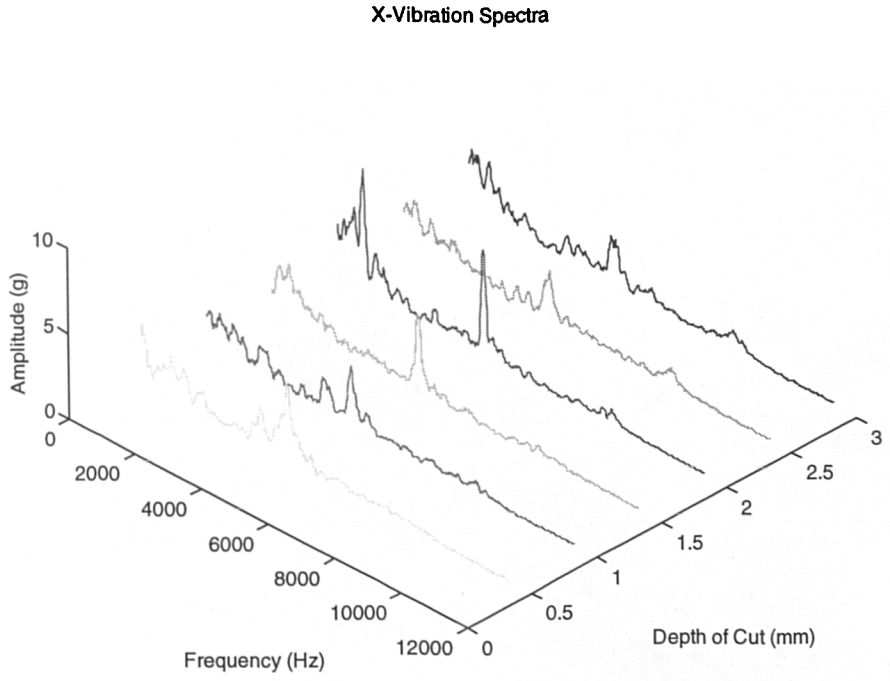

Figure 7.31: Horizontal (X) Vibration Spectra Vs. DOC

(V=200m/min. & f=0.1mm/rev.)

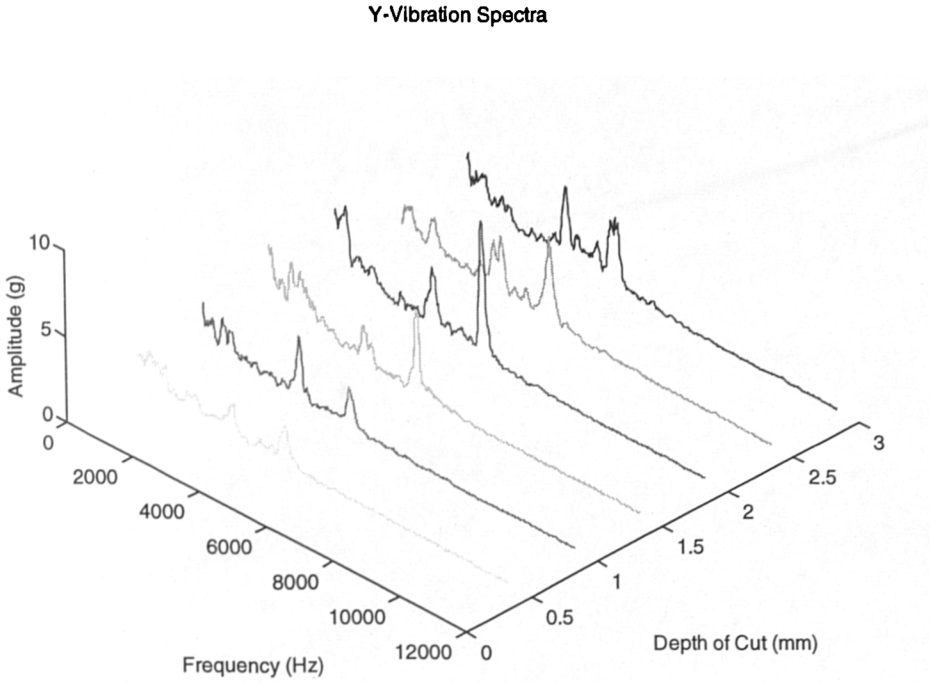

Figure 7.32: Horizontal (X) Vibration Spectra Vs. DOC

(V=200m/min. & f=0.1mm/rev.)

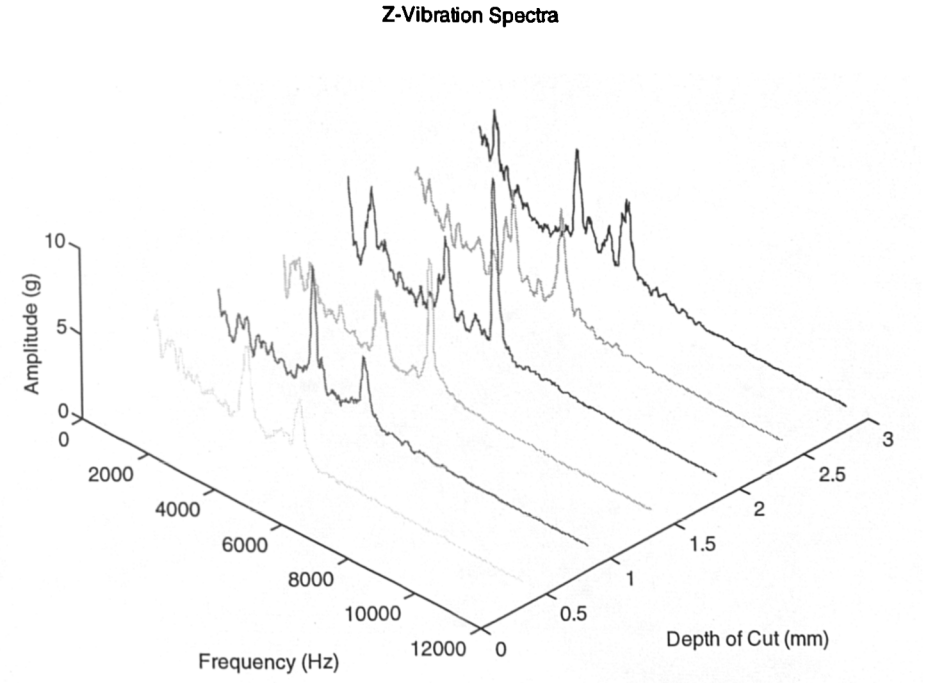

Figure 7.33: Vertical (Z) Vibration Spectra Vs. DOC

(V=200m/min. & f=0.1mm/rev.)

P10 FIGURES

(WORN)

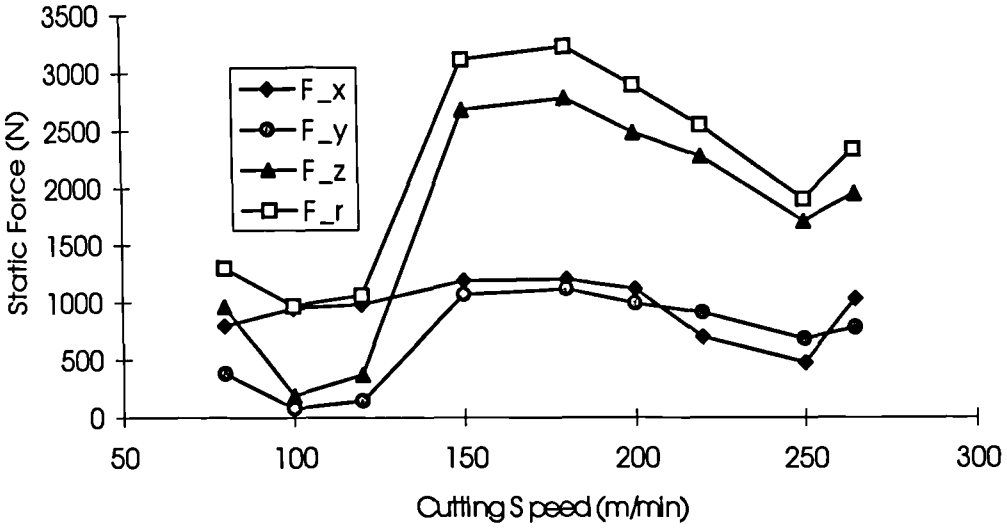

Figure 7.34: Static Force Vs. Cutting Speed -Worn Tool (f=0.2mm/rev. & a=2mm)

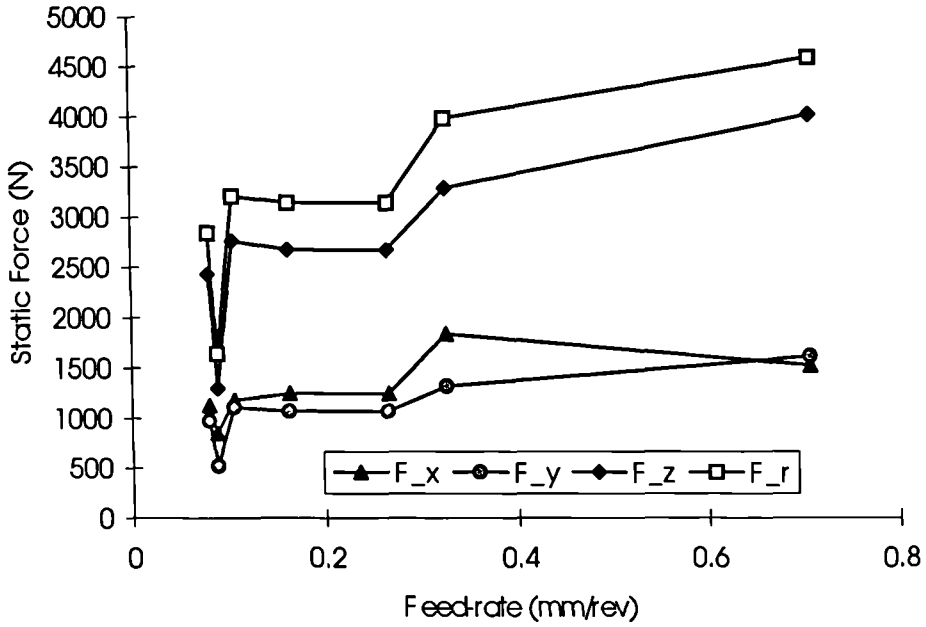

Figure 7.35: Static Force Vs. Feed-rate - Worn Tool (V=200m/min. & a=2mm)

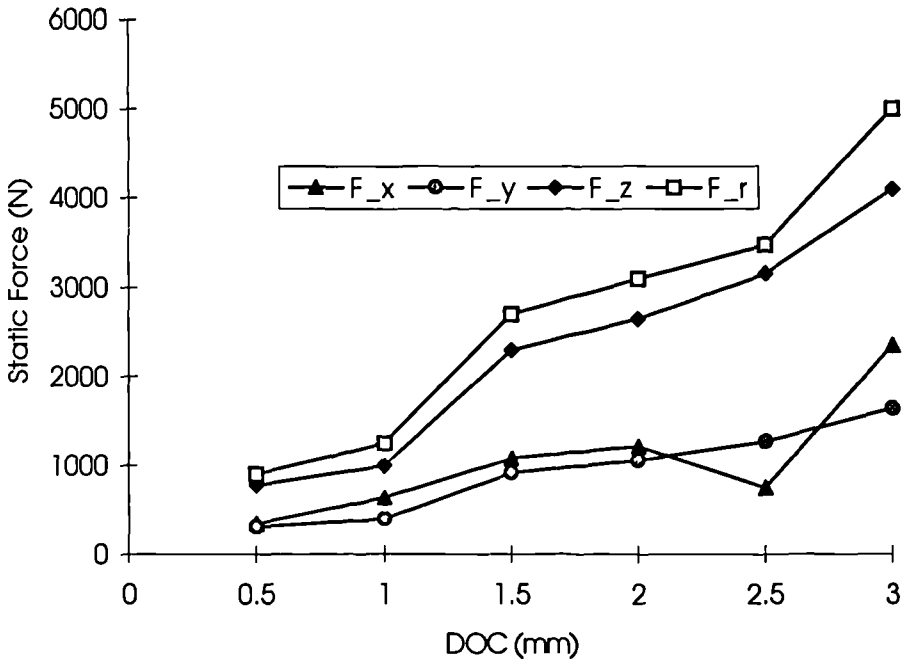

Figure 7.36: Static Force Vs. DOC - Worn Tool (V=200m/min. & f=0.2mm/rev.)

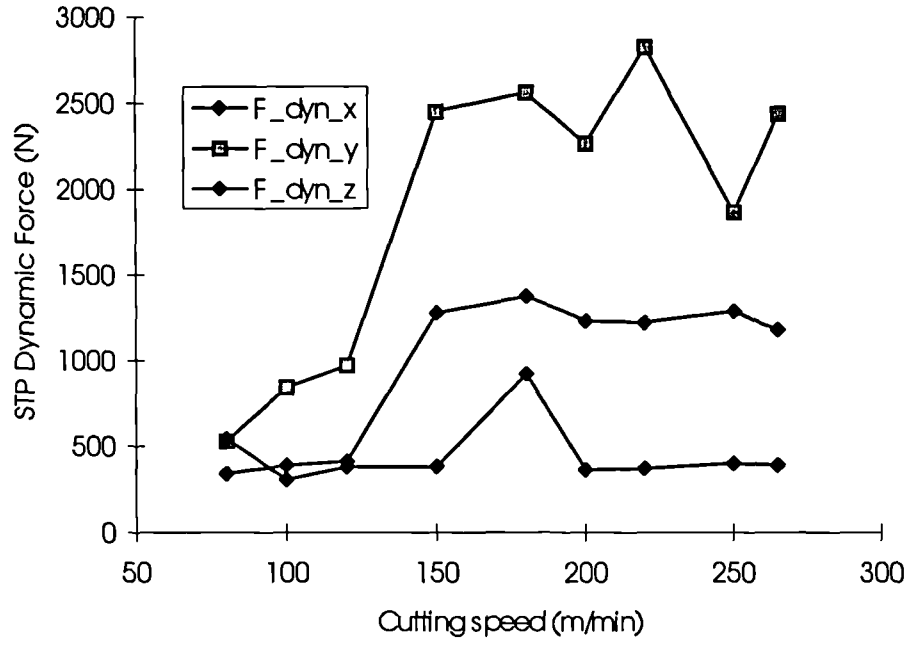

Figure 7.37: STP in Dynamic Force Signal Vs Cutting speed - Worn Tool (f=0.2mm/rev. & a=2mm)

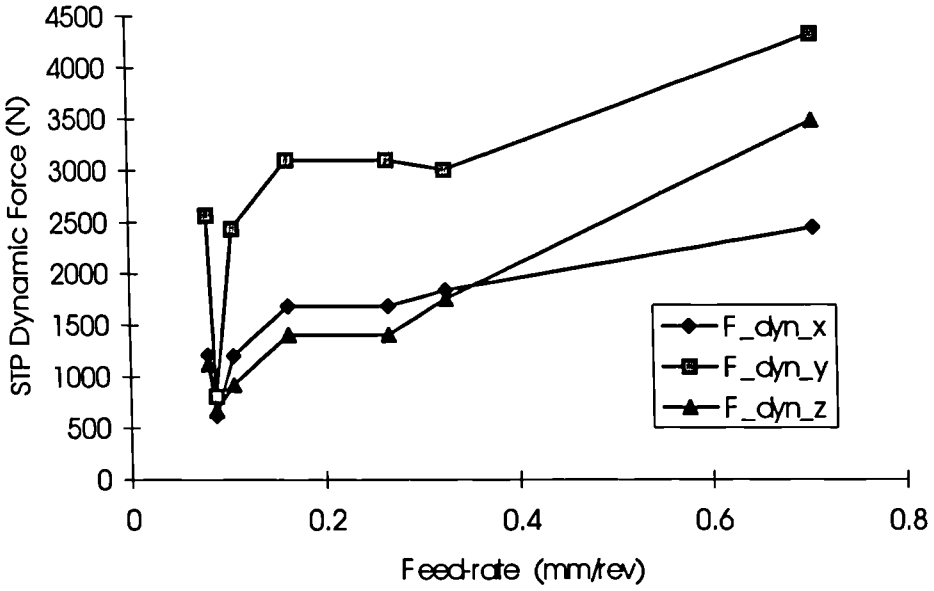

Figure 7.38: STP Dynamic Force Vs. Feed-rate - Worn tool (V=200m/min. & a=2mm)

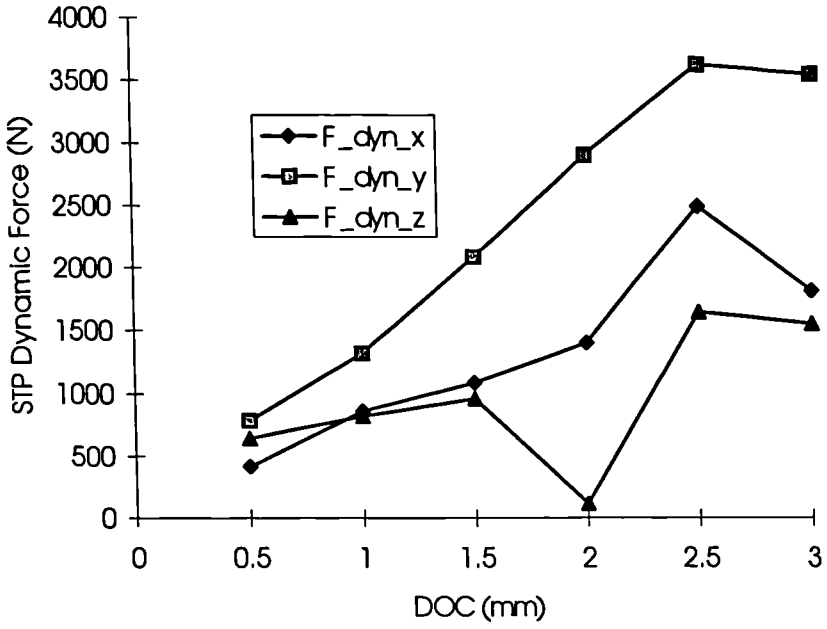

Figure 7.39: STP Dynamic Force Vs DOC - Worn Tool (V=200m/min. & f=0.2mm/rev.)

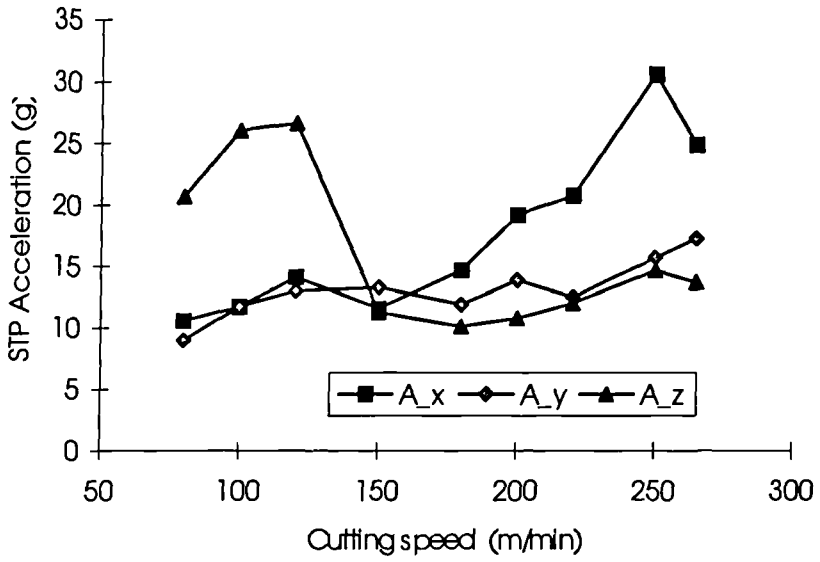

Figure 7.40: STP Acceleration Signal Vs. Cutting speed - Worn tool (f=0.2mm/rev. & a=2mm)

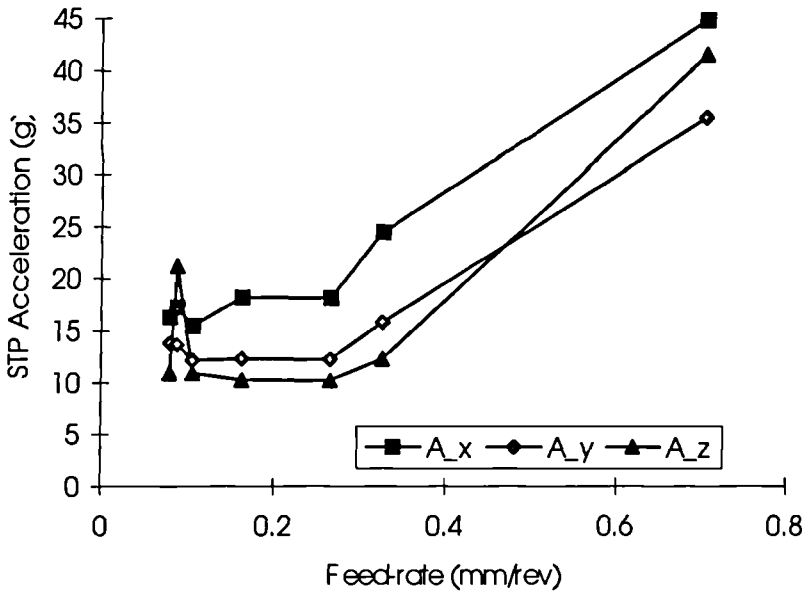

Figure 7.41: STP Acceleration Signal Vs. Feed-rate - Worn Tool (V=200m/min. & a=2mm)

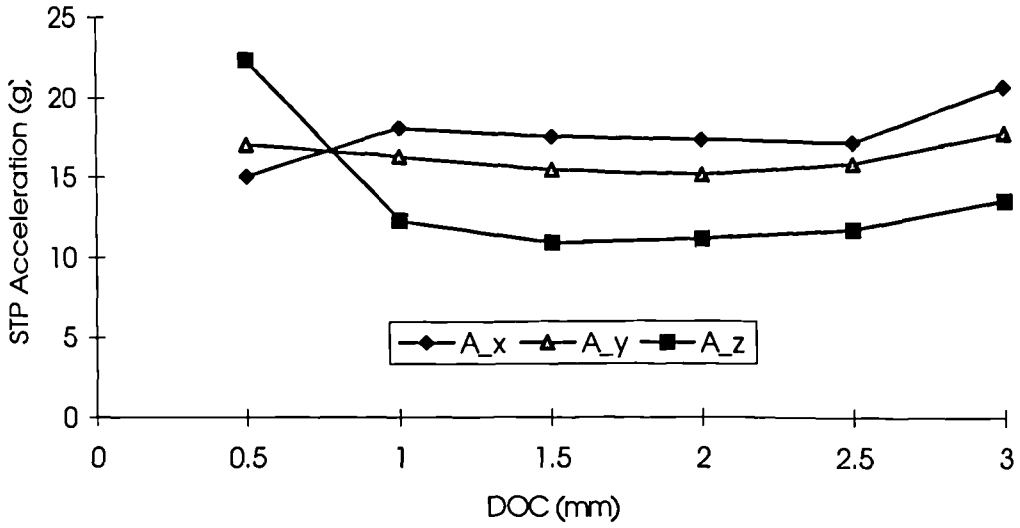

Figure 7.42: STP Acceleration Signal Vs DOC - Worn Tool (V=200m/min. & f=0.2mm)

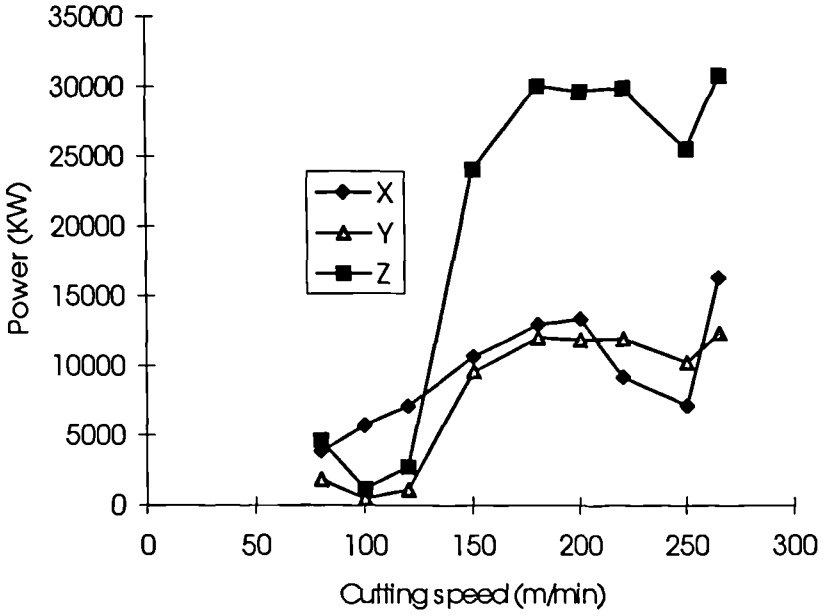

Figure 7.43: Cutting power Vs. Cutting speed - Worn Tool (f=0.2mm/rev. & a=2mm)

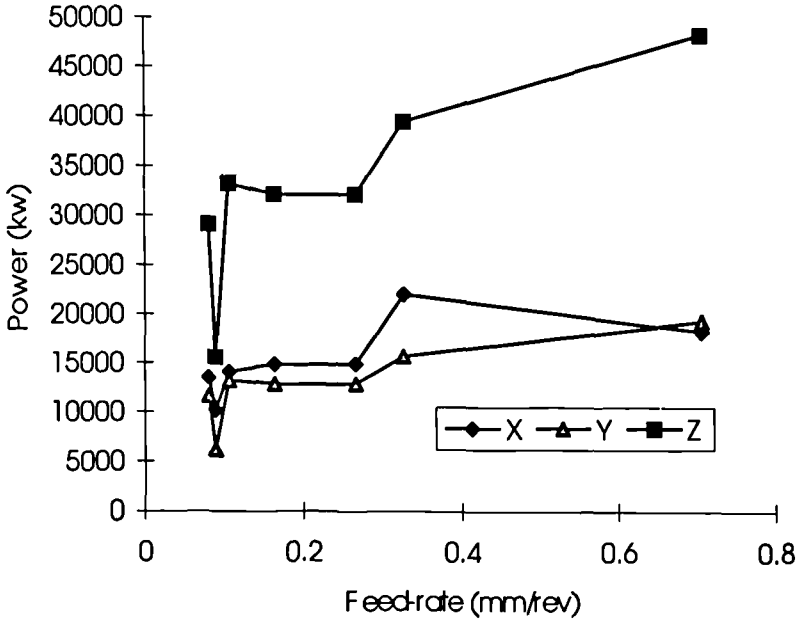

Figure 7.44: Cutting Power Vs Feed-rate - Worn Tool (V=200m/min. & a=2mm)

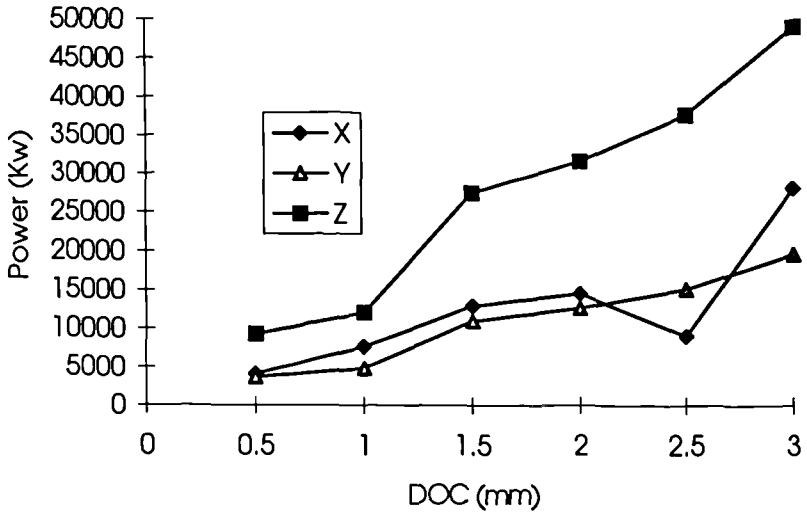

Figure 7.45: Cutting Power Vs. DOC -Worn Tool (V=200m/min. & f=0.2mm/rev.)

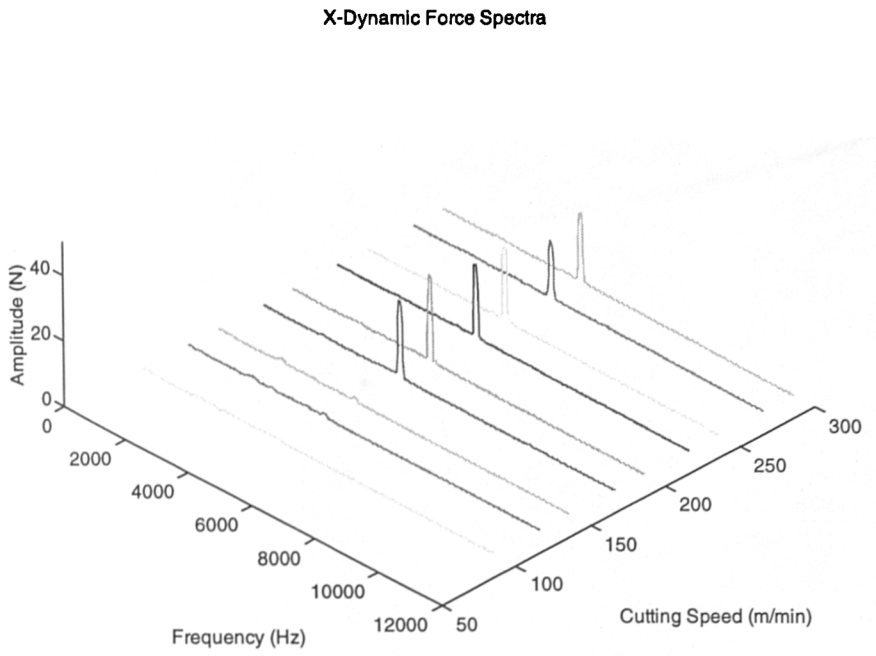

Figure 7.46: Horizontal (X) Dynamic Force Spectra Vs. Cutting Speed

(f=0.2mm/rev. & a=2mm)

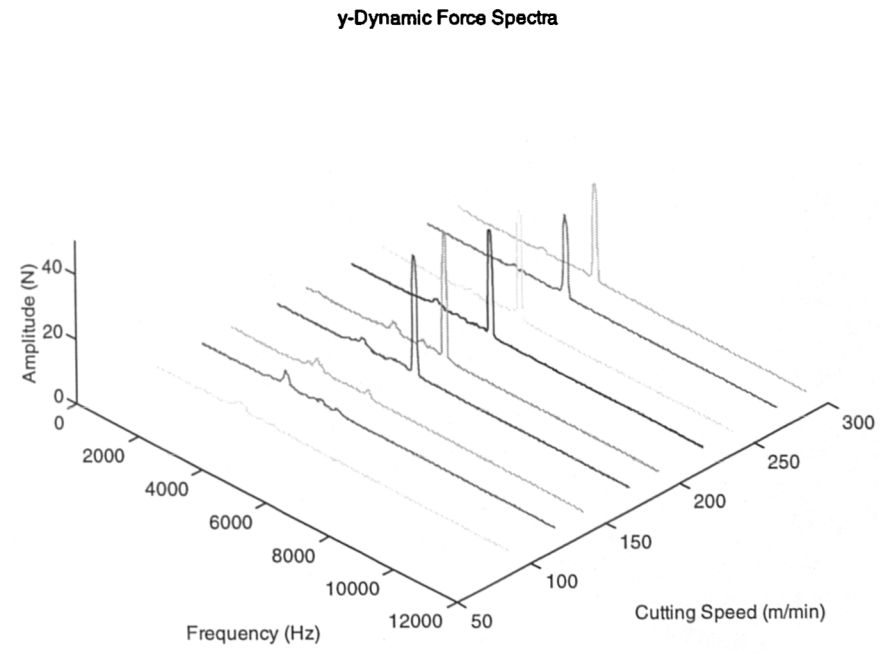

Figure 7.47: Horizontal (Y) Dynamic Force Spectra Vs. Cutting Speed

(f=0.2mm/rev. & a=2mm)

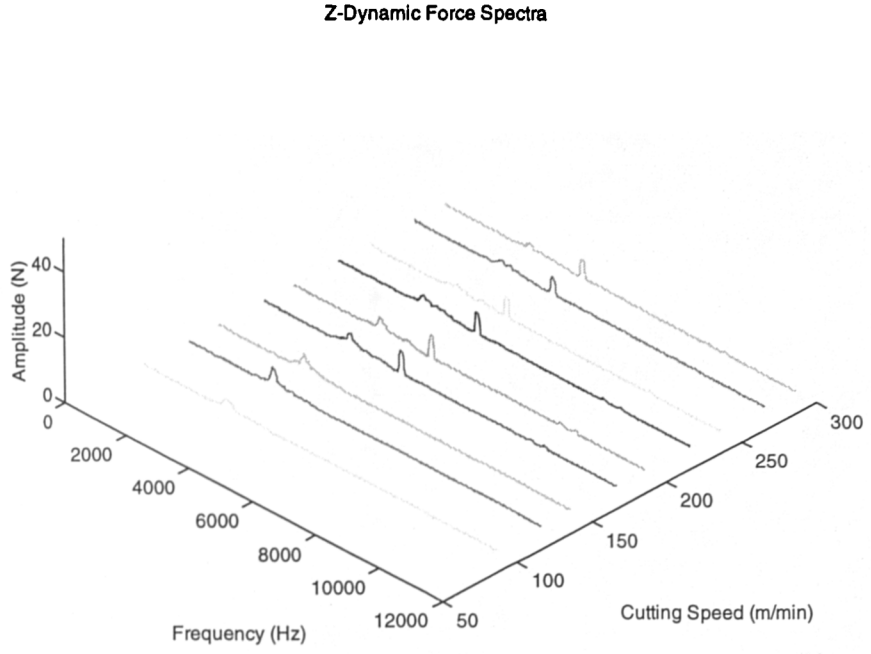

Figure 7.48: Vertical (Z) Dynamic Force Spectra Vs. Cutting Speed

(f=0.2mm/rev. & a=2mm)

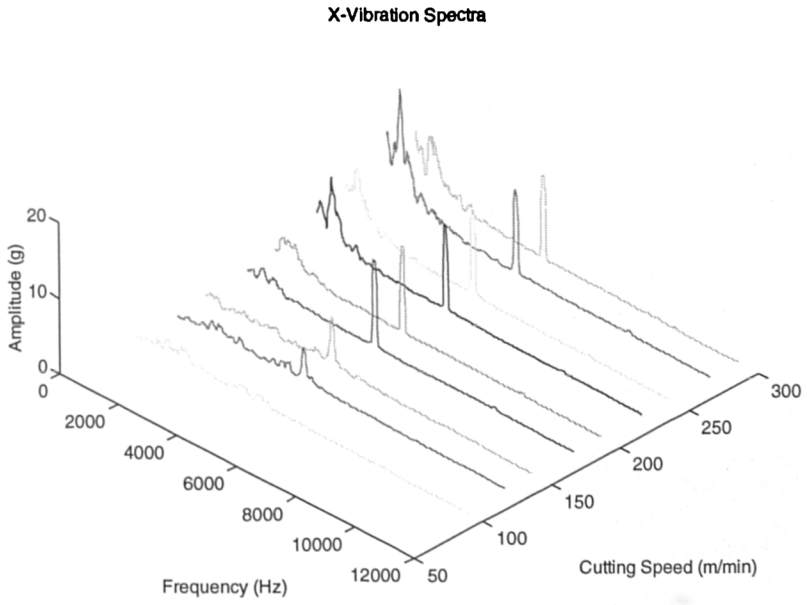

Figure 7.49: Horizontal (X) Vibration Spectra Vs. Cutting Speed

(f=0.2mm/rev. & a=2mm)

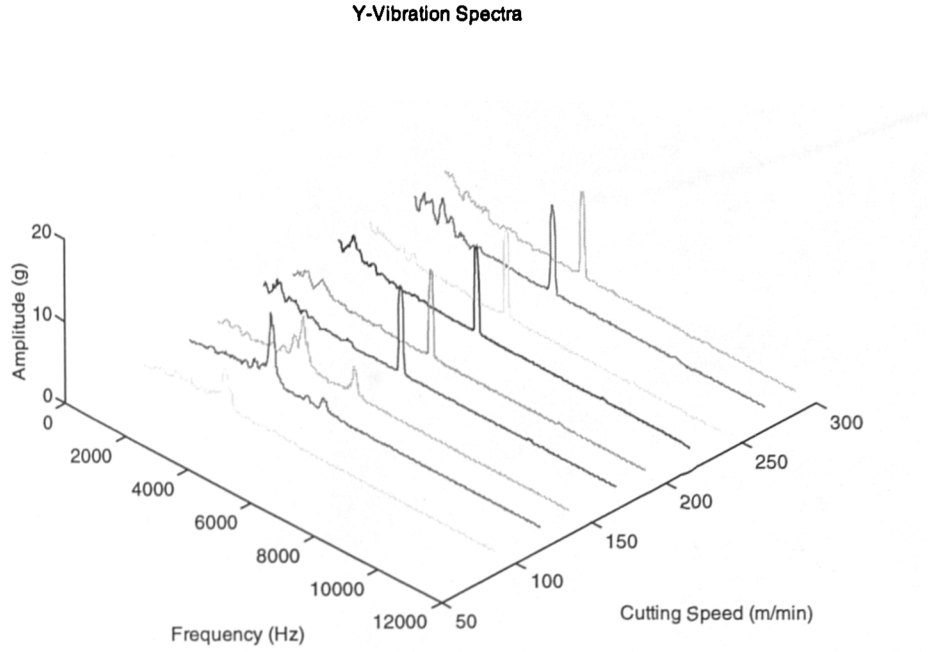

Figure 7.50: Horizontal (Y) Vibration Spectra Vs. Cutting Speed (f=0.2mm/rev. & a=2mm)

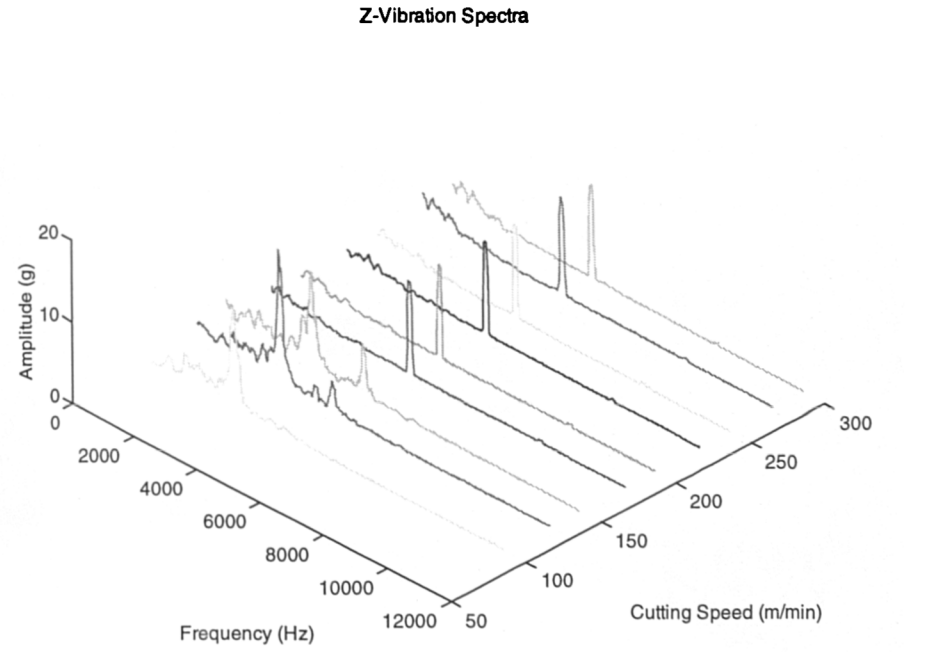

Figure 7.51: Vertical (Z) Vibration Spectra Vs. Cutting Speed (f=0.2mm/rev. & a=2mm)

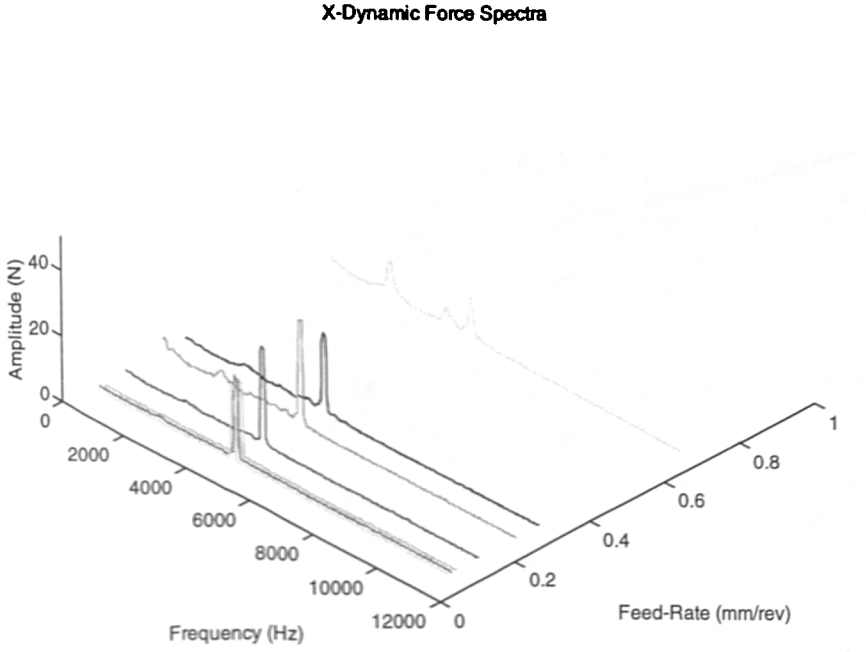

Figure 7.52: Horizontal (X) Dynamic Force Spectra Vs. Feed-Rate

(V=200m/min. & a=2mm)

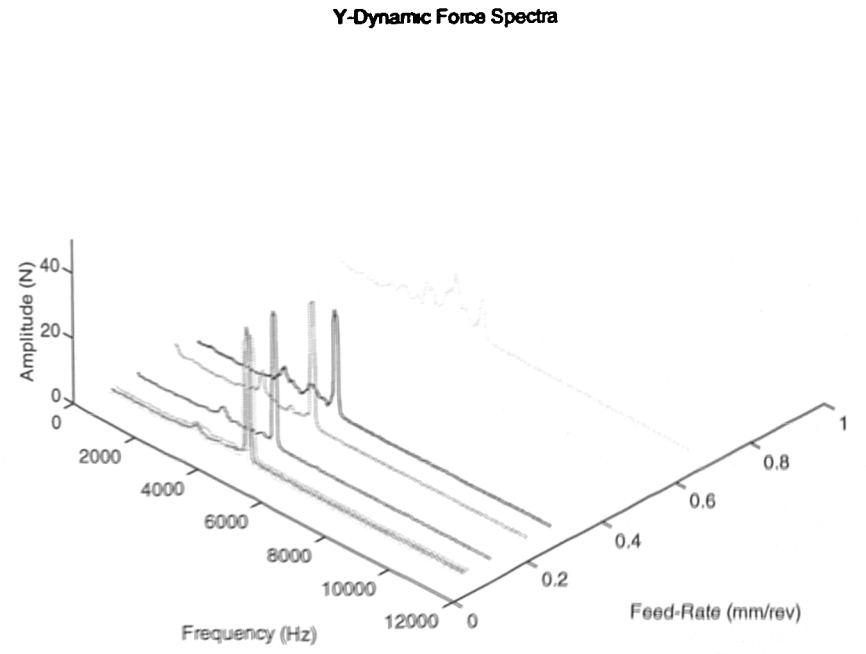

Figure 7.53: Horizontal (Y) Dynamic Force Spectra Vs. Feed-Rate

(V=200m/min. & a=2mm)

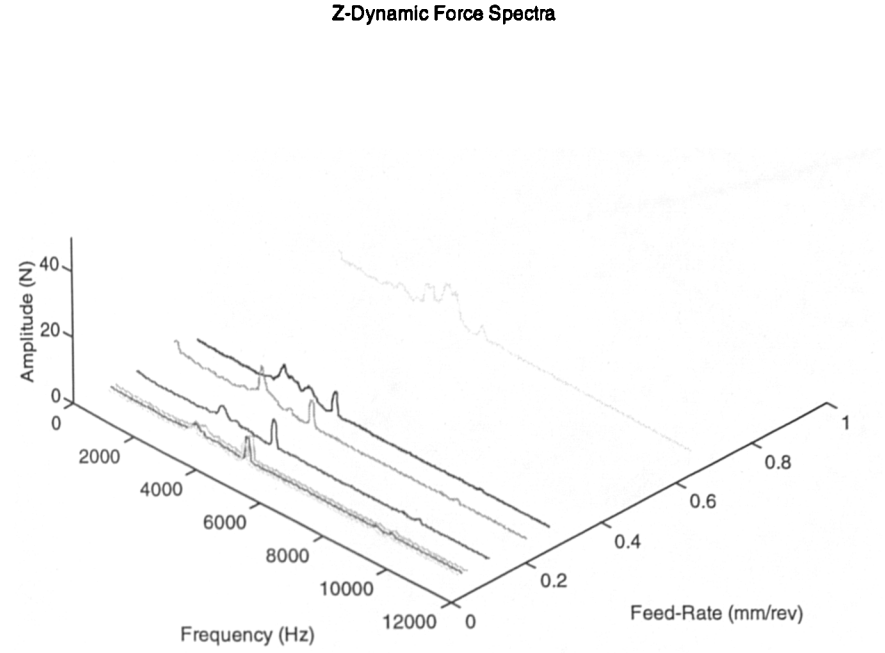

Figure 7.54: Vertical (Z) Dynamic Force Spectra Vs. Feed-Rate (V=200m/min. & a=2mm)

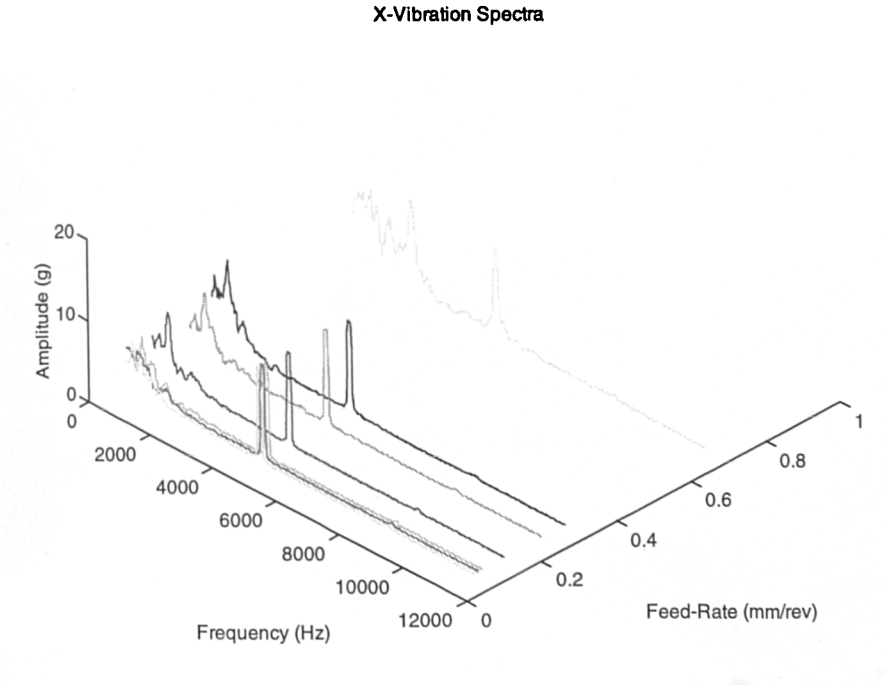

Figure 7.55: Horizontal (X) Vibration Spectra Vs. Feed-Rate (V=200m/min. & a=2mm)

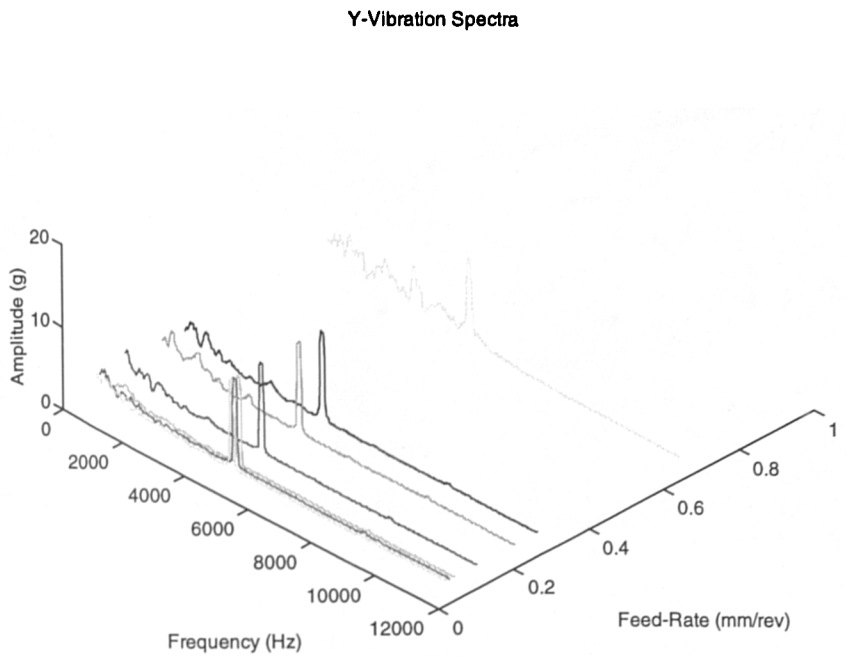

Figure 7.56: Horizontal (Y) Vibration Spectra Vs. Feed-Rate (V=200m/min. & a=2mm)

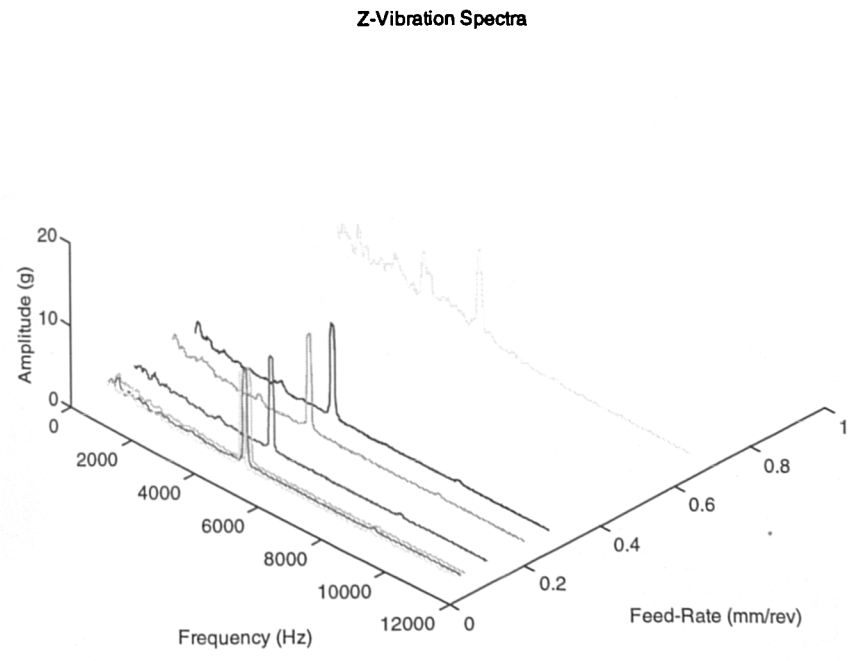

Figure 7.57: Vertical (Z) Vibration Spectra Vs. Feed-Rate (V=200m/min. & a=2mm)

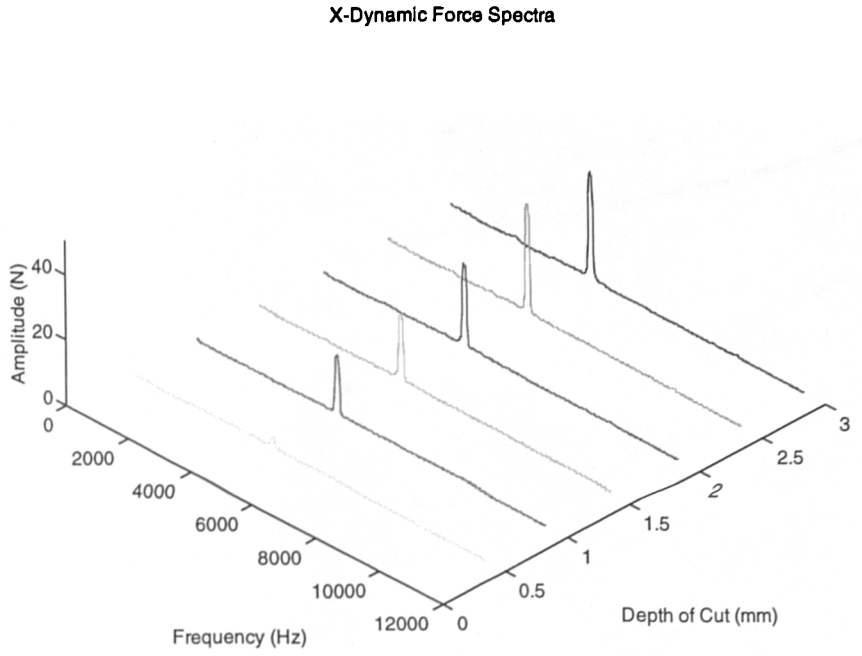

Figure 7.58: Horizontal (X) Dynamic Force Spectra Vs. DOC (V=200m/min. & a=2mm)

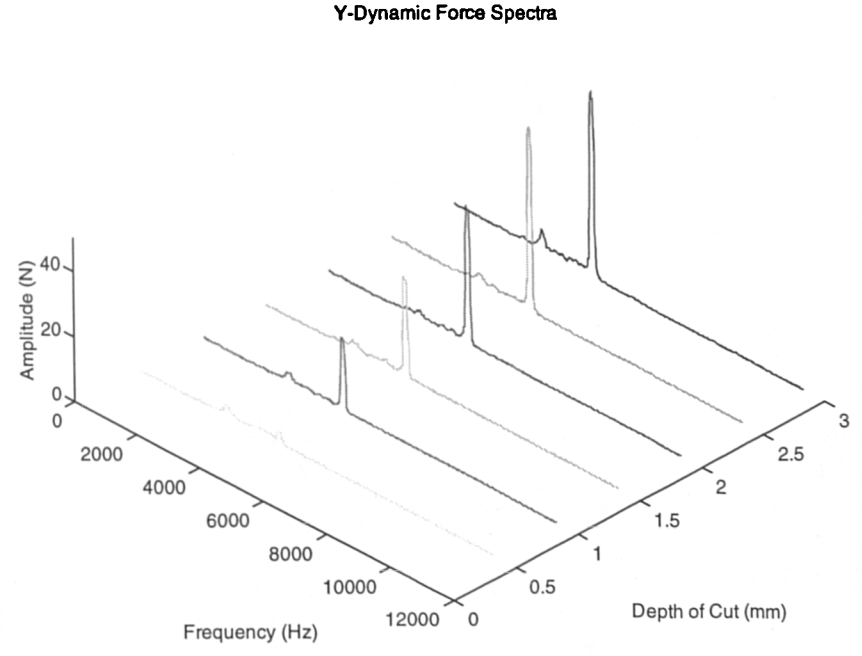

Figure 7.59: Horizontal (Y) Dynamic Force Spectra Vs. DOC (V=200m/min. & a=2mm)

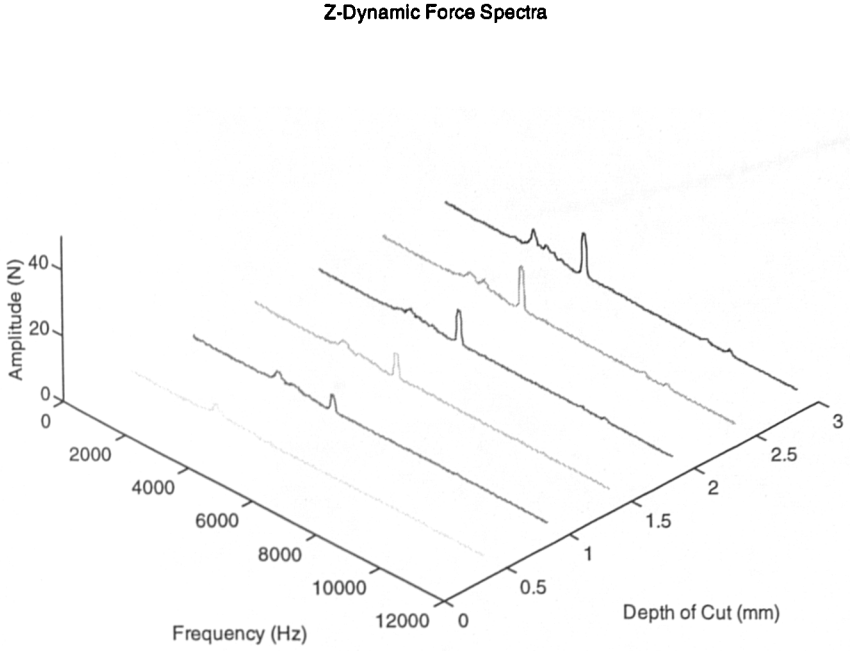

Figure 7.60: Vertical (Z) Dynamic Force Spectra Vs. DOC

(V=200m/min. & a=2mm)

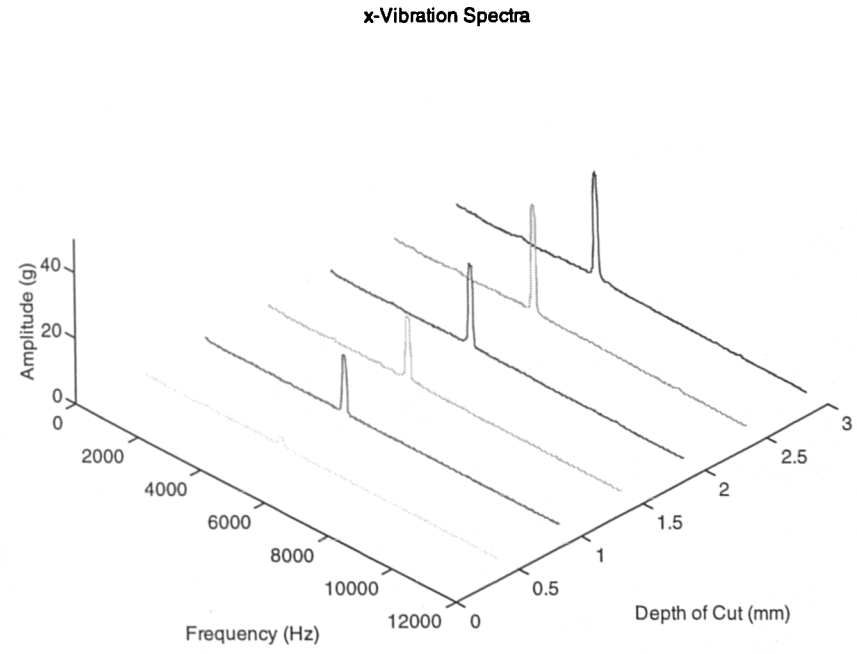

Figure 7.61: Horizontal (X) Vibration Spectra Vs. DOC

(V=200m/min. & a=2mm)

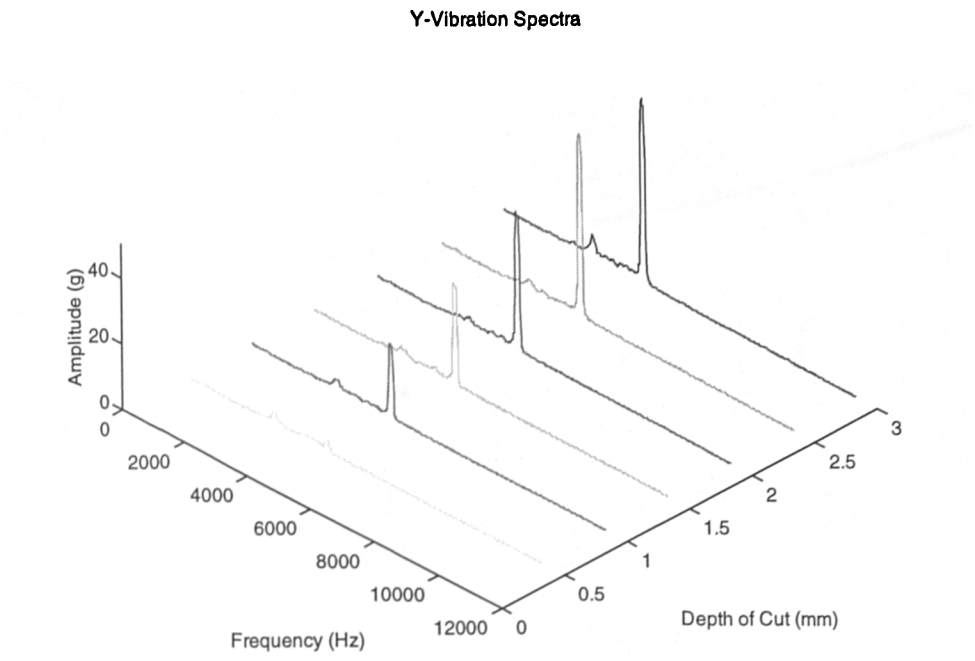

Figure 7.62: Horizontal (X) Vibration Spectra Vs. DOC

(V=200m/min. & a=2mm)

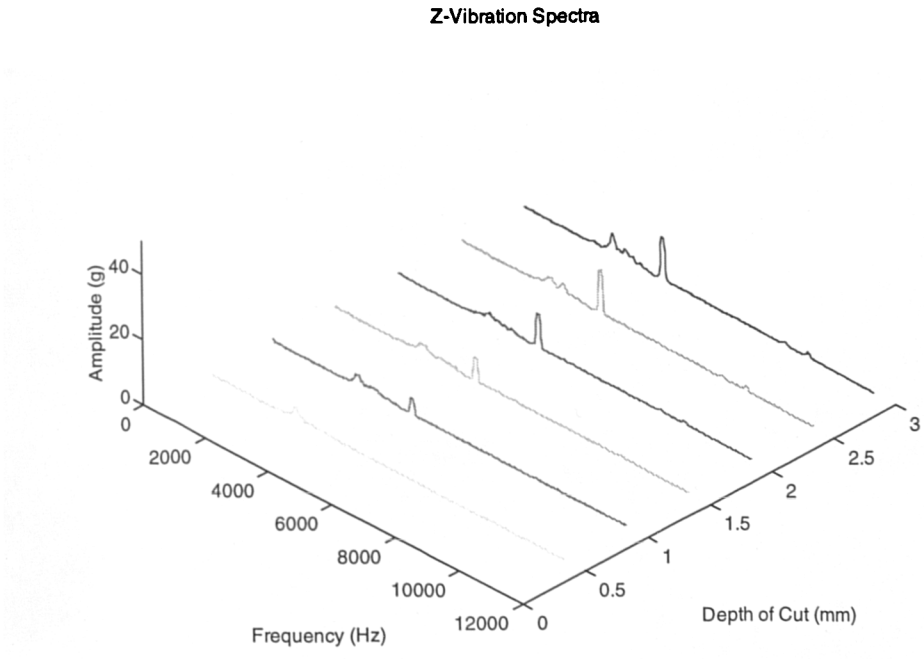

Figure 7.63: Vertical (Z) Vibration Spectra Vs. DOC

(V=200m/min. & a=2mm)

CHAPTER 8

PRELIMINARY STUDY INTO THE APPLICATION OF NEURAL NETWORKS IN TCM

8.0. Overview of Investigation

This chapter presents the results of a preliminary neural network implementation for identifying the cutting tool state. In the ensuing study, the tool state was limited to two classes: worn and sharp, whilst making use of only a single wear indicator - flank wear land-length. The results from implementing TCM through application of a linear neural network model (SLP) and a non-linear neural network model (MLP) are outlined and discussed.

8.1. Implemented Wear Criterion

In the experiments conducted, flank and crater wear were the prevalent forms of gradual tool wear observed. Whereas crater wear could be avoided by using tool inserts with a coating and chip breaker geometry, the occurrence of flank wear was wholly unavoidable. Other forms of tool wear such as notch and nose wear can be remedied by selecting appropriate cutting conditions. In line with ISO 3685, flank wear was selected in this study as the basis for tool wear. ISO 3685 states that for a cemented tool insert to be considered sharp, the minimum flank wear on an evenly distributed face should not exceed 0.3 mm, whereas, for uneven or badly grooved, chipped or scratched cutting tool faces, the maximum should not exceed 0.6 mm (ISO, 1993).

The implementation of the aforementioned wear criteria was rather subjective, i.e. percentage wear on the cutting tool used as the classification bench mark (worn or

sharp). This was necessary because tool wear is a continuous process and it is therefore difficult to pin-point exactly where the two classes could be separated exclusively. With knowledge of the possible information contained in the obtained data, it was assumed that the cutting tool performed reasonably well without any detriment to either cutting integrity or workpiece surface finish until the flank wear exceeded 0.3mm. This value, the wear criteria, was therefore used as the classification threshold. However, experience shows that there is no unique threshold value, with the end of tool life being very dependent upon the cutting conditions, tooling and workpiece materials. The mean and maximum flank wear land length and crater depth on pre-ground worn tool inserts at the beginning of the experiments were recorded and are shown in Table 8.1.

Using the validated test rig and outlined experimental procedure in the the previous chapter, plane faced tool geometry inserts, uncoated and of tooling material types P10 and P40 (both of SPUN 12 03 08 geometry) was used to cut EN8 workpiece material. Cutting data representing worn and sharp tool states was collected at various cutting conditions, but due to the high costs of the tool inserts, test cuts were limited and samples of the collected data are shown in Table 8.2 for the data used in the SLP study, while Table 8.3 shows the data used for the MLP study. Inspection of Tables 8.2 and 8.3 showed that the data had large variations in magnitude across the entire data set and therefore required a suitable method of scaling before presentation to the neural network. The network has to learn and be able to predict ensuing tool state (generalise) based on presented information only, and the nature of presented data is therefore crucial to the successful application of neural networks in practice (Bishop, 1994). In deciding the task requirement of the neural network, which was primarily the classification of the cutting process data, it was necessary to limit the cutting tool states to worn (1) and nominally sharp (0). This limitation emphasised that there were only two possible desired outputs from the network and this condition was used as the task description criteria.

In order to achieve the desired outputs (worn/sharp) it was necessary to limit the connection weight vectors of the network to small values (<1), hence, the inputs had to be within the same range. A solution to this effect was to normalise the experimental data, effected by dividing all data samples in a particular data set (e.g. the feed-force component of the static cutting force) by a normalising factor, the magnitude of which ensured that all data points in that set were subsequently reasonably well distributed between 0 and 1. Table 8.3 (T2) shows typical normalised data.

The limitation of the cutting tool classes implied that the TCM problem under consideration was one of classification, and thus dictated what the fundamental task requirements of the neural network should be. With the number of desired classes known, and the task to be undertaken being the classification of ensuing tool data into one of two classes, the next investigative step was to choose the classifier type and configuration. This meant selecting the type and configuration of neural network for the practical realisation of tool state classification. The earlier decision to attempt to classify the data into only two states, implied that the neural network would have to be taught what these two states were most likely to be. This condition implied a neural network configuration that is taught and therefore acquires its knowledge by a supervised method of learning. Essentially this involves labelling data sets corresponding to worn and/or sharp tool states. During training, the difference between network calculated output (scaled tool state descriptor) and the actual tool state (target) is found, and this error minimised as required. Based on the number of classes of output required and thereof the task requirements, a decision was made to investigate the development of a modular TCMS through application of ***Perceptron Neural Networks***. These perceptron networks generally fall into two main categories: single layer perceptron (SLP) and multi-layer perceptron (MLP). SLP is essentially a linear network model whereas MLP is non-parametric and capable of non-linear operations.

8.2. Sensitivity of SLP to Tool Wear

8.2.1. Training and Configuration

The selected normalised test cut data were divided into two groups : a separate independent training and test set. In total, 83 cutting test data were selected from test cuts performed using only a single tooling material (P10) under a range of cutting conditions. Data from 41 of these tests was used to train the perceptron with the remaining 42 tests then being used to test its performance. The two groups of data was partitioned such that each group contained an equal distribution of worn and sharp tool data, and also an equal variation in the cutting conditions.

The perceptron was designed using the MATLAB Neural Network Toolbox, and consisted of a single layer of 12 perceptron neurons and one binary output depicting tool state. An output of '0' was used to denote a sharp tool, whilst a '1' represented a worn tool. Clearly this type of output represents two extremes in the range of possibilities of tool wear, and does not distinguish between the type of wear (e.g. flank or crater wear). Sharp tool data was collected when cutting either with new tool inserts at the start of cut or were nominally sharp (i.e. wear features evident, but of minor proportions). Those involving worn tools involved cutting with a tool exhibiting at least 0.3 mm of flank wear (mean) and 0.02 mm crater depth measured using a tool maker's microscope and a dial test tool indicator respectively.

The data set used for training the SLP comprised equal proportions of the two tool states (worn/sharp) and was designated P. P contained 41 x 12 normalised values. P was targeted to a 41 element column vector of binary values of tool status (1 for worn and 0 for sharp). Such a configuration did not permit successful classification, i.e. it was not possible for the perceptron training algorithm to converge on finite values of weights and a bias. For successful classification using a perceptron, data must be linearly separable with visualisation of a 2-vector

input straightforward (cf. Fig. 8.2. and Fig. 8.3) with successful classification reliant upon separating output states with a straight line.

Similarly, a 3-vector input perceptron involves separating output states with a plane surface. Thereafter, visualisation becomes more difficult, but clearly it is natural to assume that some data points of the 12-input vector data sets are encroaching into what may be considered to be the wrong sector. During training it became evident that the data could not be linearly separated into two tool states. As such, no convergence would be reached in any length of time by the perceptron.

By trial and error (i.e. accumulatively increasing the input data dimension) the first 31 sets of data from the initial training set of 41 were found to converge after less than 1000 epochs (training cycles), and thus, were linearly separable (Fig. 8.3). It was therefore evident that in so far as linearity was concerned, 'undesirable' patterns occurred between the 32nd and 41st data set. These undesirable patterns were labelled as those that encroached into the wrong tool class.

Omission of the overlapped data for training but cross-validating the trained perceptron for the entire range of sampled data could be expected to result in a reduction in the maximum classification accuracy as fewer than initial patterns were used to train the network. Therefore, instead of a 100% success rate, prediction may be limited to a maximum success rate of 76% (i.e. 31/41). Alternatively, if corresponding values beyond the 31st pattern data were used neither for training nor cross-validation, then a 100% success classification rate would again be achievable.

For example, when classification was strictly limited to the two classes -worn and sharp, a 2-D plot of the data showed an overlap in the tool state categories. Choosing a line that best separated the two categories, it was visualised that 10 out of 41 data points were on the wrong side. Manually removing these gave a

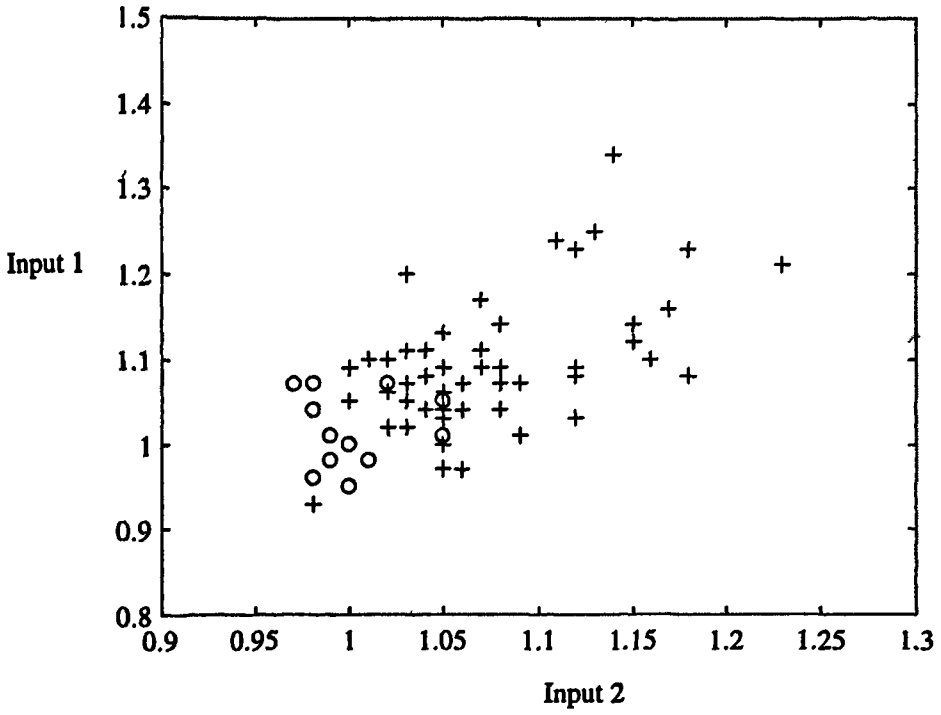

Figure 8.2: Typical two class data visualisation with overlap

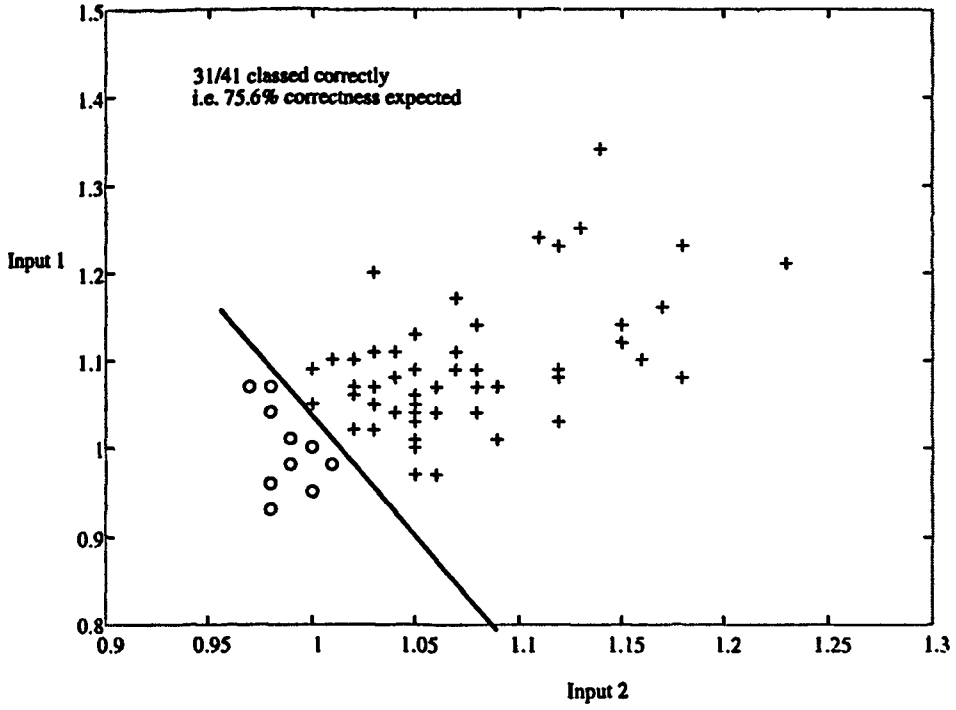

Figure 8.3: Corrected data with no overlaps

perceptron that would converge with approximately 75% chance that its future classification would be correct i.e.

$$\left(\frac{41-10}{41}\right)\times 100\% = 75.6\%$$

Essentially the training of the perceptron was undertaken by the application of the perceptron rule outlined in (Chapter 4). The main aim of the training was to obtain connection weights and biases for which sufficient convergence in the network input would have been attained. After training the perceptron, its weights and bias were noted, and used to test its performance off-line.

8.2.2. Cross-validation of Trained SLP

Testing involved presenting the trained perceptron (a linear function and values of weights and bias found in training) with data which had not been used for training. The output results were then compared to the actual values of tool wear state. It was found that 11 of the 42 data sets were classified wrongly, giving a success rate of only 74%. On examination, it was evident that 9 of the 11 failed data were associated with data sets that were broadly similar to data sets omitted in the training process, and as such it might be argued that the network had no knowledge of this type of data set. In order to investigate this proposition, broadly similar data (i.e. those that overlapped on a 2-D graph) for both training and testing were omitted and testing classification improved significantly with only 2 of the 31 data sets used for testing failing to classify correctly (i.e. a 94 % success rate).

8.2.3. Discussion of Results

The SLP is simple in operation and design, but the input data has to be enhanced in an appropriate way such that it can be mapped onto a dimensional space where it would be linearly separable. Clearly, this requirement is not suitable for this type of pattern classification problem where speed and precision are of the essence.

A comparison of the results obtained from the SLP classification without modification to the testing data show a decrease in the predicted and expected classification rate of 2% (i.e. from 76% to 74%) when all 41 patterns were considered. But the overall classification success rate increased when only the 31 data occurring in the same region as those actually employed in training were considered (i.e. from 74% to 94%).

The simplest form of the perceptron network, as used in the present study, has just one layer, and this places restriction on its computational ability. Moreover, the hard limit transfer function restricts the perceptron output to 0s and 1s.

8.2.4. Conclusions

A TCMS based on a multi-sensor integration of signals through application of a SLP has been investigated and presented. This study showed that a SLP could classify worn and sharp tool data from a turning process by partitioning the input data into subspaces using a hyperplane. Because of the amount of post data-processing required in order to enhance the data, SLP is not 'ideally' suited for TCM since it cannot cope with the non-linearity of the metal cutting process. However, if one were merely concerned with knowledge of the instantaneous state of the cutting tool (worn or sharp defined by some criteria) then it suffices as its classification performance is comparable to that of hybrid neural networks. A higher degree of confidence and accuracy is required in TCM tasks because precision and integrity are paramount. Perceptron neural networks that can handle the non-linearity of the cutting data can offer such confidence and accuracy and thus, help realise a widely applicable TCMS. Multi-layer perceptron feed-forward neural networks offer more powerful data representation and are capable of complex data manipulations and, can deal well with the non-linear nature of metal cutting data. This line of investigation is the subject of the next section

8.3. MLP Classification of Cutting Tool State

In this Section, preliminary research findings on the development of a modular TCMS implemented via application of MLP neural networks is reported. Herein, a three layered perceptron neural network has been employed to fuse multivariate data from a turning process and thereof predict the tool state. Cutting conditions were used to broaden the scope of applicability of the system. This study was also aimed at establishing an optimum MLP configuration, training methodology, and the obtained results are presented and discussed.

The data selected for this investigation (normalised) was divided into two main groups: a training set consisting of data from a P10 tool insert only, and cross-validation sets from (i) P10 insert of known tool state (worn and sharp), henceforth T1 for referencing; (ii) P10 insert whose tool state was known only at the start and end of the cut, T2 for referencing; and (iii) P40 insert of known tool state (worn and sharp), T3 for referencing.

8.3.1. MLP Network Topology

The neural network type used was a feed-forward multi-layer perceptron commonly referred to as the MLP, which was implemented through the Neural Network Toolbox in MATLAB. Details of the general descriptive terminology of the MLP topology have already been provided in Chapter 4, and this section proceeds under the assumption of the reader's familiarity with such basic knowledge.

The MLP used in this study consisted of 12 input nodes, 1 hidden layer with variable number of nodes (100, 20, 10, 8, 5, 1) and 1 binary output node. A single hidden layer was arbitrarily chosen as earlier published works suggests that networks with two or more hidden layers actually offer no real advantage over those with only one (Sarle, 1994). The same principle could not be applied to the selection of its number of neurons. The number of neurons in this layer was

considered to be a complicated but critical issue, and an experimental approach was therefore adopted. The input and output nodes corresponded to the number of input signals and desired output respectively, i.e. the input sensors were as described earlier in addition to the feed-rate, depth of cut and cutting speed. The designed architectures were trained via back-propagation (BP) with the learning rate and momentum coefficients set respectively to 0.2 and 0.85, and a Mean Square Error (MSE) goal of 0.009 (<1%). These values as with the number of hidden nodes were chosen experimentally and deemed to give optimum convergence of the MLP. The addition of the momentum term to the BP training algorithm ensured that the network was not caught in a shallow minima, but rather sensitive to larger trends in the calculated error (MathWorks, 1994). Chosing favourable initial conditions (weights) and the implementation of adaptive learning rate reduced training time, but did not affect network outcome. The Nguyen-Widrow method (MathWorks, 1994) was used to set the initial conditions, which sets the initial weights to random values of between 0-1. A sigmoid transfer function ('squashing') was employed in both layers of the network.

8.3.2. MLP Training

The training data consisted of data sampled using tool inserts that could be classed only as worn or sharp (fresh), and the un-normalised experimental data are shown in Table 8.3. The various neural network configurations were trained using the designated training set until the error converged to the desired value. Convergence of the error indicated completion of training to the required specification (MSE <1%). Training stopped in MATLAB only when the error had converged to a desired value or the specified number of training cycles (epoch) had been exhausted. In training a neural network using BP, overfitting or underfitting could easily result if testing was not simultaneously performed on the network as it was trained. The possibility of such an occurrence was not overlooked, but testing was not implemented mainly because based on past

experience, it was unlikely to occur.

The trained networks were cross-validated using the designated data sets, and the results are presented in Table 8.4.

8.3.3. Results and Discussion

The results obtained from the cross-validation exercise showed that some network outputs were not binary as expected. The reason for this it would seem was that network outputs were weighted probabilities. A decision was made whereby network output values above 0.5 were rounded to 1 and those below 0.5 rounded to 0.

Table 8.4 shows the predicted success rates attained by each of the networks considered. In addition to data recorded using P10 inserts, the networks were also presented with data recorded using a P40 tool insert, T3 (new variable class). This data was successfully classified with a much higher degree of success rate than the P10 data.

The cross-validation process also showed that with a fresh P10 insert (T1), the neural network architectures predicted exactly the same percentage success rates regardless of the number of hidden nodes (83 %). Presentation of data sampled with a P10 tool that was not fresh at the beginning of the cut but completely worn at the end of the cut (T2) showed some disparity. The network initially predicted the tool state correctly, but as the tool continued to cut its cutting edge deteriorated, and the network became erratic. About midway through the test, it was apparent that the maximum tool wear threshold for the flank and crater wear had been exceeded. Since the data sampled at this stage was a half-way house between worn and sharp, explains the high misclassification rate. A closer inspection of the results showed that the networks were sensitive to changes in the cutting conditions (DOC and feed-rate), especially in the transition zone between sharp and worn. This, it was judged, accounted for the instability of the network

outputs in the transition zone. Hong *et al.* (1996) reported the occurrence of such phenomenon in their work, but had intentionally left out training samples in this region since they were of the opinion that the worn tool condition in the region was unclear. At the end of tests T2, the wear conditions on the tool were measured (V_BMean = 0.32 mm, V_BMax = 0.45 mm and K_td = 0.008 mm) and were found to be within the bounds of a worn tool as defined in the implemented wear criteria. This confirmed that the networks had correctly predicted the ensuing tool state. Thus, the network had been able to monitor the cutting tool state from when the tool insert was sharp (though not fresh), until when the wear increased above the set threshold value, and consistently did so for all the network architectures validated.

Inspection of the misclassified data sets in all the categories of tool inserts investigated showed that some of the failed cases corresponded to when the chip form pattern changed from continuous to discontinuous. This change resulted in an increase in the magnitude of the dynamic variables, which the network detected, but attributed it to the onset of tool wear. The sensitivity of the networks to the phenomenon of chip type formation and breakage could be eliminated by using tool inserts with chip breaker geometry, making it possible to concentrate on tool state detection. Experience shows that it is important to control chip form because inconvenient chip formation may lead to operator injury, poor surface finish or peripheral damage to machine tool (Jawahir and van Luttervelt, 1993).

A comparison of the performance of all the network architectures showed that those that produced the highest percentage of successful classifications were those with either 5 or 20 nodes in the hidden layer. Generally, if one were to choose one architecture for TCM in this context, that with 20 nodes would be preferred as it optimises more variables and thus would generalise better in subsequent applications. However, in this investigation, the network with 5 nodes performed better, i.e. attained 98% success compared to 96% for that with 20, but it could be

argued that the difference is statistically insignificant .

8.3.4. Conclusions

A multi-sensor neural network TCMS based on fusion of independent and different source sensor signals has been investigated and presented. Initial tests showed the system to be capable of correctly identifying the tool state with accuracy of well over 90% when previously unseen data though for the same tooling material (T1, T2) was used. It also correctly diagnosed the state of cutting tool inserts (T3) using data that had not previously been presented to it. Compared to research work performed in this area by other researchers, the method presented avoids complicated feature extraction. Instead, the principal independent sensor signal components are used.

Further conclusions reached in this study can be summarised as follows:

- As the cutting process continually changes (workpiece inhomogeneity, voids, bearing friction, steady-state speed errors), the process of training and cross-validation of the performance of the neural network on data sampled at different cutting conditions provides valuable insight into how best to explore the generalisation capabilities of these networks.

- Though the implemented cutting cycles were limited in scope (i.e. range of cutting parameters used), this inadequacy was compensated for by exploring the ability of P10 data trained network to classify data sampled using a different tooling material type (P40) whilst the training was performed entirely on P10 data. The networks were capable of reasonable tool state identification regardless of the insert type.

- The cross-validation data sets consisted of data whose wear state were widespread, but nonetheless still within the maximum threshold value of the training data.

- The number of hidden nodes in an MLP does not seem to be of significant importance as far as classification success accuracy was concerned, i.e. there exists no specific number of such nodes for best performance. In so far as the training time was concerned, topologies with higher number of hidden nodes take longer to train, as more variables have to be optimised since more connections and weights are encountered. With more neurons in the hidden layer, there exist a higher chance of minimising the overall MSE of the network.

The preliminary investigation outlined involved the utilisation of multi-sensors implementing intelligent sensor fusion through application of perceptron neural networks of the lower order SLP and a higher order MLP, with the sensor inputs being the principal components of different source signals. The performance of the SLP system was deemed inadequate for any possible or anticipated on-line application requiring planning and scheduling. The MLP system fared better, attaining 95% accuracy on data of a non-linear nature. Further work is required to be carried broadly based on the following aspects:

- Attempt to eliminate network sensitivity to chip form by employing controlled contact tool insert geometries,
- Improve the MLP design and training method, and
- Extend the application to a broader range of tool insert states (i.e. part worn, worn, severely worn, to include fractured/chipped tools).

TABLE 8.1: Tool insert wear level at start of experiments

Insert type (Data Designation)	V_BMean (mm)	V_BMax (mm)	K_td (mm)
P10 (T1)	0.56	0.75	0.02
P10 (T2)	0.07	0.09	0.0028
P40 (T3)	0.2	0.33	0.006

TABLE 8.2: Experimental data used for SLP study

Cut	Speed	Feed-rate	DOC	Static Force			STP Dynamic Force			STP Acceleration		
No.	(m/min)	(mm/rev)	(mm)	(N)			(N)			(g)		
				X	Y	Z	X	Y	Z	X	Y	Z
1	100	0 163	1 5	311	115	392	127	151	143	4.89	2.32	5.25
2	130	0.163	1 5	339	164	459	156	202	212	4.45	2.49	5.4
3	150	0.163	1 5	338	162	462	127	177	159	4.41	2.47	5.33
4	180	0 163	1 5	318	154	438	124	173	153	4.08	2.36	5.22
5	200	0 163	1.5	308	147	440	127	168	148	4.41	2.64	5.11
6	230	0 163	1 5	298	146	436	111	145	129	5.15	2.63	4.32
7	250	0 163	1 5	286	136	424	113	132	122	4.71	2.58	3.86
8	280	0 163	1 5	291	138	431	104	120	113	5.08	2.9	3.54
9	300	0 163	1 5	339	164	459	169	153	148	5.08	3.07	3.39
10	200	0 106	1 5	308	147	176	127	168	148	4.41	2.64	5.11
11	200	0 163	1	348	180	241	160	208	181	4.93	3.17	5.92
12	200	0 265	1 5	422	276	357	290	563	494	8.61	6.76	9.18
13	200	0 3256	1 5	427	294	415	367	674	754	8.91	7.61	10.54
14	200	0 163	0 5	436	382	875	651	701	497	18 87	13.59	20.89
15	200	0 163	1	846	506	1605	616	790	670	17 28	13.67	21.22
16	200	0 163	1 5	1068	186	1850	619	894	714	17.42	18.2	22.3
17	200	0 163	2	1406	458	2265	637	1508	1017	22.6	20.4	26.8
18	200	0 163	2 5	1880	546	2955	570	1134	887	18.5	18.9	28.1
19	200	0 163	3	2758	1118	4700	560	1459	1078	20.2	21.2	29.9
20	80	0 163	1 5	796	384	960	340	529	544	10.6	9	20.7
21	100	0 163	1 5	948	78	195	390	844	306	11.74	11.73	26.04
22	120	0 163	1 5	982	150	375	413	975	379	14.13	13.03	26.66
23	150	0 163	1 5	1188	1072	2680	1280	2453	381	11.6	13.3	11.3
24	180	0 163	1 5	1200	1114	2785	1377	2570	925	14.7	11.9	10.1
25	200	0 163	1 5	1118	992	2480	1236	2269	365	19.2	13.9	10.8
26	220	0 163	1 5	702	910	2275	1227	2830	373	20.8	12.5	12
27	250	0 163	1 5	478	684	1710	1292	1866	402	30.6	15.7	14.7
28	265	0 163	1 5	1032	778	1945	1183	2443	390	24.9	17.3	13.7
29	200	0 08	1 5	1128	972	2430	1210	2570	1118	16.3	13.8	10.9
30	200	0 0882	1 5	852	520	1300	622	805	671	17.29	13.67	21.23
31	200	0 106	1 5	1178	1108	2770	1204	2437	923	15.5	12.2	10.9
32	200	0 163	1 5	1242	1072	2680	1682	3101	1402	18 2	12.3	10.2
33	200	0 265	1 5	1242	1072	2680	1682	3101	1402	18.2	12.3	10.2
34	200	0 3256	1 5	1838	1314	3285	1838	3009	1756	24.5	15.8	12.3
35	200	0 7056	1 5	1524	1612	4030	2445	4322	3485	44.8	35.5	41.5
36	200	0 163	0 5	342	310	775	418	787	643	15.04	17.03	22.34
37	200	0 163	1	638	400	1000	860	1321	823	18.1	16.3	12.3
38	200	0 163	1 5	1080	920	2300	1088	2083	960	17.5	15.4	10.9
39	200	0 163	2	1210	1058	2645	1401	2897	116	17.2	15	11.1
40	200	0 163	2 5	752	1260	3150	2495	3626	1649	17.1	15.8	11.7

41	200	0.163	3	2352	1640	4100	1814	3549	1552	20.6	17.7	13.5
42	100	0.163	2	2244	1236	3455	559	913	814	17.73	20.45	32.61
43	120	0.163	2	2138	1192	3430	621	1091	965	21.7	21.5	39.6
44	140	0.163	2	1958	1128	3325	698	1440	1200	26.7	30	44.9
45	160	0 163	2	1894	1082	3275	1028	1718	1337	33	30.5	49.1
46	180	0.163	2	104	1056	3265	908	1542	1247	30.6	27.5	46.5
47	200	0 163	2	1742	976	3145	927	1484	1231	31.4	31.2	44.2
48	220	0 163	2	1702	978	3225	874	1291	1074	32.1	36.6	38.5
49	240	0 163	2	1628	946	3170	834	1042	923	30.6	30.2	32.8
50	250	0 163	2	1614	122	90	741	1048	946	29	31.9	30.2
51	200	0 08	2	1212	650	1950	490	767	676	19.15	20.36	26.38
52	200	0 088	2	1294	690	2070	582	835	734	18.12	23.38	27.8
53	200	0 106	2	1396	758	2365	634	984	857	22.87	24.94	32.8
54	200	0 163	2	1606	930	3060	779	1323	1106	28.3	26	38.9
55	200	0 265	2	1878	1212	4515	1198	2004	1551	40.3	46	52
56	200	0 326	2	1976	1382	5370	2980	3885	3311	53.1	51.4	66.4
57	200	0 163	0 5	410	544	885	580	608	561	18	22.86	21.42
58	200	0 163	1	544	222	820	723	879	763	24.22	27.37	28.23
59	200	0 163	1 5	992	342	1525	886	1203	987	29.7	40.7	37.5
60	200	0 163	2	1822	1094	3300	1117	1522	1242	32.5	36	46.2
61	200	0 163	2 5	1968	808	3090	989	1669	1352	34.8	30.5	47.6
62	200	0 163	3	2298	892	3795	1043	1612	1205	33.7	31.8	44.7
63	100	0 163	2	1692	1068	3085	856	964	930	23.34	25.86	37.63
64	120	0 163	2	1836	1148	3235	623	1175	1029	23.1	24.9	42.2
65	140	0 163	2	1764	1124	3160	683	1392	1163	26.1	21.8	45.8
66	160	0 163	2	1812	1148	3190	897	1553	1222	24.6	35.6	45.8
67	180	0 163	2	1676	1034	3125	697	1366	1126	26.9	24.7	40.4
68	200	0 163	2	1616	926	3120	741	1317	1082	29.5	26.3	39.9
69	220	0 163	2	1522	1008	3155	753	1254	1030	27.1	28.4	35.5
70	240	0 163	2	1486	986	3155	856	1315	1099	29.2	28.6	40.9
71	200	0 08	2	1236	778	2025	548	971	850	21.01	23.16	161.48
72	200	0 088	2	1266	814	2095	602	1181	1032	26.4	22.8	33.6
73	200	0 106	2	1332	870	2310	616	1289	1119	27.7	24.4	36.2
74	200	0 163	2	1570	1074	3200	823	1790	1446	38.1	34.1	48.2
75	200	0 265	2	1918	1386	4615	955	2417	1887	44.2	38.3	56.5
76	200	0 326	2	1994	1448	5335	1777	3303	2842	50.5	44.8	63.3
77	200	0 706	2	2298	2288	9870	2588	4481	2001	64.2	50.3	72.7
78	200	0 163	0 5	400	512	1000	527	922	819	18.95	18.02	31.71
79	200	0 163	1	840	628	835	743	1388	1188	27.5	24.3	38.4
80	200	0 163	1 5	900	502	1495	764	1927	1565	36.6	22.4	44.3
81	200	0 163	2	1650	1172	3360	737	2018	1630	38.1	29.4	48.6
82	200	0 163	2 5	1666	2076	3560	1058	6823	5201	49.4	39.6	27.4
83	200	0 163	3	2556	826	3770	913	2600	1820	43.7	44.1	54.8

TABLE 8.3 (T1): Experimental data used for MLP study

Cut No.	Speed	Feed	DOC	Static Force (/N)			STP Dynamic Force (/N)			STP Acceleration(/g)		
	m/min	mm/rev	mm	X	Y	Z	X	Y	Z	X	Y	Z
1	100	0 163	2	1620	960	1060	671	952	857	20 26	29 4	36 32
2	120	0 163	2	1560	960	1040	681	1011	895	21.3	21.6	38.5
3	140	0 163	2	1420	860	980	857	1236	1091	25.6	31.3	42.9
4	160	0 163	2	1380	840	980	720	1193	1010	23.3	23.9	41.3
5	180	0 163	2	1340	800	960	883	1277	1064	24.1	26.4	41.1
6	200	0 163	2	1220	780	950	1133	1600	1372	32	31.3	30.5
7	220	0 163	2	1200	760	940	746	996	853	20.1	31.34	30.15
8	240	0 163	2	1180	660	900	706	812	780	19.64	29.42	27.14
9	250	0 163	2	1160	660	920	742	869	786	19 27	31.8	27.94
10	200	0 079	2	940	540	600	531	702	616	12.98	18.07	23.65
11	200	0 088	2	980	560	620	564	702	631	14.49	19.05	24.39
12	200	0 106	2	1040	580	700	669	892	808	18.79	24.46	30
13	200	0 163	2	1220	740	940	815	1096	853	22.9	30 3	34.02
14	200	0 192	2	1260	840	1080	1172	1566	1369	32 4	35.9	43.2
15	200	0 244	2	1340	900	1260	1131	1487	1248	33.4	34.1	44.5
16	200	0 326	2	1460	1140	1620	1934	2939	2696	54 2	47.1	60.8
17	200	0 423	2	1500	1200	1920	2501	4319	3874	64 8	57.9	64.1
18	200	0 163	0 5	240	420	280	452	600	574	12.81	15	23
19	200	0 163	1	560	520	500	693	899	802	19 19	22.78	30.49
20	200	0 163	1 5	880	660	760	784	1092	857	23 8	27	35.2
21	200	0 163	2	1220	740	960	808	1096	934	24 4	27.9	35
22	200	0 163	2.5	1340	820	1020	833	1394	1084	30.4	26.1	40.4
23	200	0 163	3	1680	940	1120	859	1337	1053	27 9	28	38.1
24	200	0 163	3 5	2180	1060	1600	1009	1643	1332	34 4	29 6	44.9
25	200	0 163	4	2640	1240	1700	991	1796	1359	35 8	27.9	44
26	100	0 163	2	1620	960	2650	540	1255	1141	24	48	43
27	120	0 163	2	1420	860	2550	747	1394	1231	25	47	46
28	140	0 163	2	1280	780	2450	823	1734	1540	32	29	54
29	160	0 163	2	1260	780	2450	1043	1654	1394	29	35	48
30	180	0 163	2	1240	760	2450	1113	1745	1964	28	131	49
31	200	0 163	2	1220	740	2450	1215	1490	1230	28	38	44
32	220	0 163	2	1080	700	2350	794	1332	1222	27	50	45
33	230	0 163	2	1040	640	2250	798	1193	1031	24	44	39
34	200	0 079	2	840	500	1450	509	819	752	16	31	33
35	200	0 088	2	920	520	1600	500	960	867	17	22	35
36	200	0 106	2	940	530	1700	616	998	888	18	30	34
37	200	0 163	2	1100	700	2500	1090	1511	1268	26	87	48
38	200	0 192	2	1140	740	2600	1052	1502	1255	27	78	47
39	200	0 244	2	1340	900	3150	1604	2273	1805	37	143	58
40	200	0 326	2	1460	1120	4100	1755	2964	2121	48	115	71
41	200	0 423	2	1466	1300	4750	1741	3077	2702	64	50	83
42	200	0 163	0 5	240	400	700	497	722	697	15	21	26
43	200	0 163	1	560	520	1250	832	1128	1026	23	35	42
44	200	0 163	1 5	800	580	1800	883	1214	1130	23	31	43
45	200	0 163	2	1120	680	2300	1009	1465	1284	26	29	47
46	200	0 163	2 5	1180	940	2600	1090	1780	1523	32	35	53
47	200	0 163	3	1860	980	3550	857	1690	1381	32	31	48
48	200	0 163	3 5	2180	1100	4150	810	1922	1568	36	40	57
49	200	0 163	4	2600	1240	4700	1181	2693	1976	53	50	62

TABLE 8.3 (T2): Normalised data used for MLP study

Cut	Speed	Feed	DOC	Static Force (/N)			STP Dynamic Force (N)			STP Acceleration (g)		
	m/min	mm/re	mm	X	Y	Z	X	Y	Z	X	Y	Z
98	0.33	0.50	0.15	0.10	0.04	0.07	0.04	0.02	0.02	0.05	0.02	0.03
99	0.50	0.50	0.15	0.11	0.05	0.08	0.04	0.03	0.02	0.04	0.02	0.03
100	0.67	0.50	0.15	0.10	0.05	0.07	0.04	0.02	0.02	0.04	0.03	0.03
101	0.83	0.50	0.15	0.10	0.05	0.07	0.04	0.02	0.02	0.05	0.03	0.02
102	1.00	0.50	0.15	0.11	0.05	0.08	0.06	0.02	0.02	0.05	0.03	0.02
103	0.67	0.50	0.23	0.12	0.06	0.04	0.05	0.03	0.03	0.05	0.03	0.03
104	0.67	0.50	0.46	0.14	0.10	0.07	0.12	0.10	0.11	0.09	0.08	0.05
105	0.67	0.33	0.23	0.28	0.17	0.27	0.21	0.11	0.10	0.17	0.14	0.11
106	0.67	0.67	0.23	0.47	0.15	0.38	0.21	0.22	0.15	0.23	0.20	0.13
107	0.67	1.00	0.23	0.92	0.37	0.78	0.19	0.21	0.15	0.20	0.21	0.15
108	0.33	0.50	0.15	0.32	0.03	0.03	0.13	0.12	0.04	0.12	0.12	0.13
109	0.50	0.50	0.15	0.40	0.36	0.45	0.43	0.35	0.05	0.12	0.13	0.06
110	0.67	0.50	0.15	0.37	0.33	0.41	0.41	0.32	0.05	0.19	0.14	0.05
111	0.83	0.50	0.15	0.16	0.23	0.29	0.43	0.27	0.06	0.31	0.16	0.07
112	0.67	0.50	0.11	0.38	0.32	0.41	0.40	0.37	0.16	0.16	0.14	0.05
113	0.67	0.50	0.15	0.39	0.37	0.46	0.40	0.35	0.13	0.16	0.12	0.05
114	0.67	0.50	0.38	0.41	0.36	0.45	0.56	0.44	0.20	0.18	0.12	0.05
115	0.67	0.50	1.00	0.51	0.54	0.67	0.82	0.62	0.50	0.45	0.36	0.21
116	0.67	0.33	0.23	0.21	0.13	0.17	0.29	0.19	0.12	0.18	0.16	0.06
117	0.67	0.67	0.23	0.40	0.35	0.44	0.47	0.41	0.02	0.17	0.15	0.06
118	0.33	0.23	0.67	0.75	0.41	0.58	0.19	0.13	0.12	0.18	0.20	0.16
119	0.47	0.23	0.67	0.65	0.38	0.55	0.23	0.21	0.17	0.27	0.30	0.22
120	0.60	0.23	0.67	0.03	0.35	0.54	0.30	0.22	0.18	0.31	0.28	0.23
121	0.73	0.23	0.67	0.57	0.33	0.54	0.29	0.18	0.15	0.32	0.37	0.19
122	0.83	0.23	0.67	0.54	0.04	0.02	0.25	0.15	0.14	0.29	0.32	0.15
123	0.67	0.12	0.67	0.43	0.23	0.35	0.19	0.12	0.10	0.18	0.23	0.14
124	0.67	0.23	0.67	0.54	0.31	0.51	0.26	0.19	0.16	0.28	0.26	0.19
125	0.67	0.46	0.67	0.66	0.46	0.90	0.99	0.56	0.47	0.53	0.51	0.33
126	0.67	0.23	0.33	0.18	0.07	0.14	0.24	0.13	0.11	0.24	0.27	0.14
127	0.67	0.23	0.67	0.61	0.36	0.55	0.37	0.22	0.18	0.33	0.36	0.23
128	0.67	0.23	1.00	0.77	0.30	0.63	0.35	0.23	0.17	0.34	0.32	0.22
129	0.33	0.23	0.67	0.56	0.36	0.51	0.29	0.14	0.13	0.23	0.26	0.19
130	0.47	0.23	0.67	0.59	0.37	0.53	0.23	0.20	0.17	0.26	0.22	0.23
131	0.60	0.23	0.67	0.56	0.34	0.52	0.23	0.20	0.16	0.27	0.25	0.20
132	0.73	0.23	0.67	0.51	0.34	0.53	0.25	0.18	0.15	0.27	0.28	0.18
133	0.67	0.11	0.67	0.41	0.26	0.34	0.18	0.14	0.12	0.21	0.23	0.81
134	0.67	0.15	0.67	0.44	0.29	0.39	0.21	0.18	0.16	0.28	0.24	0.18
135	0.67	0.38	0.67	0.64	0.46	0.77	0.32	0.35	0.27	0.44	0.38	0.28
136	0.67	1.00	0.67	0.77	0.76	1.65	0.86	0.64	0.29	0.64	0.50	0.36
137	0.67	0.23	0.33	0.28	0.21	0.14	0.25	0.20	0.17	0.28	0.24	0.19
138	0.67	0.23	0.67	0.55	0.39	0.56	0.25	0.29	0.23	0.38	0.29	0.24
139	0.67	0.23	1.00	0.85	0.28	0.63	0.30	0.37	0.26	0.44	0.44	0.27

TABLE 8.3 (T3): Experimental data used for MLP study

Cut No.	Speed	Feed	DOC	Static Force (N)			STP Dynamic Force (N)			STP Acceleration (g)		
	m/min	mm/rev	mm	X	Y	Z	X	Y	Z	X	Y	Z
50	100	0.163	2	1960	1040	3650	1100	1020	966	19.9	8.31	34
51	120	0.163	2	1980	1040	3200	1346	1271	1218	28.2	46.3	43.4
52	140	0.163	2	1940	1020	3000	1403	1730	1588	33.6	50.2	58.8
53	160	0.163	2	1780	980	2750	1445	1837	1645	40.2	65.3	61
54	180	0.163	2	1740	936	2500	1790	1885	1443	93.8	63.9	66.7
55	200	0.163	2	1700	920	2600	1665	1907	1378	45	68.3	56.5
56	220	0.163	2	1660	958	2500	1706	1807	1407	40.8	68.9	54.6
57	240	0.163	2	1680	940	2250	1636	1584	1149	42.4	103.5	53.9
58	200	0.079	2	1020	540	1500	1006	1108	895	35.6	28.2	38.7
59	200	0.088	2	1160	640	1650	1238	1464	941	78.1	40	48.3
60	200	0.106	2	1338	740	1900	1429	1623	1024	79.7	64.7	49.6
61	200	0.163	2	1740	1000	2550	2562	2594	1652	97	102.8	57
62	200	0.192	2	1698	1120	3050	1791	2528	1863	59.4	81.1	62.3
63	200	0.244	2	1740	1140	3400	2429	3324	2484	65.8	63.8	77.1
64	200	0.326	2	1760	1220	4200	2241	3410	2647	51.4	70.9	86.8
65	200	0.423	2	1740	1340	5050	1891	3377	2588	56.3	55.1	84.6
66	200	0.163	0.5	480	440	850	940	996	881	21.8	33.1	32
67	200	0.163	1	880	640	1450	1292	1688	1230	31.2	43.3	49.4
68	200	0.163	1.5	1120	700	1950	1449	1807	1300	32.5	41.7	48.6
69	200	0.163	2	1560	920	2600	2011	2468	1535	42.6	80.6	50.1
70	200	0.163	2.5	2220	1240	3350	2914	3342	1917	61	77.4	48.4
71	200	0.163	3	2860	1540	4250	3270	4278	2297	94	96.9	51.5
72	200	0.163	3.5	2960	1660	4450	4014	4594	2364	71.2	107.3	51.5
73	200	0.163	4	3240	2100	5100	3778	5533	2809	88.1	105.4	46.7
74	100	0.163	2	2100	1080	3400	1015	1722	1381	27.9	25.8	60.2
75	120	0.163	2	2020	1120	3300	1277	2584	2179	56.2	44.2	138.1
76	140	0.163	2	1960	1020	3200	1675	4554	3723	65.3	75.9	375.8
77	160	0.163	2	1840	880	3050	1893	7810	6423	186.4	167.5	276.2
78	180	0.163	2	1700	900	3000	2283	7291	5988	104.7	121.4	379.7
79	200	0.163	2	1900	880	2850	1988	3134	2710	171.4	42.6	506.4
80	220	0.163	2	1720	940	2850	2343	3699	3133	181	49.5	434.7
81	240	0.163	2	1720	800	2750	2103	2543	2534	227.5	32.9	475.9
82	200	0.079	2	900	640	2950	1048	7495	6556	261.1	182.7	233.4
83	200	0.088	2	1020	660	3100	1137	8409	7260	272.2	195.6	259.4
84	200	0.106	2	1300	820	2800	1184	6371	5670	267.3	145	354.7
85	200	0.163	2	1840	920	2950	2175	4218	3658	243.4	59.5	502.9
86	200	0.192	2	1920	640	3350	2287	5429	4704	256.9	96	419.8
87	200	0.244	2	1820	660	3750	1951	6609	5846	308.5	108	353.1
88	200	0.326	2	1760	740	4400	1647	5962	4943	258.5	88.1	488.8
89	200	0.423	2	1780	580	5100	1778	4778	4065	272.3	73.7	417.2
90	200	0.163	0.5	380	180	750	664	1148	979	32.2	15.6	299.1
91	200	0.163	1	840	940	2650	1580	6458	5631	201.5	140.9	236.4
92	200	0.163	1.5	1320	1220	3600	1732	7825	6515	196.2	168.2	227.8
93	200	0.163	2	1560	460	2800	1741	3663	3241	213.8	64.2	360.1
94	200	0.163	2.5	2200	940	3900	1657	7091	5695	196.7	136.8	361
95	200	0.163	3	2760	1200	4700	1853	8716	6565	91.1	147	251.3
96	200	0.163	3.5	3160	1580	5700	1621	11012	8373	123	151	304
97	200	0.163	4	3380	1540	6000	2374	13254	10064	125	178	229

TABLE 8.4: Summary of cross-validation results

No. Nodes	% Success for Each Data Type and Designation		
	P10 (T1)	P10 (T2)	P40 (T3)
100	83	73	98
20	83	82	96
10	83	63	92
8	83	73	98
5	83	82	98
1	83	73	98
Total No. of Data	42	49	49

CHAPTER 9

IMPACT OF CUTTING CONDITIONS ON SENSOR SIGNALS - CHIP BREAKER GEOMETRY TOOL INSERTS

9.0. Overview

This chapter is concerned with investigating the effects of cutting conditions on sensor signals, employing tool inserts with chip breaker geometry and a harder workpiece material. Medium Sandvik Coromant double coated carbide grade tool inserts (integral groove chip-breaker geometry type) of the P25 (Al_2O_3 outer coating and TiCN inner coating) and P15 (TiN outer coating and Al_2O_3 inner coating) types were used to cut EN24 steel. Further details of the cutting conditions, material and tooling inserts are provided in summary Table 9.1. Experimental results are analysed in both the time and frequency domains.

9.1. Effects of Process Parameters

For this investigation, test cuts were conducted using P15 inserts, hence the ensuing discussion is based solely on the results obtained that is outlined in Table 10.2. The duration of each test cut was such that stabilisation of the cutting process would have been attained, and recording of the sensor signals was carried out after 5-10 seconds had elapsed. The active cutting time or time of tool engagement, chip samples as well as features of significance on the tool surface such as wear and BUE were noted. The obtained data was analysed and presented as time displays and frequency spectra plots. Analysis of results involved extracting the static and dynamic cutting forces from the sampled cutting force components as described in Chapter 8, and these together with the vibration

(acceleration) signals were studied when each of the three process parameters were varied. In summary, test cuts were conducted under the following conditions:

- Test set 1: Involved investigating the effects of cutting speed on the sensor signals. The cutting speed was varied from 100 m/min to 300 m/min at 20 m/min intervals at a feed-rate of 0.2 mm/rev and DOC of 2 mm (Cut No. 1-11).

- Test set 2: The feed-rate was varied from 0.076 mm/rev to 0.42 mm/rev with five values between. The cutting speed used was 200 m/min and constant DOC of 2 mm (Cut No. 12-18).

- Finally, the 3rd set of tests involved investigating the effects of DOC variation on the signals. The DOC was varied from 0.5 mm to 3 mm at 0.5 mm intervals with a feed-rate and cutting speed of 0.1 mm/rev and 200 m/min respectively (Cut No. 19-24).

For the time domain analysis, the static force and the Sum Total Power (STP) of both dynamic and acceleration signals were plotted against the cutting parameters. The objective of the time domain analyses was to establish the nature and level of sensor signal component change i.e. their sensitivity to process parameter variation. Frequency analysis involved interpretation of the dynamic force and vibration signature spectra plots for various cutting conditions.

9.2. Time Domain Analysis

9.2.1. Effects of Speed Change

Inspection of the data table and static force displays (Figures 9.1 - 9.3) showed that the three static force components were only slightly affected, and to a varying degree, by cutting speed changes. The x-component magnitude (418N) initially decreased as the speed was increased from 100 m/min. but then decreased to a minimum value of 407 N at V = 180 m/min. It then rose to 450 N at V = 300

m/min. The z-component decreased erratically, with no discernible trend immediately apparent. The STP dynamic force also showed sensitivity to changes in the cutting speed, with the z-axis component being the most sensitive to cutting speed changes. Increases in the cutting speed lead to a concurrent rise in STP dynamic forces, peaking at 180 m/min. and then decreasing gradually. The STP acceleration signals tended to behave similarly to the STP dynamic force signals, but with the x-component being the most sensitive to speed changes.

9.2.2. Effects of Feed-rate

The static force plots (Figures 9.4 - 9.6) showed that the z-component was the most sensitive to feed-rate changes and the y-component the least. At faster feed-rates (i.e. above 0.1 mm/rev), the force components behave in a linear manner with larger changes occurring in the z-axis than the x- and y-axes. Both the STP dynamic force components were sensitive to feed-rate variation, with the z-component being the most sensitive, increasing nearly 25% in magnitude for a step increment in feed-rate. The z- and x-STP acceleration behaved identically to the STP dynamic force, while the x-component was not sensitive at all.

9.2.3. Effects of DOC

As the DOC increased from 0.5 mm to 3 mm both the x- and z-components of the static force showed a linear sensitivity with a constant slope (Fig. 9.7 - 9.9). The y-component of static force showed only a slight increase. As for the STP dynamic force, all three components were sensitive (to an extent) to DOC increments with the z-STP dynamic force component having the largest slope and the y-axis the least. The acceleration components showed that the x- and z-vibrations were most affected by increases in the DOC.

The sensitivity of the sensor signals to changes in the cutting conditions can be summarised by building a sensitivity index table by assigning numbers (i.e. high when sensitive and low when not). Such a table was constructed using the

following indices: 3- most sensitive; 2-moderately sensitive; 1-least sensitive; and 0-when not sensitive at all.

From the matrix table shown in Table 9.3, it is evident that all three sensor signals show a varying degree of sensitivity to changes in the process parameter in all three directions. The y- and z-dynamic forces, x- and z-static forces, and x- and z-acceleration were the most sensitive as their sum total response were largest. Bearing in mind that a score of 9 was the highest absolute total response, any score above (9/2) or 5 would be indicative of good sensitivity to changes in the cutting conditions. Inspection of the matrix indices table shows that 6 components scored 5 and above (shown in bold and underlined). Effectively, the y-, x- and y-components of the static forces, STP dynamic forces and acceleration signals respectively were less sensitive to process parameter changes.

9.3. Frequency Spectra Analyses

The interpretation of frequency analysis results was carried out through spectra displays and contour plots. Each plot was presented as a series of three displays:

- The complete frequency spectrum (15 KHz) shown in Figures 9.10 - 9.16
- With a cut-off frequency at 5 KHz examples of which are shown in Figures 9.17 and 9.18, and
- With a cut-off frequency at 2 KHz typical examples shown in Figures 9.19 and 9.20.

Frequency analysis was undertaken mainly to identify specific directions or points that had a high dynamic tendency which could not be visualised in the time domain. The data was first passed through a forward FFT to yield the frequency distribution data, and then the FFT data was smoothed using a seventh order filter. The final data was presented as spectra and contour plots. Frequency spectra

presentation allows visualisation of the sensor signal behaviour of single axis spectrum for each cutting condition. This allows a comprehensive establishment of the relationship between frequency and amplitude of the sensor signals for the complete sampled frequency range. Contour plots, Figures 9.21- 9.23, show the behaviour of the complete cutting condition range (desired variable) with the complete (or thereof cut-off) frequency range, thereby allowing visualisation of the dominant frequencies. Generally, vertical rows of peaks on the contour plots are indicative of a resonant or dominant frequency, and the more compact and close the line, the steeper the peaks.

Inspection of the obtained spectra and contour plots showed that there was a consistent peak at 500 Hz, 2-4 KHz, and 8-10 KHz. With the vibration spectra, the higher frequency components were dominant whereas the 2-4 KHz components were sharpest on the dynamic force spectra. The lower frequency band was rather difficult to interpret. This frequency was most likely associated to the chip breaking and approximate calculations of the chip fracture frequency indicated this to be the case. Change in amplitude of the chip fracture frequency as the cutting speed increased suggested far more than just a mere chip fracture frequency, and therefore warranted further investigation. The effects of spindle motor speed on the frequency spectra with the lathe idle was studied. Obtained spectra results indicated that the 0-500 Hz frequency band was sensitive to spindle speed increments, and its magnitude increased proportionally to the spindle motor speed. This phenomenon was associated with background noise from the motor drive belt, linkages and the hydraulic systems. The noise could not be eliminated since chip formation and fracture also had a similar frequency range. A decision was therefore taken not to filter this band. No other peaks or higher frequency bands appeared.

9.3.1. Effects of Cutting Speed

The cutting speed did not seem to have any substantial effects on the magnitude of the dynamic and vibration signals in the spectra. As expected, an increase in the magnitude of the peak at 500 Hz was visible when increasing cutting speed for reasons already outlined. Unlike the dynamic force spectra with no apparently noticeable features, the acceleration spectra peaks shifted from 2-3 KHz band to concentrate in the 10 KHz band (i.e. increasing the cutting speed altered the chip lamination frequency).

9.3.2. Feed-rate

The general effect on the dynamic force spectra was an increase in the bandwidth of the resonant frequencies at 2-4 KHz and 10 KHz. These observations were visible on the three force components, with visualisation stronger on the z-component, and least on the x-components. Inspection of the vibration spectra showed that the *10 KHz peak was the most sensitive to feed-rate changes.* Generally, peaks appeared at ≈5 KHz and 10-12 KHz, which tended to increase proportionally to the feed-rate. However, magnitudes of the latter frequency band were more than 5 times larger than those in the former frequency band, with the x-direction spectra more sensitive to feed-rate changes and y-axis the least.

9.3.3. Effects of DOC

The 500 Hz and 2-3 KHz peaks were more sensitive to DOC changes on the x- and y-dynamic force spectra. They generally increased while the 10 KHz peak remained constant and therefore less sensitive. On the z-force displays the spectra behaviour were similar to those of the x- and y-displays with the 10 KHz peak more sensitive to DOC changes. The vibration spectra showed that the sharpest response occurred with the 10 KHz peak. The x-component increased as the DOC increased. this increase was also aobserved with the z-component but less eminent in the y-component.

On the whole, as the DOC increased, the noise in the data tended to increase and the region of maximum concentration of the spectra energy became rather dispersed. This effect was most prominent in the z-component at a DOC of 3 mm.

9.4. Discussion of Results and Conclusions

This work was partly motivated by the current lack of TCMS for tool inserts with chip-breaker geometry configurations, and the effects such control has on the sensor signals. Almost all existing methods are based on plane-faced tool geometry, and this investigation makes a substantial contribution to knowledge in this field.

An important observation made from these tests was that under fixed sets of cutting conditions, the characteristic resonant frequencies of the tool holder and chip lamination remained constant and therefore variations on its peak frequency or bandwidth indicated a sensitivity to changing parameters. It was also noticed that there was an amplitude peak at a low frequency spectrum on the free running lathe, indicative of substantial noise from the electric motors.

Increases in the force components were principally influenced by feed-rate and DOC with other changes attributable to either the effects of tool wear or material inhomogeneities.

This investigation demonstrated that the well known effect of cutting speed on plane-faced tool static force behaviour was only partly valid. The first discrepancy involved the cutting forces remaining largely unchanged as the cutting speed increased. Normally, a slight reduction in the force components accompany moderate to high cutting speed increases for a nominally sharp plane-faced tool. The reason for this did not seem immediately apparent, but a possible logical reason could be the tool insert geometry effect. The workpiece used in this investigation, EN24, had been hot rolled, quenched in oil and tempered, and

was considerably harder to machine. The normal or expected trend, based on studies where machining was performed using plane-faced tool inserts and the only variable being the cutting speed, would have been a slight decrease in the static cutting force components with an increase in cutting speed. Most of the obtained plots showed that the static cutting forces tended to remain constant with very slight variation as the surface cutting speed increased. It could be argued that the relative hardness of the workpiece was the main contributing factor. Once a tool had been used, the cutting edges began to crumble (i.e. wear); this had the effect of increasing force levels because the contact area would have increased. Continued cutting with a partly worn tool insert led to an increase in the frictional forces. Increased friction caused the cutting temperature to rise, hence softening the material being machined. It could be argued that a slight decrease in static cutting forces due to increases in the cutting speed may have therefore been offset by wear effects.

Another significant contribution to the uniqueness of this study is the supposed effect of mechanical and chemical interaction between the tool insert and the workpiece. Unlike previous studies that used un-coated inserts, the wear mechanisms were deemed to have been severely altered by the currently employed material combinations. A possible reason for the high wear resistance of these inserts was the reduction in abrasion and diffusion wear (especially abrasion wear) rate in the primary and secondary phases of tool wear. Naturally, if two materials of equal hardness are rubbed together, it takes a long time and considerable effort to scratch their surfaces i.e. harder materials have high abrasion resistance. Beyond the secondary phase i.e. on the threshold of the tertiary phase, the wear rate was found to accelerate as the abrasion resistance was weakened, resulting in the erosion of the coating, and plastic deformation of the cutting edges. This phenomena was primarily due to changes in the coating thickness, thermal reduction of the cohesive strength of the materials, an increase in the coefficient of friction between coating layer and chips, and elastic properties of the substrate deposit (Audy *et al.*, 1995).

The similarity between the current results and those from plane-faced tool insert geometry with respect to static force components were expected, i.e. a larger magnitude for the main cutting force (F_z), similar radial cutting force (F_x) and a smaller axial force (F_y).

Chip formation depended largely on the cutting conditions. Both types of chip patterns, continuous and discontinuous, were simultaneously produced. The discontinuous chip formation in these experiments were a direct consequence of the utilisation of chip-breaker geometry tool insert, i.e. controlled tool chip contact. This was partly due to the danger uncontrolled chip formation posed to the machine operator, and to a lesser extent, chipping of the cutting tool edge by any entangled chip. Another consideration in utilising chip breaker configuration was to reduce the volume of solid chip material. While unbroken continuous chip has a bulk ratio of $\approx$ 50, broken chips have a bulk ratio of $\leq$ 3, offering a volumetric reduction of more than 17 times, serving handling and removal time, and cost (AB Sandvik, 1995). The use of the chip breaker configuration inserts in this study was first and foremost to control and break the chip (i.e. integral obstruction).

Based on the results discussed herein, the effects of the cutting parameters on the sensor signals cannot be ignored. All three cutting conditions affect the magnitude of the process parameters (feed-rate and DOC) or the rate of tool wear (cutting speed). In order to develop what might be termed a universal TCMS, it is prudent not to limit the operational functioning range of the system, hence the reason for using all three cutting parameters as independent inputs to the envisaged system.

Table 9.1: Details of Cutting Material and Cutting Conditions

Machine Tool		Lang J6
Workpiece Material		
	Work Material	EN24T BS 970 817M40
	Hardness	Brinell 255
	Composition	0.4% C, 0.28% Si, 0.27% Mo 1.18% Cr, 0.5 % Mn, 1.4% Ni
Tooling Material:	Tool Holder	Sandvik SSBCR 2020 K12
	Tool Type	SCMT 12 04 08 UM
	Tool Material	Sandvik Coromant P25 4025 P15 4015
	Overhang (mm)	50
Cutting Conditions	Speed (m/min.)	100 - 300 @ 20 intervals
	Feed (mm/rev)	0.08 - 0.42 (5 values between)
	Depth /mm	0.5 - 3 @ 0.5 intervals
Cutting fluid	None	

Table 9.2: Experimental Results

Cut No.		Static Force (N)			STP Dynamic Force (N)			STP Acceleration (g)		
		X	Y	Z	X	Y	Z	X	Y	Z
Variable Speed										
1	100	418	222	725	125	258	215	83	39	124
2	120	412	227	705	104	128	145	85	42	121
3	140	412	231	712	110	142	165	131	58	176
4	160	409	236	707	100	154	223	464	61	251
5	180	407	245	691	132	211	396	575	75	281
6	200	419	250	696	90	154	273	335	78	201
7	220	423	250	700	85	144	206	264	83	171
8	240	439	249	700	88	142	192	213	69	185
9	260	440	253	715	89	155	185	195	85	213
10	280	447	248	694	81	139	166	151	67	155
11	300	450	251	707	88	143	172	159	61	148
Variable Feed										
12	0.076	336	178	369	47	68	91	102	31	73
13	0.08	343	187	389	46	61	82	90	29	66
14	0.088	349	184	410	49	64	86	114	32	76
15	0.106	351	191	450	47	63	83	145	33	82
16	0.163	394	215	617	82	135	200	364	62	175
17	0.235	418	226	700	98	171	284	412	79	209
18	0.42	466	248	857	140	256	391	581	97	346
Variable DOC										
19	0.5	90	119	132	33	38	49	38	17	34
20	1	185	148	243	44	56	86	85	25	78
21	1.5	262	164	338	48	63	91	112	30	80
22	2	344	181	456	54	73	106	134	33	92
23	2.5	418	190	550	53	84	115	135	34	101
24	3	488	196	614	63	94	138	104	41	117

Table 9.3: Sensitivity Matrix Index

Process Parameter	Static Force			Dynamic Force			Vibration		
Components	x	y	z	x	y	z	x	y	z
Speed	1	1	1	1	2	3	3	1	2
Feed	2	1	3	1	2	3	3	1	2
DOC	2	1	3	2	2	3	3	1	3
Total Response	**5**	3	**7**	4	**6**	**9**	**9**	3	**7**

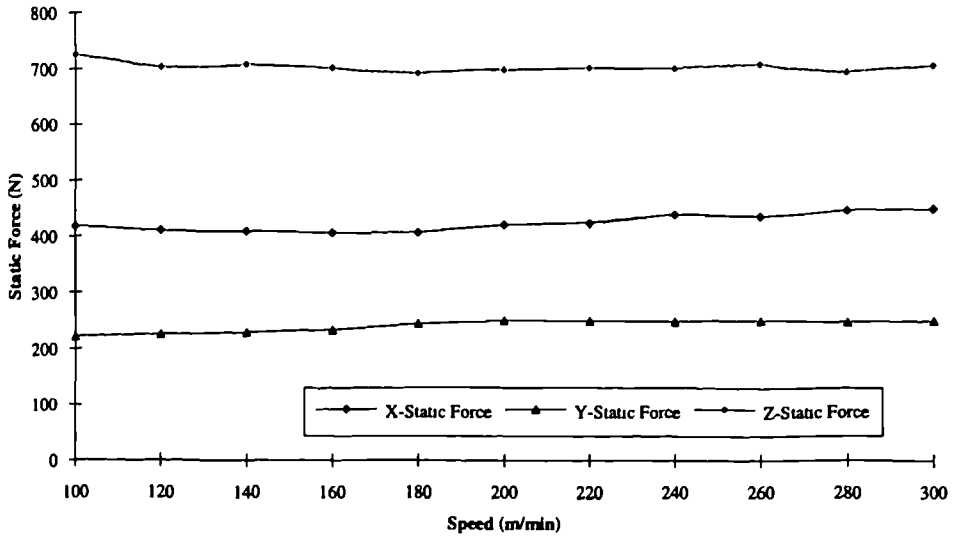

Figure 9.1: Static Force Vs Cutting Speed (f=0.2mm/rev. & a=2mm)

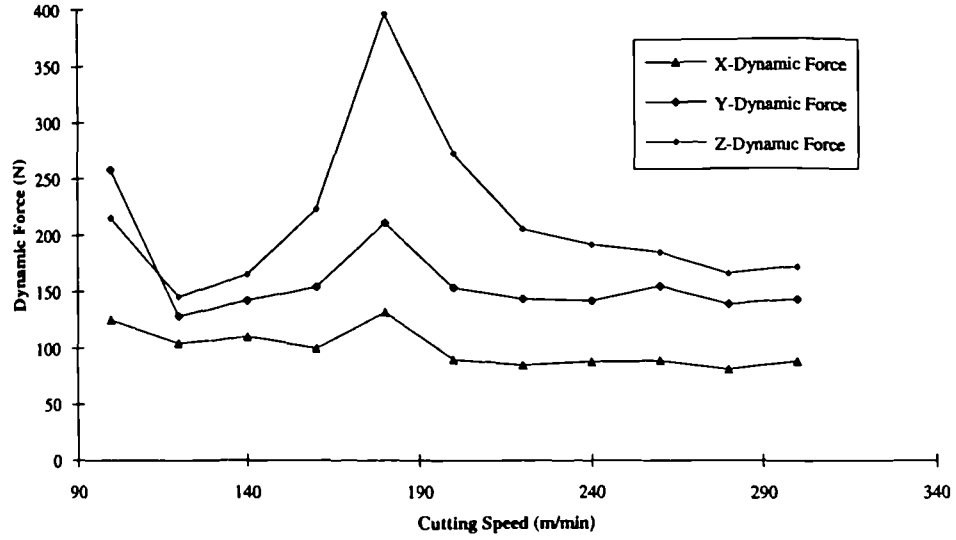

Figure 9.2: STP Dynamic Force Vs Cutting Speed (f=0.2mm/rev. & a=2mm)

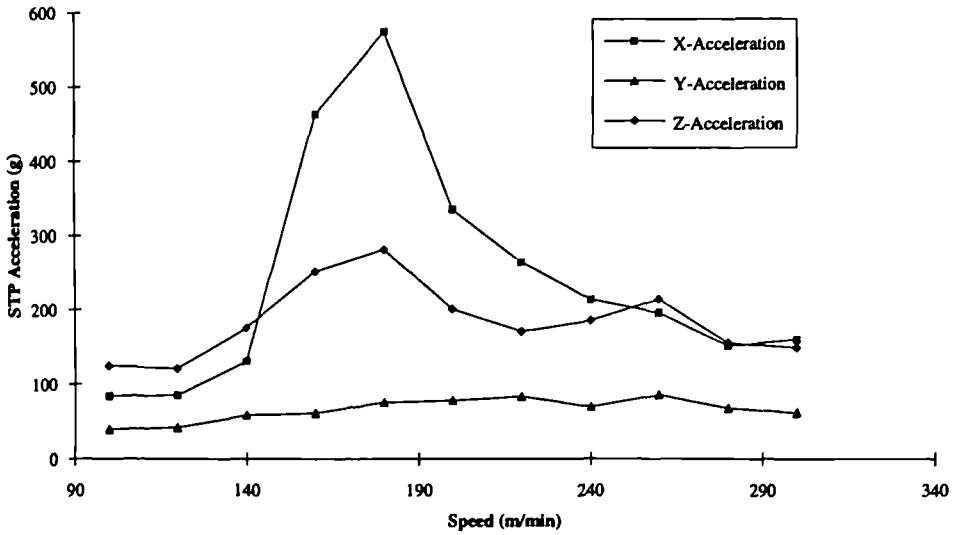

Figure 9.3: STP Acceleration Vs Cutting Speed (f=0.2mm/rev. & a=2mm)

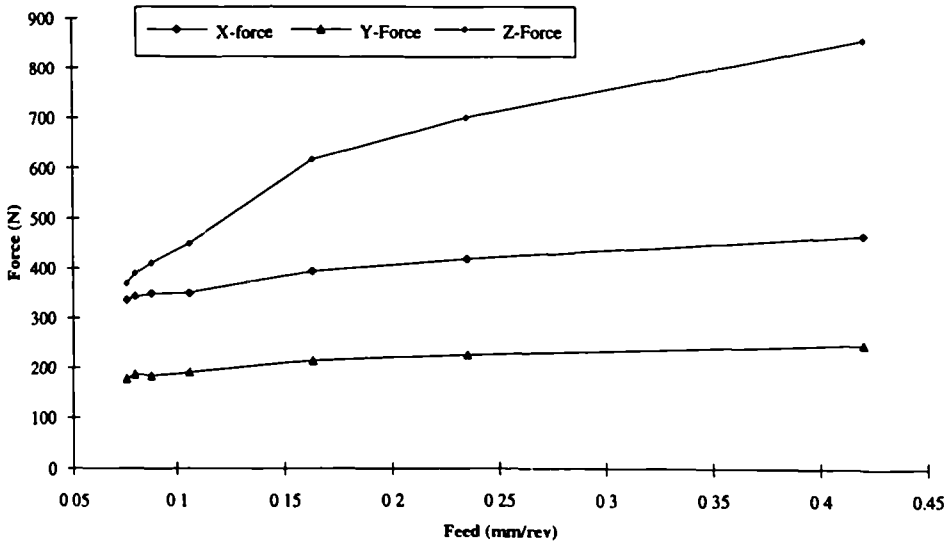

Figure 9.4: Static Force Vs. Feed (V=200m/min. & a=2mm)

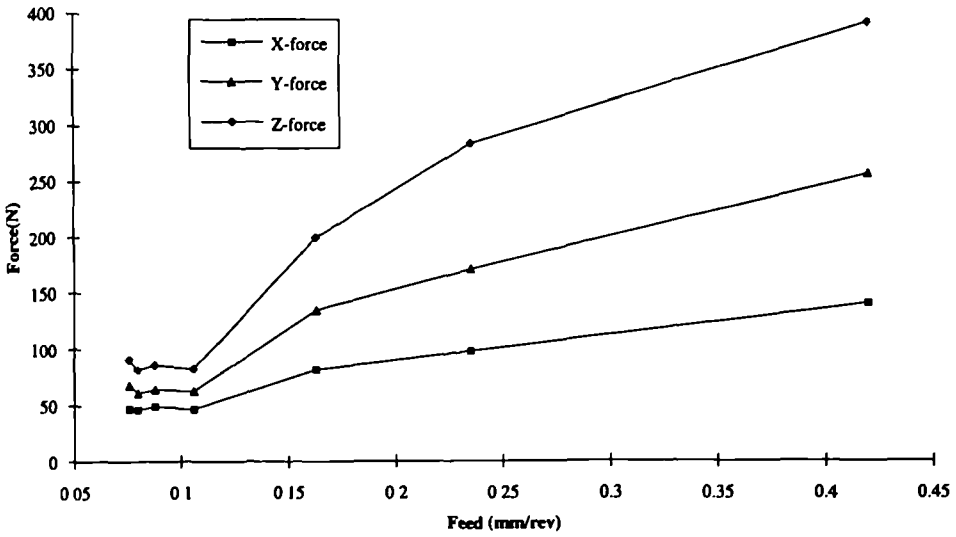

Figure 9.5: STP dynamic Force Vs. Feed-rate (V=200m/min. & a=2mm)

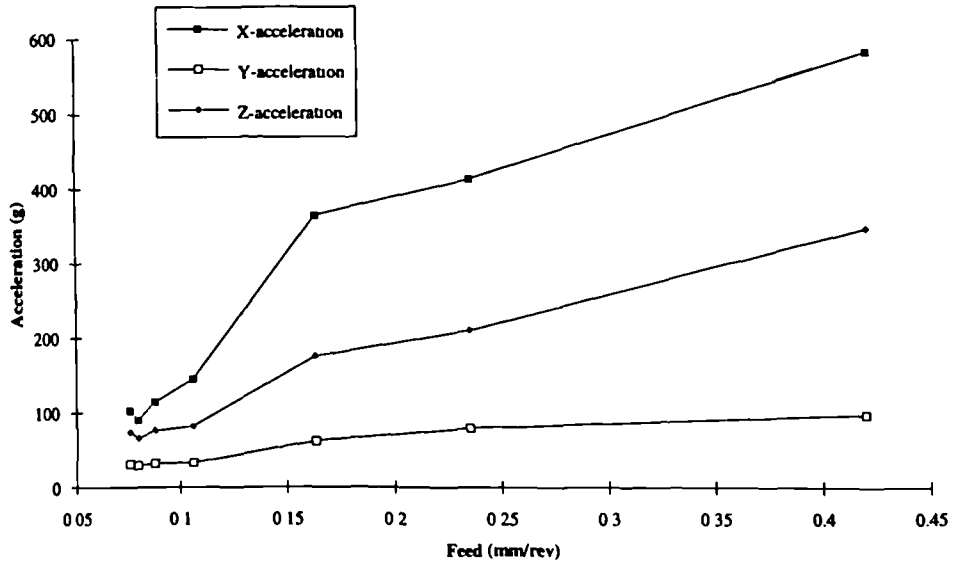

Figure 9.6: STP Acceleration Vs. Feed-rate (V=200m/min. & a=2mm)

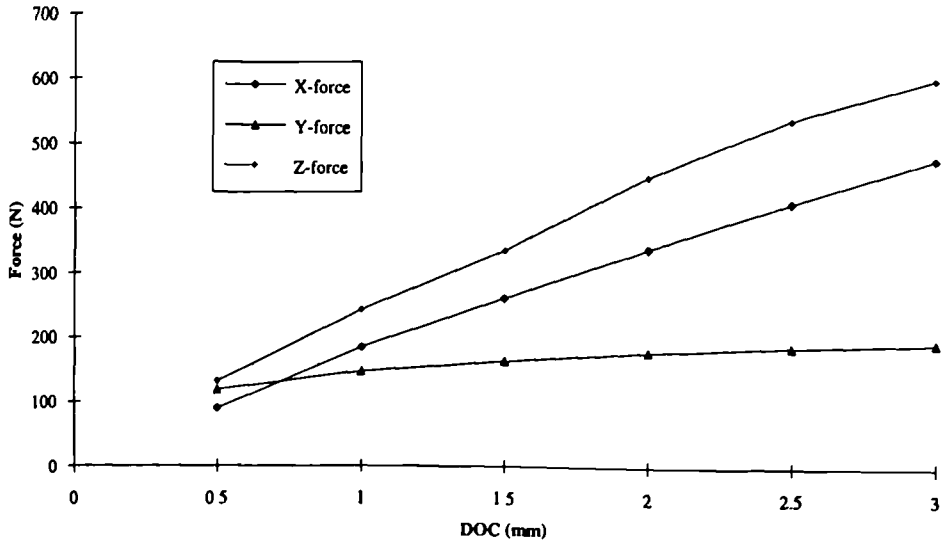

Figure 9.7: Static Force Vs. DOC (V=200m/min. & f=0.2mm/rev.)

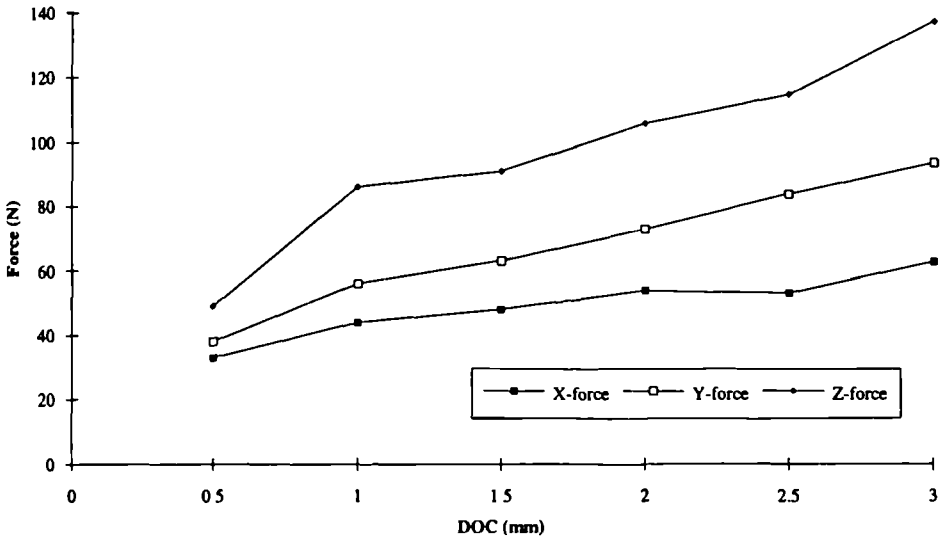

Figure 9.8: STP Dynamic force Vs. DOC (V=200m/min. & f=0.2mm)

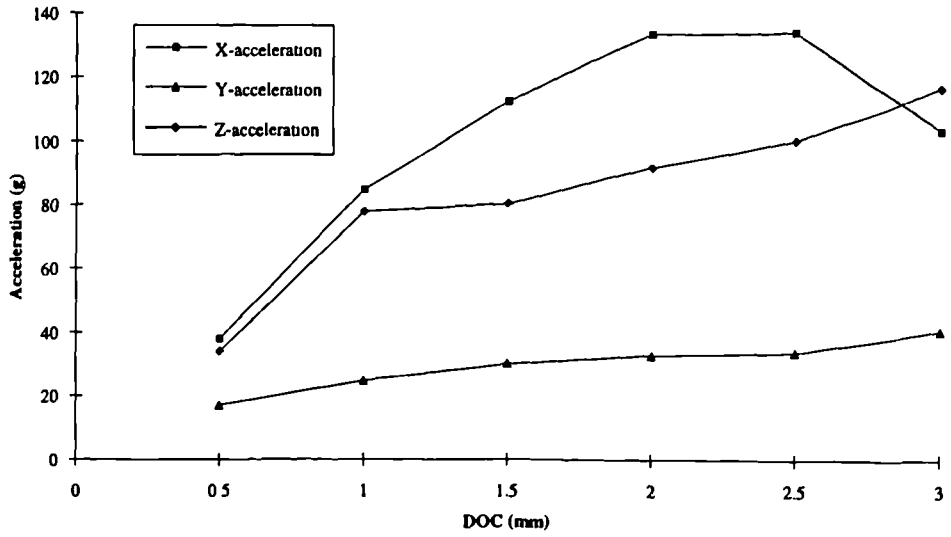

Figure 9.9: STP Acceleration Vs DOC (V=200m/min. & f=0.2mm/rev.)

Key to Waterfall and Contour Plots:

Variable Designation	Cutting Speed (m/min)	Feed-rate (mm/rev)	DOC (mm)
1	100	0.076	0.5
2	120	0.08	1
3	140	0.09	1.5
4	160	0.1	2
5	180	0.16	2.5
6	200	0.24	3
7	220	0.42	
8	240		
9	260		
10	280		
11	300		

Figure 9.10: Y-Dynamic Force Spectra Vs. Cutting Speed

(f=0.2mm/rev. & a=2mm)

Figure 9.11: X-Vibration Spectra Vs. Cutting Speed

(f=0.2mm/rev. & a=2mm)

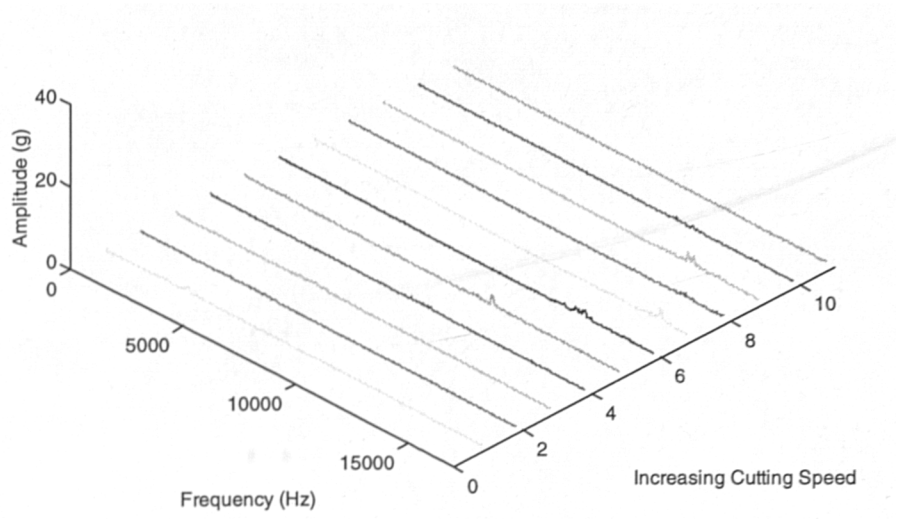

Figure 9.12: Y-Vibration Spectra Vs. Cutting Speed

(f=0.2mm/rev. & a=2mm)

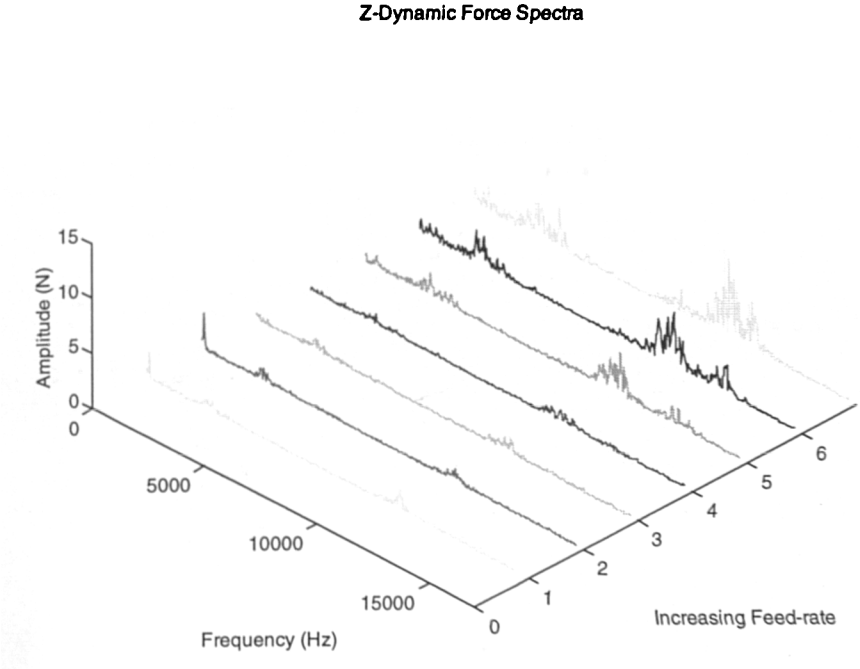

Figure 9.13: Z-Dynamic Force Spectra Vs. Feed-Rate

(V=200m/min. & a=2mm)

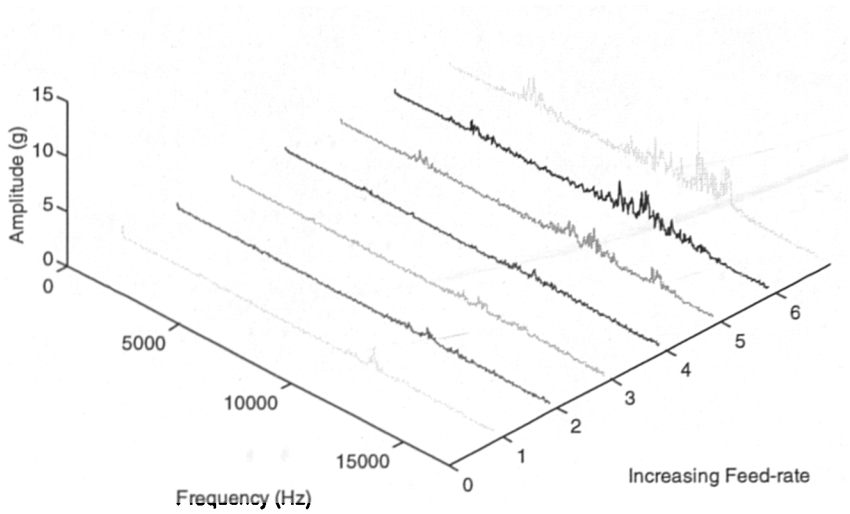

Figure 9.14: Z-Vibration Spectra Vs. Feed-Rate

(V=200m/min. & a=2mm)

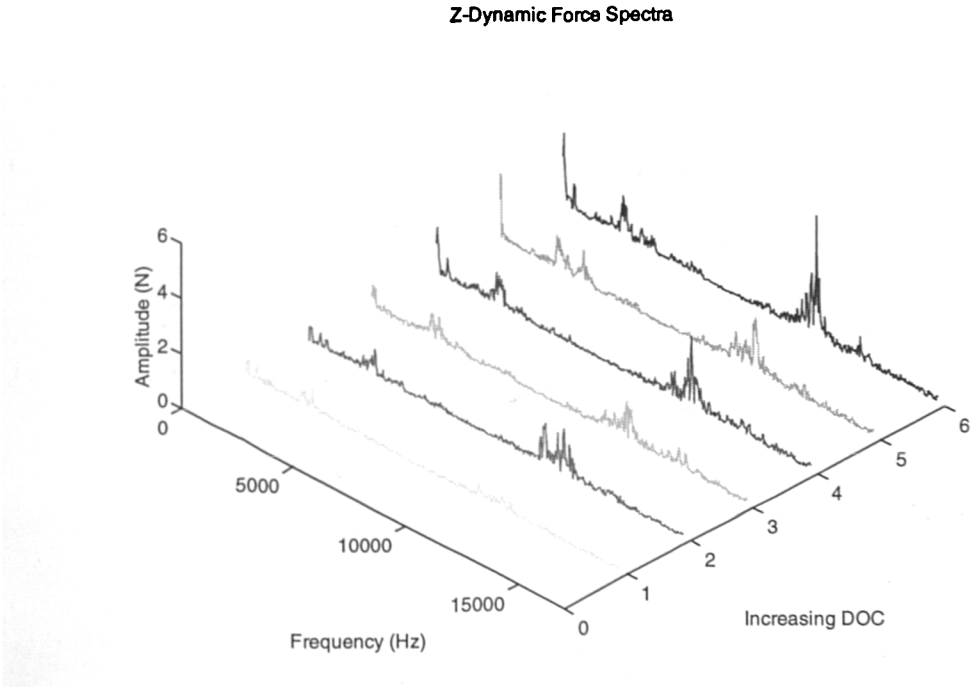

Figure 9.15: Z-Dynamic Force Spectra Vs. DOC

(V=200m/min. & f=0.2mm)

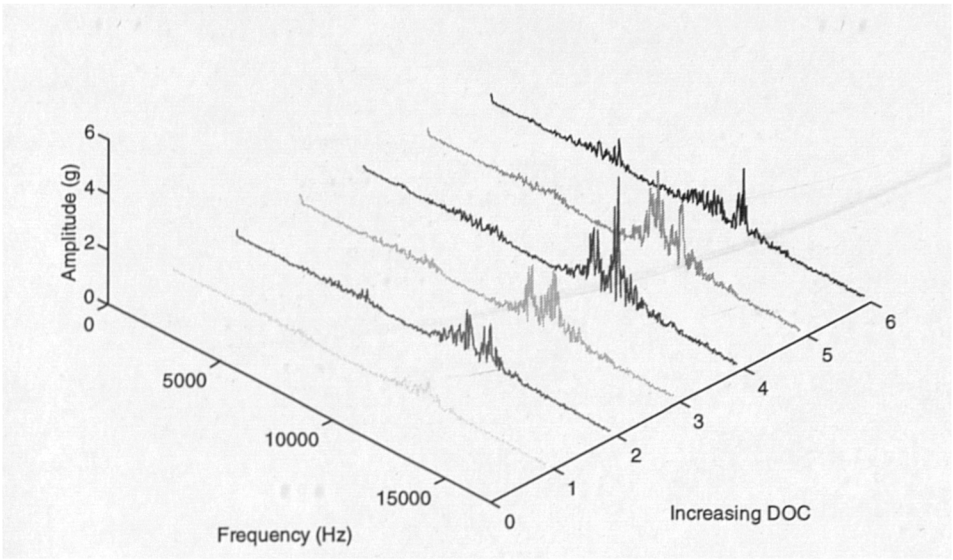

Figure 9.16: X-Vibration Spectra Vs. DOC

(V=200m/min. & f=0.2mm/rev.)

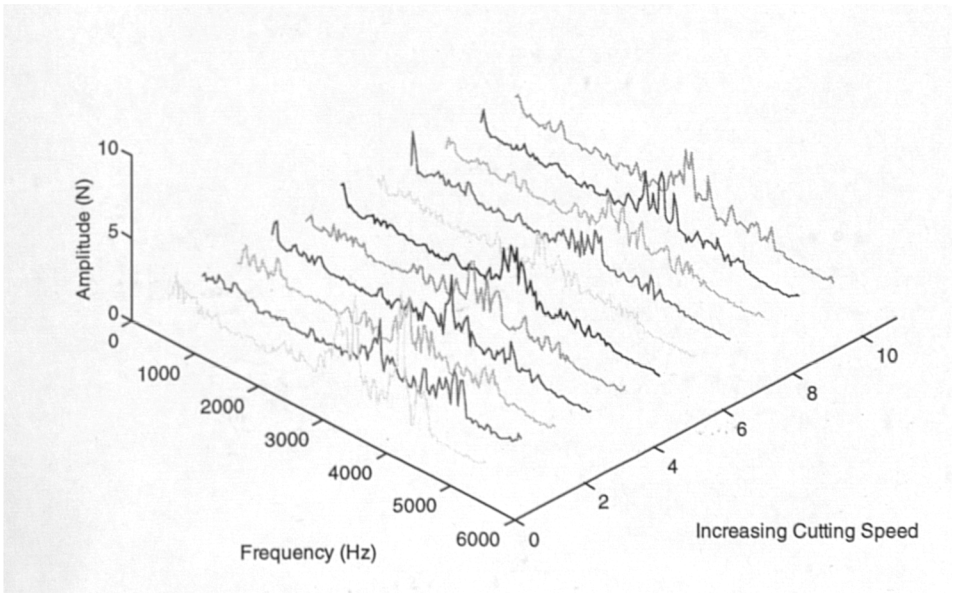

Figure 9.17: Z-Dynamic Force Spectra Vs. Cutting Speed - 5 KHz cut-off
(f=0.2mm/rev. & a=2mm)

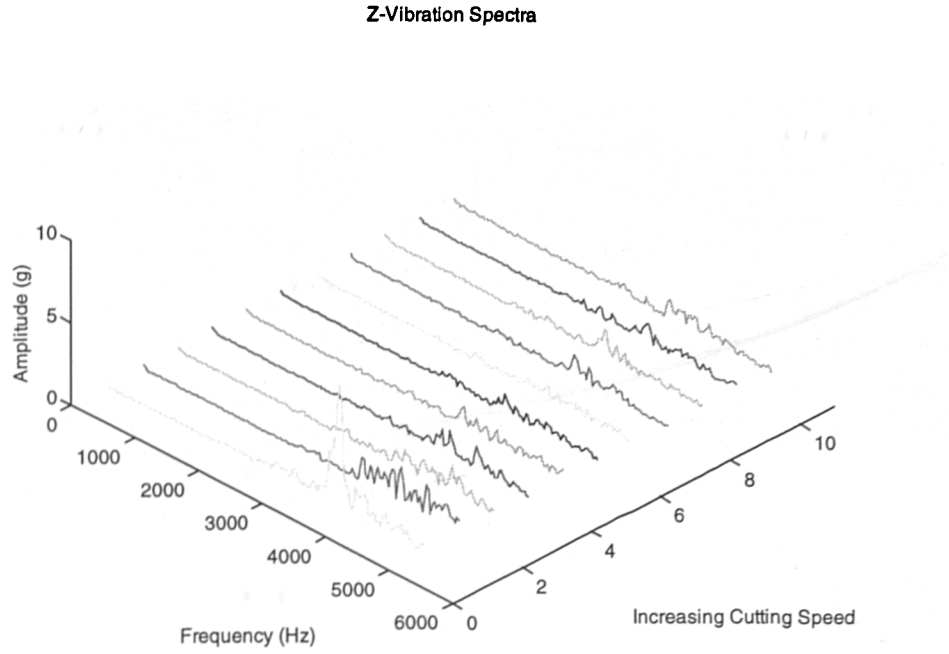

Figure 9.18: Z-Vibration Spectra Vs. Cutting Speed - 5KHz cut-off (f=0.2mm/rev. & a=2mm)

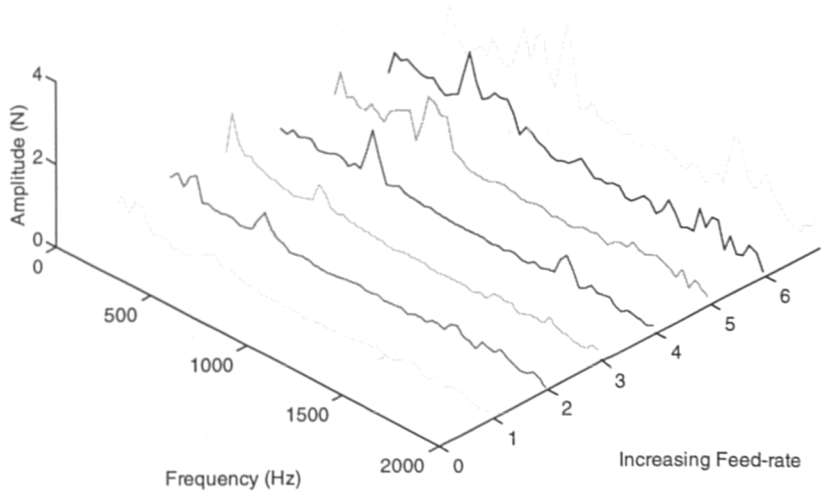

Figure 9.19: X-Dynamic Force Spectra Vs. Feed-Rate - 2 KHz cut-off (V=200m/min. & a=2mm)

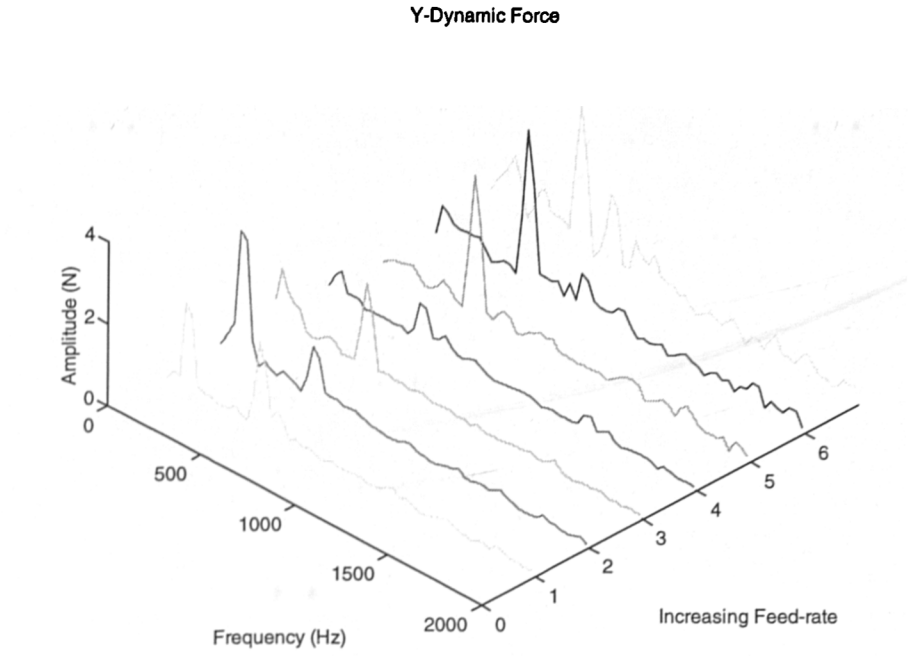

Figure 9.20: Y-Dynamic Force Spectra Vs. Feed-Rate - 2 KHz cut-off (V=200m/min. & a=2mm)

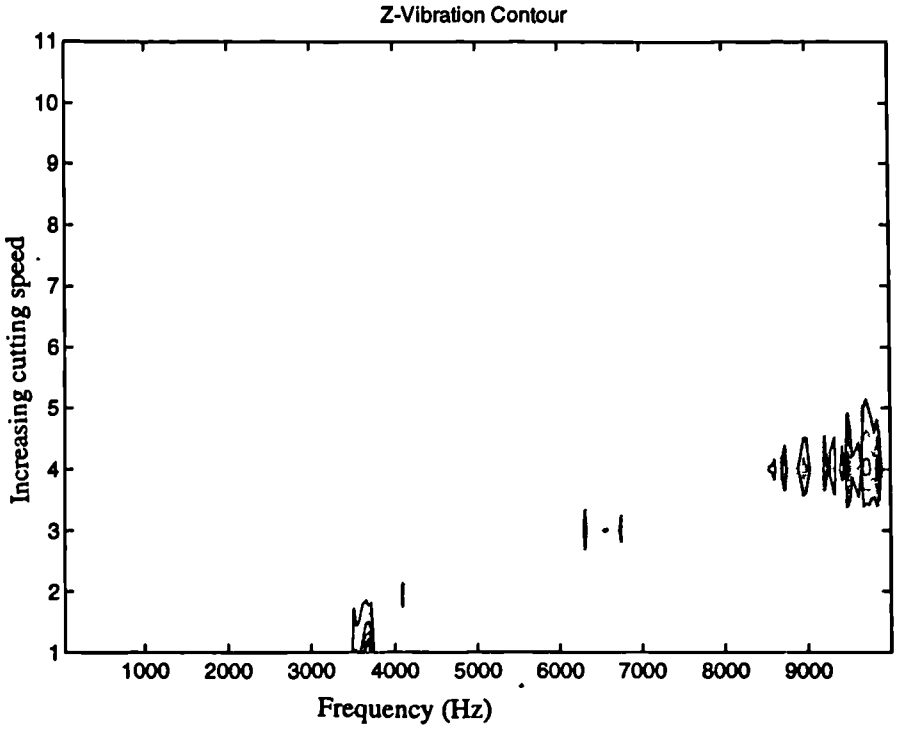

Figure 9.21: Z-Vibration Contour Vs. Cutting Speed

(f=0.2mm/rev. & a=2mm)

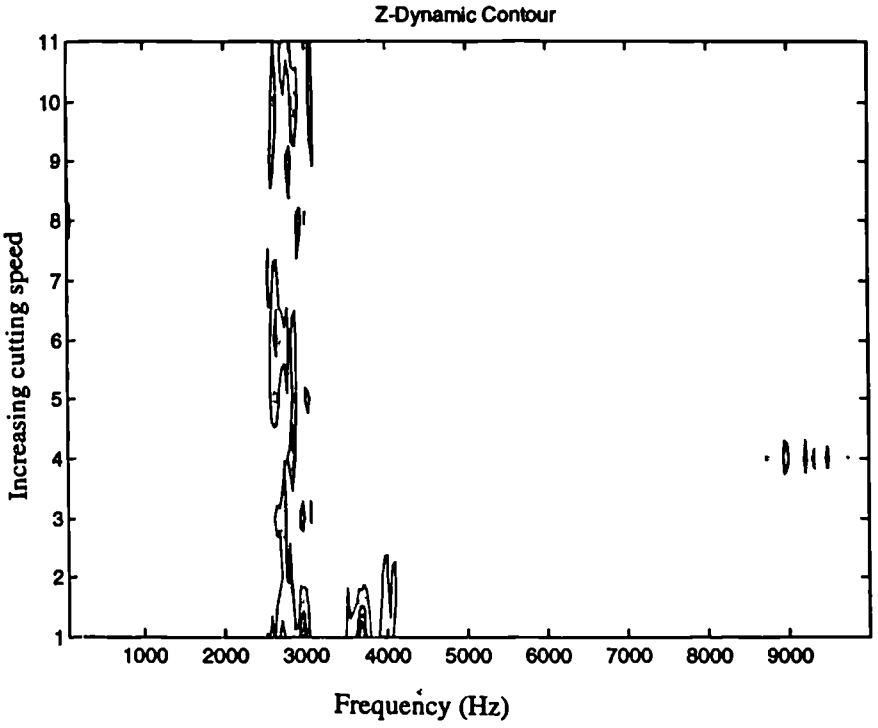

Figure 9.22: Z-Vibration Contour Vs. Cutting Speed

(f=0.2mm/rev. & a=2mm)

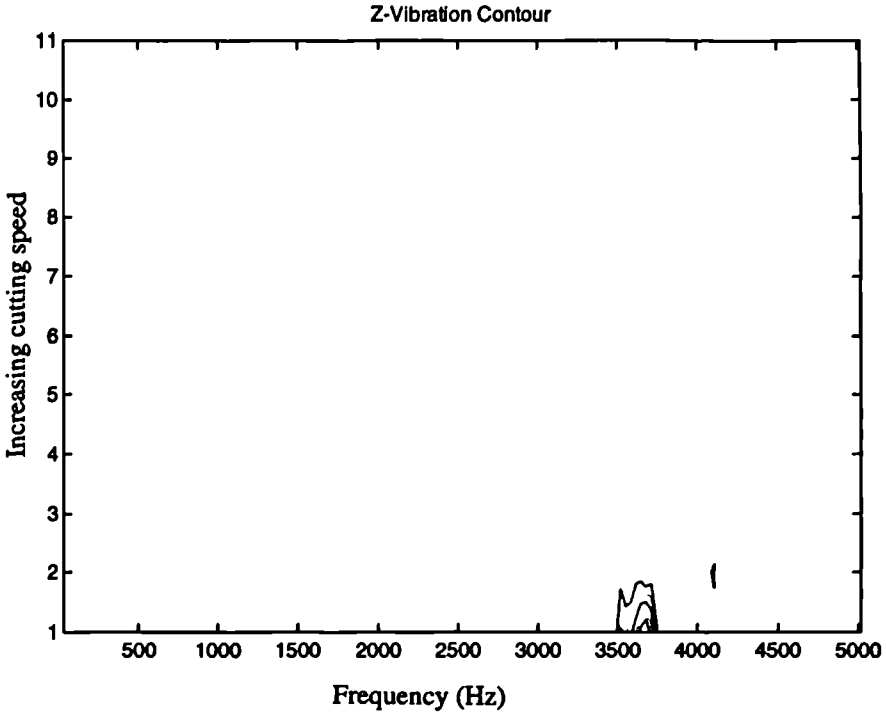

Figure 9.23: Z-Vibration Contour Vs. Cutting Speed (cut-off at 5 Khz) (f=0.2mm/rev. & a=2mm)

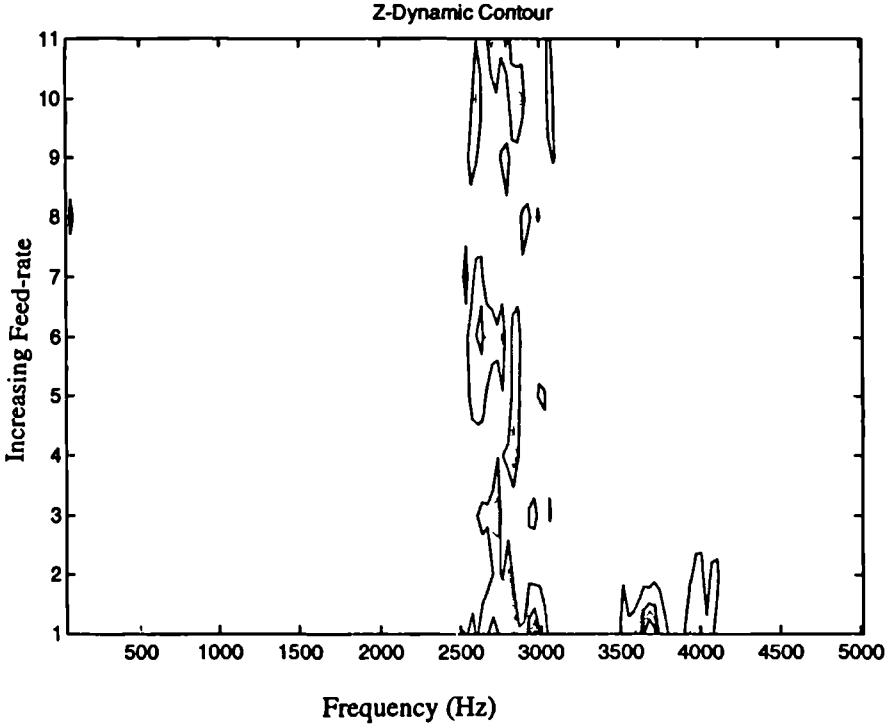

Figure 9.24: Z-Vibration Contour Vs. Feed-Rate (cut-off at 5 Khz) (V=200m/min. & a=2mm)

CHAPTER 10

PROGRESSIVE WEAR STUDIES

10.0. Overview of the Study

In this chapter, results of progressive cutting tool wear studies utilising P15 and P25 tool inserts and a harder EN24 workpiece to accelerate the tool wear are presented and discussed. The cutting conditions employed followed the tool insert manufacturer's guidelines. For each set of cutting conditions the cutting process was occasionally interrupted to take measurements of the wear types formed. It was then possible to build a picture of the active tool life, and also trace and study the tool wear profile.

10.1. Scope of the Tool Wear Study

The study mainly involved conducting interrupted test cuts at fixed cutting conditions with fresh tool inserts until failure or when wear levels had accumulated at which continued cutting risked catastrophic failure (fracture). Due to the rate of tool wear, test cuts generally lasted less than 10 seconds at the beginning of each test run. As the test progressed, the duration of each test was systematically increased to well over 30 seconds for complete stabilisation of the cutting process to be achieved while at the same time allowing significant tool wear accumulation. Each test cut was interrupted after the prescribed time interval to take measurements of flank, nose and notch wear lengths just after the process parameters of interest had been recorded. Tool wear measurements were made using a tool maker's microscope, and the observations supplemented by scanning electron microscope profiling. As well as collecting chip samples, BUE and other tool features (chipping or fracture) were noted. The obtained data were analysed in order to investigate the effects wear accumulation had on the sensor signals in terms of their sensitivity and repeatability.

10.2. Range of Cutting Conditions Investigated

Using the tool insert manufacturer's guidelines, a cutting range was selected based on the insert type and the ensuing cutting parameters chosen accordingly. This involved reading the maximum and minimum values of the feed-rate and DOC values off the ISO chart that corresponded to the chosen tool inserts. For the tool selected, the recommended values were as follows: feed-rates, 0.05 mm/rev to 0.4 mm/rev while DOC varied from 0.2 mm to 4 mm. Cutting speed was selected based on the toughness of the workpiece to be machined. The recommended cutting conditions for the workpiece-tooling geometry configuration was as follows: feed-rate of 0.25 mm/rev; DOC of 1.25 mm, and cutting speed of 273m/min.

A decision was made to conducted the wear tests at a fixed DOC of 2 mm in order to minimise notch wear and also because DOC increments resulted only in a proportional increase in the magnitude of the process parameters. The test cuts will be conducted within the following conditions (though not exhaustively):

- Cutting speeds: 275 m/min., 300 m/min., 350 m/min. (so as to achieve significant various wear modes on the cutting tool within a short time since high cutting speeds lead to high temperatures) , and

- Feed-rates: 0.1 mm/rev, 0.2 mm/rev and 0.3 mm/rev (machine pre-set).

The two tool insert types used were both coated via chemical vapour deposition. P15 has a thick wear resistant coating on a hard resistant substrate. The inner coating is of 8 μm thickness comprising 6 μm thick of aluminum oxide (Al_2O_3)on top. The outer layer is thinner and of titanium nitride (TiN). This combination gives P15 excellent wear resistant properties. On the other hand, P25 has a thick (≈ 10μm) layer of Al_2O_3 on top of a medium size titanium carbon nitride (TiCN). This combination gives P25 a high wear resistance and good edge security (AB Sandvik, 1995).

10.3. P25 Insert Results

Results are shown in Table 10.1. Inspection of the obtained results showed that significant changes occurred in the measured parameters as the wear length on the cutting face increased. Increased feed-rate at constant speed decreases tool life by increasing burn-out activity. The same is true for cutting speed changes at constant feed-rate, though more significant in terms of active tool life. DOC was not investigated for reasons outlined earlier.

In total, 7 tests were conducted:

- constant speed (300 m/min.) and three feed-rates (0.1 mm/rev, 0.2 mm/rev and 0.3 mm/rev),
- constant speed (275 m/min.) and two feed-rates (0.1 mm/rev and 0.3 mm/rev).
- constant speed (350 m/min.) and two feed-rates (0.1 mm/rev and 0.3 mm/rev)

Plots of wear (nose, flank and notch) vs. time (Figures 10.1 - 10.5) were produced together with static force (Figures 10.6 - 10.10), STP dynamic force (Figures 10.11 - 10.15), and STP acceleration (Figures 10.16 - 10.20) relationship with flank wear. Dynamic force and acceleration spectra were produced as well as contour plots (Figures 10.21 - 10.64).

10.3.1. Time Domain Analyses

The wear-time plots mainly served to highlight the effective wear rate at the prescribed cutting speed and feed-rate. At low feed-rates, generally the tool wore much gradually than at higher feed rates. Inspection of the wear-time plots show that it is possible to capture the three phases of tool wear (primary, secondary and tertiary) but only at low feed-rates regardless of cutting speed. In terms of tool

life (longevity), the tool lasted longer at low cutting speeds and the wear phases were more visible and pronounced (Figure 10.4 cf. Figure 10.1, and Figure 10.3 cf. Figure 10.5). On nearly all the plots, the most noticeable indicator of imminent tool failure was the sudden escalation of nose wear to failure. Typically, when the nose wear was higher than 0.2 mm, one ran the risk of catastrophic failure. This level of wear was also found to be an applicable safety threshold for the flank wear length. Notch wear on the other hand increased steadily in the early part of the tests, then remained practically the same for the remainder of tool life.

10.3.1.1. Progressive Wear Interpretation via Static Force Plots

The table of results show that the static force generally increased, albeit slightly, as the wear on the cutting tool face increased, for both increases in feed-rate and cutting speed. A closer inspection of the obtain figures for the static force-flank wear relationship reveals a variable but increasing trend in all three axes (Figures 10.6 - 10.10). Figure 10.6 shows that beyond a flank wear length of 0.15 mm, the cutting forces increased by nearly 200%. However, these increases vary in both axes, with the x- and y-directions showing most change. This trend was observed in all the five depicted curves except in Figure 10.9 where sufficient wear had not accumulated.

10.3.1.2. Progressive Wear Interpretation using STP plots

- Dynamic Forces: Generally, at low feed-rates, the initial trend was upwards (Figure 10.11) and then fell when a flank wear length of 0.2 mm was exceeded (Figure 10.14). The other figures tended to depict a rather undulating behaviour, for which interpretation was difficult and frequency analysis required.

- Vibration Signatures: With increases in flank wear, the acceleration power increased, peaking at a flank wear length of 0.2 mm before falling. This trend

was most noticeable when cutting at high speed and feed-rate (Figures 10.16 - 10.20). Clear and meaningful observation can be made by examining the spectra plots, which is the focus of the next section.

10.3.2. Frequency Analysis

Frequency analysis involved performing a forward FFT on the data, and the results interpreted through two media: spectra and contour plots. With spectra plots, it is possible to visualise any significant amplitude variations and their corresponding frequencies, whereas the overall frequency bands were better viewed on a contour plot.

10.3.2.1. Dynamic Forces

Spectra Plots: Inspection of the spectra plots (Figures 10.21 - 10.29) showed that there were three principal frequency bands that could be associated with wear accumulation. Inspection of the x-axis spectra showed peaks at 300 Hz, 1500 Hz, 3-4 KHz and 10 KHz. The 3-4 KHz frequency peak was the most sensitive to wear levels which coincided with the dynamometer resonant frequency. This main peak remained constant for the first three wear values (primary wear) showing minor signs of oscillation with rapid increase in flank and nose wear. Once the wear values either reached or passed 0.1 mm, wear increased gradually with the contact area staying relatively the same. The increase in peak value beyond the 4th test run could be attributed to an increase in flank wear. The increase in peak height was not proportional to either the flank or nose wear value. Thus, the sensitive peak initially rises with wear accruement, then when beyond and into the tertiary wear zone, the peak falls as more damping occurs.

These observations were more pronounced on the low feed plots (0.1 mm/rev) and less so at high feeds (0.3 mm/rev). The dramatic rise in the 10 KHz peak towards tool failure reflected the rapid increase in the nose and flank wear values which in most instances coincided with tool chipping.

Contour Plots: Inspection of these plots (Figures 10.41 - 10.54)showed that three main peak frequencies were dominant. At low feed, the x-axis plot had peaks at 500 Hz, 1.5-2 KHz and 3.5-4 KHz frequency bands. On the y- and z-plots, the main energy concentrated in the 2-3 KHz frequency band with a slight energy concentration also appearing at ≈ 11 KHz. Increases in the feed-rate caused the spectra to become dispersed with the low frequency band disappearing.

10.3.2.2. Vibration Signals

Spectra Plots: Unlike the dynamic force spectra, the vibration spectra (Figures 10.30 - 10.40) had only two main peak frequency bands: a 2-4 KHz (the fundamental resonant frequency of the tool holder) and a 9-11 KHz band (chip lamination frequency). Inspection of the plots revealed the z-axis plots to be the most sensitive to wear accruements. The 2-4 KHz band increased steadily, peaking before falling to reach tool failure. Meanwhile the 9-11 KHz peak increased as wear accumulated with the last spectrum showing the largest increases. Increases in the feed-rate led to a proportional increase in the magnitude of both peaks, indicating the same trend as with low feeds. However, at high feed-rates, the spectra were more noisy and had a wider frequency band. Comparison of spectra depicting cutting at different cutting speed showed that increasing the cutting speed actually decreased the amplitudes of the resonant peak.

Contour Plots: These plots (Figures 10.55 - 10.64) clarified observations made from the spectra plots, i.e. that there existed two principal frequency peaks; a low band ≈3 KHz and a higher and larger energy concentration band at 10-12 KHz. No effects of tool wear were visible, but feed-rate and cutting speed increases tended to generally increase the energy and noisy nature of the contour. For example, increasing the cutting speed from 275 m/min. to 300 m/min. introduced a low band spectra at 2.5 KHz-3 KHz on the z-vibration at 0.1 mm/rev feed rate.

At high feed-rates, these merely became sharp with smaller bandwidths corresponding to higher cutting speeds.

10.3.3. Summary of Observation

From the results obtained, the following sensitivity summary table has been produced:

Using Static Cutting Forces:

	Cutting Force Direction		
Criteria	X	Y	Z
Sensitivity to Flank wear	3	3	2
Sensitivity to Nose wear	2	3	1
Total Response	**5**	**6**	3

Using Dynamic Force Spectra:

Criteria	X	Y	Z
Sensitivity to Flank wear	2	2	3
Sensitivity to Nose wear	2	3	2
Total Response	4	**5**	**5**

Using Vibration Spectra:

Criteria	X	Y	Z
Sensitivity to Flank wear	2	2	3
Sensitivity to Nose wear	2	3	3
Total Response	4	**5**	**6**

These summary tables show that nose and flank wear gave a far more coherent indication of tool wear. Major flank face notch wear rose as cutting increased, but once it reached a certain value, it stayed the same until the tool failed. In terms of the three wear phases, obtained notch wear values did not support the view that it had three distinct phases.

10.4. P15 Insert Results

10.4.1. Time domain Analysis

Experimental results for these tests are shown in Table 10.2. Three sets of tests were conducted for this investigation at variable cutting speed and feed-rate viz.: cutting speed (300 m/min) and feed-rates (0.1 mm/rev and 0.3 mm/rev), and cutting speed (275 m/min) and feed-rate (0.3 mm/rev). Inspection of the three plots reveal that the low feed wear-time plot (300 m/min and 0.1 mm/rev) gave a better indication of the tool life. After 100 seconds of active tool cutting a very sharp rise was followed by two further rises. Although this observation was present on the (275m/min. and 0.3 mm/rev) curve, it was not as pronounced as at low feeds (Figures 10.65- 10.67). The flank and nose wear types, as with the P25 insert, seem to be better indicators of tool wear/life than the notch wear.

Inspection of the static force-flank wear relationship (Figures 10.68 - 10.70) showed an upward tendency as flank wear increased. This trend was well pronounced especially at high feed-rates. At low feed-rates, the cutting forces increased steadily but undulated, and as flank wear length increased beyond 0.2 mm, they began to decline. Increasing the cutting speed led to magnitude increments in the forces, especially at higher wear values.

The STP dynamic force-flank wear plots (Figures 10.71 - 10.73) at low feed-rates show that the forces either remained constant (x-axis) or increased up to about 30% in magnitude as flank wear length increased (representing 160 seconds of tool life to 220 seconds at the end of tool life). Increasing the feed-rate led to a more linear plot with higher magnitudes at low wear (flank wear length < 0.1 mm) and the same magnitude beyond, regardless of wear length. When the cutting speed was decreased, the STP initially fell to reach a steady and constant value.

The STP acceleration plot against flank wear length (Figures 10.74 - 10.76), overall at low feed-rates increased as wear length increased (y and z) while the x-plot showed a fall. When the feed-rate was increased (from 0.1 mm/rev to 0.3 mm/rev) the x- and y-curves remained constant but rose slightly when the wear length exceeded 0.3 mm. At this stage, the z-value which was almost 300% higher in magnitude compared to the x- and y-values (300 g) began to show a downward trend. Increasing the feed-rate led to a proportional increase in the STP acceleration ratios (i.e. at 0.1 mm/rev and 300 m/min., the maximum value of the z-axis STP acceleration was 190g and jumped to 180g when the feed-rate was increased to 0.3 mm/rev, representing a 400% increase). Cutting speed effects were less prominent. At a low cutting speed (275 m/min), the STP acceleration decreased (z- and y-directions) until the wear reached 0.1 mm, and remained constant. The x-axis did not change until a flank wear length of 0.25 mm, at which the constant value fell suddenly.

10.4.2. Frequency Analysis

10.4.2.1. Dynamic Forces

Inspection of the spectra plots of dynamic force (Figures 10.77 - 10.87) showed that most of the energy in the spectra tended to concentrate below 4 KHz, from which three distinct bands could be identified on both the x and y-axes: 500 Hz, 1500 Hz and 2-3.5 KHz. The z-axis plots had one main dominant peak at 2.5 KHz and a small one at 10 KHz, whose magnitude changed with both wear accruement and process parameter increases. The 2-3 KHz peak seemed to undulate with its bandwidth increasing as wear length increased, thus becoming less sharp. At the same time, the 10 KHz peak's magnitude increased gradually as wear land length increased.

Closer inspection of the x- and y-spectra at low feed-rates showed that the 500 Hz peak increased proportionally to the tool wear rate, reaching a maximum peak at the fifth cut before gradually dampening. Changes in the feed-rate seem to affect only the sharper two frequency band peaks at 2-3 KHz and 10 KHz the fundamental resonance frequency of the tool holder and chip lamination frequency respectively.

A glance at the contour plots of the dynamic forces (Figures 10.96 - 10.102) confirmed the observation from the spectra plots that there were principally two peak frequencies in the x-axis (at low feed-rate) at 500 Hz and 3.5 KHz. In the y-axis, the high frequency component dropped to 2.5 KHz while the 500 Hz peak completely disappeared in the z-axis to leave only the 2.5 KHz peak. The contour plots also reveal that feed-rate increases led to dispersion of the spectra energy, especially in the 2.5-4 KHz bandwidth region. Cutting speed changes (decrease) led to a reduction in the spectra intensity at peak frequencies.

10.4.2.2. Vibration signal

The vibration spectra plots (Figures 10.88 - 10.95) generally were more noisy than those from the P25 insert (coating effect). Three main peaks again were clearly visible in all three axes: 1-1.5 KHz, 3-5 KHz and the 10 KHz bands, though, with significant variations from one another. In the x-direction, the 1.5 KHz peak had a large bandwidth which decreased as wear length increased. No significant changes occurred on the y-axis spectra. On the z-axis, the most significant change was on the 10 KHz peak. This increased considerably as the wear length increased and fell as the tool entered its tertiary wear phase. Increases in the feed-rate led to a widening of the bandwidth which further increased as the wear length increased. Cutting speed changes did not appear to have any significant effect on the spectra plots.

The contour plots (Figures 10.103 - 10.108) show that except for the z-axis plots, the y and x-plots at low and high feed-rates were scattered, covering a wide bandwidth. The z-axis had its clearest and sharpest concentration at 10 KHz. No other significant features were immediately visible.

10.5. Summary of Observation

The study undertaken showed that flank wear and nose wear were better indicators of tool wear than notch wear. A sensitivity matrix was constructed, loosely based on observations on a single set of cutting conditions. Again numbers were allocated as follows: 3 = Excellent indicator (most sensitive), 2- Good indicator and 1- bad indicator (least sensitive), and the outcome is shown in Table 10.3.

From inspection of the sensitivity matrix, it is evident that all five process parameters show some sensitivity to tool wear. Considering the combined total score for each signal component and each insert type, static force components were less sensitive to tool wear, while the STP dynamic and vibration components

were more sensitive. Additionally, test results also confirmed that these process parameters were sensitive to cutting conditions (cutting speed and feed-rate). In terms of the individual axes, the z-axis cutting direction was the most sensitive in all five cases and the x-axis was generally the least sensitive. Both tool inserts show slight differences in terms of their active tool life due to their hot hardness.

10.6 Discussion of Results

Based on measurements and analysis of the process it has been possible to identify the trend of sensor signals as the tool insert wear length increased. The determined characteristics tended to show that the sensor signals were affected by the different wear modes as well. The magnitudes of the static cutting forces were overwhelmingly dependent on the cutting conditions especially the DOC and feed-rate.

Because of the complex and stochastic nature of the cutting process, identification of actual tool condition is difficult but not impossible. During the experimental stages of the wear progression studies, it was noted that some tool inserts failed at considerably small flank wear lengths. The most likely explanation to account for these failures were partly attributed to what might be called 'Thermally Induced Premature Failure Mechanism' (Shi and Ramalingan, 1990). A common characteristics to these occurrences was that a majority of the failures tended to occur at high cutting speeds (i.e. 350 m/min). A possible shortcoming in these investigations was the relative difficulty to accurately measure the flank, nose and notch wear lengths especially when they were irregular. The reported wear values are therefore prone to error. It should be remembered that quoted wear values would be expected to deviate from the true or ideal values due to the element of subjectivity. Owing to the irregularity of the major flank wear region, the maximum flank wear length (V_BMax) was used as the standard measure of flank wear length. This was because at certain levels of wear accumulation, the previously uniform wear cross-section region (at low flank land length) suddenly

became non-uniform and accurate measurements was impossible. In almost all the tests conducted, it was found that, the end of tool life was indicated by the sudden escalation of both the flank and nose wear land lengths. These usually were accompanied by large scale increases and fluctuations in the magnitude of the static cutting forces that is attributed to bulk deformation brought about by mechanical and thermal effects (Lister, 1993).

Generally, when cutting took place at low feed-rates, the static cutting forces decreased very slightly as cutting time progressed due to increased wear levels. The decreasing static cutting forces approached a stationary value which was found to be dependent upon the amount of flank and nose wear present, and also on the nature of the tooling material. This behaviour was rather more difficult to ascertain with the P15 insert than with the P25. Principally, a noticeable difference in the two insert types was the occurrence of the so called BUE effect. While considerable BUE occurred in the P25, little or no BUE occurred when machining with the P15 insert regardless of cutting speed, feed-rate or wear levels. A common occurrence to both insert types was the fact that beyond the stationary wear value, nose wear was found to rise at a faster rate than flank wear land length. This seems to suggest that catastrophic tool failure occurred largely at the tool nose, and nose wear perhaps was a better indicator of end of tool life. Chipping of the cutting edge often accompanied such dramatic rise in nose wear length. Oraby and Hayhurst (1991) attributed tool failure as actually originating at the nose area then triggering failure from either the flank or notch areas. Observations from these experiments seem to concur with that view, but only in so far as nose and flank wear were concerned. No evidence was found that would seem to suggest that tool failure might have been triggered by flank face notch wear. Under such circumstances, it would be possible to use nose wear to signal the end of tool life and its imminent replacement. A practical approach would be to track both flank and nose wear levels and know exactly which wear regime the tool was in (i.e. its wear phase). Then the rise in nose wear would signal the approach of the catastrophic failure region and therefore, an ideal time to replace

the tool insert. The limitations of using static forces alone include disturbances on their magnitude arising from variations in the workpiece material, DOC, feed-rate and possibly tool edge geometry. In practical applications such as a TCMS, it is prudent to supplement tool wear information by using signals from other sources particularly those that indicate the dynamic characteristics of the cutting process. The primary motive for this suggestion hinges on the fact that the aforementioned variations can result in the static forces magnitudes changing in the same order as those due to tool wear effects. It was therefore thought necessary to examine the nature of both kinematics describing quantities viz.: the dynamic cutting forces spectra and the vibration signatures spectra and their correlation to wear levels assessed.

Methods for evaluating vibration signature and dynamic cutting forces signals involved the transformation of the measured signals from time to frequency domain by FFT. Through this method, one was able to view properties or characteristic information of the cutting process. Since tool wear features on the signals were of prime importance, the analysed and presented spectra began with those describing the tool characteristics at first contact (i.e. when tool was new and therefore sharp) and ended with those spectra describing the severely worn tool characteristics (or the occasional chipping/failure modes). From the spectra obtained, it was possible to establish the distinct differences in signal characteristics when cutting was performed with a new insert to that which had accrued a detrimental level of wear. The characteristic rise in amplitude of the fundamental resonance frequency peak of the dynamic force signal was attributed to the cyclical stick-slip effect in the contact area. The physics of this effect is due mainly to the fact that when the tool is sharp (i.e. new), the sharp edges minimise contact between the tool and workpiece. This results in small movements, hence small dynamic forces indicated on the spectra by peak magnitudes at the resonant frequency on the spectra. Increasing wear levels led to an increase in the contact area due to crumbled cutting edges. The transition of friction from static to sliding generates high signal pulses that contribute to increasing the magnitude of

the fundamental resonant peak as well as appearing as secondary peaks around the 10 KHz band region. Beyond a certain flank wear value, the fundamental frequency peak begins to dampen as the contact area increases monotonically, partly due to increased contact friction and thereof plastic deformation and the development of accelerated nose wear. It could therefore be argued that the occurrence of monotonic nose wear causes the resonant peak magnitude to decrease. Inspection of the chips formed indicated that the high burst was due to increases in the lamination frequency (from >1KHz to around 10 KHz) arising from the change in deformation behaviour of the material in the shear zone. A theoretical base for the decline in resonant frequency peak amplitude when the tool was severely worn could be due to an increase in the rake angle from the rubbing effect of the deformed chip (Lee *et al.*, 1992; 1989).

Since the dynamic force and vibration signature consist mainly of a combination of stochastic, periodic and superposed harmonic signals (Warnecke *et al.*, 1990), a method of observation that combines both aspects of signal and process behaviour was desired. The computation of the sum total power contained in each sampled signal by adding up all the FFT points seemed the best, logical, and most appropriate approach. This approach delivered the probability that the most significant properties affected by the accruement of wear on the tool surface was inclusive in the analysed signal.

Based on the analyses performed and interpretations of features on the presented graphs, selection of the sensor signals has been justified. The cutting conditions, self-evidently would be incorporated into the input vector set for reasons already outlined.

The analysed data was used as input data to a neural network paradigm, and that exercise sought to use the capability of ANNs in distinguishing tool state. The procedure, results and discussion are outlined in the next chapter.

Table 10.1: Experimental results from P25 test cuts

		Wear (mm)			Static Forces			Dynamic Forces			Vibration (g)		
Test No.	Time (s)	Notch	Nose	Flank	x	y	z	x	y	z	x	y	z
V= 300 & f=0.1													
A1	5	0.05	0.01	0.02	301	165	389	87	114	146	79	54	109
A2	12	0.09	0.03	0.05	303	163	384	68	103	129	78	53	99
A3	17	0.11	0.05	0.07	305	167	390	72	96	118	74	53	100
A4	26	0.13	0.06	0.08	306	169	400	75	111	139	75	53	117
A5	34	0.14	0.08	0.1	316	172	433	78	109	136	92	59	113
A6	47	0.15	0.09	0.11	333	180	431	88	128	161	91	66	129
A7	64	0.15	0.1	0.12	332	180	400	82	115	152	74	54	110
A8	82	0.16	0.15	0.13	339	197	385	96	136	174	85	62	122
A9	113	0.16	0.18	0.14	364	208	399	106	125	164	90	65	127
A10	135	0.16	0.2	0.16	374	202	453	111	136	169	90	64	123
A11	155	0.16	0.3	0.21	722	447	520	145	173	245	122	92	205
V=300 & f=0.2													
A12	5	0.05	0.02	0.04	343	186	626	147	220	295	127	97	226
A13	12	0.07	0.05	0.06	346	187	636	148	250	311	130	98	229
A14	22	0.09	0.07	0.07	349	183	617	128	218	273	118	92	216
A15	34	0.11	0.08	0 1	356	190	624	126	221	252	138	99	239
A16	47	0.14	0.11	0.13	384	199	684	137	236	284	153	108	254
A17	66	0.16	0.13	0.15	428	223	668	153	249	310	154	115	267
A18	79	0.17	0.16	0.17	449	248	680	170	263	333	159	108	272
A19	95	0.17	0.18	0.19	501	286	675	173	281	357	144	105	260
A20	103	0.17	0.21	0.2	550	318	657	168	270	339	146	100	245
A21	115	0.17	0.35	0.22	771	536	727	181	277	333	167	108	276
V=300 & f=0.3													
A22	8	0.04	0.02	0.03	435	238	988	378	606	784	344	228	642
A23	21	0.1	0.08	0.12	468	259	999	316	637	749	293	212	571
A24	32	0.11	0.14	0.15	538	304	1038	333	667	790	325	218	597
A25	50	0.15	0.15	0.16	602	370	1096	359	738	831	352	238	651
A26	62	0.17	0.22	0.18	608	431	1037	333	600	733	367	230	640
A27	73	0.17	0.24	0.19	649	530	1073	352	623	757	368	244	667
A28	83	0.17	0.4	0.2	790	1211	1172	364	633	833	408	278	748
V=275 & f=0.1													
A29	9	0.03	0.01	0.02	295	169	435	90	138	162	102	59	126
A30	17	0.06	0.03	0.05	296	169	443	89	135	160	100	64	126
A31	29	0.09	0.07	0.08	297	166	446	82	128	150	97	60	126
A32	42	0.1	0.09	0 09	291	171	435	90	134	165	104	71	141
A33	56	0.11	0.1	0 1	301	176	430	101	141	183	107	68	138
A34	75	0.12	0.11	0.11	302	172	439	98	141	170	114	69	143
A35	100	0.13	0.13	0.12	297	175	441	108	145	170	91	64	136
A36	123	0.14	0.13	0.13	297	169	442	114	160	210	93	69	141
A37	159	0.15	0.14	0.14	301	176	439	120	175	214	100	70	146
A38	181	0.16	0.16	0.15	300	172	423	115	149	198	110	66	132
A39	220	0.17	0.17	0.16	307	175	446	119	152	204	117	71	143
A40	253	0.18	0.18	0.17	306	178	460	112	164	211	102	75	158
A41	313	0.2	0.19	0.18	299	170	436	120	163	207	108	77	158
A42	403	0.21	0.2	0.19	298	168	473	126	176	226	117	90	189
A43	479	0.21	0.22	0.21	291	176	452	111	164	215	98	80	173
A44	569	0.21	0.27	0.24	303	169	464	100	167	187	106	79	165
V=275 & f=0.3													
A45	3	0.01	0.04	0.02	439	235	1081	378	595	769	459	259	653
A46	13	0.07	0.06	0.07	461	240	1102	333	605	739	379	240	610
A47	24	0.08	0.1	0.1	493	255	1028	360	679	863	394	260	655
A48	35	0.12	0.12	0.12	504	265	1010	340	632	812	392	254	687
A49	45	0.13	0.13	0.14	538	281	1045	348	632	784	377	260	660
A50	53	0.15	0.14	0.15	551	297	1029	355	631	747	386	263	681
A51	64	0.15	0.15	0.16	576	310	1062	361	670	821	429	283	750
A52	76	0.15	0.16	0.17	613	347	1051	378	704	894	414	274	746
A53	98	0.15	0.17	0.18	643	385	1078	358	676	838	433	275	737
A54	119	0.15	0.18	0.19	670	422	1067	346	669	835	403	257	677
A55	139	0.15	0.2	0.2	662	428	1060	342	653	810	407	262	681
A56	157	0.15	0.23	0.22	683	465	1095	377	728	892	444	267	746
A57	192	0.15	0.37	0.3	832	823	1179	392	689	907	506	278	776

Table 10.2: Experimental results from P15 test cuts

Test No.	Tims	Wear Form (mm)			Static Force (N)			STP Dynamic Force (N)			STP Acceleration (g)		
	(s)	Notch	Nose	Flank	X	Y	Z	X	Y	Z	X	Y	Z
B1	13	0.04	0.03	0.05	352	188	423	105	143	160	94	64	126
B2	28	0.06	0.06	0.07	348	182	436	83	121	139	73	56	121
B3	46	0.07	0.07	0.09	362	197	453	117	162	186	90	64	149
B4	64	0.08	0.09	0.1	362	201	448	108	152	184	96	66	137
B5	101	0.09	0.1	0.11	370	210	458	103	143	171	108	65	133
B6	134	0.1	0.1	0.12	383	208	446	114	156	182	105	73	144
B7	167	0.11	0.1	0.13	375	209	471	114	154	179	104	67	125
B8	212	0.12	0.1	0.14	401	232	498	106	161	178	92	69	136
B9	274	0.12	0.1	0.15	407	220	464	119	157	179	63	69	146
B10	319	0.12	0.1	0.16	394	207	484	109	142	173	111	68	136
B11	376	0.12	0.1	0.17	392	223	472	106	156	175	91	66	133
B12	425	0.12	0.1	0.18	395	214	504	114	162	176	65	74	164
B13	528	0.12	0.12	0.19	368	195	484	107	165	187	50	75	183
B14	654	0.12	0.13	0.2	354	187	478	110	166	197	99	78	189
B15	775	0.12	0.14	0.21	331	175	459	108	152	186	82	71	179
B16	1006	0.12	0.15	0.22	317	167	432	100	169	196	82	79	171
B17	1113	0.12	0.17	0.24	309	169	428	110	174	200	75	76	175
B17R	1185	0.12	0.18	0.26	319	155	479	119	184	219	87	86	175
V=300 & f=0.3													
B18	9	0.03	0.04	0.06	533	299	1011	451	769	1006	300	319	860
B19	20	0.05	0.08	0.1	557	299	1033	366	635	851	309	264	737
B20	35	0.07	0.11	0.13	591	330	1064	381	716	911	272	267	780
B21	74	0.12	0.16	0.19	723	441	1098	397	729	914	289	293	820
B22	123	0.15	0.17	0.28	951	659	1134	402	709	940	310	289	808
B23	150	0.15	0.25	0.35	1185	953	1240	394	667	865	358	378	735
V=275 & f=0.3													
B24	8	0.04	0.02	0.05	462	249	947	511	698	1058	308	461	838
B25	33	0.06	0.08	0.09	586	283	1111	383	656	863	312	410	760
B26	84	0.08	0.11	0.1	588	310	1013	360	673	814	308	352	666
B27	134	0.12	0 13	0.11	660	350	1078	365	618	753	370	327	608
B28	180	0.13	0.14	0.18	727	401	1024	365	620	783	344	333	653
B29	224	0.15	0.17	0.25	798	450	1058	386	664	802	317	342	685
B30	268	0.15	0 19	0.27	865	493	1124	395	667	805	123	353	673

Table 10.3: Sensitivity matrix of process parameters to tool wear

	x		y		z		
Tool insert Used	P15	P25	P15	P25	P15	P25	Total
Static Forces	1	2	1	2	2	3	11
STP Dynamic Forces	1	2	2	2	3	3	13
STP Acceleration	1	2	2	2	3	3	13
Dynamic Force Spectra	1	1	1	1	2	2	8
Acceleration Spectra	2	1	1	1	2	3	10
Total	6	8	7	8	13	14	

FIGURES

P25 FIGURES

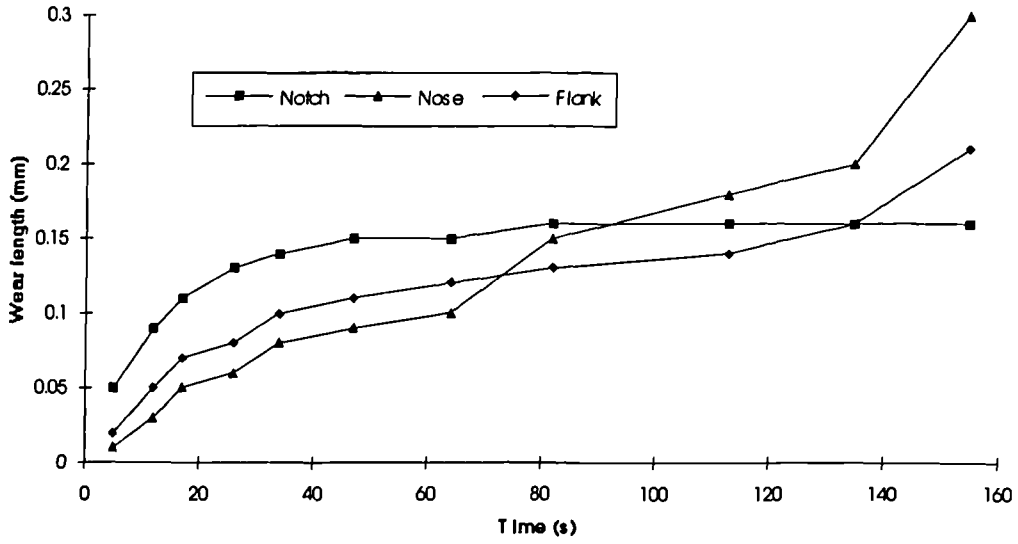

Figure 10.1: Wear-time plot (V=300m/min. & f=0.1mm/rev.)

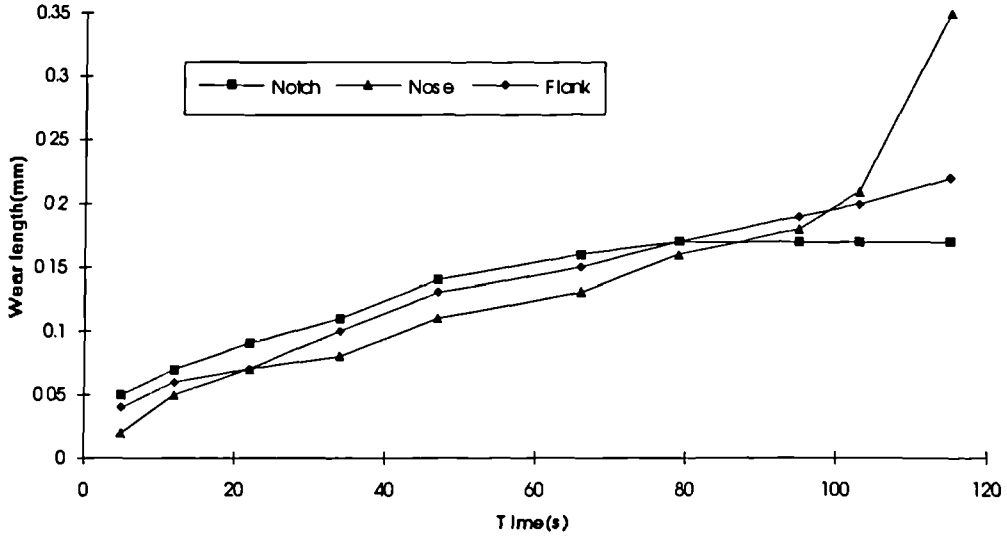

Figure 10.2: Wear-time plot (V=300m/min. & f=0.2mm/rev.)

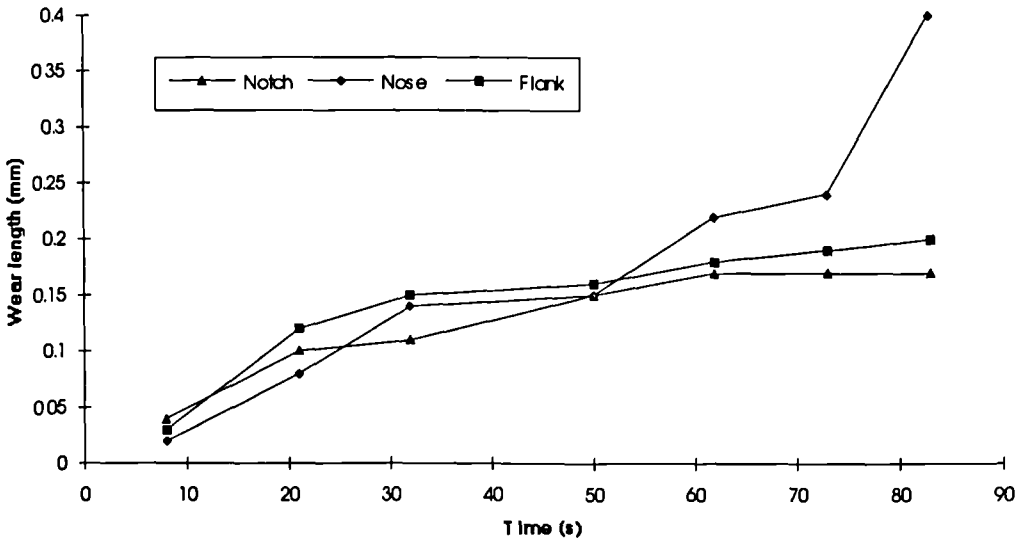

Figure 10.3: Wear-time plot (V=300m/min. & f=0.3mm/rev.)

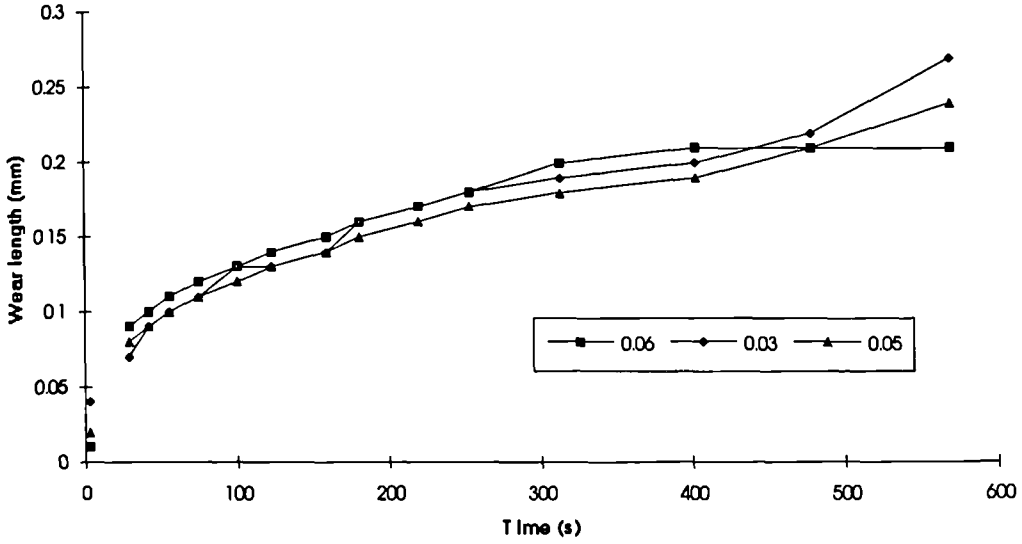

Figure 10.4: Wear-time plot (V=275m/min. & f=0.1mm/rev.)

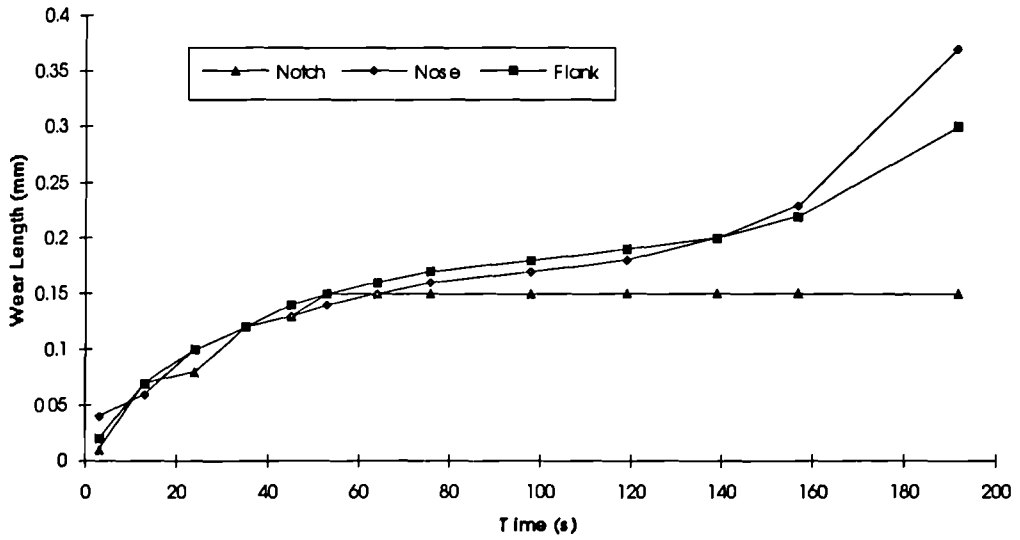

Figure 10.5: Wear-time plot (V=275m/min. f=0.3mm/rev.)

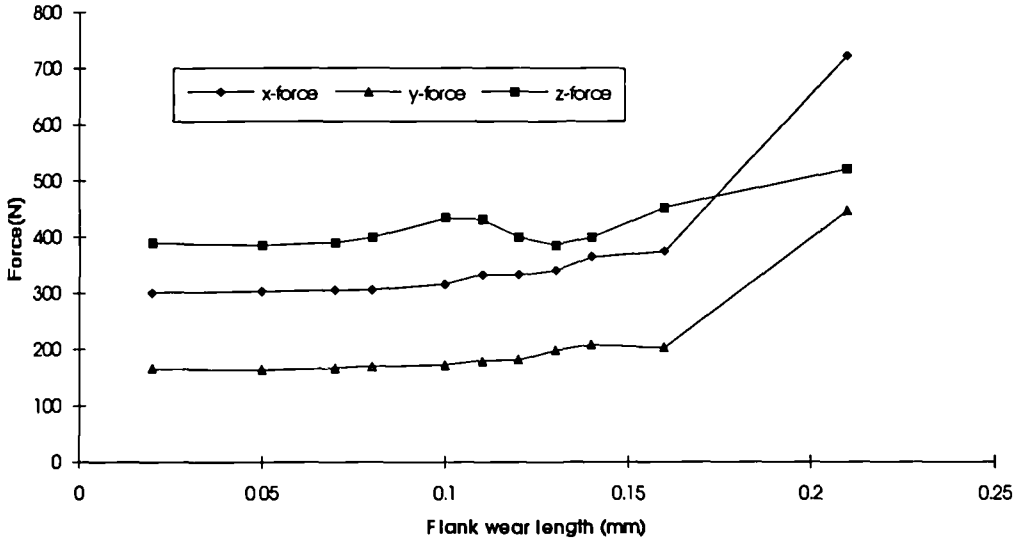

Figure 10.6: Static force-flank wear relationship (V=300m/min. & f=0.1mm/rev.)

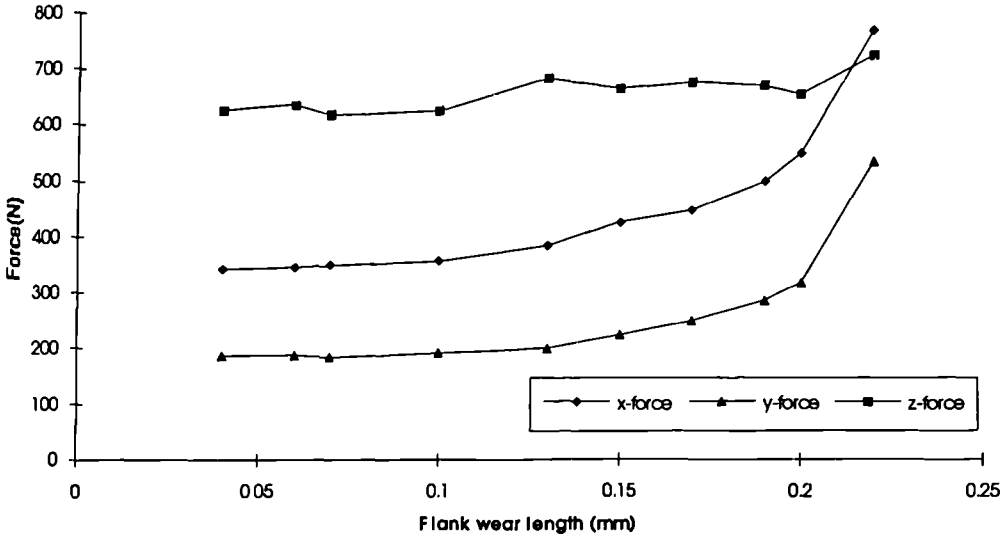

Figure 10.7: Static Forces Vs Flank wear length (V=300m/min. & f=0.2mm/rev.)

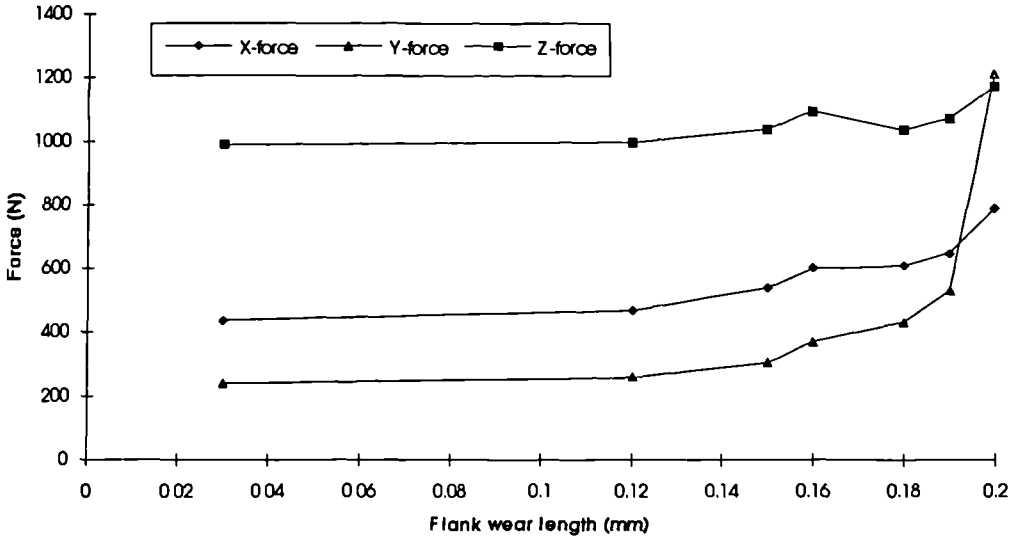

Figure 10.8: Static Forces Vs Flank wear length (V=300m/min. & f=0.3mm/rev.)

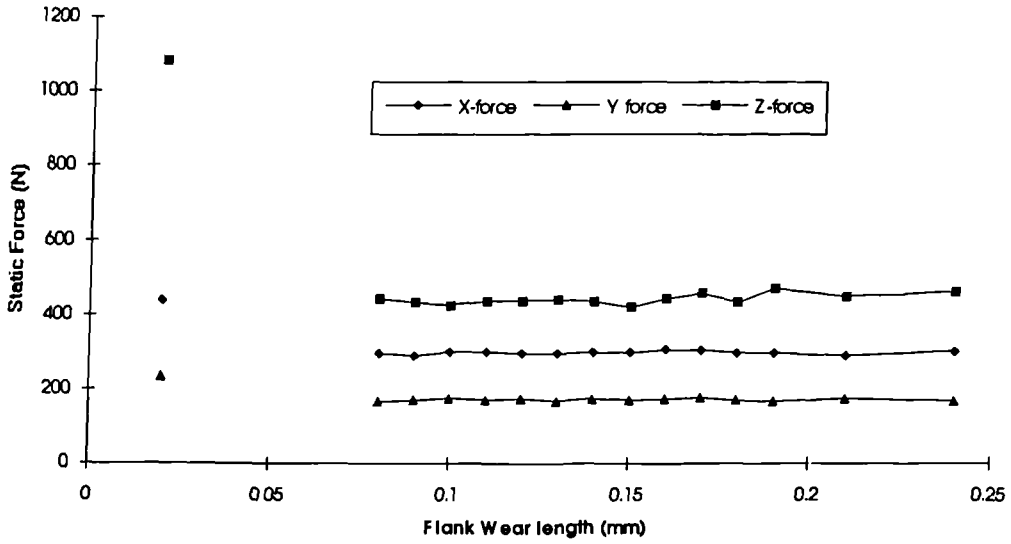

Figure 10.9: Static Forces Vs. Flank Wear (V=275m/min. & f=0.1mm/rev.)

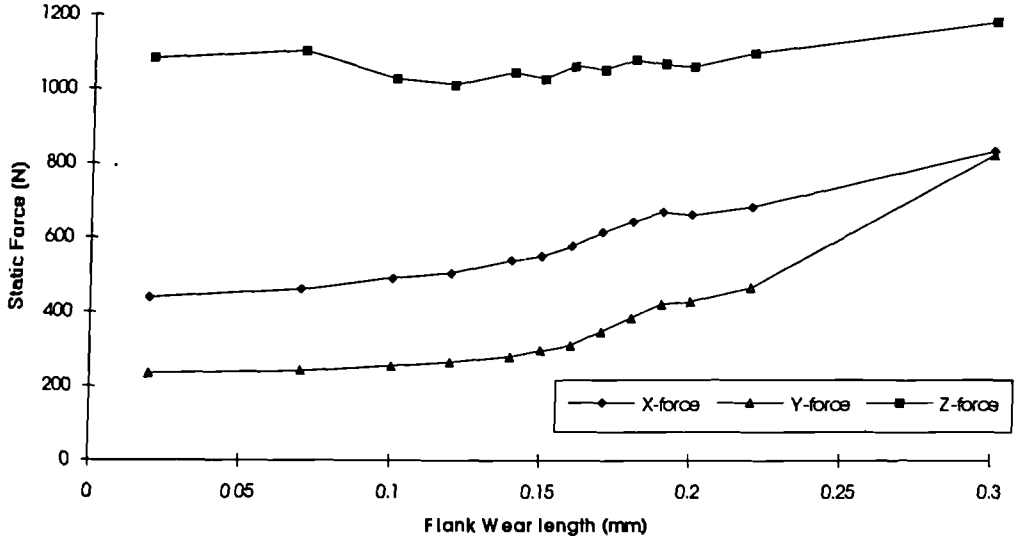

Figure 10.10: Static Forces Vs. Flank Wear Length (V=275m/min. & f=0.3mm/rev.)

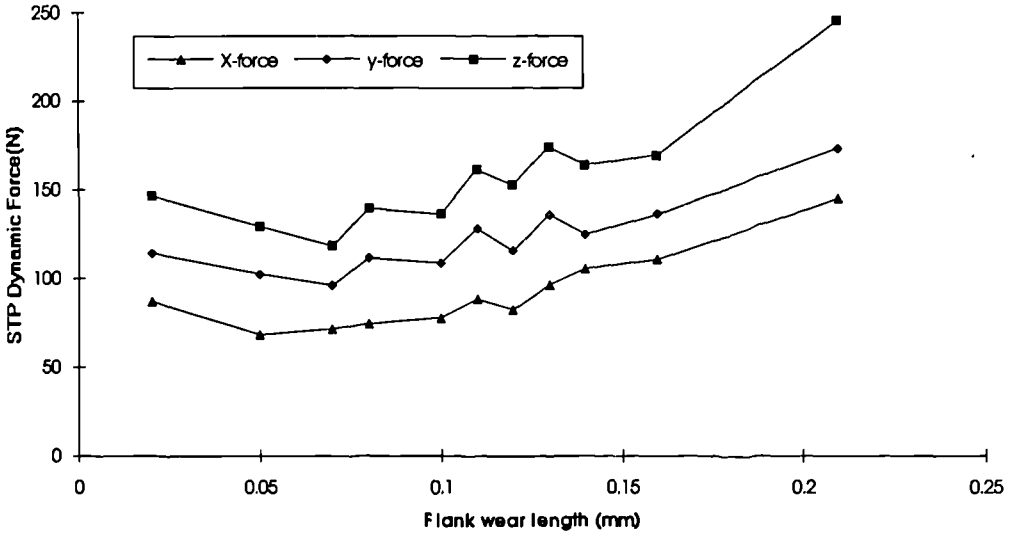

Figure 10.11: STP in Dynamic force spectra Vs Flank wear (V=300m/min. & f=0.1mm/rev.)

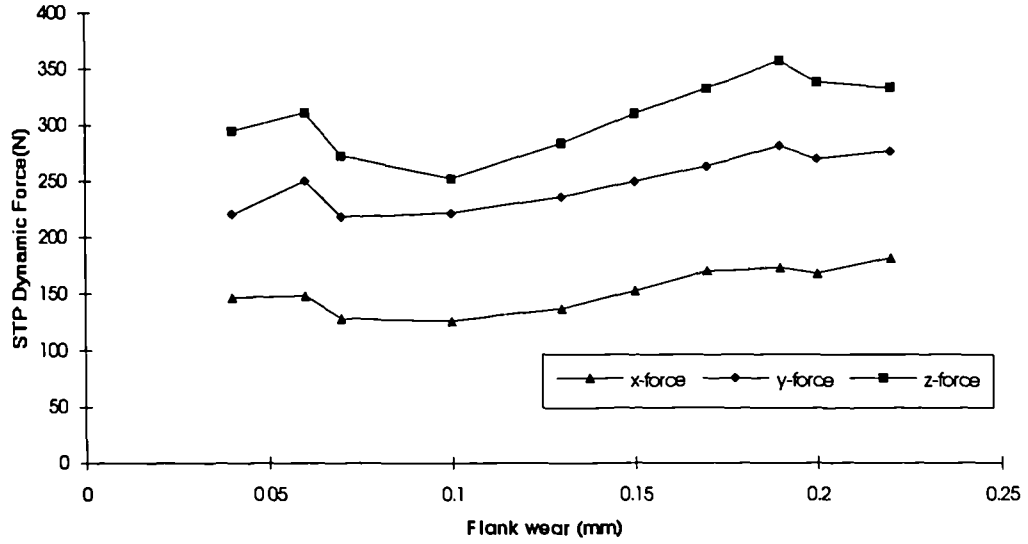

Figure 10.12: STP in Dynamic force spectra Vs Flank wear length (V=300m/min. & f=0.2mm/rev)

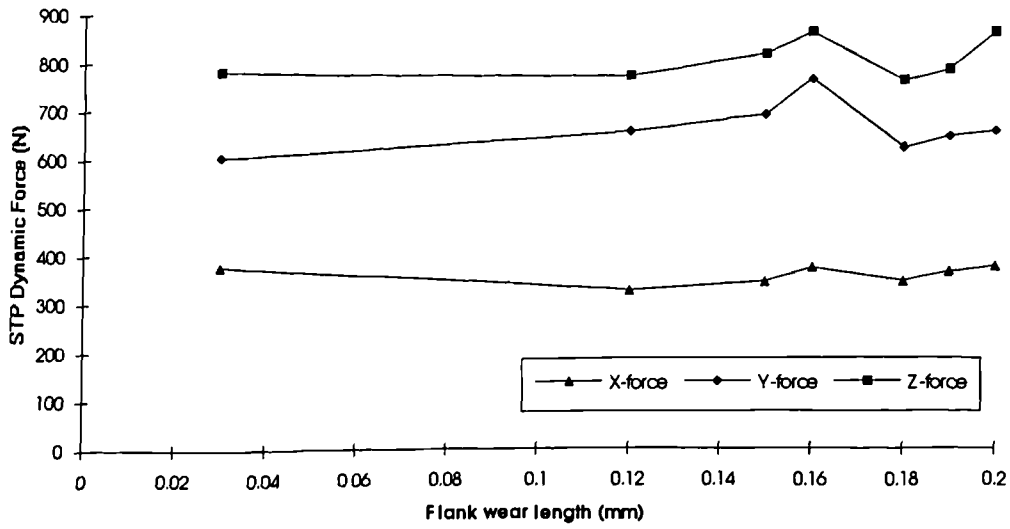

Figure 10.13: STP in Dynamic force spectra Vs. flank wear (V=300m/min. & f=0.3mm/rev.)

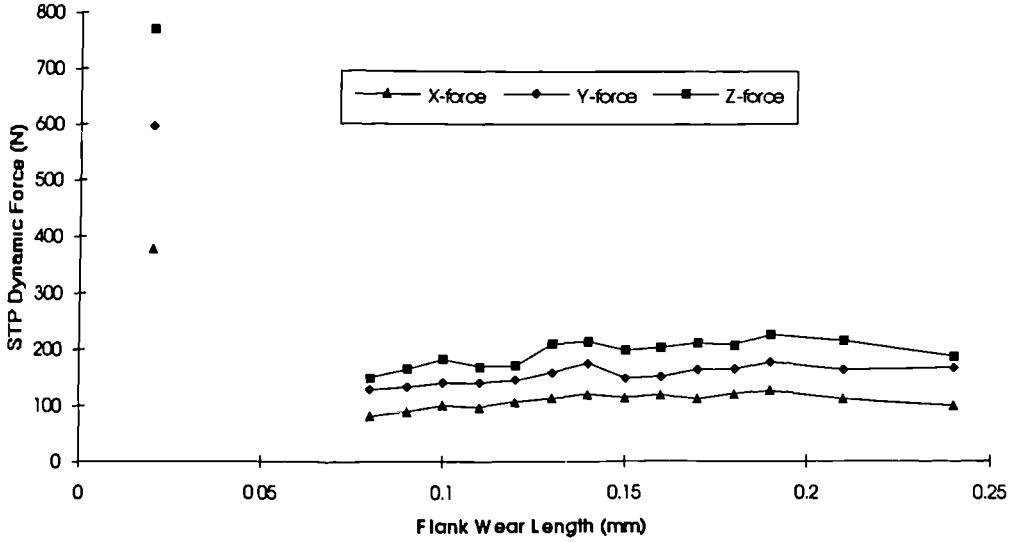

Figure 10.14: STP in Dynamic Force Spectra Vs. Flank Wear (V=275m/min. & f=0.1mm/rev.)

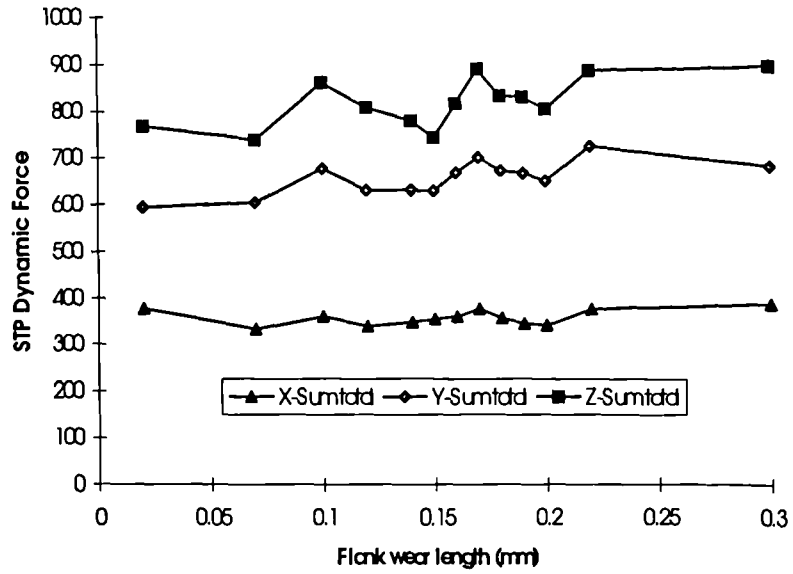

Figure 10.15: STP in Dynamic Force Spectra Vs. Flank Wear (V=275m/min. & f=0.3mm/rev.)

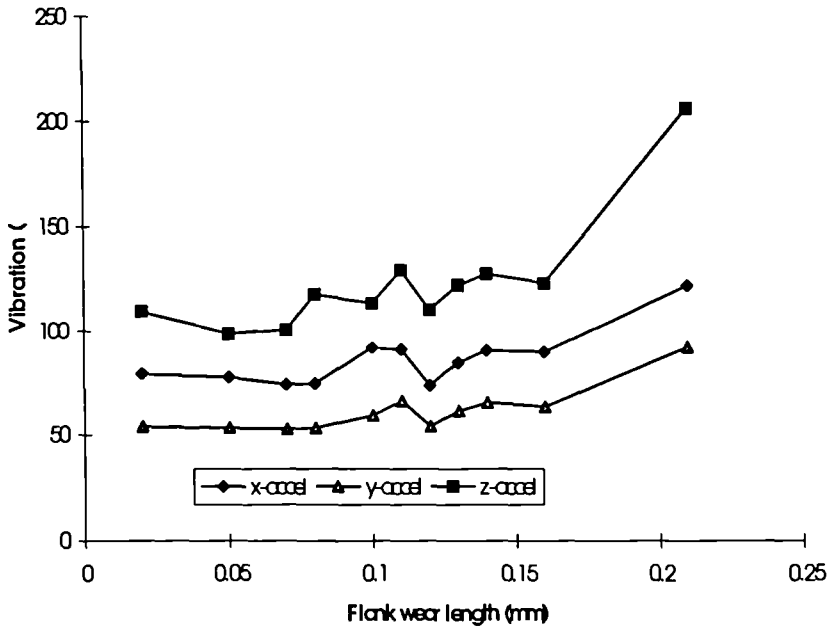

Figure 10.16: STP in Vibration Spectra Vs Flank Wear (V=300m/min. & f=0.1mm/rev.)

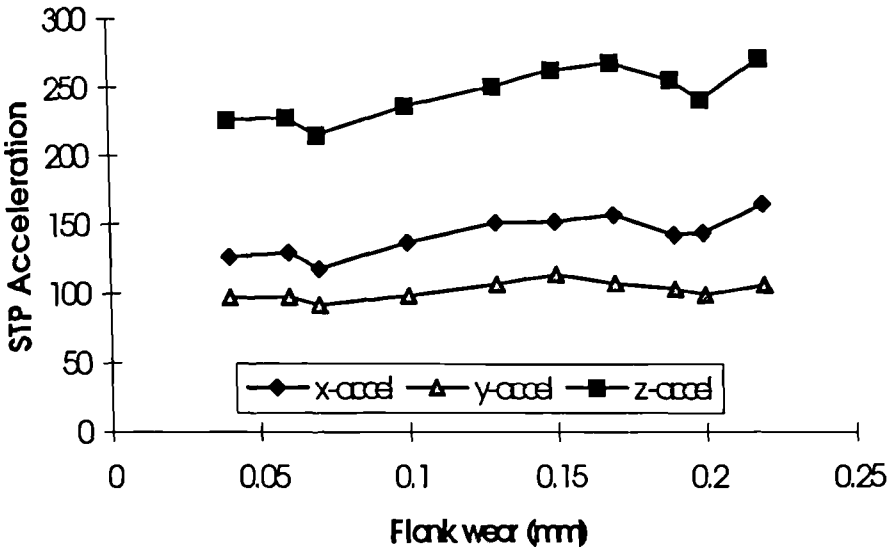

Figure 10.17: STP of Vibration Spectra Vs Flank Wear (V=300m/min. & f=0.2mm/rev)

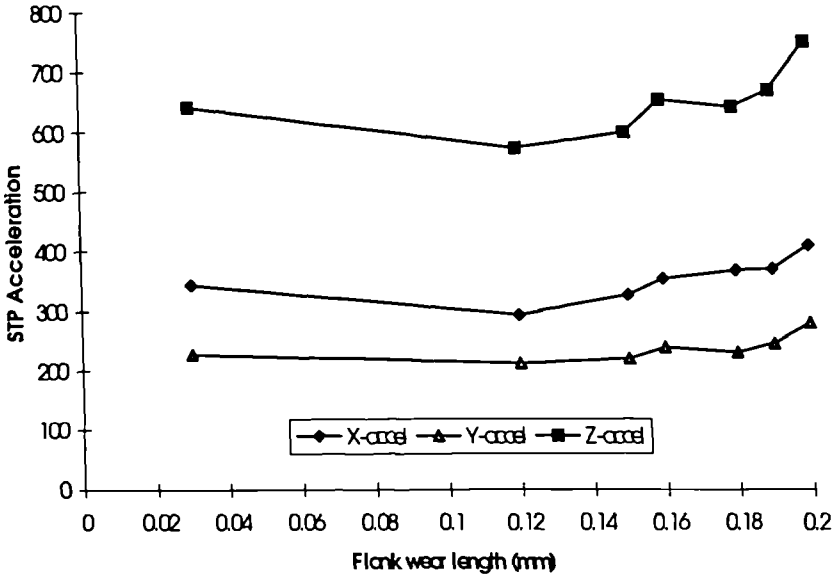

Figure 10.18: STP in Vibration Spectra Vs. Flank Wear (V=300m/min. & f=0.3mm/rev.)

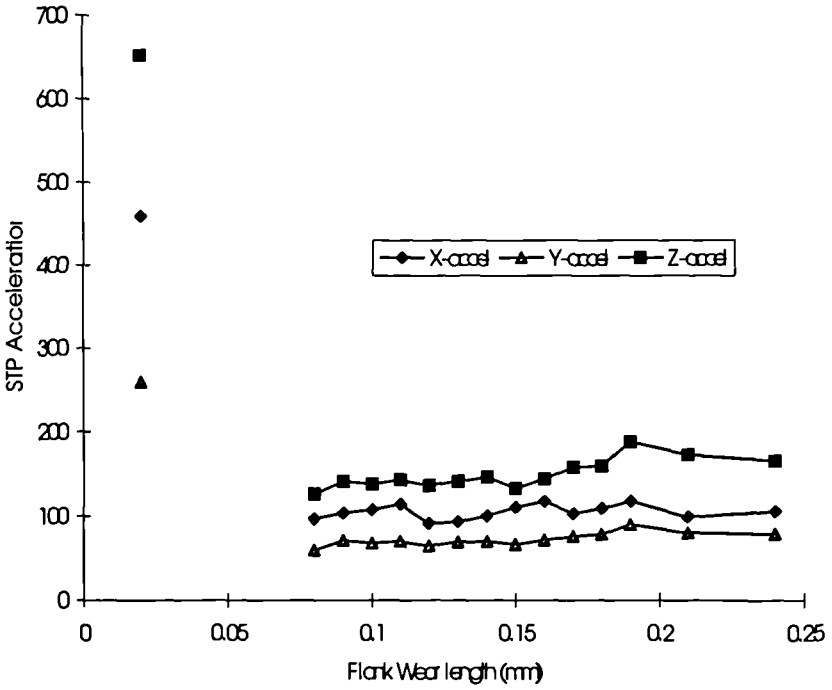

Figure 10.19: STP in Acceleration Spectra Vs. Flank Wear (V=275m/min. & f=0.1mm/rev.)

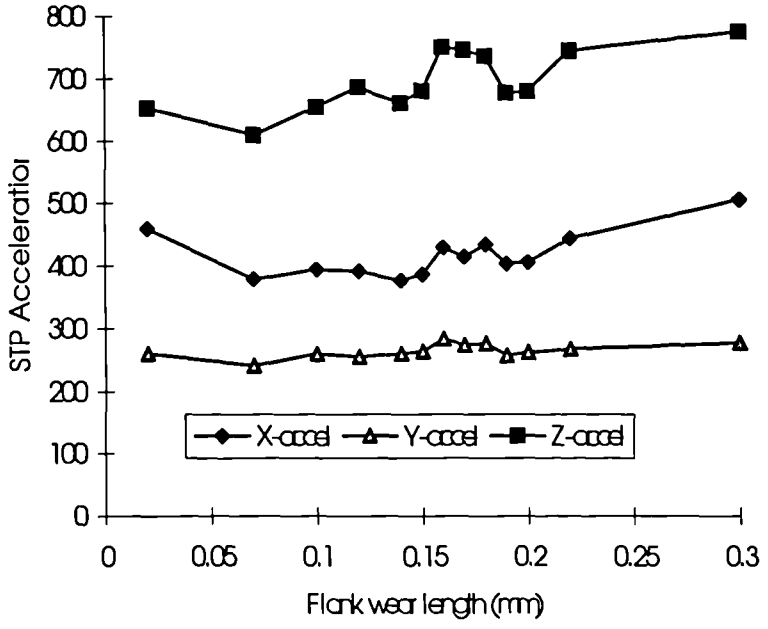

Figure 10.20: STP in Acceleration Spectra Vs. Flank Wear (V=275m/min. & f=0.3mm/rev.)

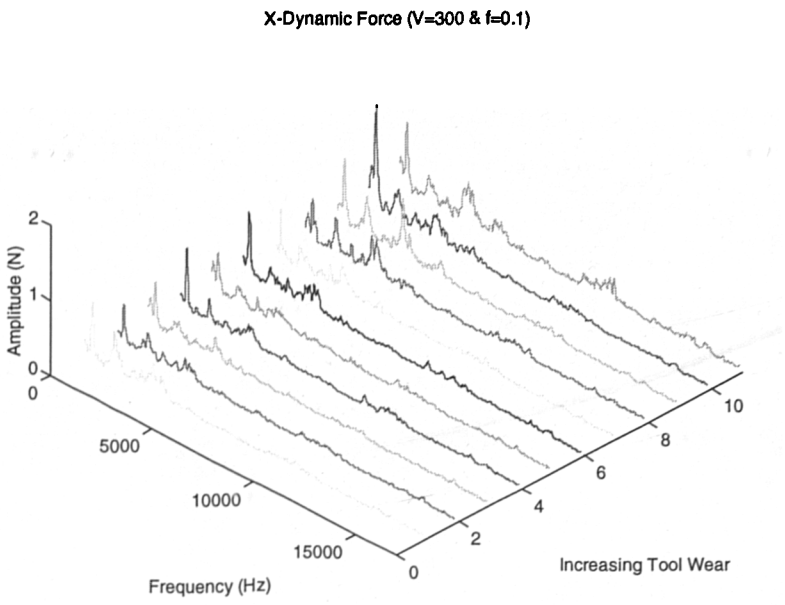

Figure 10.21: X-Dynamic Force Spectra Vs. Flank Wear

(V=300m/min. & f=0.1mm/rev.)

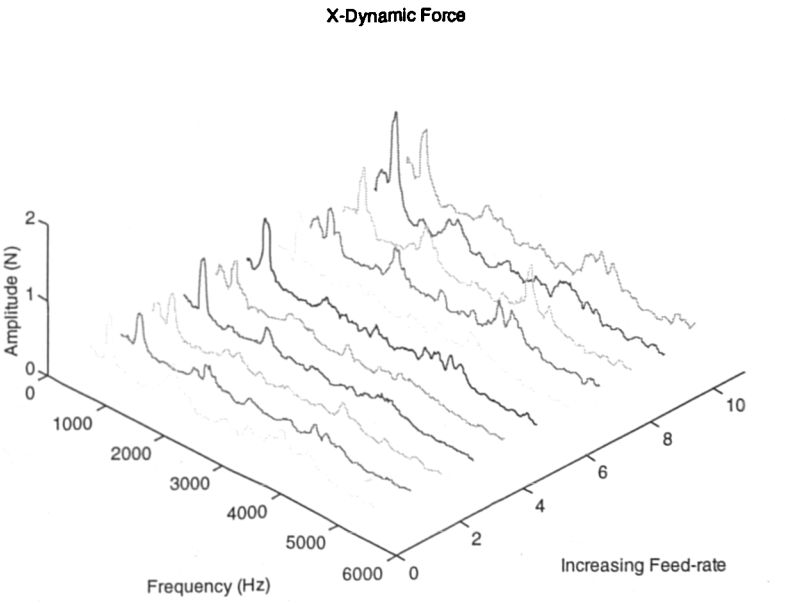

Figure 10.22: X-Dynamic Force Spectra Vs. Flank Wear

(V=300m/min. & f=0.1mm/rev.) -cut-off at 5KHz

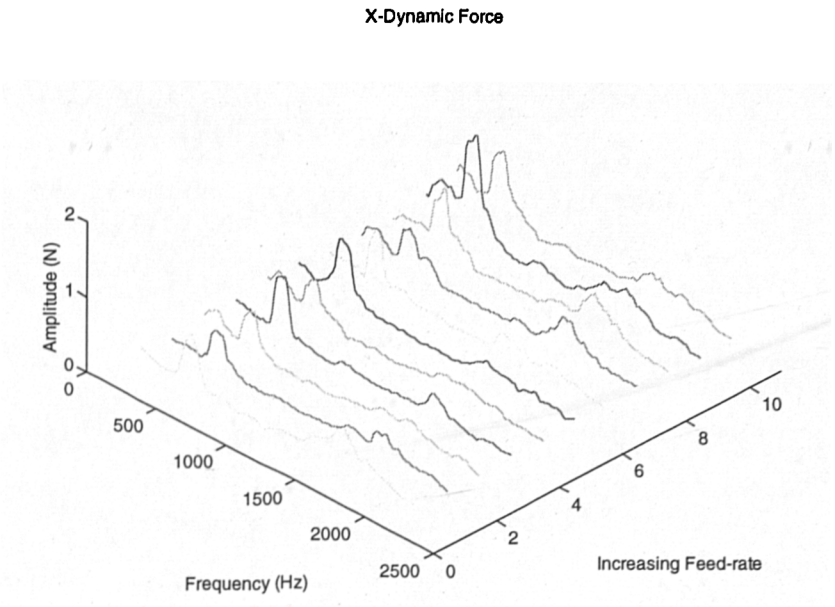

Figure 10.23: X-Dynamic Force Spectra Vs. Flank Wear

(V=300m/min. & f=0.1mm/rev.) cut-off at 2khz

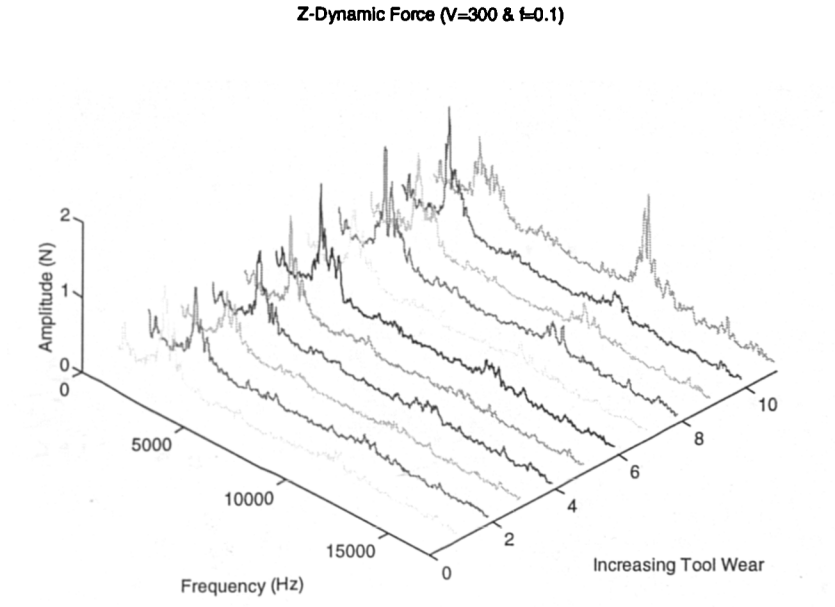

Figure 10.24: Z-Dynamic Force Spectra Vs. Flank Wear

(V=300m/min. & f=0.1mm/rev.)

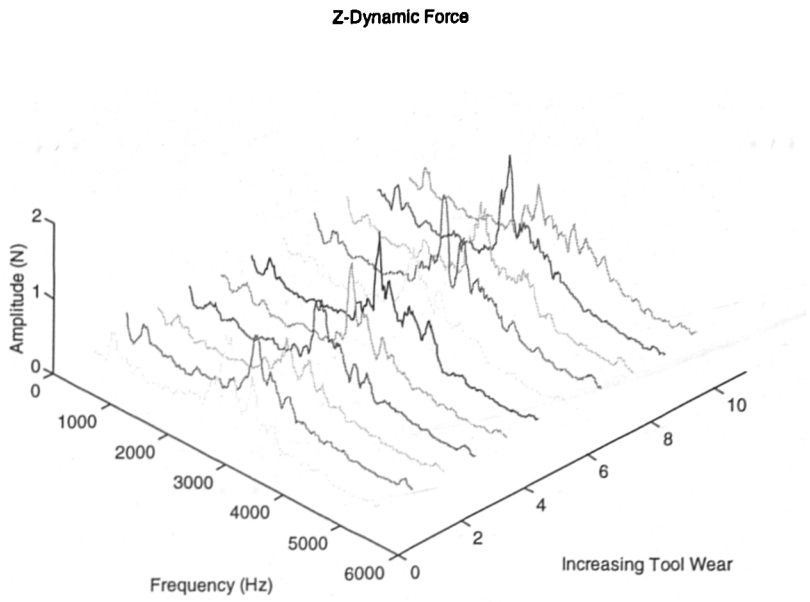

Figure 10.25: Z-Dynamic Force Spectra Vs. Flank Wear

(V=300m/min. & f=0.1mm/rev.) - cut-off at 5 KHz

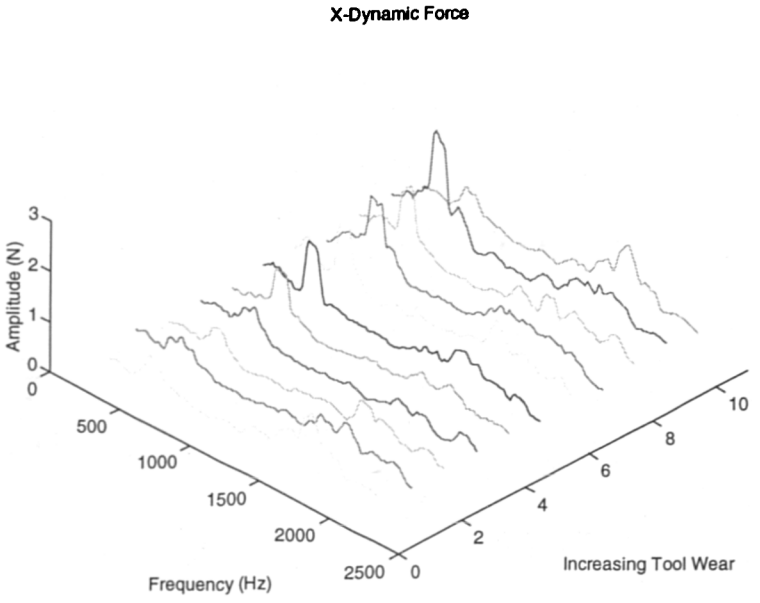

Figure 10.26: X-Dynamic Force Spectra Vs. Flank Wear

(V=300m/min. & f=0.2mm/rev.) - cut-off at 2 KHz

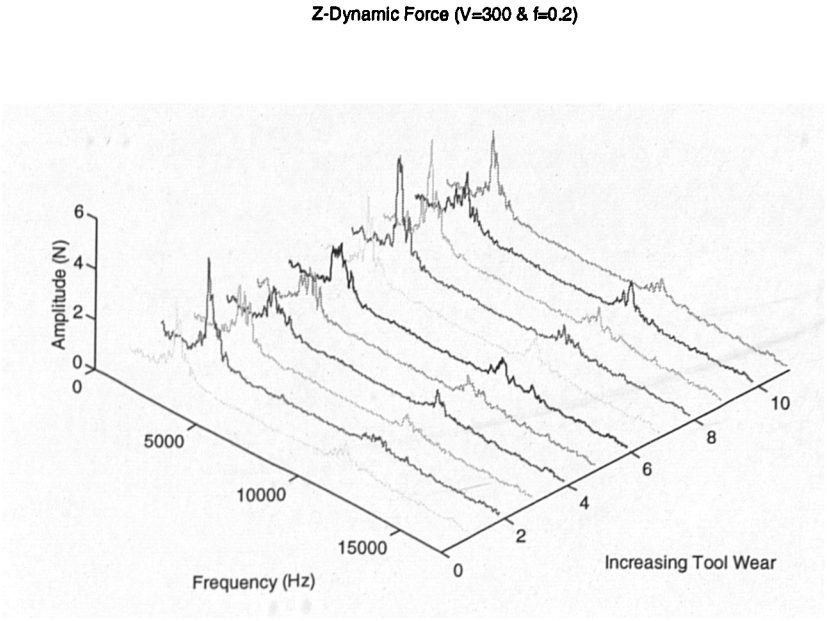

Figure 10.27: Z-Dynamic Force Spectra Vs. Flank Wear

(V=300m/min. & f=0.2mm/rev.)

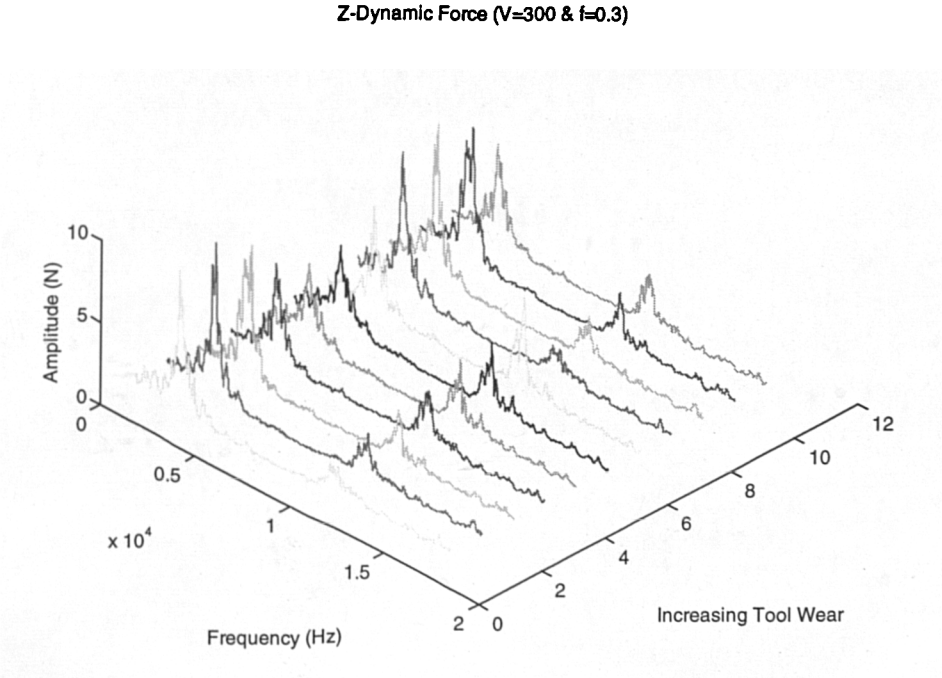

Figure 10.28: Z-Dynamic Force Spectra Vs. Flank Wear

(V=300m/min. & f=0.3mm/rev.)

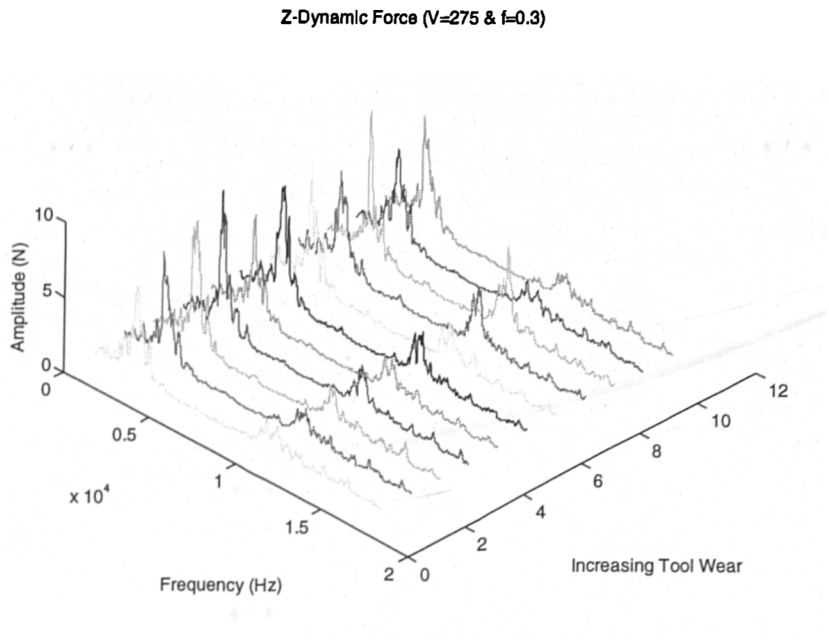

Figure 10.29: Z-Dynamic Force Spectra Vs Flank Wear

(V=275m/min. & f=0.3mm/rev.)

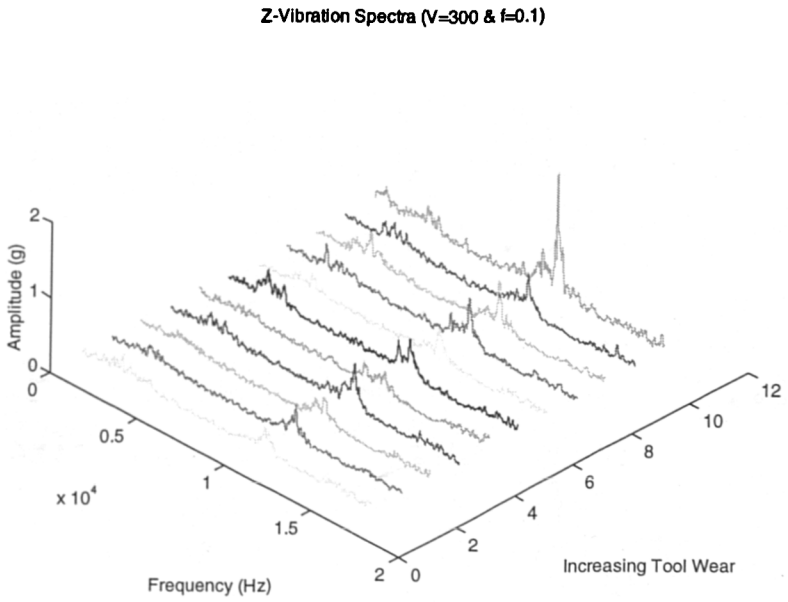

Figure 10.30: Z-Vibration Spectra Vs. Flank Wear

(V=300m/min. & f=0.1mm/rev.)

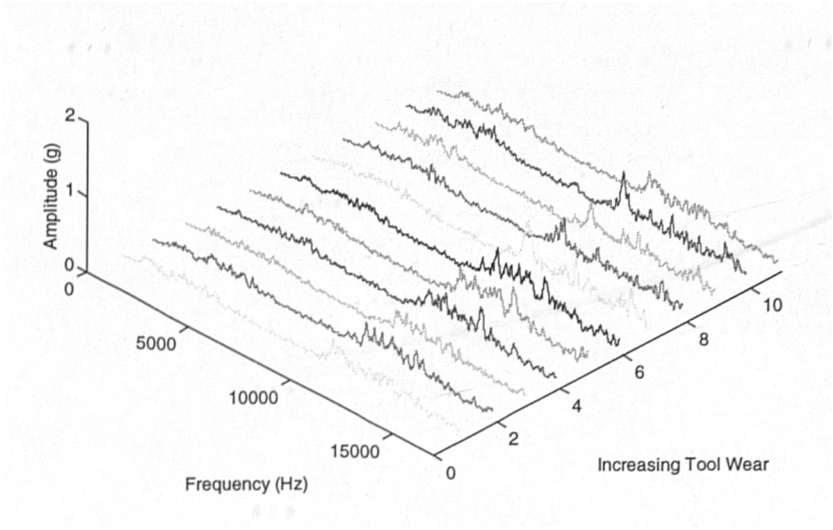

Figure 10.31: X-Vibration Spectra Vs. Flank Wear

(V=300m/min. & f=0.2mm/rev.)

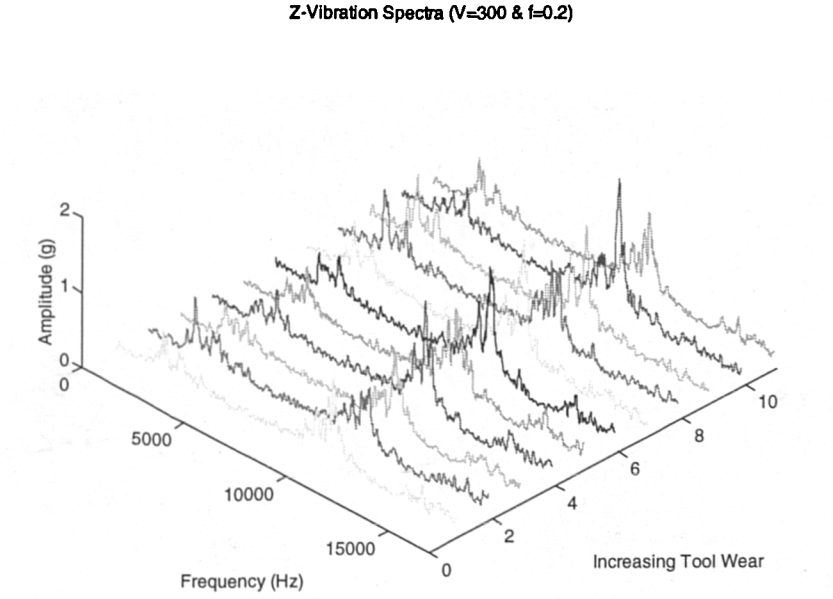

Figure 10.32: Z-Vibration Spectra Vs. Flank Wear

(V=300m/min. & f=0.2mm/rev.)

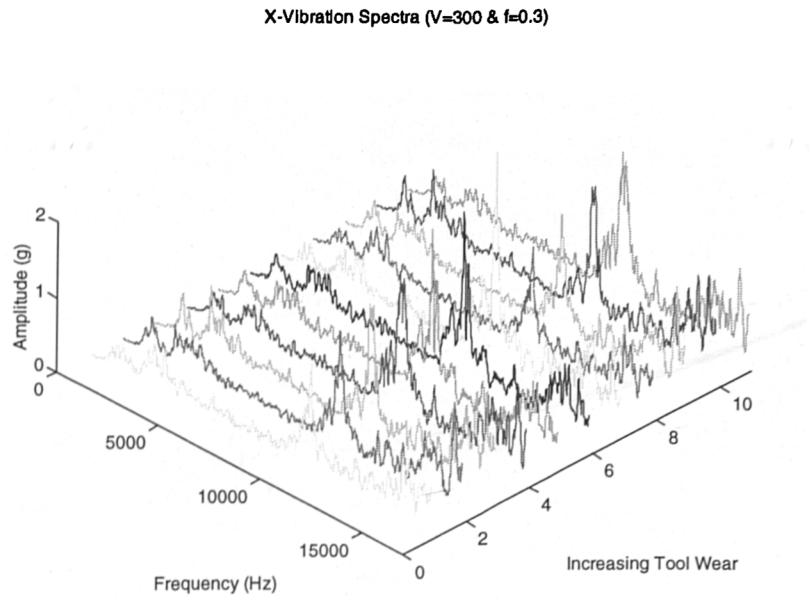

Figure 10.33: X-Vibration Spectra Vs. Flank Wear

(V=300m/min. & f=0.3mm/rev.)

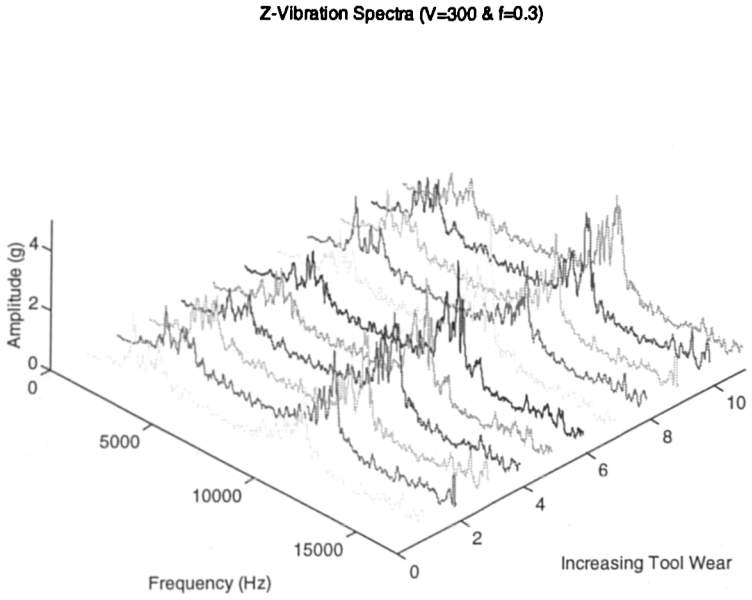

Figure 10.34: Z-Vibration Spectra Vs. Flank Wear

(V=300m/min. & f=0.3mm/rev.)

Figure 10.35: X-Vibration Spectra Vs. Flank Wear

(V=275m/min. & f=0.1mm/rev.)

Figure 10.36: Y-Vibration Spectra Vs. Flank Wear

(V=275m/min. & f=0.1mm/rev.)

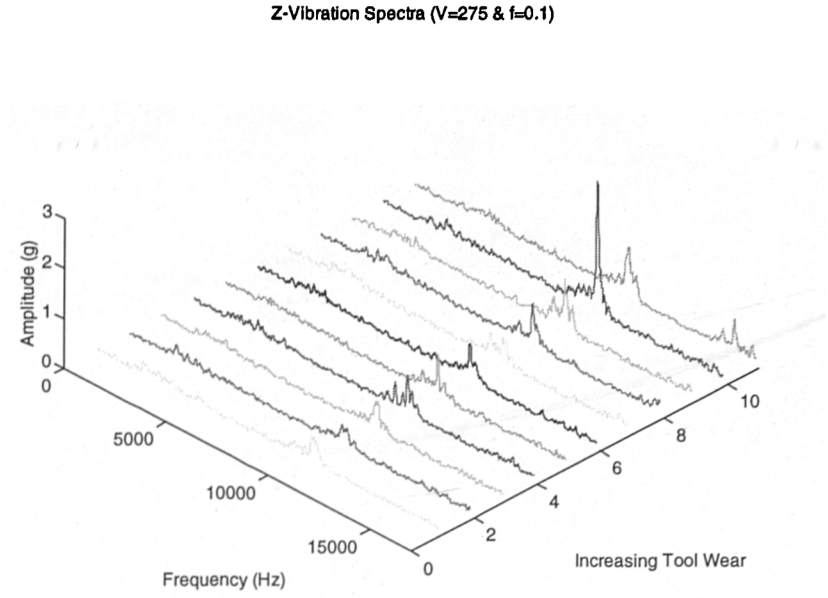

Figure 10.37: Z-Vibration Spectra Vs. Flank Wear

(V=275m/min. & f=0.1mm/rev.)

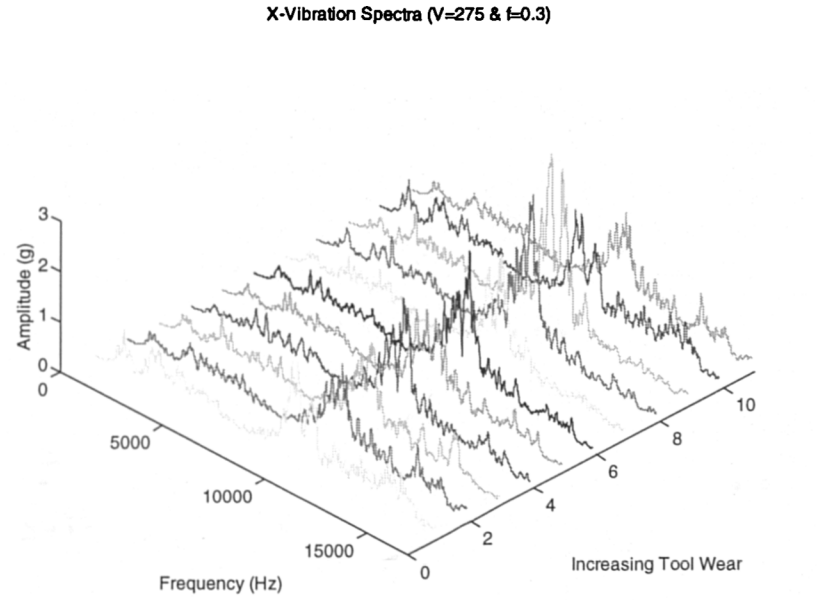

Figure 10.38: X-Vibration Spectra Vs. Flank Wear

(V=275m/min. & f=0.3mm/rev.)

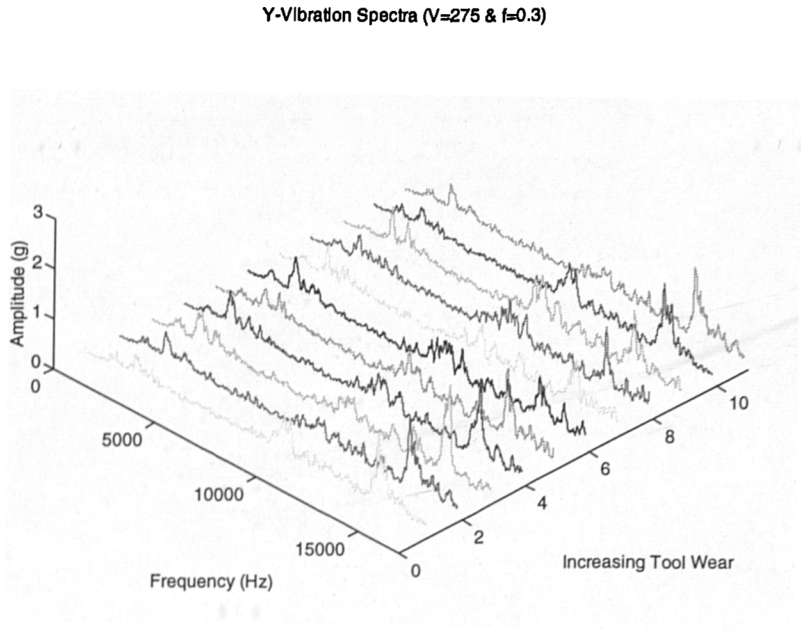

Figure 10.39: Y-Vibration Spectra Vs. Flank Wear

(V=275m/min. & f=0.3mm/rev.)

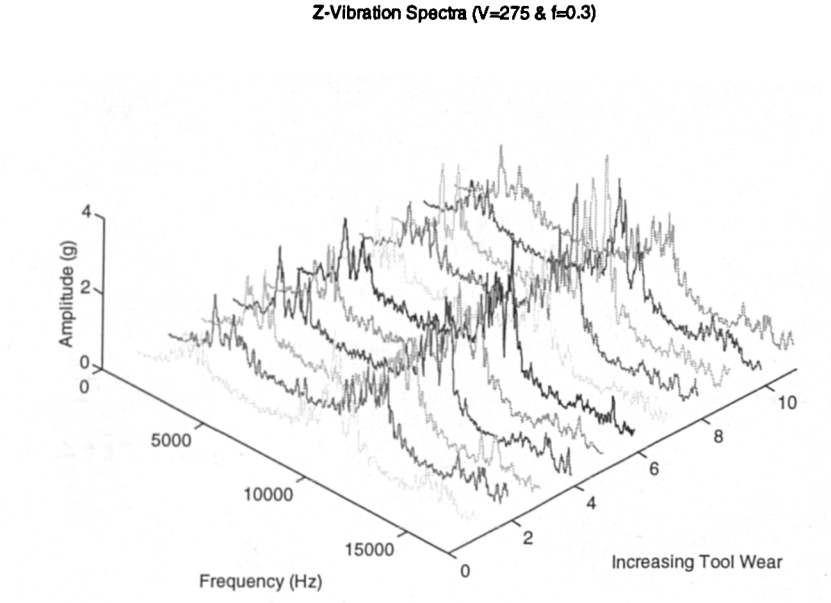

Figure 10.40: Z-Vibration Spectra Vs. Flank Wear

(V=275m/min. & f=0.3mm/rev.)

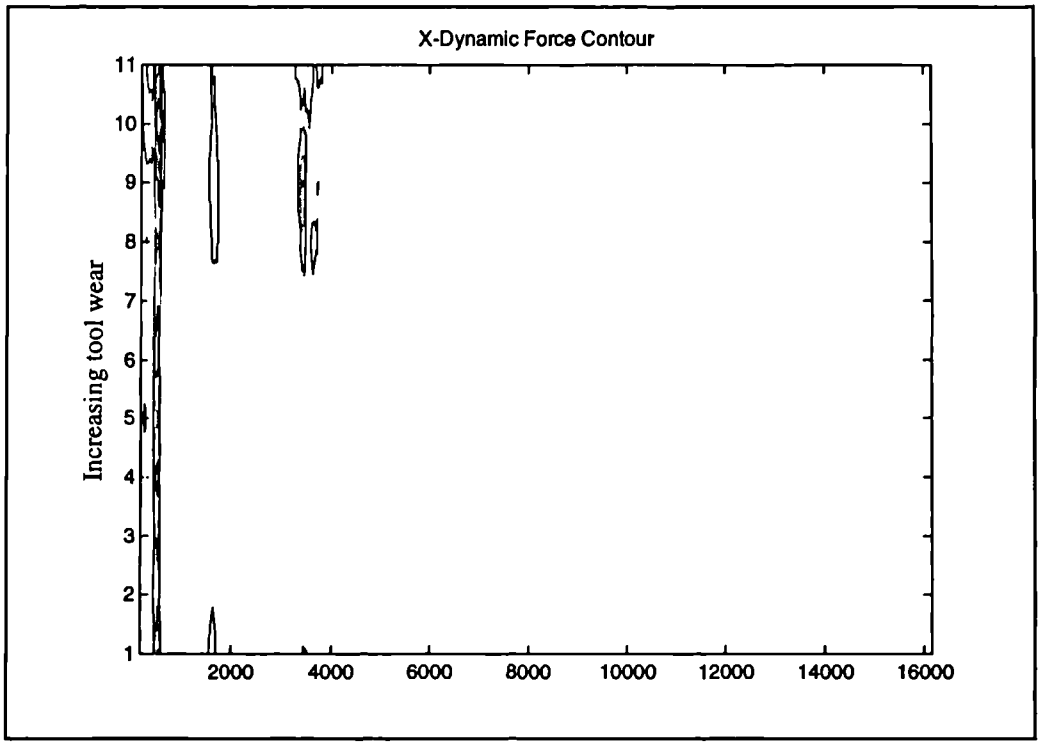

Figure 10.41: X-Dynamic Force Contour (V=300m/min. & f=0.1mm/rev.)

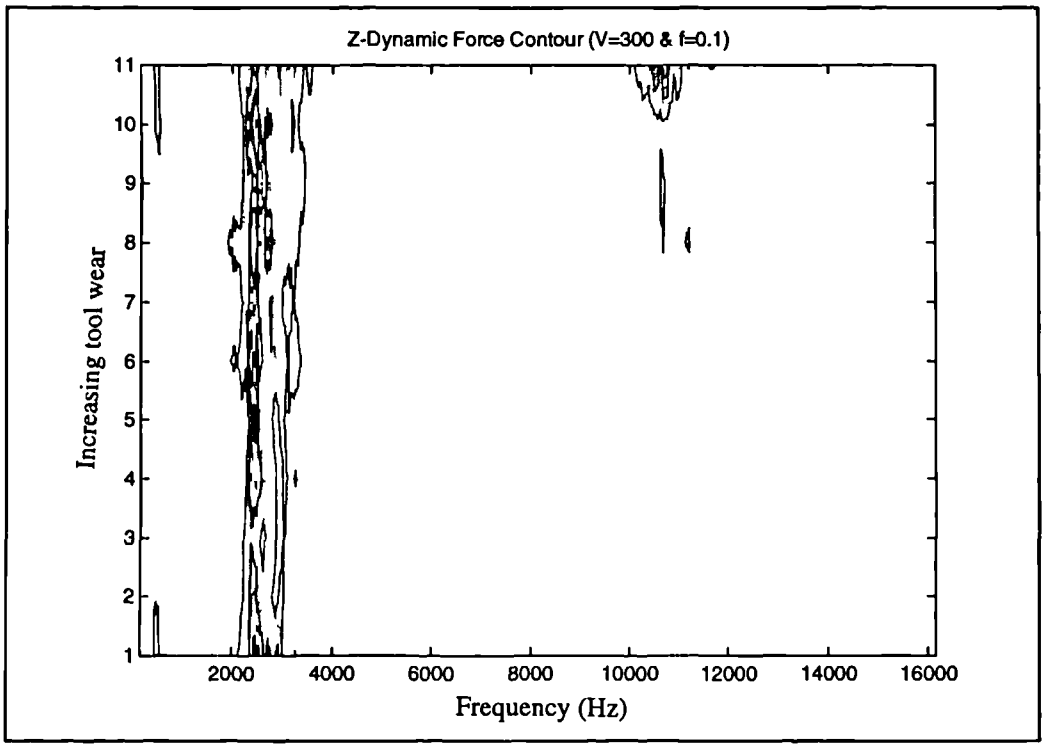

Figure 10.42: Z-Dynamic Force Contour (V=300m/min. & f=0.1mm/rev.)

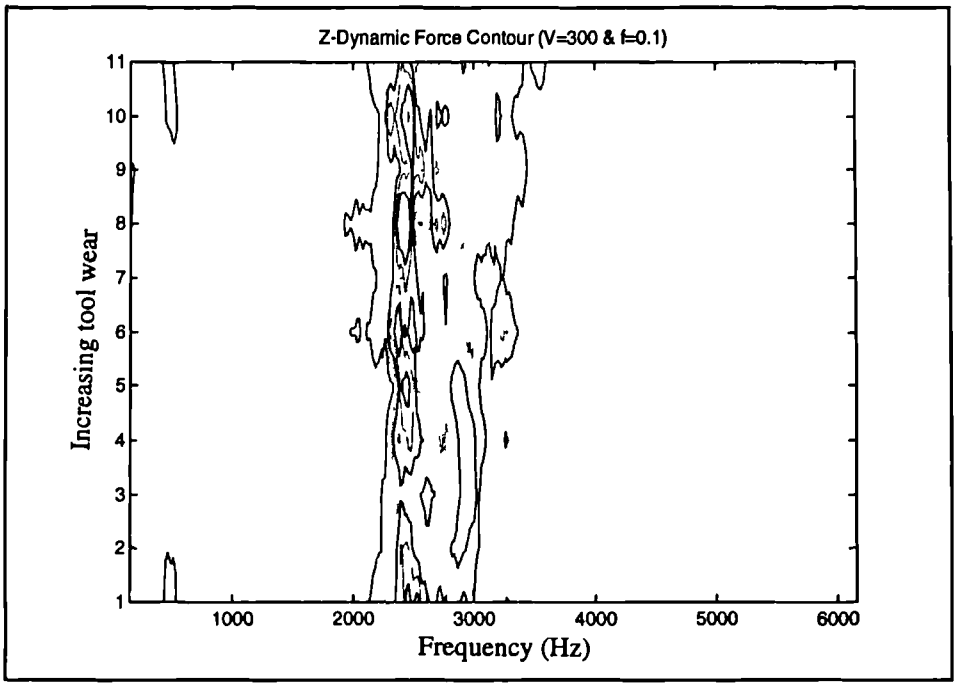

Figure 10.43: Z-Dynamic Force Contour

(V=300m/min. & f=0.1mm/rev.) cutoff at 5 Khz

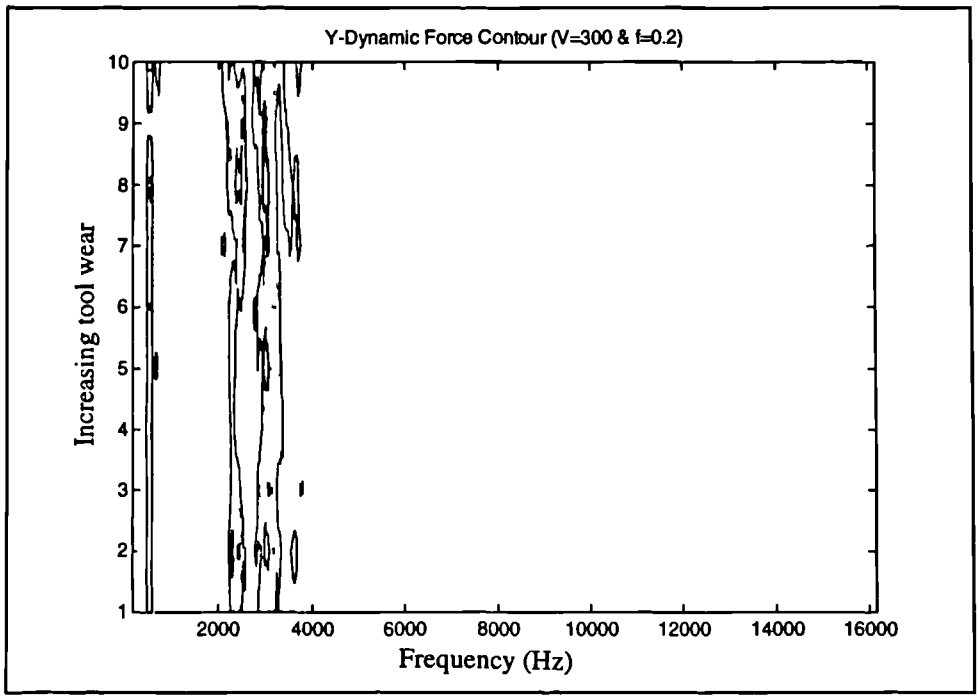

Figure 10.44: Y-Dynamic Force Contour (V=300m/min. & f=0.2mm/rev.)

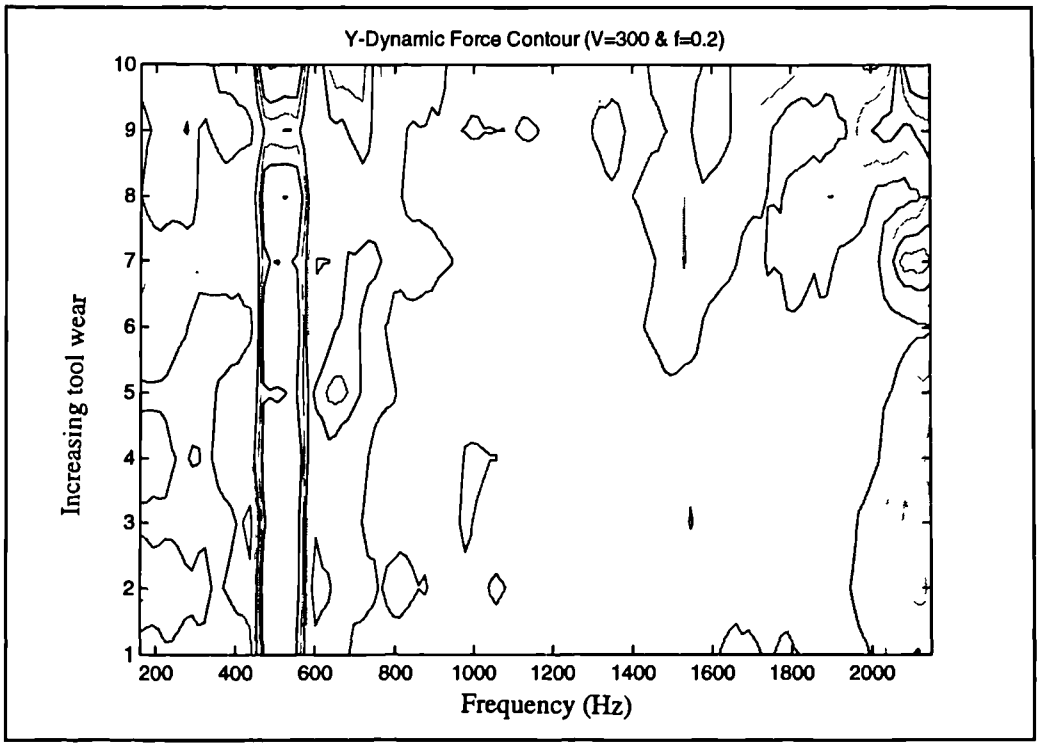

Figure 10.45: Y-Dynamic Force Contour (V=300m/min. & f=0.2mm/rev.) cutoff at *2 KHz*

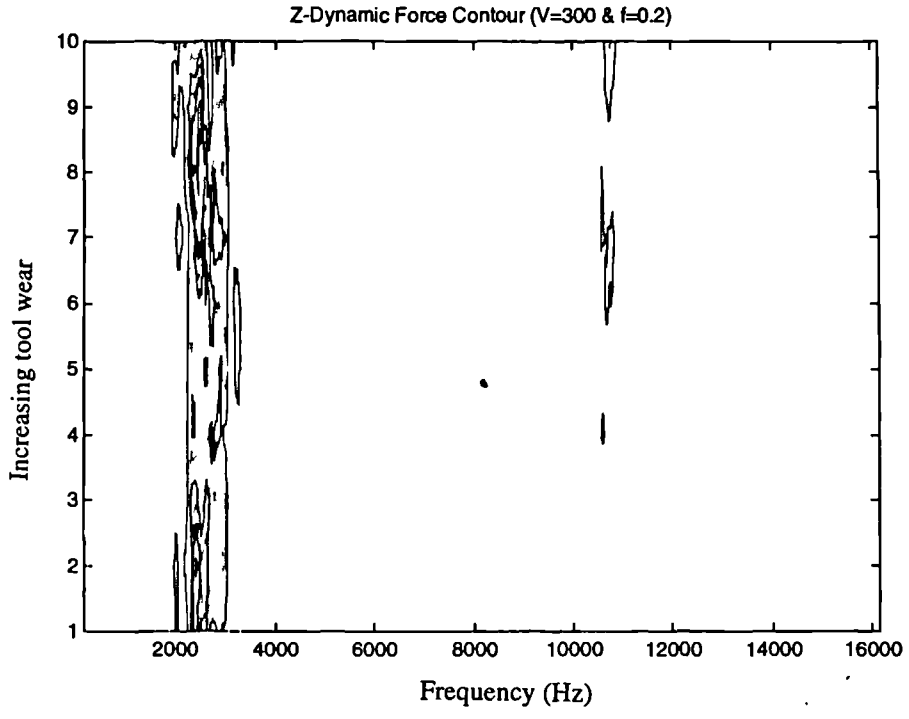

Figure 10.46: Z-Dynamic Force Contour (V=300m/min. & f=0.2mm/rev.)

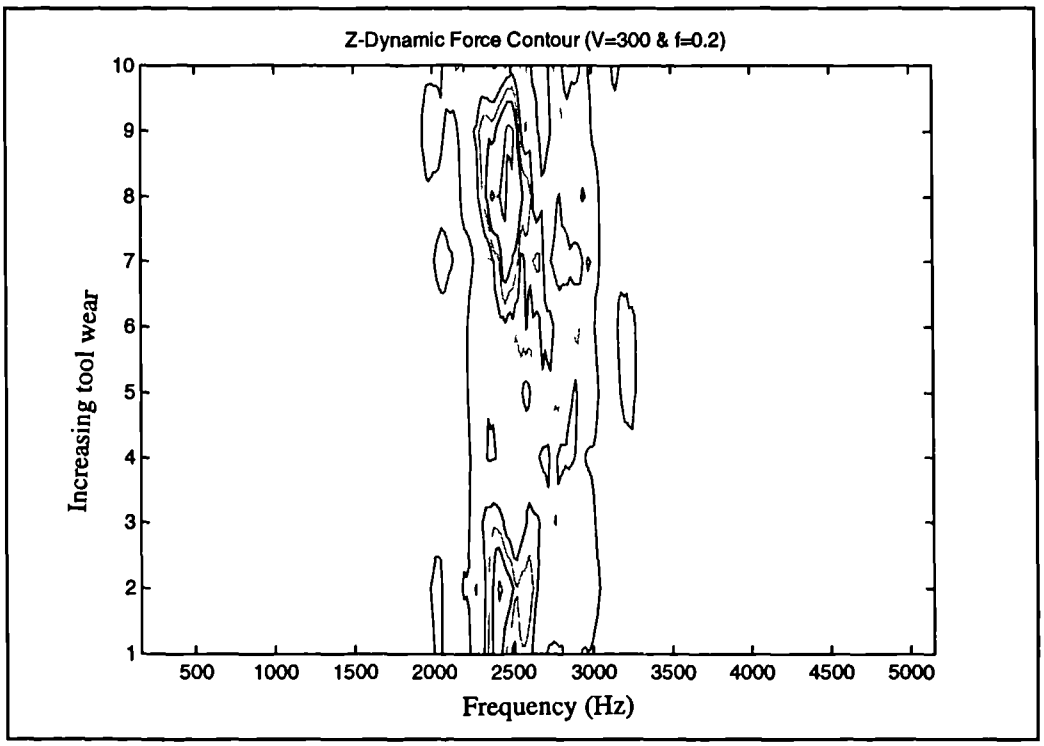

Figure 10.47: Z-Dynamic Force Contour (V=300m/min. & f=0.2mm/rev.) cutoff at 5 Khz

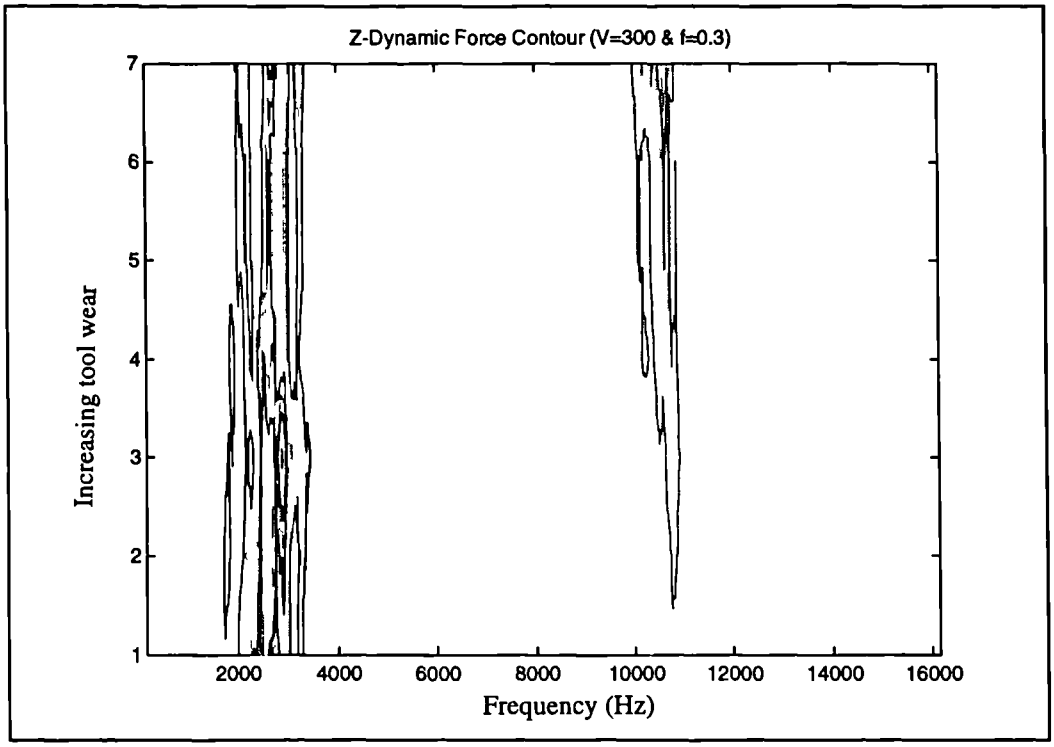

Figure 10.48: Z-Dynamic Force Contour (V=300m/min. & f=0.3mm/rev.)

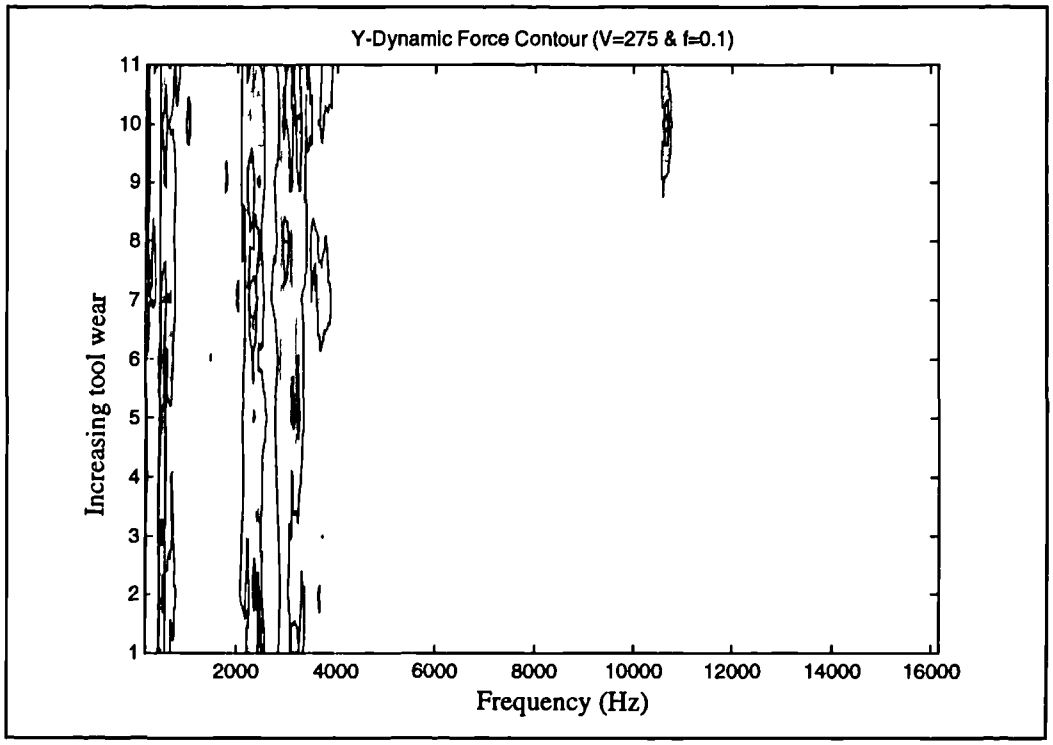

Figure 10.49: Y-Dynamic Force Contour (V=275m/min. & f=0.1mm/rev.)

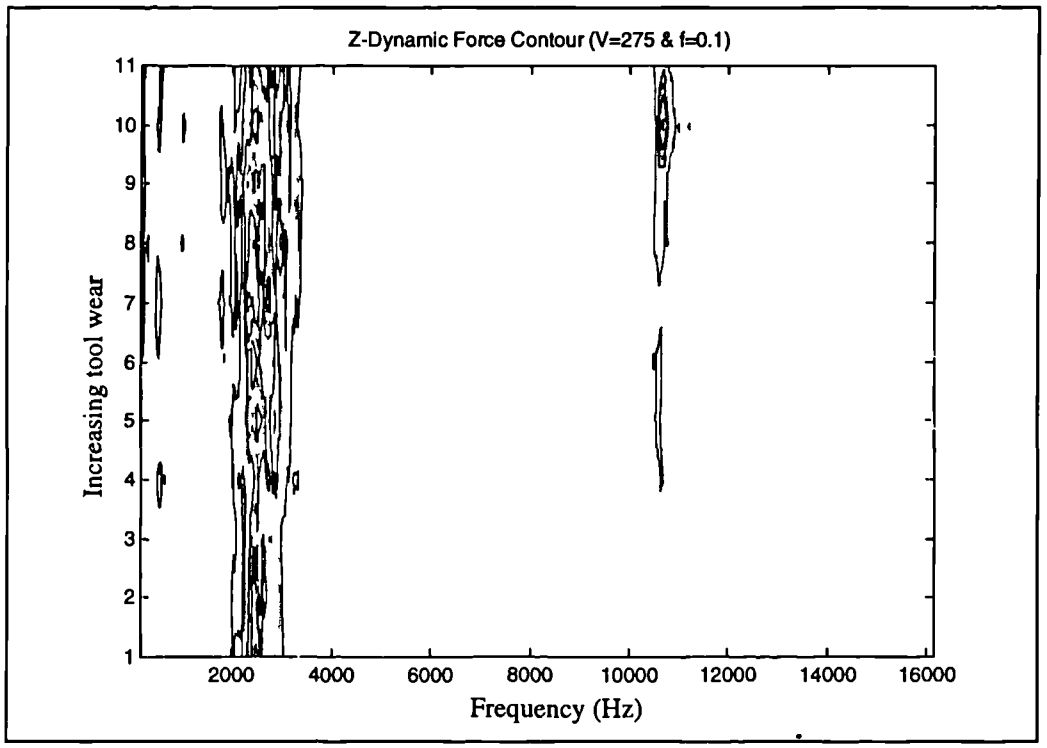

Figure 10.50: Z-Dynamic Force Contour (V=275m/min. & f=0.1mm/rev.)

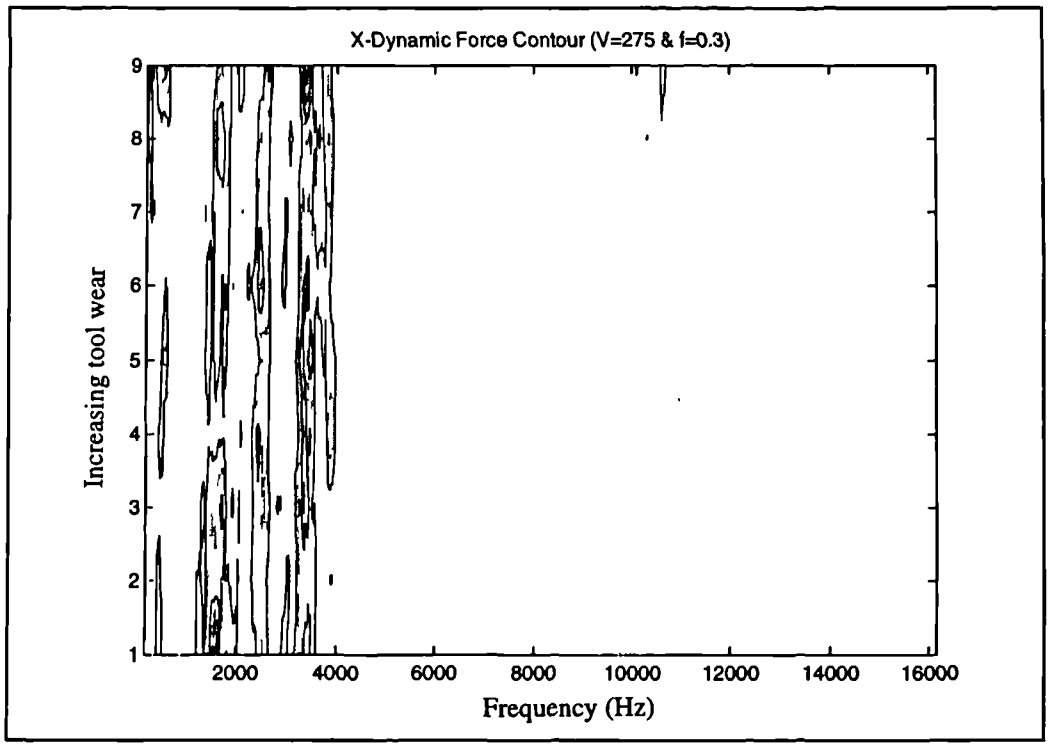

Figure 10.51: X-Dynamic Force Contour (V=275m/min. & f=0.3mm/rev.)

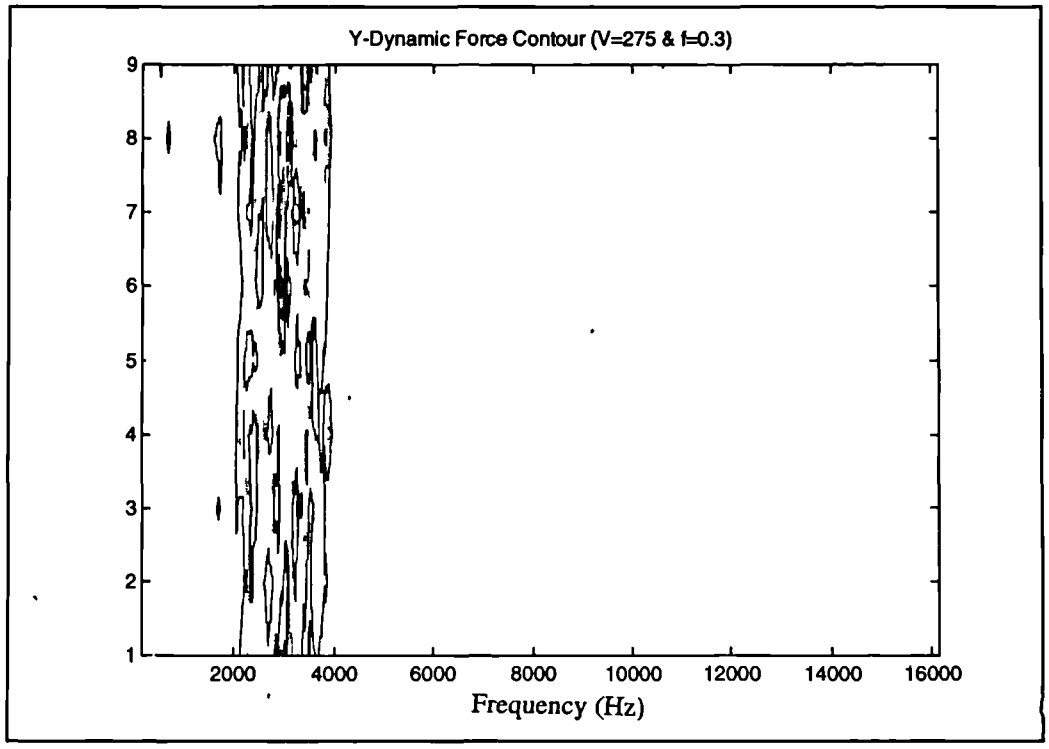

Figure 10.52: Y-Dynamic Force Contour (V=275m/min. & f=0.3mm/rev.)

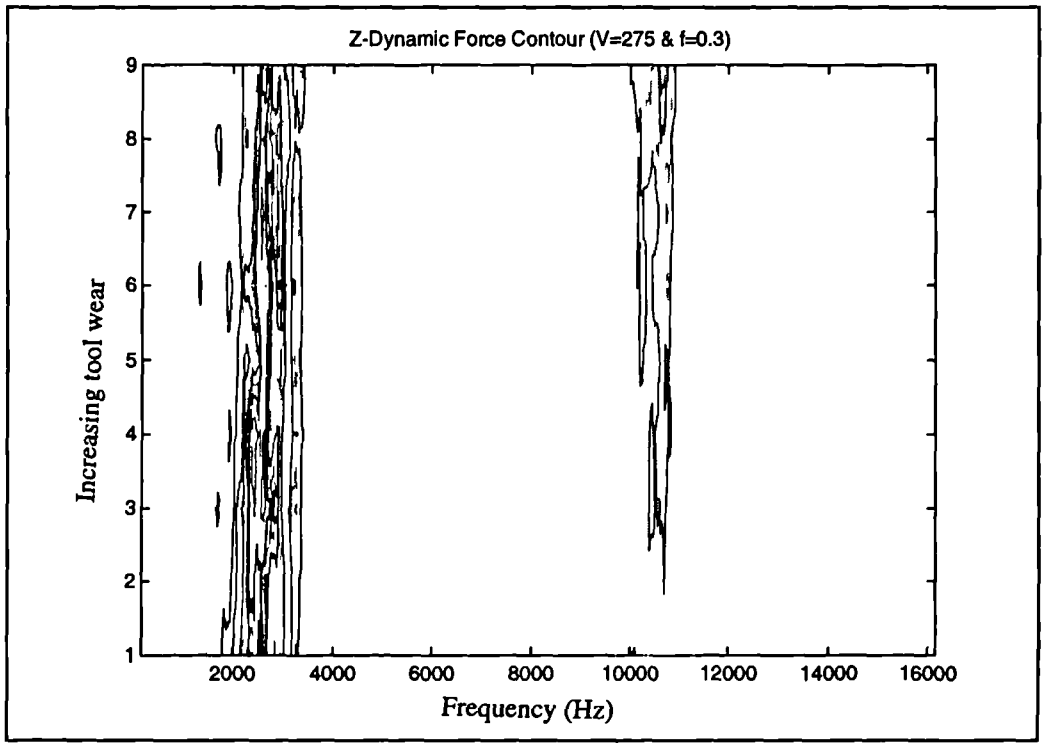

Figure 10.53: Z-Dynamic Force Contour (V=275m/min. & f=0.3mm/rev.)

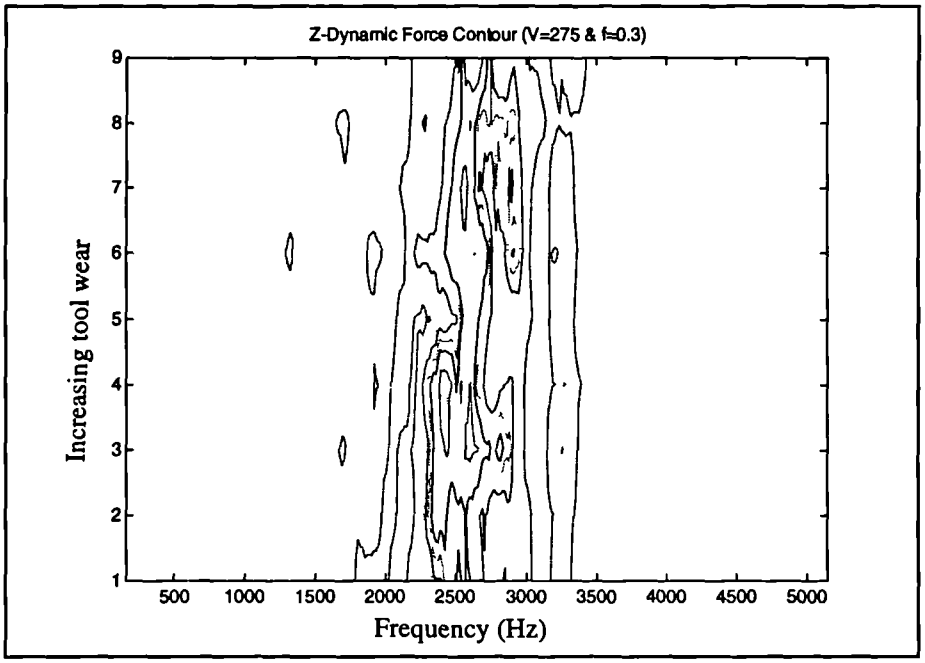

Figure 10.54: Z-Dynamic Force Contour (V=275m/min. & f=0.3mm/rev.) cutoof at 5 Khz

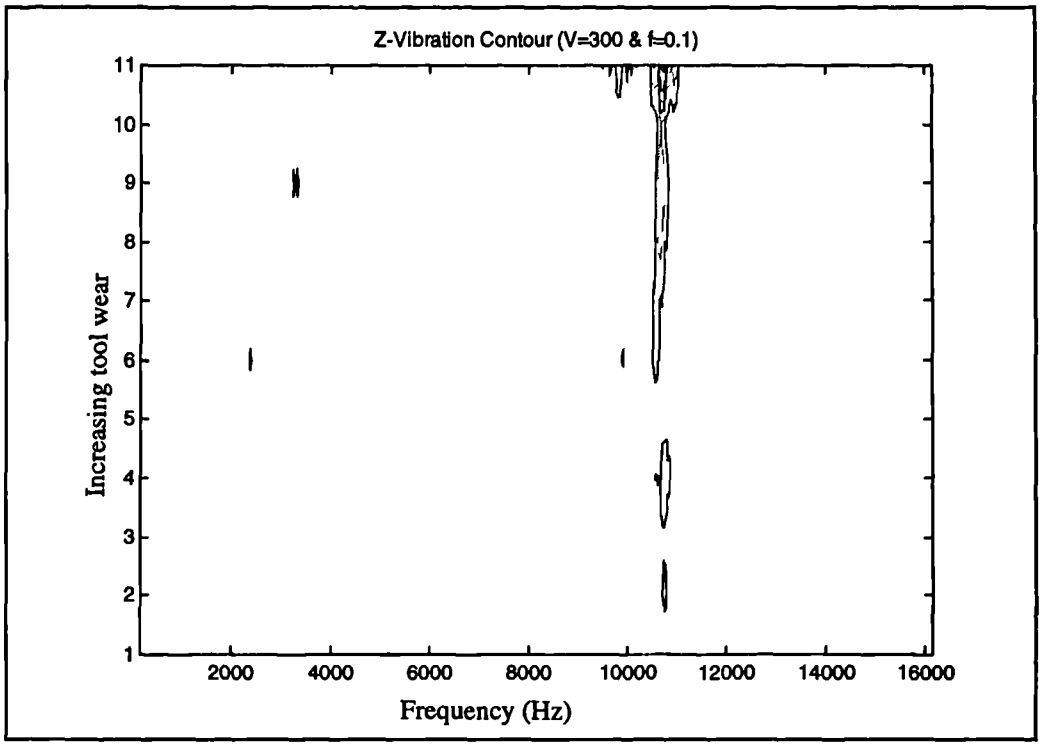

Figure 10.55: Z-Vibration Contour (V=300m/min. & f=0.1mm/rev.)

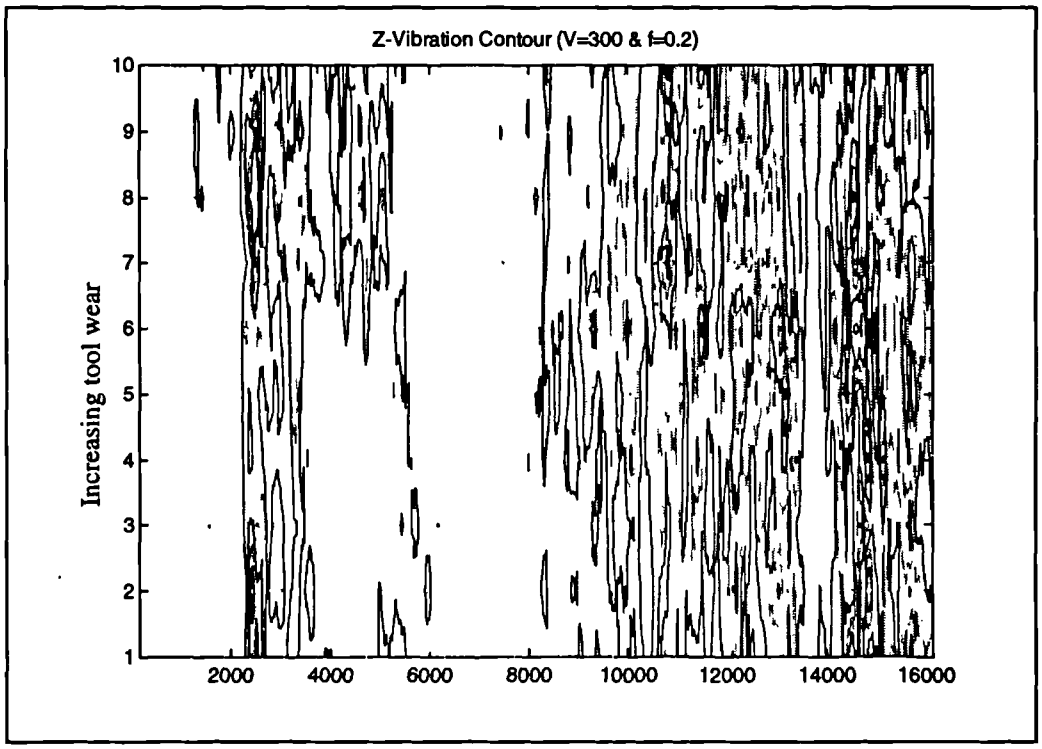

Figure 10.56: Y-Vibration Contour (V=300m/min. & f=0.2mm/rev.)

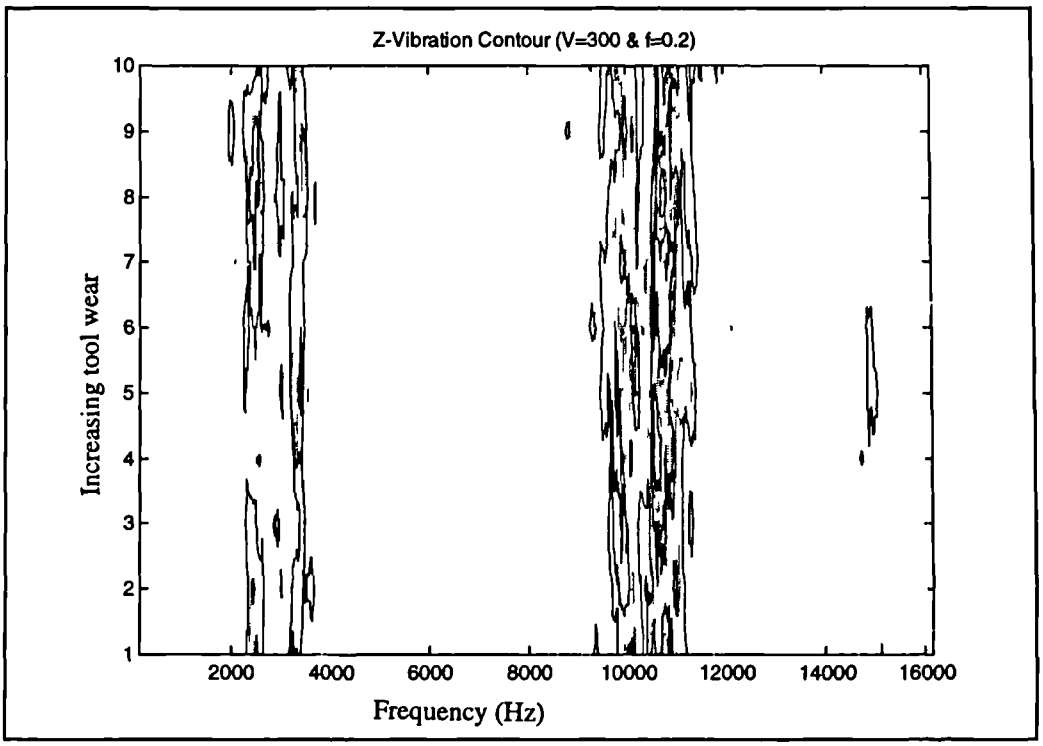

Figure 10.57: Z-Vibration Contour (V=300m/min. & f=0.2mm/rev.)

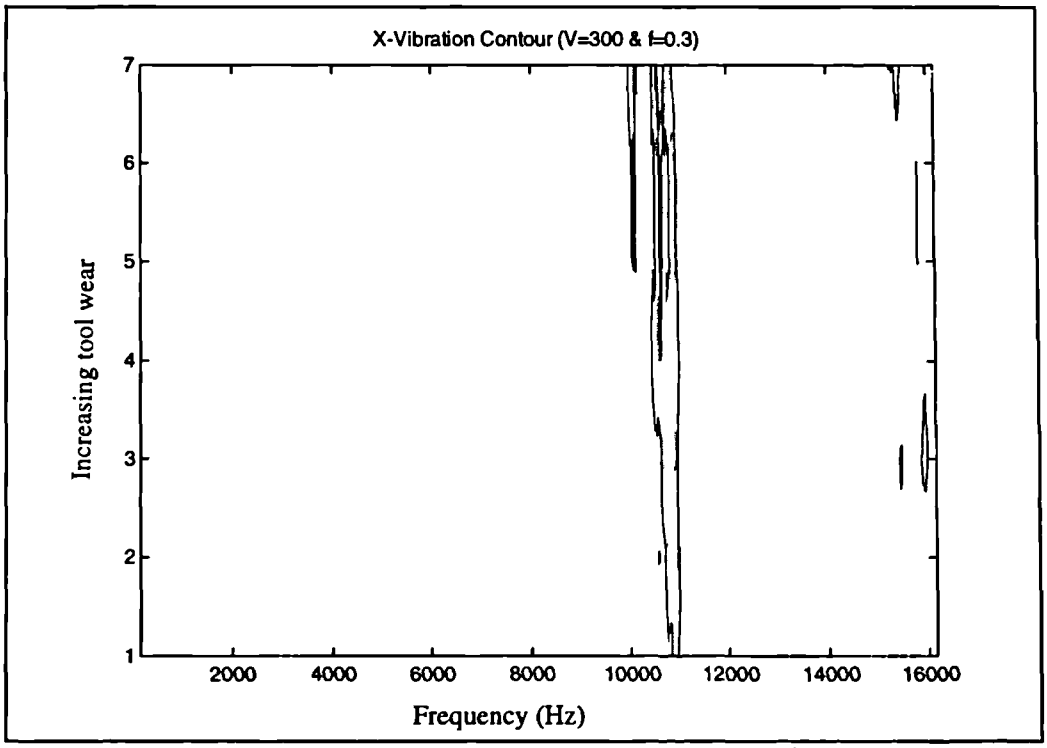

Figure 10.58: X-Vibration Contour (V=300m/min. & f=0.3mm/rev.)

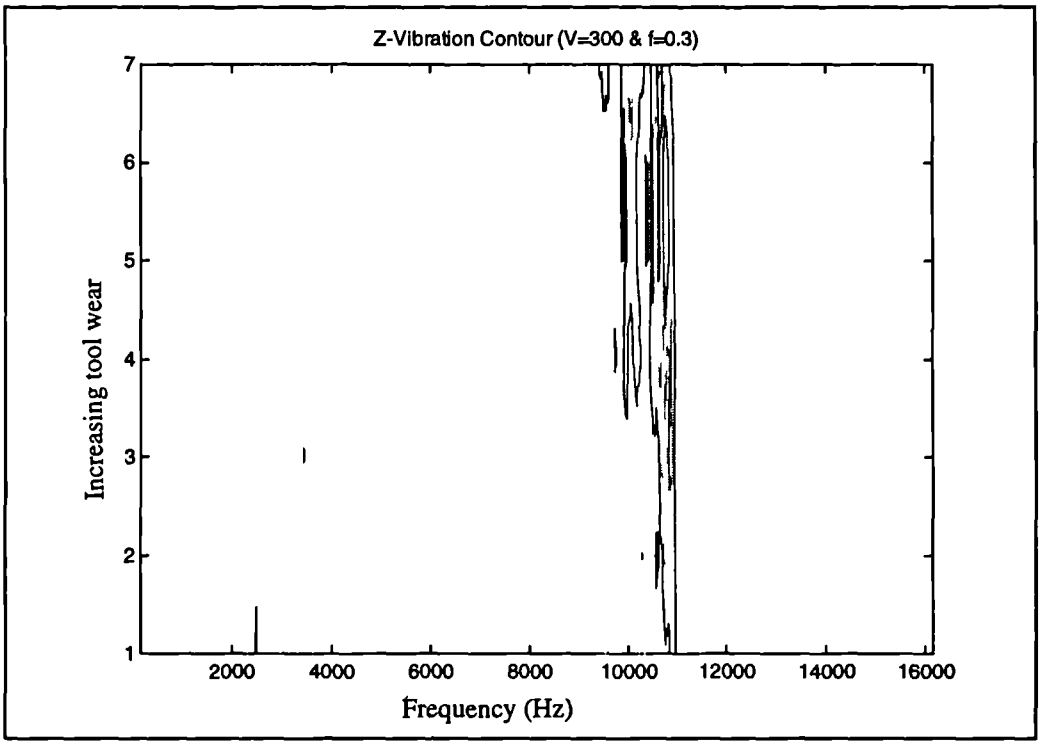

Figure 10.59: Z-Vibration Contour (V=300m/min. & f=0.3mm/rev.)

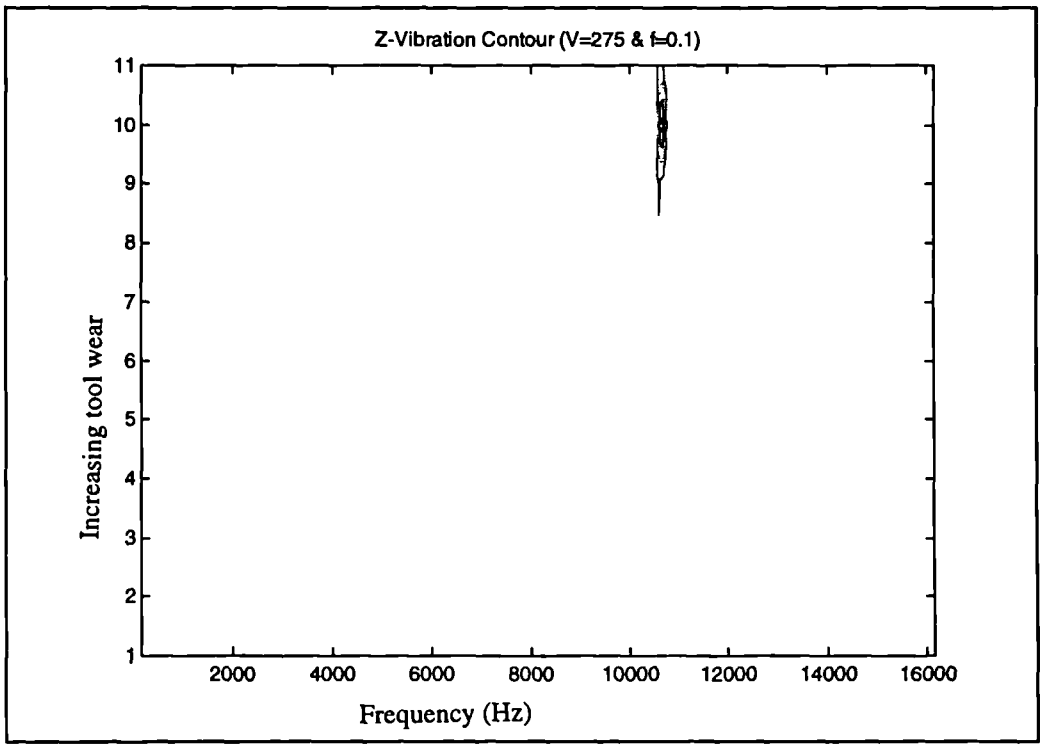

Figure 10.60: Z-Vibration Contour (V=275m/min. & f=0.1mm/rev.)

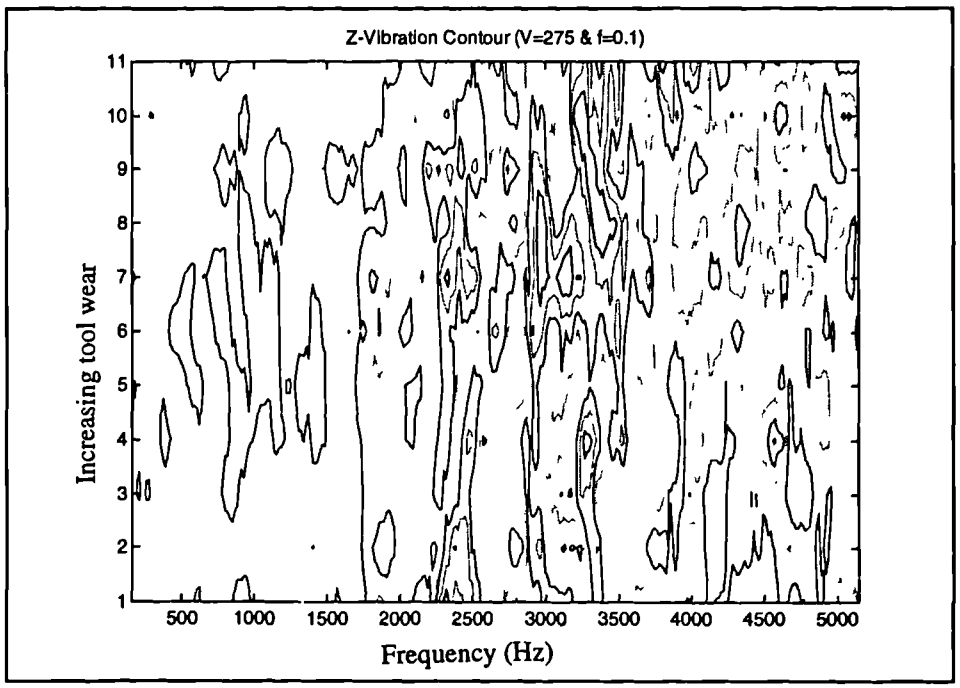

Figure 10.61: Z-Vibration Contour (V=275m/min. & f=0.1mm/rev.) cutoff at 5 KHz

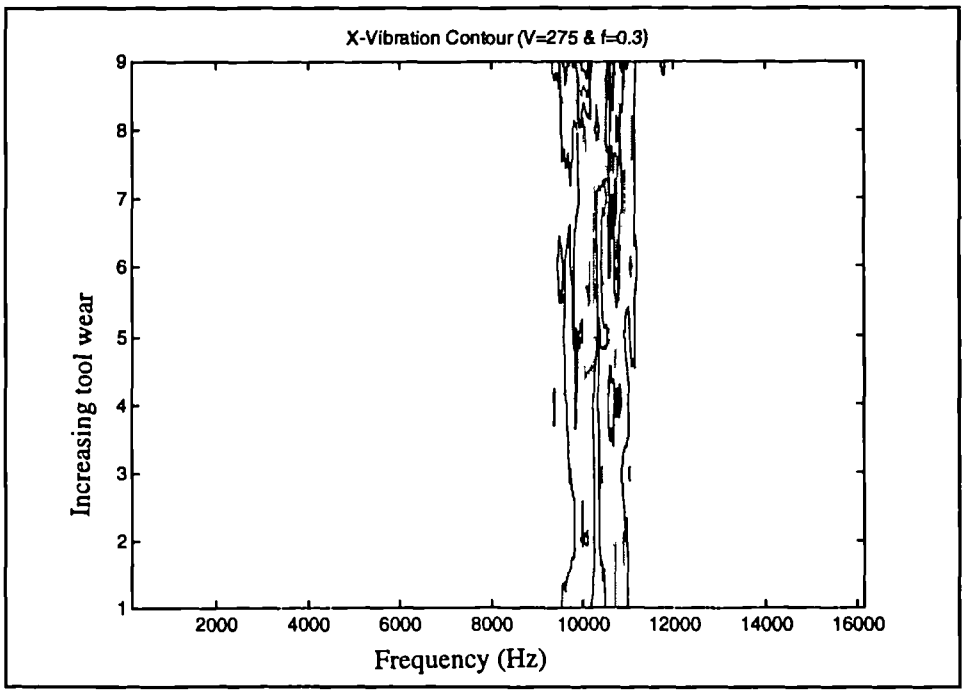

Figure 10.62: X-Vibration Contour (V=275m/min. & f=0.3mm/rev.)

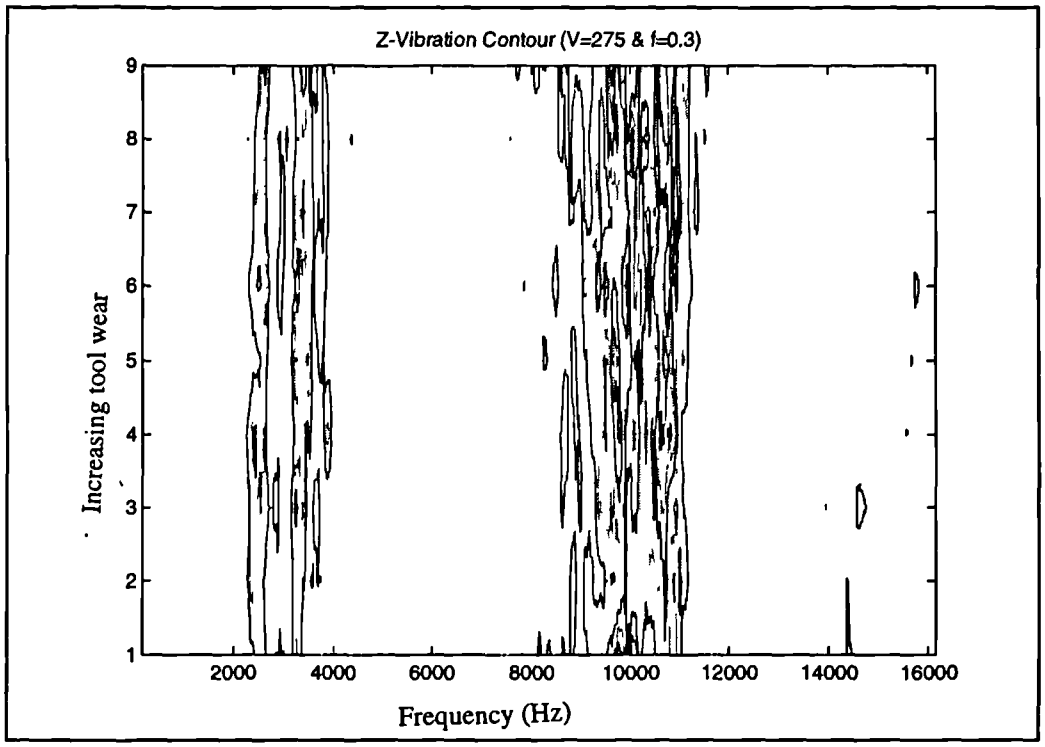

Figure 10.63: Z-Vibration Contour (V=275m/min. & f=0.3mm/rev.)

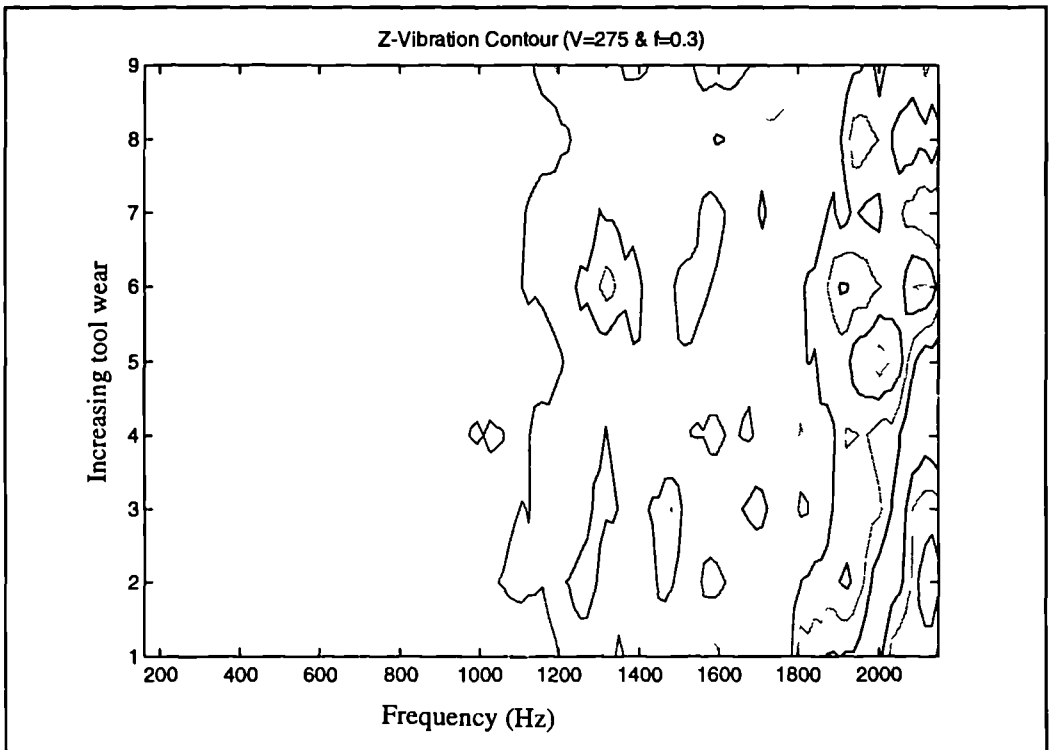

Figure 10.64: Z-Vibration Contour (V=275m/min. & f=0.3mm/rev.) cutoff at 2 Khz

P15 FIGURES

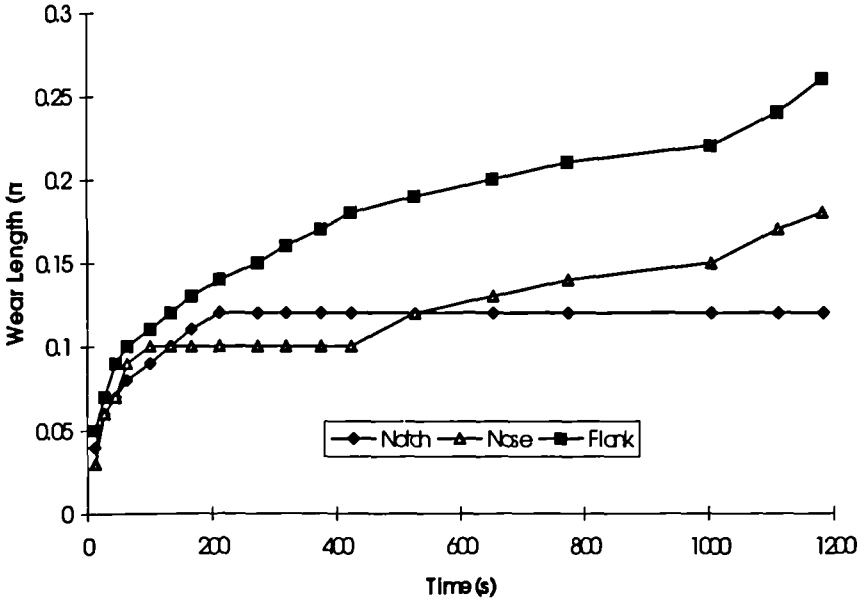

Figure 10.65: Wear - Time Plot (V=300m/min. & f=0.1mm/rev.)

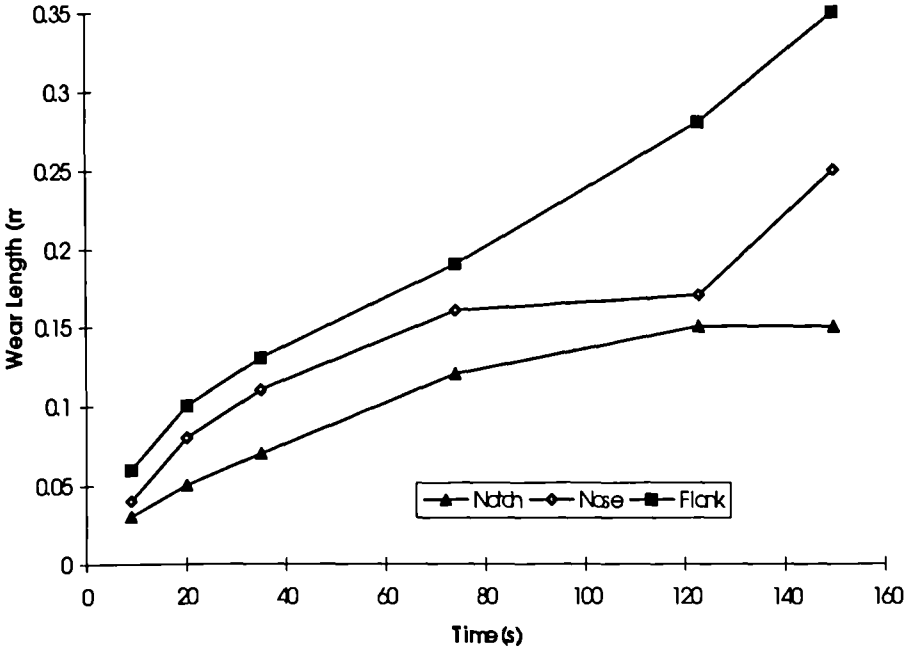

Figure 10.66: Wear-Time plot (V=300m/min. & f=0.3mm/rev.)

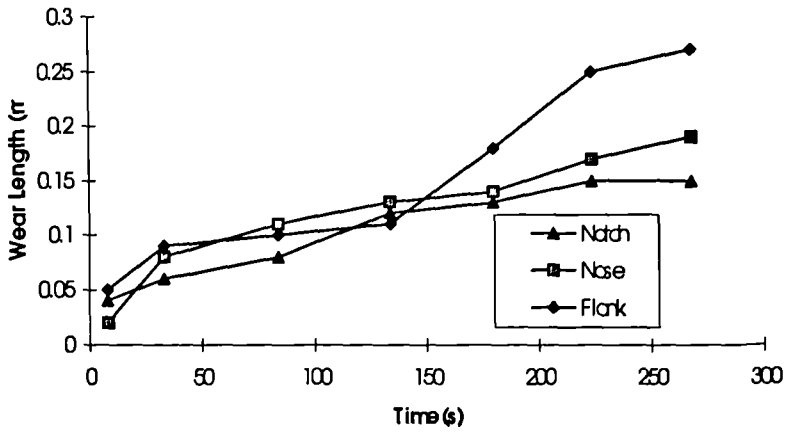

Figure 10.67: Wear - Time plot (V=275m/min. & f=0.3mm/rev.)

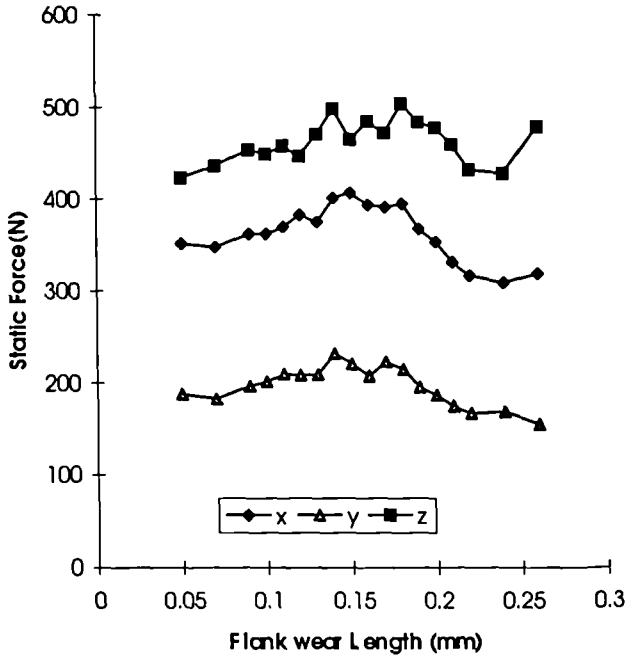

Figure 10.68: Static Forces Vs. Flank Wear Length (V=300m/min. & f=0.1mm/rev.)

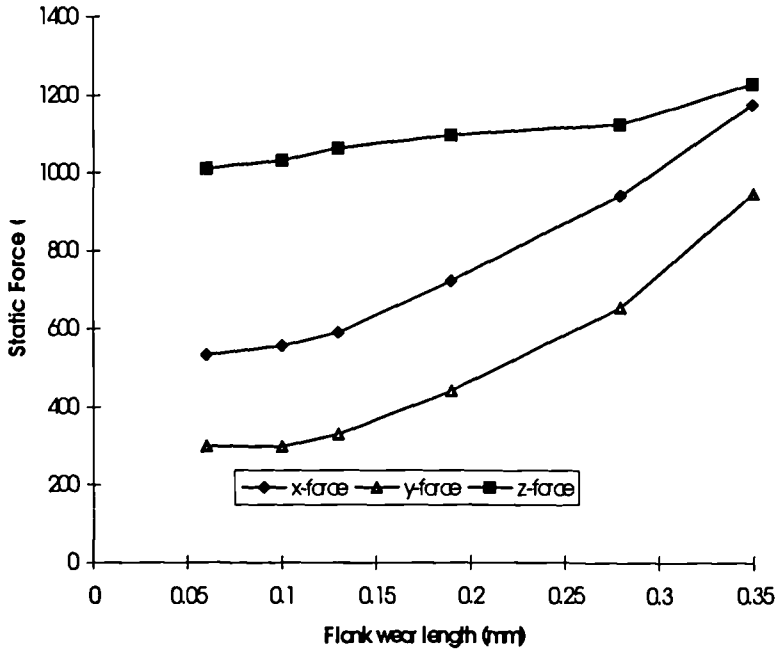

Figure 10.69: Static Forces Vs. Flank Wear Length (V=300m/min. & f=0.3mm/rev.)

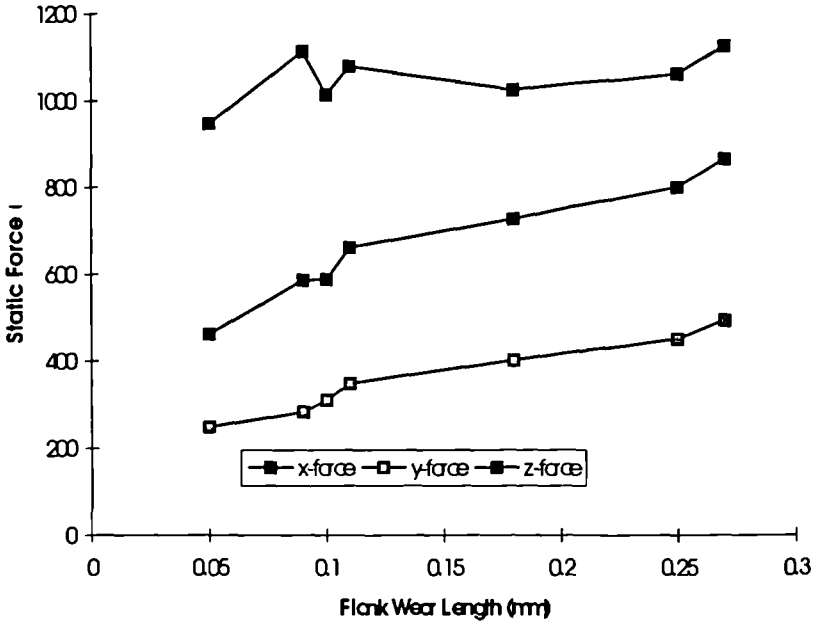

Figure 10.70: Static Cutting Forces Vs. Flank Wear Length (V=275m/min. & f=0.3mm/rev.)

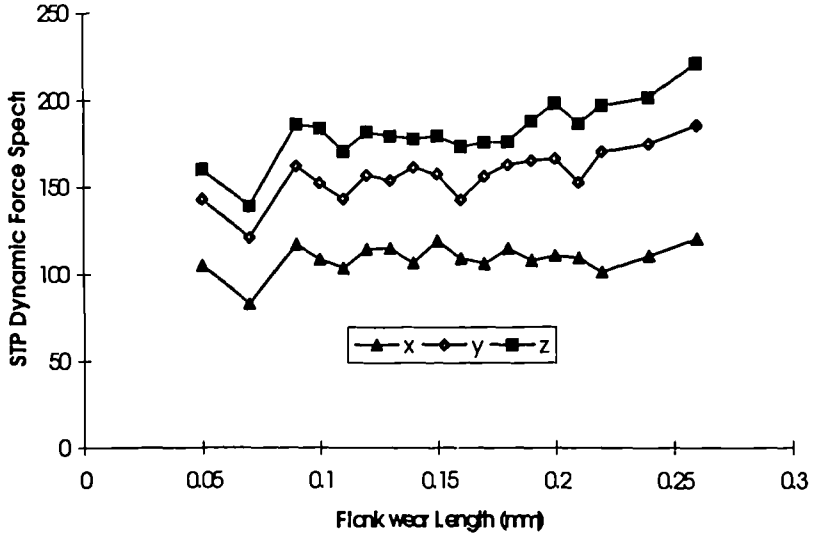

Figure 10.71: STP Dynamic Force Spectra Vs. Flank Wear Length (V=300m/min. & f=0.1mm/rev.)

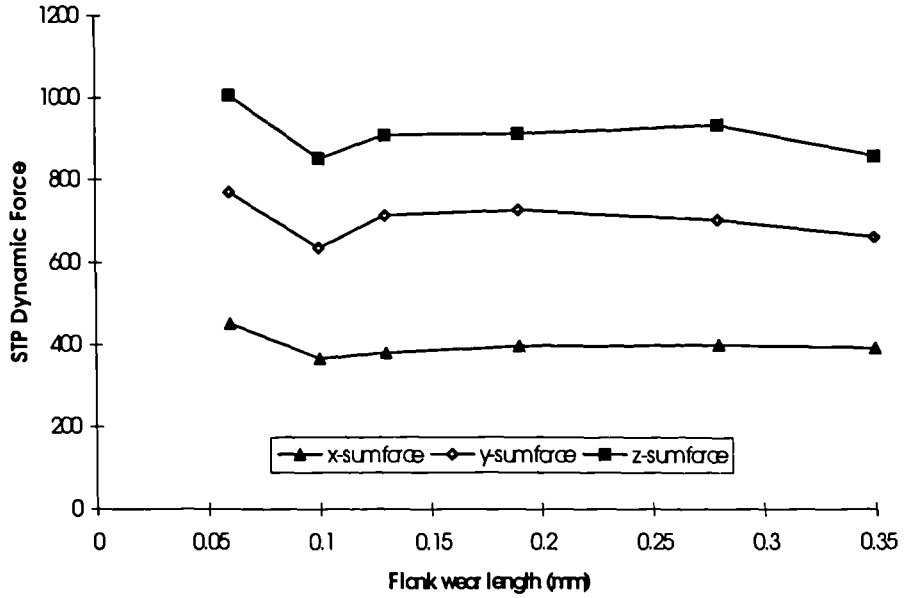

Figure 10.72: STP Dynamic Spectra Vs. Flank Wear (V=300m/min. & f=0.2mm/rev.)

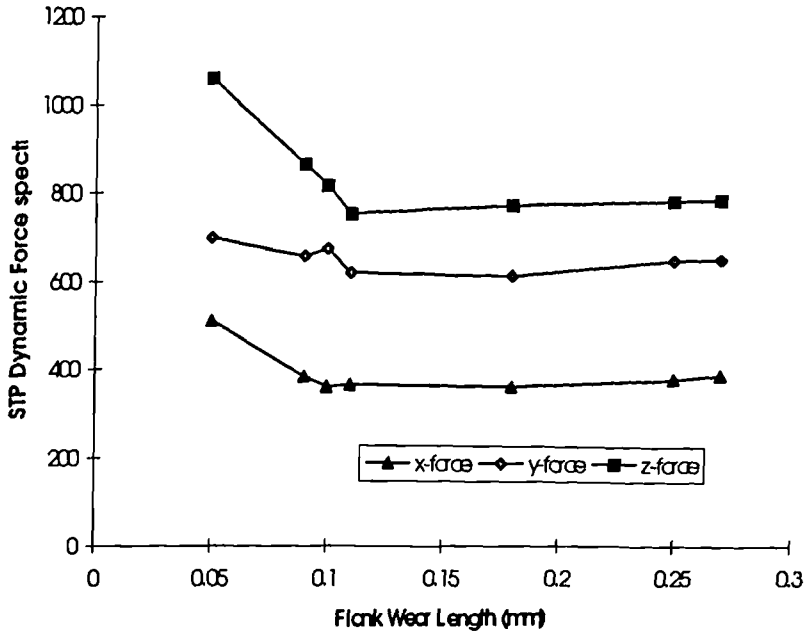

Figure 10.73: STP in dynamic force spectra Vs. Flank Wear Length (V=275m/min. & f=0.3mm/rev.)

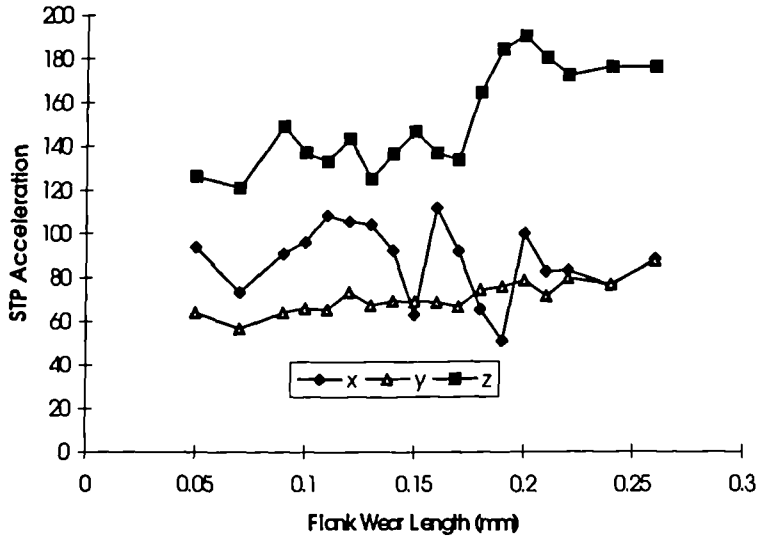

Figure 10.74: STP Acceleration Spectra Vs. Flank Wear Length (V=300m/min. & f=0.1mm/rev.)

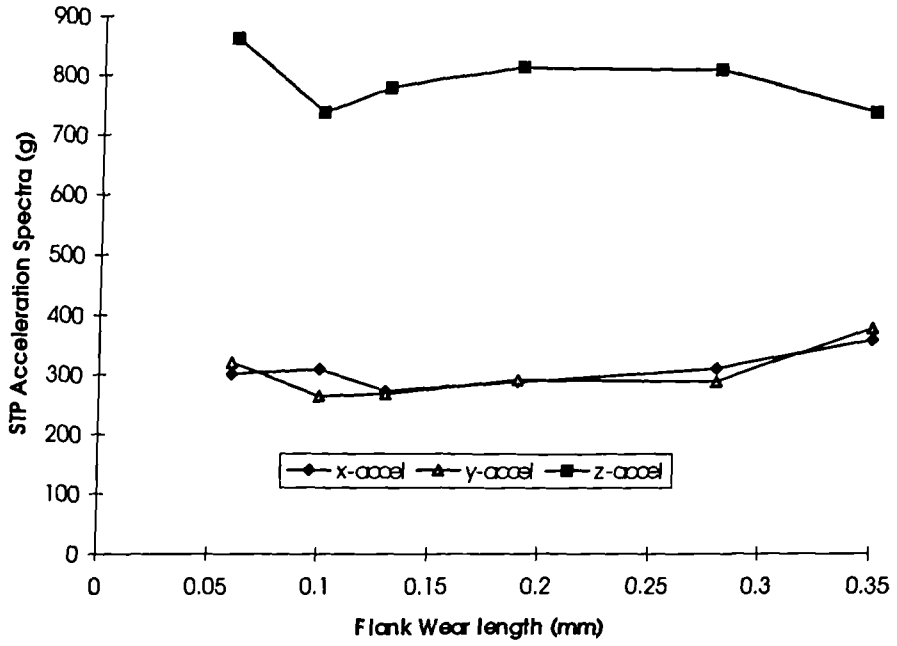

Figure 10.75: STP Acceleration Spectra Vs. Flank Wear length (V=300m/min. & f=0.3mm/rev.)

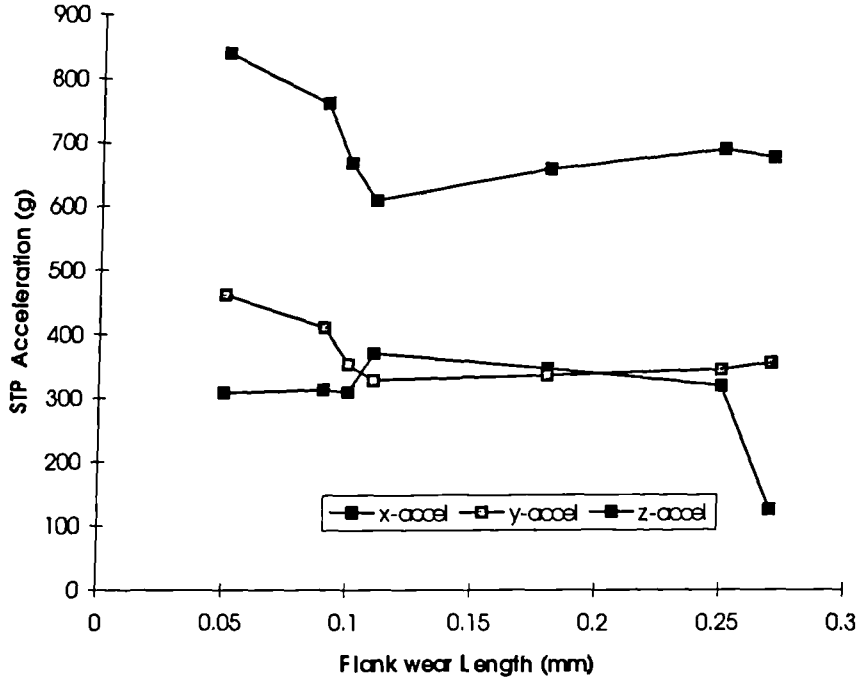

Figure 10.76: STP Acceleration Spectra Vs. Flank Wear Length (V=275m/min. & f=0.3mm/rev.)

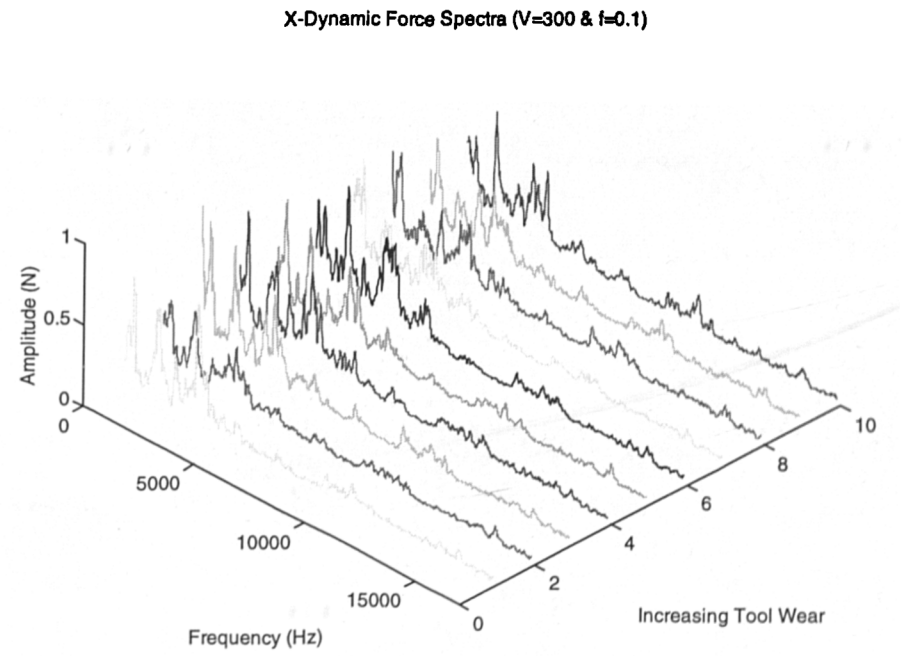

Figure 10.77: X-Dynamic Force Spectra Vs. Flank Wear

(V=300m/min. & f=0.1mm/rev.)

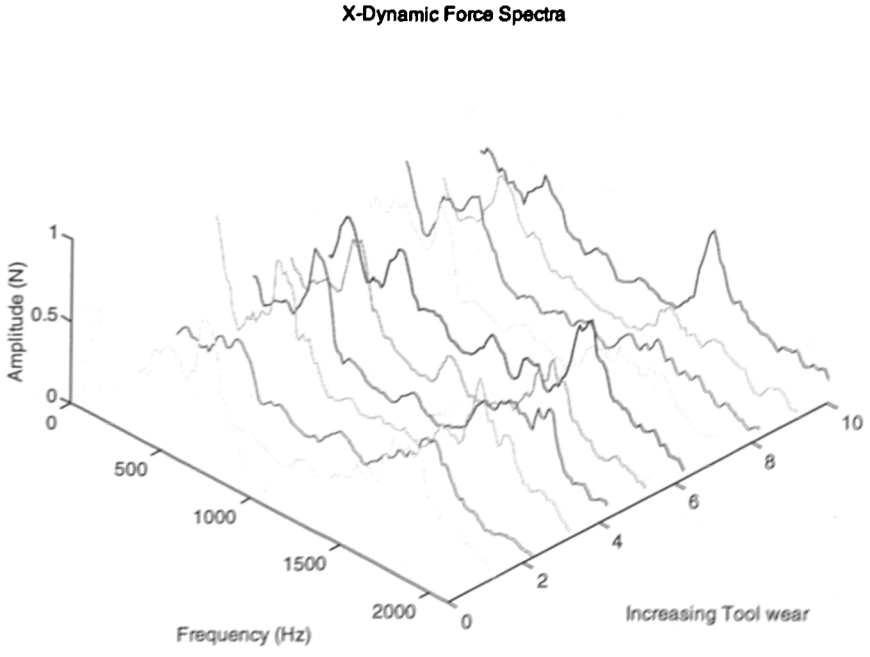

Figure 10.78: X-Dynamic Force Spectra Vs. Flank Wear

(V=300m/min. & f=0.1mm/rev.) - cut-off at 2 KHz

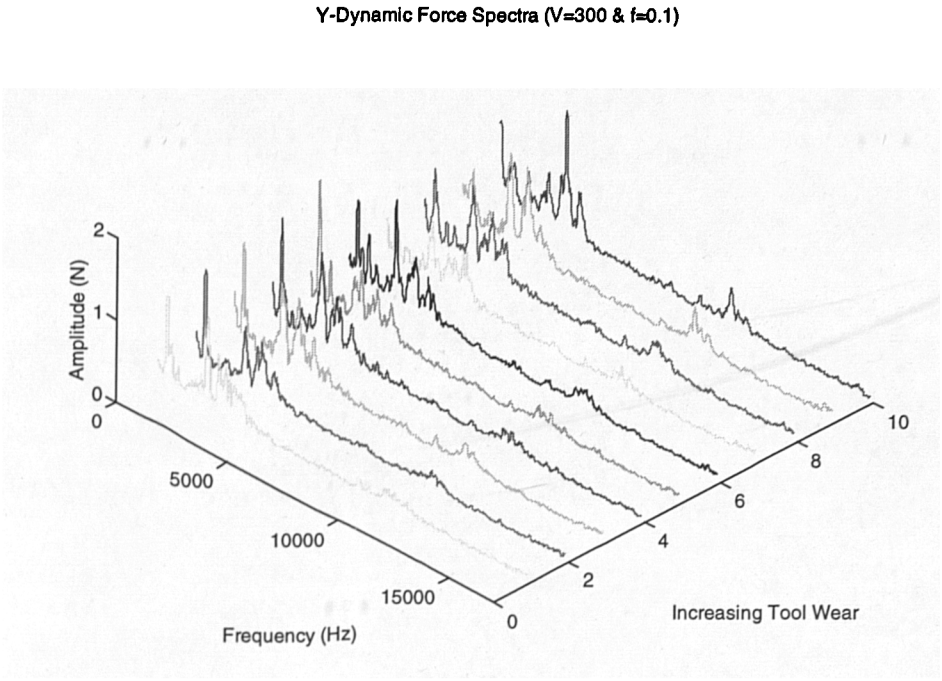

Figure 10.79: Y-Dynamic Force Spectra Vs. Flank Wear

(V=300m/min. & f=0.1mm/rev.)

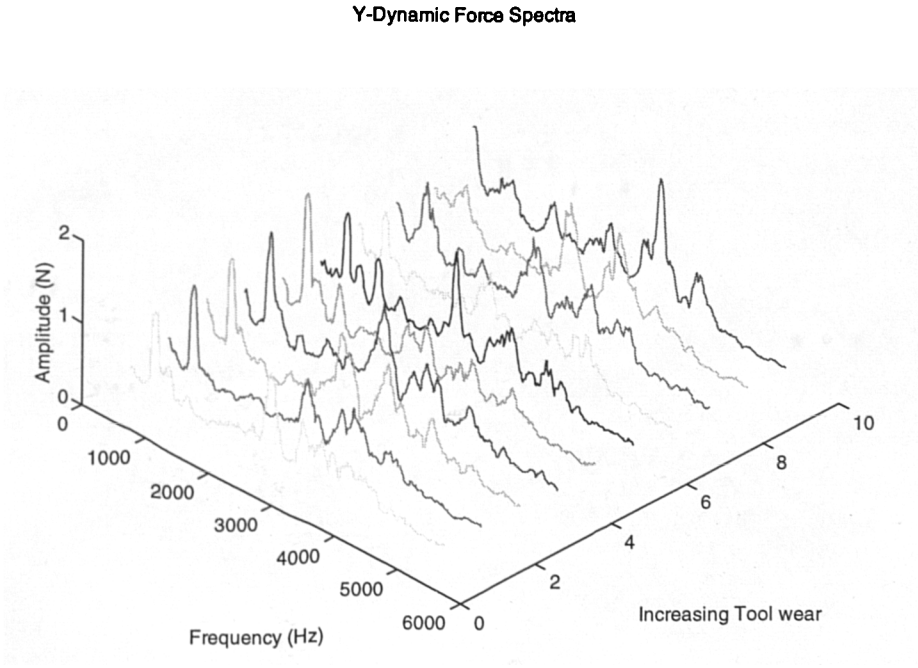

Figure 10.80: Y-Dynamic Force Spectra Vs. Flank Wear

(V=300m/min. & f=0.1mm/rev.) - cut-off at 5 KHz

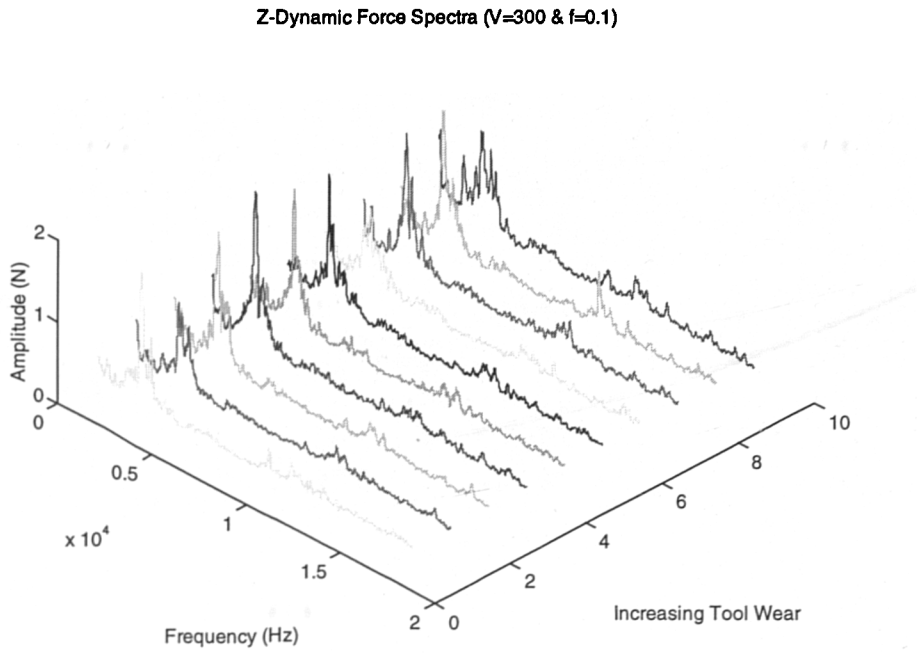

Figure 10.81: Z-Dynamic Force *Spectra Vs. Flank Wear*

(V=300m/min. & f=0.1mm/rev.)

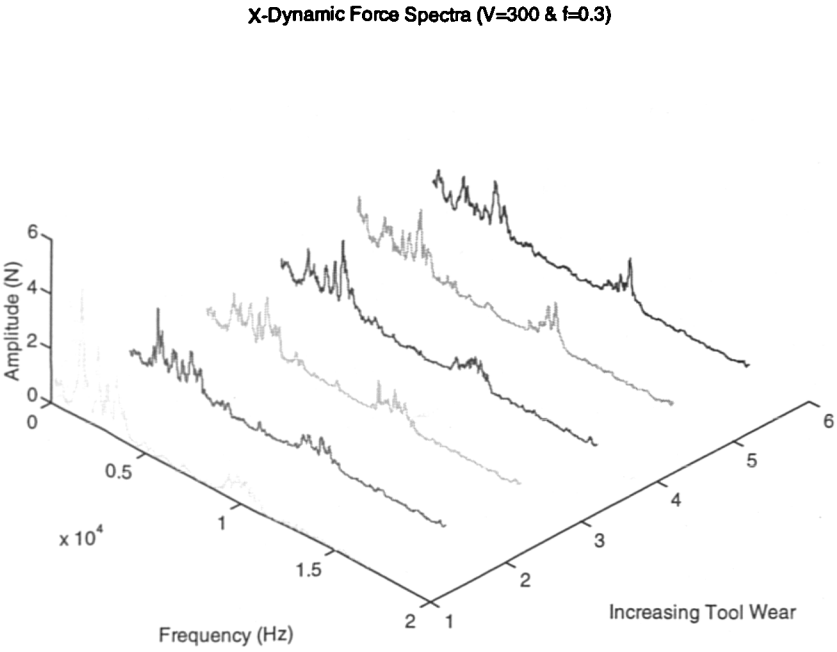

Figure 10.82: X-Dynamic Force Spectra Vs. Flank Wear

(V=300m/min. & f=0.3mm/rev.)

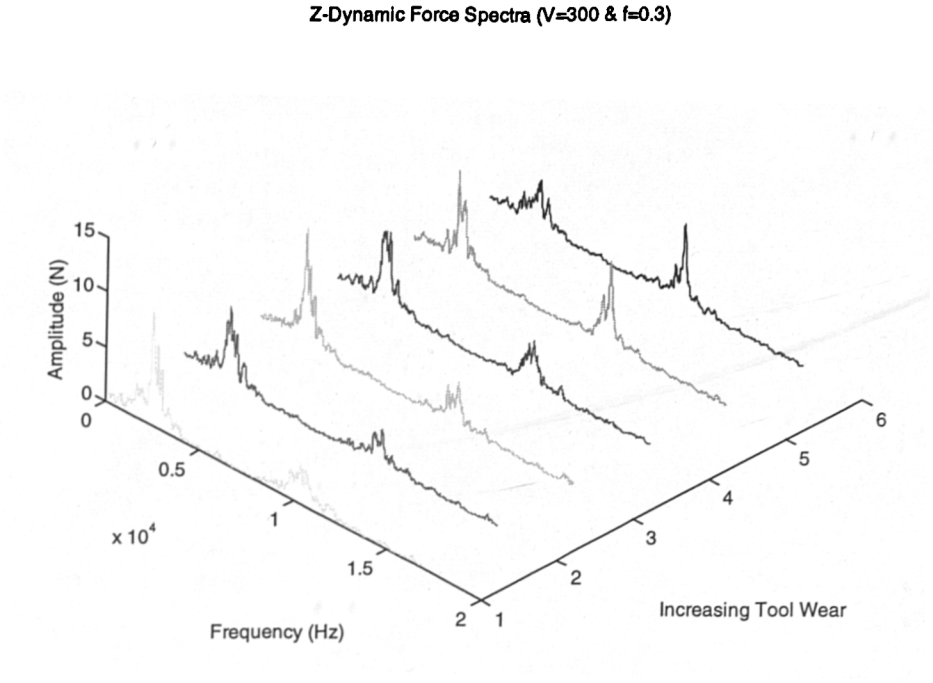

Figure 10.83: Z-Dynamic Force Spectra Vs. Flank Wear

(V=300m/min. & f=0.3mm/rev.)

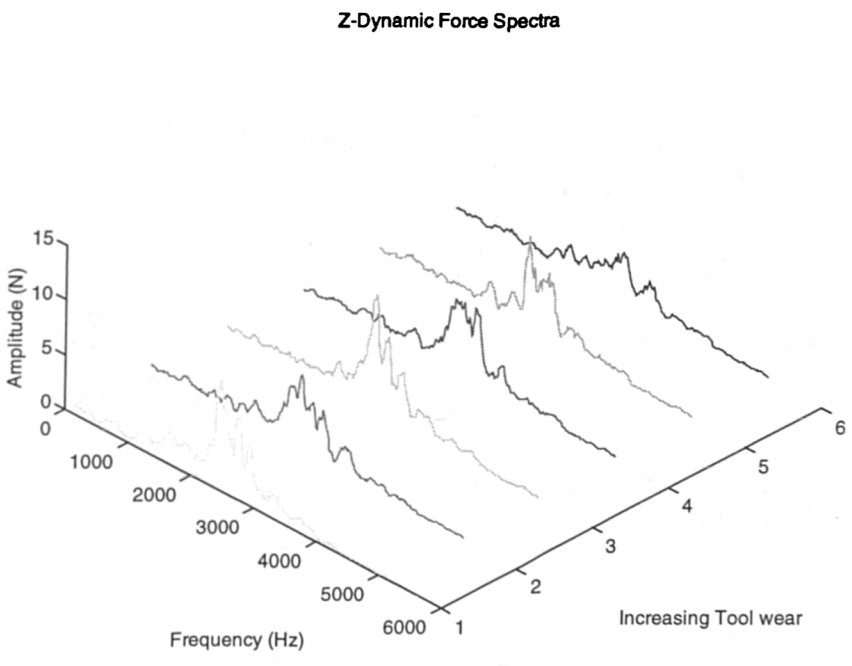

Figure 10.84: Z-Dynamic Force Spectra Vs. Flank Wear

(V=300m/min. & f=0.3mm/rev.) - cut-off at 5 KHz

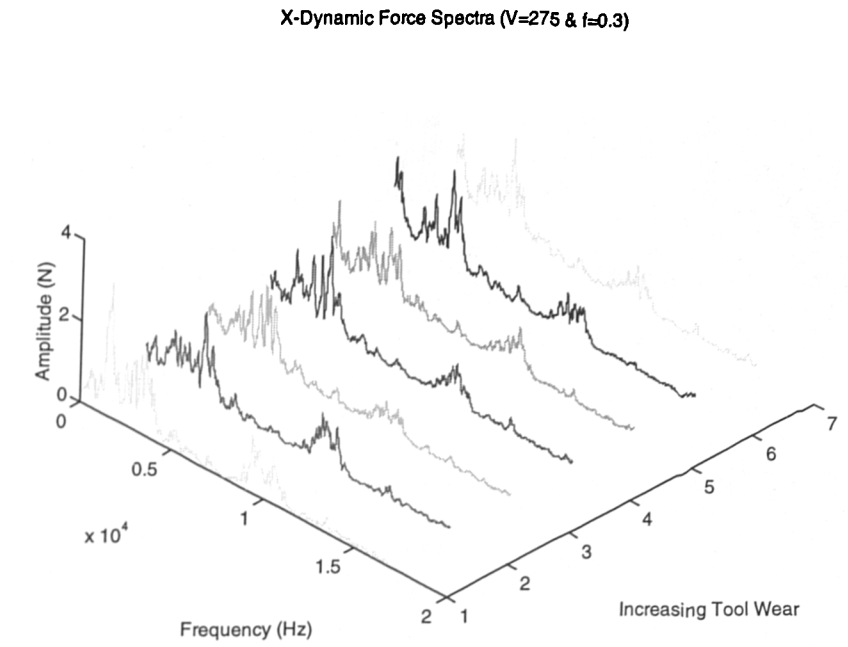

Figure 10.85: X-Dynamic Force Spectra Vs. Flank Wear

(V=275m/min. & f=0.3mm/rev.)

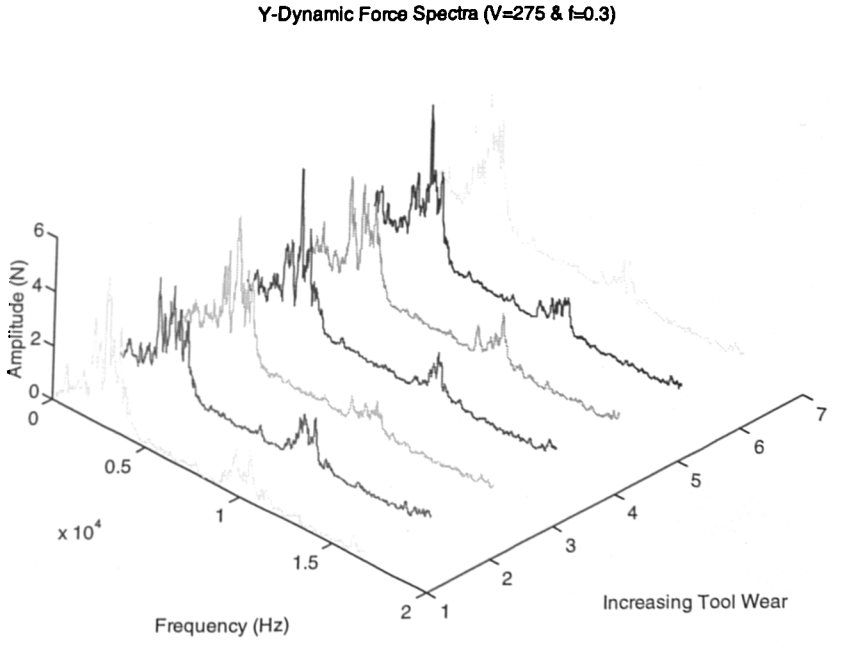

Figure 10.86: Y-Dynamic Force Spectra Vs. Flank Wear

(V=275m/min. & f=0.3mm/rev.)

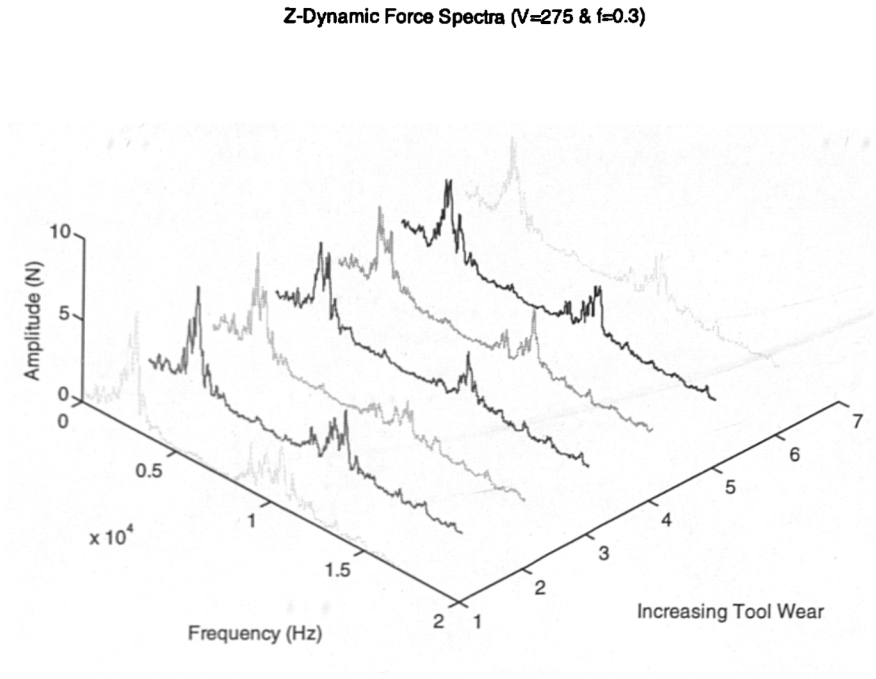

Figure 10.87: Z-Dynamic Force Spectra Vs. Flank Wear

(V=275m/min. & f=0.3mm/rev.)

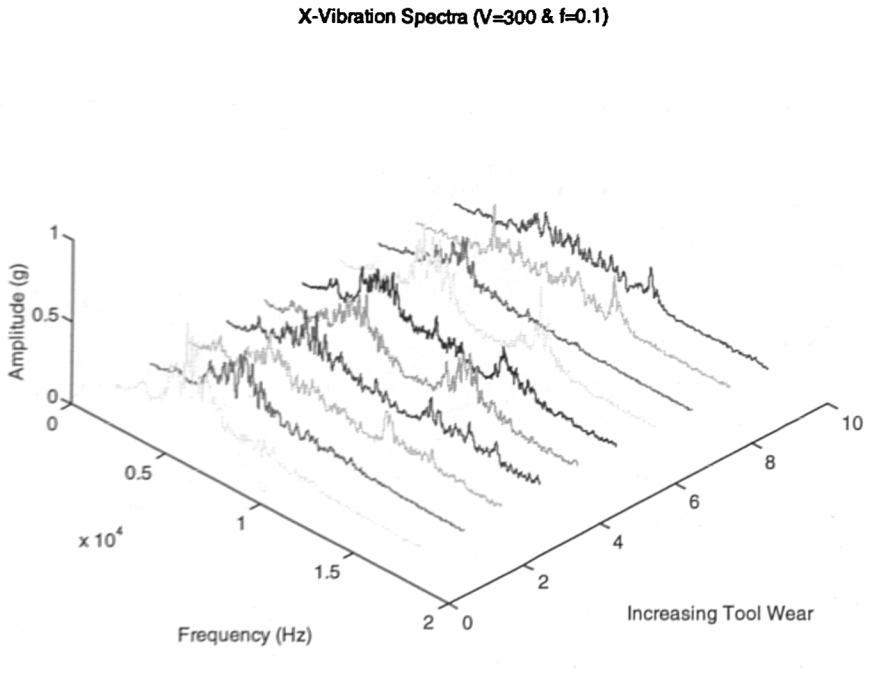

Figure 10.88: X-Vibration Spectra Vs. Flank Wear

(V=300m/min. & f=0.1mm/rev.)

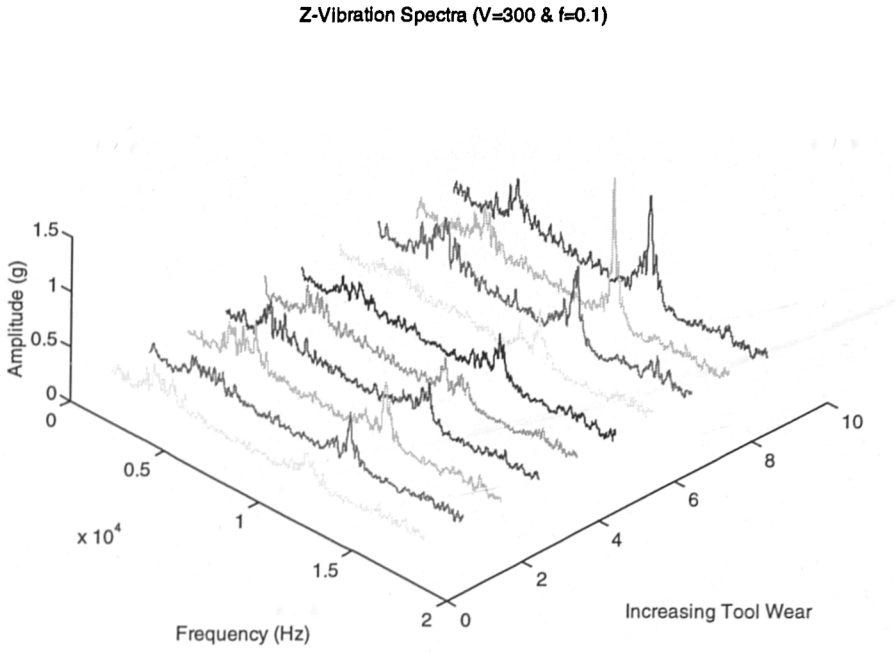

Figure 10.89: Z-Vibration Spectra Vs. Flank Wear

(V=300m/min. & f=0.1mm/rev)

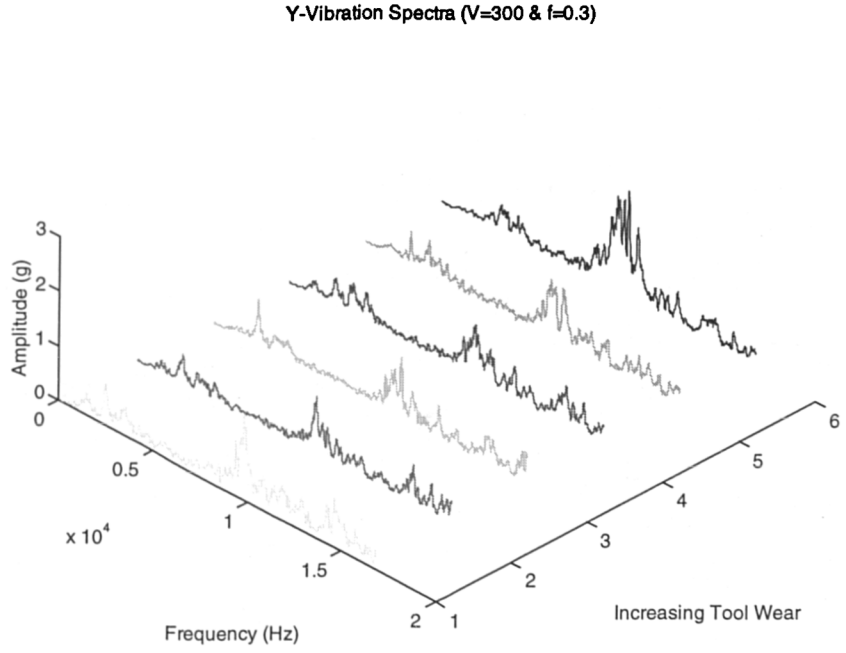

Figure 10.90: Y-Vibration Spectra Vs. Flank Wear

(V=300m/min. & f=0.3mm/rev.)

Figure 10.91: Y-Vibration Spectra Vs. Flank Wear

(V=300m/min. & f=0.3mm/rev.) cut-off at 5 KHz

Figure 10.92: Z-Vibration Spectra Vs. Flank Wear

(V=300m/min. & f=0.3mm/rev.)

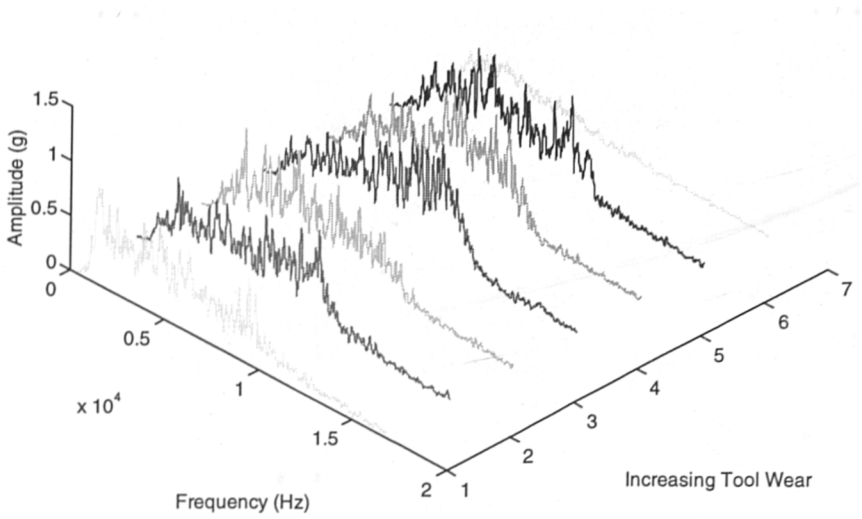

Figure 10.93: X-Vibration Spectra Vs. Flank Wear

(V=275m/min. & f=0.3mm/rev.)

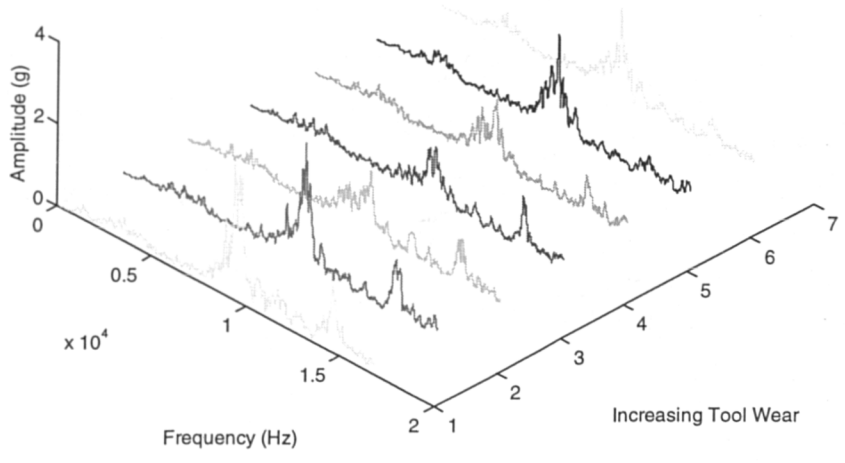

Figure 10.94: Y-Vibration Spectra Vs. Flank Wear

(V=275m/min. & f=0.3mm/rev.)

Z-Vibration Spectra (V=275 & f=0.3)

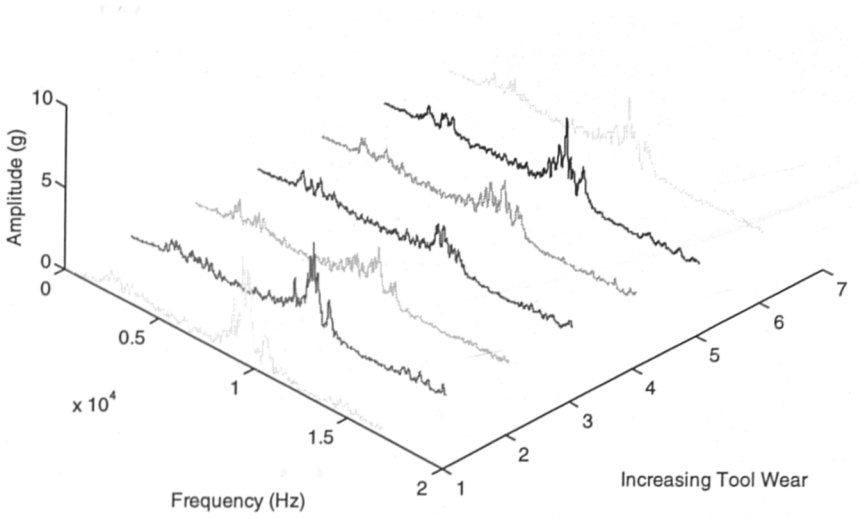

Figure 10.95: Z-Vibration Spectra Vs. Flank Wear

(V=275m/min. & f=0.3mm/rev.)

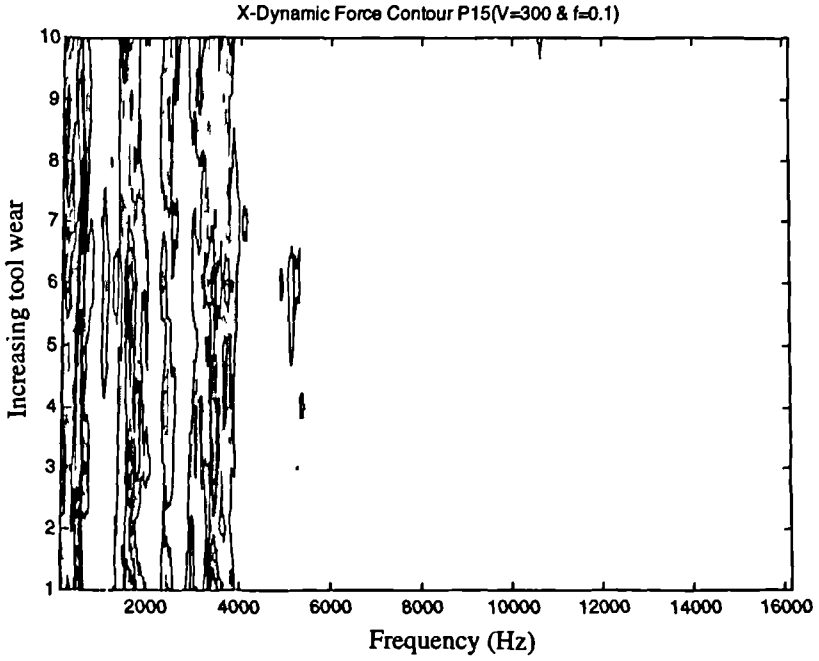

Figure 10.96: X-Dynamic Contour Vs. Tool Wear

(V=300m/min. & f=0.1mm/rev.)

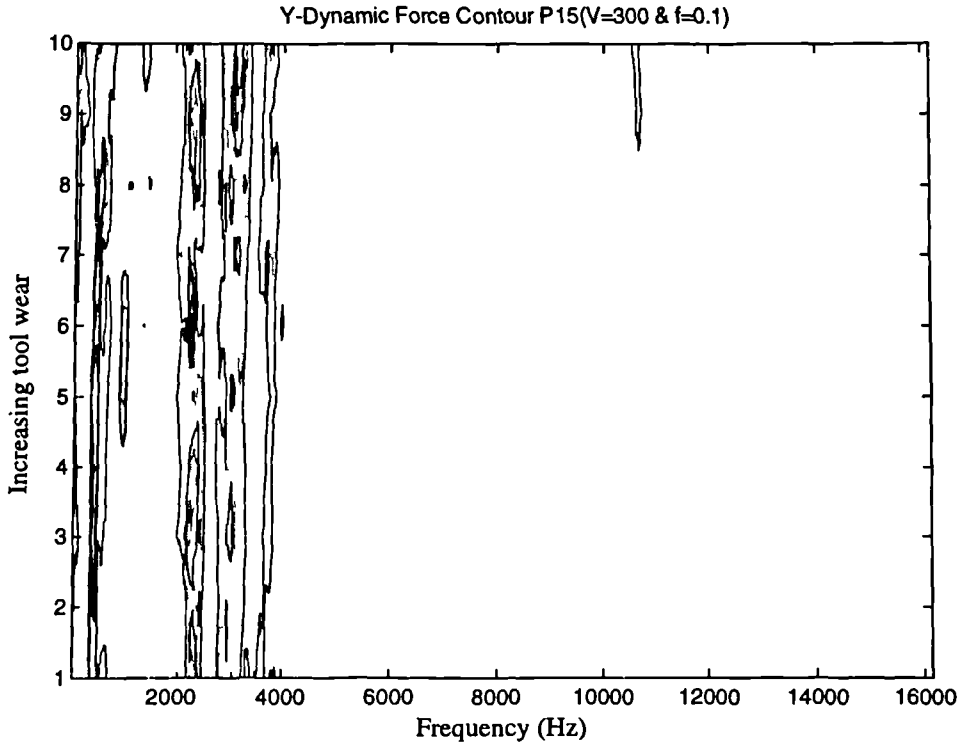

Figure 10.97: Y Dynamic Contour Vs. Tool Wear

(V=300m/min. & f=0.1mm/rev.)

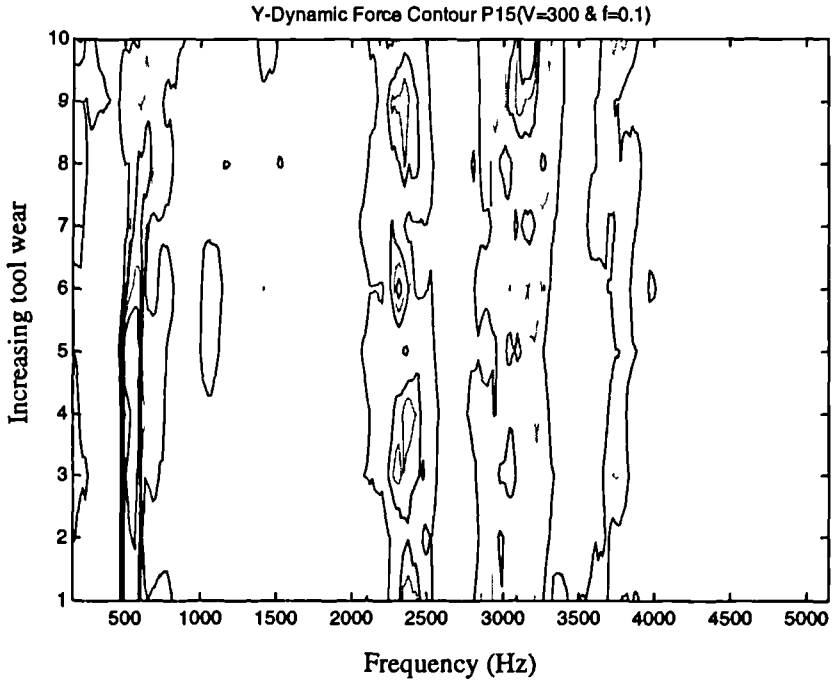

Figure 10.98: Y Dynamic Contour Vs. Tool Wear

(V=300m/min. & f=0.1mm/rev.) Cut-off at 5 KHz

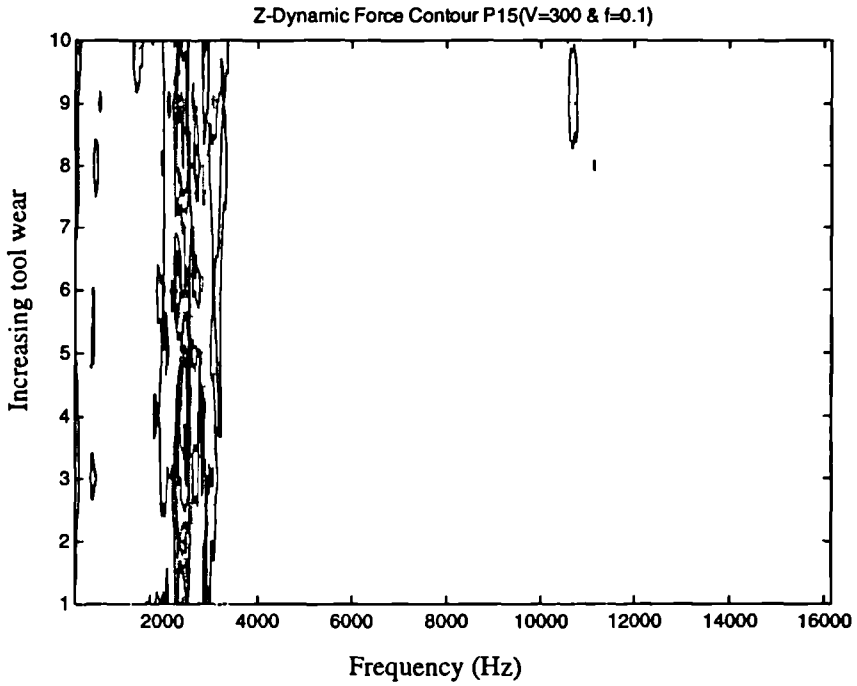

Figure 10.99: Z-Dynamic Contour Vs. Tool Wear

(V=300m/min. & f=0.1mm/rev.)

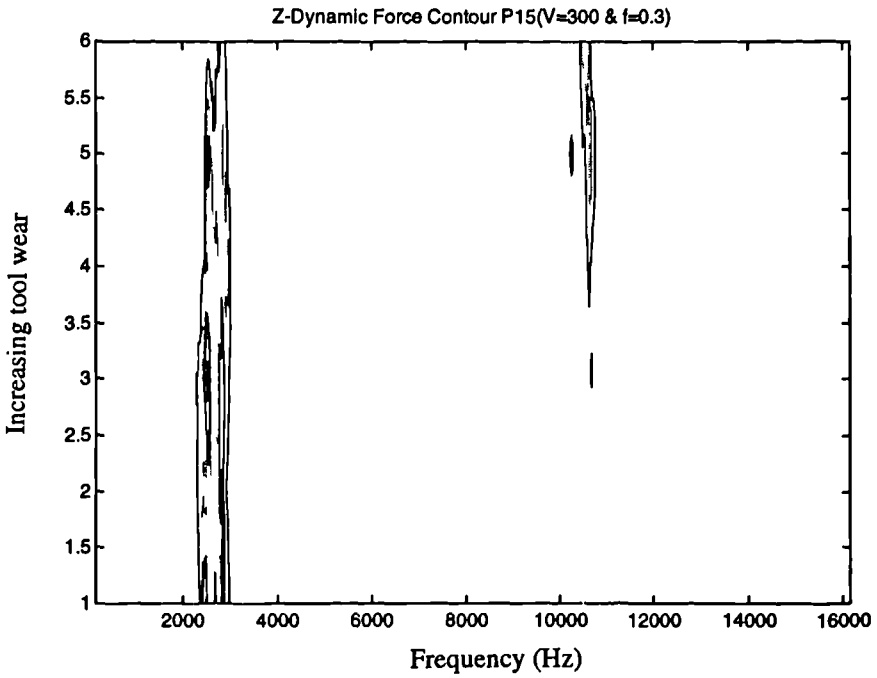

Figure 10.100: Z-Dynamic Contour Vs. Tool Wear

(V=300m/min. & f=0.3mm/rev.)

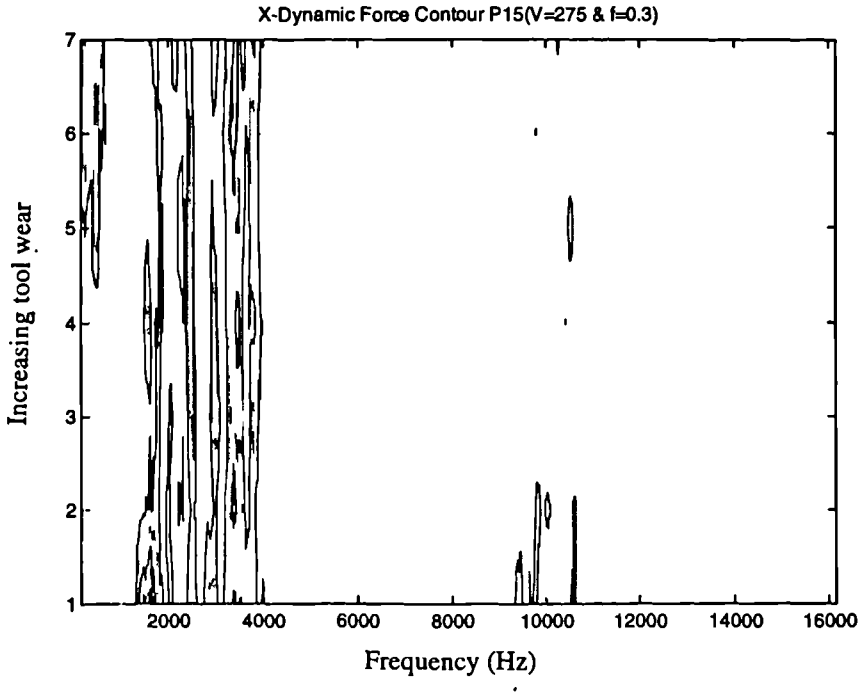

Figure 10.101: X-Dynamic Contour Vs. Tool Wear

(V=275m/min. & f=0.3mm/rev.)

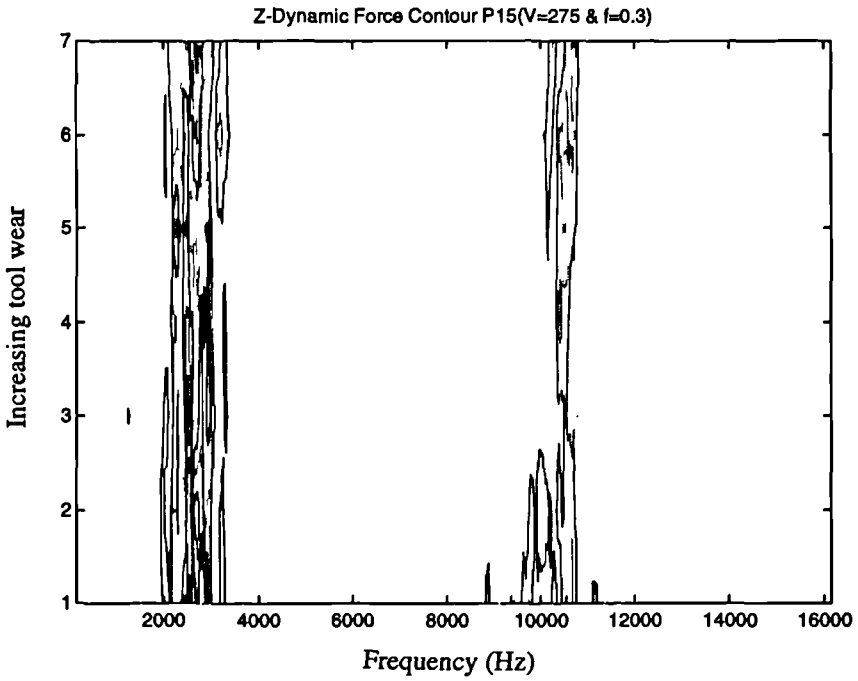

Figure 10.102: Z-Dynamic Contour Vs. Tool Wear

(V=275m/min. & f=0.3mm/rev.)

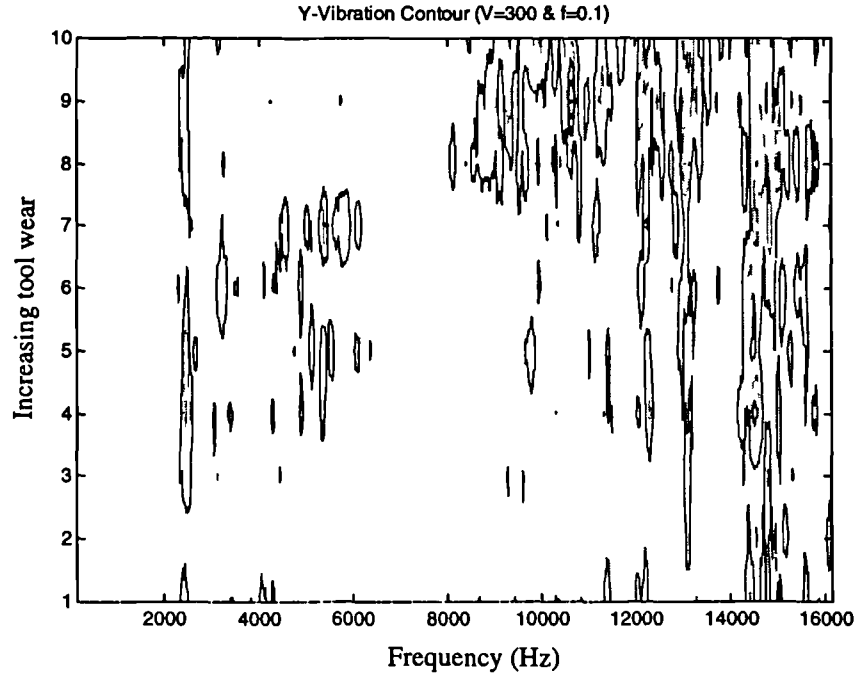

Figure 10.103: Y-Vibration Contour Vs. Tool wear

(V=300m/min. & f=0.1mm/rev.)

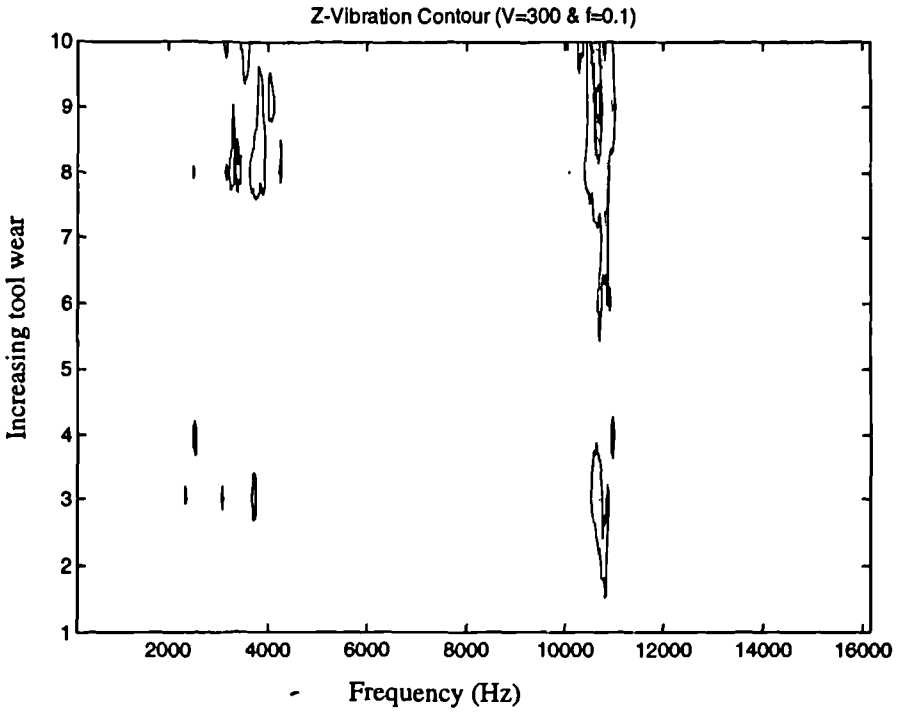

Figure 10.104: Z-Vibration Contour Vs. Tool wear

(V=300m/min. & f=0.1mm/rev.)

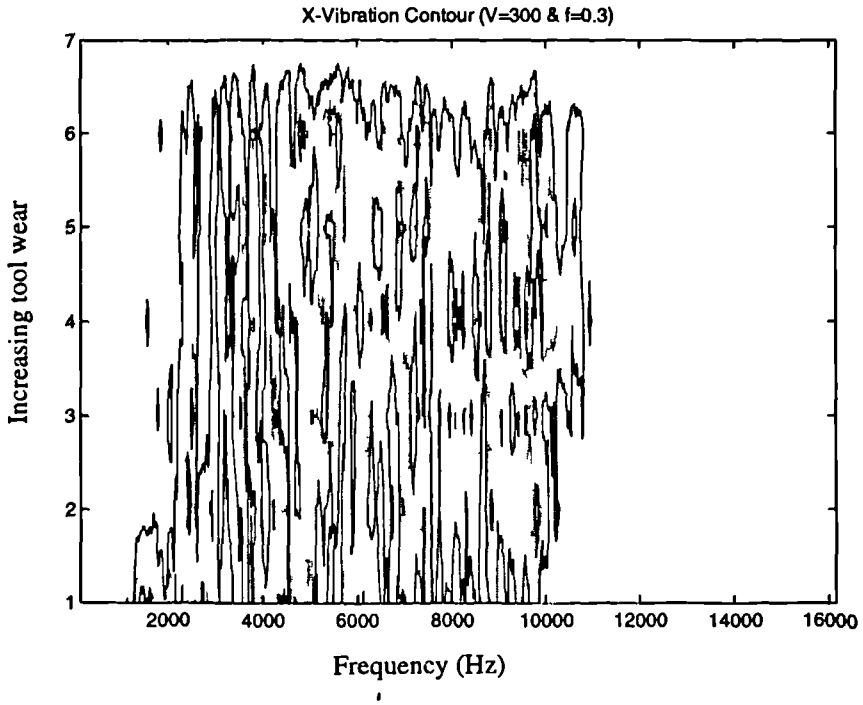

Figure 10.105: X-Vibration Contour Vs. Tool Wear

(V=300m/min. & f=0.3mm/rev.)

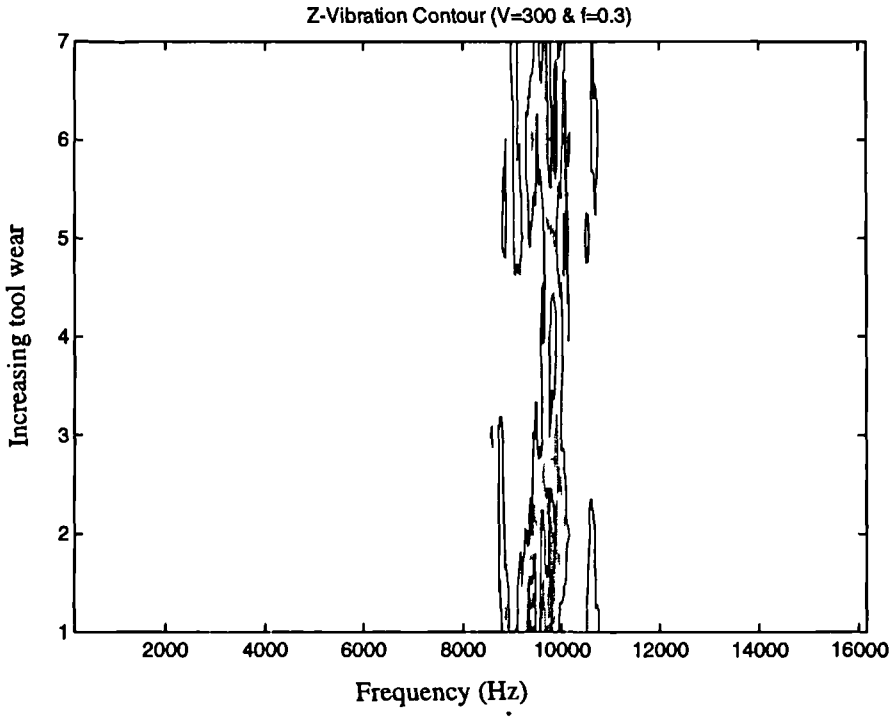

Figure 10.106: Z-Vibration Contour Vs. Tool Wear

(V=300m/min. & f=0.3mm/rev.)

CHAPTER 11

TOOL STATE CLASSIFICATION USING MLP NEURAL NETWORKS

11.0. Overview

This chapter outlines the results of the analytical investigation to attempting to develop a modular TCMS for tool state classification using MLP network. In the first part of the investigation, effort concentrates on utilising a single wear indicator, and thereafter progress to employ two wear indicators. The developed system was tested for a variety of cutting conditions and its ability to distinguish changes in tooling material and cutting conditions from those arising from tool wear assessed.

11.1. Objectives of the Investigation

Existing data on metal cutting is mostly based on plane-faced tool geometry, with flank wear often the main mode of tool life measurement. The effects of utilising chip breaker geometry insert alter the mechanics of machining, and experience shows that flank wear alone is not the single most important factor affecting tool life. In this study, experiments were conducted using P25 and P15 types of tool inserts both with chip breaker geometry in cutting EN24 steel (AISI 4340). Three different wear forms (flank, nose and notch) were measured, and occasionally, data was recorded when the tool inserts had chipped or fractured. Unlike in Chapter 8 where the tool was artificially worn to achieve desired flank wear before use in the test cuts, tests for these experiments began with a fresh insert and progressed until it was worn. The cutting conditions were incorporated in the input vector sets to ensure that the underlying process parameters would be less sensitive to changes in the cutting conditions (cutting speed, feed-rate and DOC).

The analysis of the experimental data via neural network was performed in three parts. The first phase involved using only flank wear length as the wear indicator with the task requirement being to classify the data into one of two tool classes - worn or sharp. This was followed by employing two wear indicators (flank and nose wear), and the primary task was still to classify the data into one of two tool states. The last investigation centred on expanding the wear classes to include an intermediary part-worn class, and a further class to represent the fractured/chipped tool state. The final modular TCMS and its scope of applicability was assessed and defined, by evaluating its performance and ability to recognise changes in the cutting area and in tooling material.

11.2. Classification of Worn and Sharp Tool - Flank Wear Only as Indicator

In most metal turning processes, flank wear is usually the more prevalent form of tool wear when cutting with plane-faced geometry inserts, and its occurrence is unavoidable. A judicious choice of cutting conditions and tool material can remedy other forms of wear such as cratering, frittering and notch wear. The cutting process was interrupted occasionally to record the flank wear lengths measured with the aid of a tool maker's microscope. Clearly, the tool wear process was a gradual and continuous event for which a precise transition point from sharp to worn did not exist. The decision for percentage wear on the cutting tool used as the classification bench mark as either worn or sharp was rather subjective. In the initial phase of MLP application to controlled contact insert data, an interim decision was made to categorise the data into two classes (worn/sharp) as follows:

NOMINALLY SHARP, for flank wear land length < 0.15 mm;

WORN, when the flank wear land length was > 0.15 mm.

11.2.1. Training Data

In essence, 88 data sample sets were recorded from experiments with P15 tool insert and 68 data sample sets from the P25 inserts. Of these data (156 total), less than 10% could be said to, represent worn tool state while the rest were for a nominally sharp tool. The obtained data were normalised such that the distribution for each signal was within 0.1 - 0.9 range, had zero mean with an equal variance distribution for similar learning rates and weight convergence. The samples were divided into training and test sets unavoidably containing a non-uniform distribution of worn and sharp tool data.

11.2.2. The MLP Neural Network Topology

The configuration of the MLP employed in this study was chosen from the study performed in Chapter 8. An MLP with 12 inputs, 1 binary output (representing worn {1} or sharp {0}) and a single hidden layer with 20 nodes was used. The number of hidden nodes was selected based on the experimental approach outlined earlier in Chapter 8. This essentially consisted of training several networks containing different number of nodes in a single hidden layer (1-100). The network with the least error after a prescribed number of training cycles (epoch) was selected. The momentum and learning rate coefficients were set to 0.85 and 0.2 respectively, while the Mean Squared Error (MSE) goal was set to 0.01. Connection weights were initialised through a randomised method with values in the region of -1 and 1. Network outputs from the cross-validation exercise that were not binary were rounded i.e. network predicted values below 0.5 were rounded to 0, whereas those above and including 0.5 were approximated to 1. Results are presented in Table 11.1.

11.2.3. Discussion and Conclusion of Results

Inspection of Table 11.1 shows that the best results were obtained when similar data i.e. when training and testing was performed using data obtained from

experiments with the same tool. The worst cases occurred when dissimilar data was used. This translated to success rates of 87.5% and 75% for the best and worst cases respectively. The change in test score results, it could be argued, proved that the neural network was sensitive to the tool insert type. For example, using the P15 data, the overall success rate when the network was trained and cross-validated using similar data was 87.5 %, but when cross-referenced with P25 data nearly twice as much misclassification occur. These discrepancies can be attributed to the differences in properties of the tooling material interacting with the much harder and tempered EN24 workpiece material.

Overall, with the network trained on P15 data and tested on both P15 and P25 data, a combined success rate of 83.6% (i.e. (6+13)/(48+68)) was achieved, whilst with P25 trained network, the value was 77.6 % ((22+4)/(88+28)). A comparison with results obtained in Chapter 8 would seem to contradict the findings in this study, as the cross-validation results for cross referencing (i.e. change in tooling material for the training and cross-validation sets) were lower than those obtained in Chapter 8 for the P10 trained and P40 cross validated. In the previous study, a much higher success rate was achieved when the 'softer' P40 data was used to cross-validate a mainly P10 data trained network. This discrepancy makes the sensitivity of the neural network to the tooling material rather inconclusive.

It can be concluded from this brief study that, the subjective nature of the wear threshold value and the limited number of worn tool data used in the investigation contributed significantly to the overall low success rate of the TCMS model. The employed wear criteria led to a network that was not only sensitive to flank wear levels but also to the tooling material, though in an indeterminate manner. It was deemed necessary at this stage of the investigation to expand the wear classification categories from mere sharp/worn to include two further tool state classes between the extremes.

11.3. Classification of Tool Wear and Fracture Identification - Multiple Tool Wear Indicators

11.3.1 Classification of Worn/Sharp Tool Using Flank and Nose Wear

This section extends tool wear state classification from utilising flank wear only as the wear indicator to employing flank and nose wear. Nose wear length and chipping/fracture have been incorporated into the model development, aiming for a system that would be capable of providing advanced diagnostic knowledge on the condition of the cutting tool.

11.3.1.1. Wear Data Encoding

The data used for this investigation was obtained from progressive and interrupted wear test cuts using P25 inserts ONLY and EN24 workpiece. The corresponding wear mark values for both flank and nose wear lengths were recorded and used to train and test the classification ability of MLP neural networks to the tool wear states investigated.

The first step in the data encoding process comprised setting the wear thresholds for the two wear forms. The wear mark values for the two wear forms were categorised into two principal groups as follows:

- flank wear mark value < 0.15 mm, tool insert nominally sharp,
- flank wear mark value ≥ 0.15 mm, tool insert worn (high flank),
- nose wear length < 0.2 mm, nominally sharp,
- nose wear length ≥ 0.2 mm, tool worn (nose fractured/chipped)

These wear categories were then coded in binary form as follows:

- 000 - nominally sharp (low flank, low nose)

- 100 - high flank wear,
- 010 - high nose wear,
- 001 - chipped/fractured nose,
- 110 - high flank and high nose, and
- 111 - high flank, high nose and fractured or chipped.

11.3.1.2. Results and Discussion

The data used comprised a total of 119 normalised sample sets which was divided into a training set of 50 sample sets, and a test set of 69 sample sets. MLPs with 20 and 5 hidden nodes in the middle layer, three output nodes, and an MSE value of 0.009 (<1%) were designed and simulated in the MATLAB environment, and trained using BP. Network outputs values that were not binary (i.e. 0.1 - 0.49) were manually rounded down to 0, while those in the range 0.5 - 0.99 were rounded up to 1. Results are presented in Table 11.2.

Inspection of the result indicates a significantly high classification rate for the networks investigated. The classification accuracy ranged from 89.9% to 97.1% for the individual wear categories. Recognition of flank wear scored the highest (95.8 - 97.1%). Meanwhile, nose wear was reasonably well classified achieving a minimum score of 89.9% and a maximum of 94.2%. Fracture/chipping was detected with an accuracy of 91.3 - 94.2 %.

The discrepancies in the classification results initiated the investigation of the underlying cause of the occurrence of errors, i.e. establish whether misclassifications were data dependent or network instigated. For this verification exercise an automated means of network topology selection (PREDICT) was adopted which required minimal external influence. The same pattern of errors were achieved when the network was trained and tested. This suggested that the most likely source for the errors was data dependent.

A further inspection of the mis-classified data sets was carried out for the implemented neural networks. This showed that the same data points were consistently mis-identified by all the network paradigms investigated (both user defined MLP and PREDICT chosen MLP). This coincidence was susceptible to misinterpretation and therefore warranted further investigation to establish the consistency. The following approach was adopted in order to verify the nature and characteristics of the entire data:

- Identify redundant data, and
- Reduction of the input data dimension.

11.3.2. Data Dimension Reduction

11.3.2.1. Identification of Redundant Data

The identification and elimination of redundant data as it does not contribute to the network learning was paramount. The identification of such data could in theory be performed either through network weights pruning (i.e. on-line learning and adaptations of network weights and neurons with those contributing the least eliminated) or employ a correlation-sensitivity analysis of the input-output patterns (off-line). The latter examines the weight vectors of the trained networks and eliminated links whose weights did not contribute significantly to the network learning.

Generally, when inputs are provided to a network and carry no useful underlying features, no contribution is made to the network learning by that particular input. Two approaches were employed to investigate the possible existence of such redundant sensor signal inputs in the data: cross-correlation of the input signals (i.e. measure of the extent to which signals correlate with each other as a function of time displacement) or sensitivity analysis of the input-output patterns. During training and MLP topology selection, the PREDICT neural network configuration generator transforms the input vector fields (a field here corresponded to each

component of static force, dynamic force and acceleration), into various transformed feature variable components (e.g. inverse, linear, log, ln x/1-x, etc.). A correlation analysis is then carried out on the obtained variables when building the network. The results showed that only 7 active variables (from the 12 input field) bore features that the network found useful in selecting the network configuration. These selected variables were the feed-rate, all components of the static force, x- and z-direction dynamic force and the x-direction vibration, an indication that the rest were redunctant.

A control investigation for the reduced data set was implemented using all the 12 input data, and this showed that training errors were in the order of 2, 1 and nil for flank, nose and chipped tools respectively. Testing achieved 5, 9 and 3 failed cases respectively. When the network was trained with the reduced input vectors, it predicted a training success rate of 100% for the chipped tool state, and 98% each for nose and flank wear classification. Testing however showed a drastic increase in the number of mis-classified data points, increasing by 50% to 10 each for flank and nose wear, whereas chipped state increased to 7 cases from 3 out of a total data of 68 (training and testing used the P25 data referred to in Section 11.2.1). Inspection of the failed data sets for the training set suggested that a pair of the failed testing set appear in sequence of recording to the said data. The same could not be said of the remainder of the failed cases, as they had no relationship to the sequentially recorded data. No apparent sources for the error could be immediately identified or accounted for by data inspection. The data that failed were either fundamentally different or the network simply overfitted the training data. The latter was the most plausible reason as the training and test sets were selected from a single pool of experimental results. The test and training data were swapped, and the training and test procedure repeated to find out whether the errors were dependent upon specific data points, and therefore avoidable. Exactly the same rate of classification were achieved as before. It could therefore be argued that, the network actually over-trained and over-specialised.

11.3.2.2. Reduction of Input Data Dimension

The goal was to establish and identify any unusual peculiarity in the input data that could otherwise affect neural network learning. The investigation primarily concentrated on identifying outliers in the entire data range through application of bar chart plots, cluster and discriminant analyses, and feature maps (Kohonen Feature Maps) to determine conspicuous data points. Bar charts of the inputs were constructed which gave an indication of the magnitude of each input compared to the rest of the inputs. None of the bar chart plots seemed to suggest a uniquely occurring outlier in the entire data set or gave any indication to suggest an association with outlier. The nature of data clustering using a single linkage dendrogram and re-scaled distance cluster combined was also employed together with feature maps. No data point seemed to have any peculiar characteristics that might suggest the existence of outlier data. It was therefore concluded that the failed data points were overlapped data classes i.e. worn and sharp, worn and chipped.

Finally, the use of binary codes and the implementation of a logistic sigmoid transfer function, it could be argued, were incompatible as the binary network outputs represented extremes of the sigmod function (Figure 4.11). Rounding the network outputs though desirable, was not the right thing to do. Instead, a threshold point should have been determined and established. A careful inspection of the actual network output results before rounding showed that about 50% of the failed cases actually had values of between 0.25 and 0.49, 'the ambiguity zone', which were rounded down to zero. When compared to actual wear values as displayed on a typical wear-time plot with a gradual wear increment (Fig. 6.1), instantaneous wear mark values are continuous rather than abrupt as binary coding implies.

11.3.3. Conclusions

The following conclusions were deduced from this study:

- It was found that in order to identify the input data features that the neural network utilises during learning and subsequent generalisation, it was necessary to exclude inputs that did not contribute to network learning.

- Data used in this investigation was checked for characteristics that otherwise present (i.e. such as outliers or a minority of data containing features uniquely common to them alone) would cause the network to over-specialise and therefore undermine the general trend of the bulk of the data. This would inevitable lead to higher mis-classification. It was found that, no outliers existed in both training and test data sets.

11.4. Tool State Classification Using Multiple Membership Classes For Flank and Nose Wear Measurements

This section describes the results of the investigation that involved expanding the wear classes for each of the two wear forms to include an intermediary category depicting partly worn tools. The automated neural network model builder (PREDICT) was used, and the selected variable fields compared to the assessment of tool wear sensitivity of the sensors performed in Chapters 9 and 10.

11.4.1. Wear Data Encoding

The flank and nose wear forms were categorised into three classes viz. - nominally sharp, part worn or medium wear, and severely worn. The fractured/chipped states were individually represented.

A two bits binary code was used to encode the wear mark factors as follows:

Flank wear

Wear mark value (mm)	Tool state (wear level)	Binary code
< 0.1	nominally sharp	00

0.1 - 0.15	medium	10
> 0.15	high/severe	11

Nose wear

Wear mark value (mm)	Tool state (wear level)	binary code
< 0.1	sharp	00
0.1 - 0.2	medium	01
≥ 0.2	high/severe	11

When the two wear types and their various representations were combined, a 4 bits binary coding below was achieved.

0000	low nose/flank
0001	low flank/medium nose
1000	medium flank/low nose
1001	medium flank/nose
1101	high flank/medium nose
1011	medium flank/high nose
1111	high flank/nose (chipped/fractured)

Thus, an additional output was included depicting the presence/absence of chipping/fracture.

11.4.2. Results and Discussion

The experimental data and their respective tool state (binary coded) were randomised such that the same pattern of data did not appear in sequence of recording. The automated method of variable selection and transformations was performed. 60 data sets were used to train and 59 to test. During network building and training, a comprehensive variables search and transformation was performed.

The model selected 10 active transforms from 7 active fields (cf. 12 input fields). A summary of the transformations is presented in Table 11.3. The chosen MLP configuration was 10:24:5 with a design test success of 95.81%. Learning was through adaptive gradient, utilising a sigmoid transfer function. The MSE reached was 0.003 and, implementation of direct and cascaded connections was performed with weight decay values of 0.01 for the outputs, and 0.05 for the hidden nodes. The learning rate coefficient was 0.01. The trained network was tested using previously unseen data.

From the training results, 3 misjudgements were recorded: 1 misinterpreted flank wear (sharp rather than medium) and two nose wear. The test results had a higher proportion of misjudgements compared to the training set. Eight misclassifications were made on flank wear identification, 6 on the nose wear and 3 for tool chipping.

For comparison, the MATLAB neural network was trained using all the 12 inputs as well as a separate network trained with the active inputs fields from the automated system only. With all 12 inputs, no training misclassification occurred. The testing with unseen data achieved 9, 8 and 1 errors for flank, nose and chipping identification respectively. Using the 7 active field input, the errors were

8, 13 and 7 respectively for flank, nose and chipping classification. Overall, this represented an increase in the misclassification of nose and chipping.

Clearly, the nature and type of inputs seem to alter the network learning abilities. One would have assumed that, using only the inputs seemingly containing useful variables, as identified by the automated system, compared to when all input fields were used, the former would yield better results. In terms of training, both networks successfully trained and converged to MSE = 0.009 fairly well, with no training classification errors. No immediate reason could be put forward that would reliably account for the increase in misclassifications with reduced input fields. The main question however was why the network selected the variables that it did. A study and comparison of the automated selected variables was made to their wear sensitivity. A summary of the wear results discussed earlier in Chapter 10 was reproduced (Table 11.4) for comparison. Numbers were assigned to process parameter's sensitivity to wear as follows: 3- when most sensitive and 1-when least.

From Table 11.4, the x- and y-static force, the y- and z-dynamic force, and the y- and z-vibrations reportedly showed most sensitivity to both flank and nose tool wear. The results of the effects of the cutting conditions on the sensor signals were also reproduced, and shown in Table 11.5. The sensitivity matrix indices for cutting process parameters, again showed a varied response. The total response recorded in the analysis shows that the x- and z-static force, the y- and z-dynamic force and the x and z-vibrations were sensitive to the cutting conditions.

The effects of cutting conditions and wear on the sensor signals can be combined by adding corresponding weightings vector (Table 11.6), and the most sensitive sensor component to both process parameters and tool wear deduced. Inspection of Table 11.6 showed no similarity to the transformed and selected variables (Table 11.3) obtained from the PREDICT automated system. The automated model generator simply does not employ the principal component of the sensor

signal, but instead develops alternative sets of transforms according to user defined level of complexity (exhaustive, comprehensive, etc.). It then selected and combined those variables that produced the best network output through application of genetic algorithm (GM). GM is loosely based on some aspects of the evolution processes where a set of variables derive their fitness from how successful a model can be built based on just those variables.

To investigate which variables were important during training in the MATLAB model, it was necessary to deduce the contribution of the weight matrices from the input to hidden layer connection. Those that contributed significantly to the learning process ought to have high weight values, while the less important ones have small connection weights. The sum total in the weight connections from each input to the hidden layer were as follows: 7.3, - 15.4, 0.2, 19.8, 7.2, - 3.8, 15, 34, - 18, - 5.5, 15 and 14 - for speed, feed-rate, DOC, x-, y-, z-static forces, x-, y- and z-dynamic forces, and x-, y- and z-vibration respectively. This clearly showed that the third input did not contribute to the learning process as its weight vector was very small. This represented the link for the DOC that was kept constant in all the experiments conducted. Similarly, if a threshold of $\pm$ 10 was set, for example, as a value beyond which that particular weight vector affected learning, then, only the feed-rate, x-component static force, x-, y- and z-components of the dynamic force, and the y- and z-components of acceleration contributed to the network learning. These inputs compared fairly well with the active fields selected by the PREDICT automated system.

11.4.3. Conclusions

A comparison was made between the results, input features and general neural network topology of an automatically generated MLP, and a user determined MLP neural network model. The automated system selected features from the input fields after performing data analysis by creating transformed data sets that were then used to train the network. The generated features selection could be viewed

as an extension of dimension features selection with more than one active input selected from the same field in any given instance. The user determined MLP model on the other hand performed training and testing according to user instructions utilising the principal components of input fields. Similar results were achieved by both models. However, when the user designed system was instructed to make use only of inputs that the automated system suggested were most effective in learning, its performance deteriorated.

11.5. Scope of TCMS Model Applicability

In this part of the investigation, the focus was on testing the scope of applicability of the modular TCMS model. The sole aim was to establish whether or not the model had any potential for broader applicability (i.e. response to changes in the cutting environment). The testing exercise concentrated on feeding data from the considered scenarios to an already trained network, and the following two themes were investigated:

- The ability of the neural network model (trained on P25 data) to categorise and classify tool wear when fed with P15 data (tooling material effect).

- Test the ability of the neural network model to distinguish both increments and decrements in process parameters brought by new cutting conditions (i.e. not encountered in training) from tool wear events.

11.5.1. Effects of Tooling Material on the Trained Model

The first line of investigation involved presenting the trained network with data from experiments where the tool insert used had been changed (P25 training to a P15 type) for testing. The data required for the investigation was already available as it had been collected together with those used in the training performed earlier. Inspection of the neural network predicted tool wear states indicated that overall, the model was capable of reasonably accurate tool wear

classification when fed with P15 data, though it had been exclusively trained with P25 data. Changing the tooling material did not significantly affect the network's performance in recognising tool fracture/chipping events in particular. The network classified the presented data for fracture/chipped tool state with an accuracy of 93% (4 mis-classified cases only). For sharp and partly worn tool states, the network was incapable of reasonably distinguishing the tool state classes. In so far as severely worn tool categorisation was concerned, the network scored a 100% recognition accuracy, but this dropped dramatically when the network was presented with sharp and nominally worn tool state data. In most of the instances, it misappropriated nominally sharp and partly worn tool state to severely worn.

11.5.2. Effects of Cutting Conditions on the Trained Model

The second part of the validation was concerned with the trained network's ability to distinguish changes in the cutting conditions as opposed to those emanating from wear events. Incorporation of the cutting conditions into the input data pattern and the subsequent normalisation of the data was aimed at reducing model sensitivity to significant changes in the magnitude of either process or cutting parameters. During the course of this investigation, it was established that the cutting speed did not seriously effect changes on the process parameters if the cutting speeds were over 200 m/min. The feed-rate and DOC significantly affected the sensor signal and largely determine the area of cut. It was therefore necessary to investigate the effects of a change in the area of cut on a trained model. Successful implementation of this exercise would provide valuable insight into the potential applicability of the TCMS model.

11.5.2.1. Reduced Cutting Area Effect on Trained Model

Initial investigations were carried out using interrupted test cut data with a DOC of 1 mm , cutting speed of 250 m/min and feed-rates of 0.1 mm/rev, 0.2 mm/rev

and 0.3 mm/rev. During these tests, the flank and nose wear lengths were measured and recorded.

Inspection of obtained results showed that the network was capable of distinguishing without any ambiguity a change in feed-rate. The network could in addition to distinguishing feed-rates, recognise the progressive wear mark increments for the two forms of tool wear investigated. Evidence of this process was the fact that the predicted network outputs could be seen to progress from nominally sharp tool states to severely worn and fracture. The network was better at nominally sharp tool classification as it scored 100% success accuracy. As the tool wear increased, the network's performance became much more erratic and its accuracy deteriorated, scoring only 63% accuracy for chipping/fracture classification.

A reduction in the area of cut brought about by a change in the DOC resulted in more erratic network performance than that brought about by changes in the extent of tool wear. The changes are in effect, more pronounced (i.e. represent an absolute change in magnitude). Another possible cause of the erratic behaviour lies in the nature of the process parameter changes. While tool wear is a gradual process and the process parameters generally change gradually, a change in the DOC results in an abrupt change in the process parameters as does tool failure.

Compared to the test results of the training conditions, data from test cuts performed with a DOC of 1 mm, were poorly identified and classified. Nominally sharp tool states were recognised and correctly classified with an accuracy of 100%. As tool wear mark increased, the recognition and classification rates deteriorated. Chipped and fractured tool state classification accuracy decreased to 63% success only. A 1 mm DOC implied that the cutting process was primarily limited to the nose region of the tool and therefore complicated, thus, possibly adding to the erratic nature of the predicted results.

11.5.2.2. Increased Cutting Area Effect on the Trained Model

As the cutting process for a DOC of 1 mm involved complicated cutting mechanics, the results were difficult to interpret. It was sensible and logical to use higher DOC. There was no need to take measurements of the nose and flank wear lengths since interest laid in the ability of the network to recognise an increase in the cutting area. The collected data for DOC of 3 mm and 4 mm, feed-rates of 0.1 mm/rev and 0.2 mm/rev and speed of 250 m/min were normalised as per training and previous sets, and then fed to the trained network. The primary aim was to find out whether it was possible that a network trained to recognise tool wear changes by observing both the process and cutting conditions parameters could detect and differentiate a change in DOC from a change in tool wear level.

A new tool face was used for each cut in order to minimise the effects of tool wear on the sensed sensor signals. It was not however possible to conduct tests at 0.3 mm/rev feed-rates as the tool often fractured at the start of the cutting. Inspection of the results seemed to indicate that well over 90% of the data was mis-classified. Further inspection showed that the bulk of the correctly classified data occurred at a DOC of 3 mm and feed-rate of 0.2 mm. These data points would appear to fall within the range of those used in training the network (V = 350m/min and 275 m/min, feed-rates of 0.1 mm/rev, 0.2 mm/rev and 0.3 mm/rev and DOC of 2 mm).

Further inspection of both results (for increased and decreased DOC) show that, for reduced cutting area compared to the training conditions, the network generally classified the nominally sharp tool state data correctly. On the other hand, increasing the area of cut led to a very poor tool state classification (< 10% correct identification). It could be concluded therefore that a network trained for tool wear recognition incorporating cutting conditions as inputs is unable to classify tool state when the area of cut is increased. Increases in the area of cut

were interpreted as a failed tool, primarily due to the increased magnitude of the cutting forces and vibrations originating from increasing the area of cut.

11.6. Identification of Change of Area of Cut through Classification of DOC

The previous section suggested that a TCMS was unable to classify tool state accurately when the area of cut is changed compared to those used in the training. A brief investigation was conducted in order to verify the ability of a purposely trained neural network model for DOC identification using as inputs process parameters, feed-rate and the cutting speed. New test cuts were not required as data had already been acquired that contained information when cutting was conducted at four different DOCs (1 mm, 2 mm, 3 mm and 4 mm). The combined data was randomised and divided into a training and test set comprising 100 and 110 data sets respectively.

An automated neural network model selection approach was adopted with no prior knowledge of the network topology. During the investigation, an MLP with 9 inputs, 28 hidden nodes in a single hidden layer and 1 real number output depicting the DOC was selected. The activation functions used were logistic sigmoid (with option to change to softmax with cross-entropy error of <1%). The nine active transforms selected were chosen from 6 active fields and were as follows: 1 feature from cutting speed, 2 features from the feed-rate, 3 feature from the x-direction static force, and 1 feature each from the y-dynamic force, x-vibration and z-vibration.

The approach in this investigation compared to previous model building shifted to predicting the DOC values rather than classifying them into the defined four categories. Two main reasons were taken into consideration when devising this method. Firstly, the nature of the data for some categories of the DOC were such that it had not been reciprocated in others, i.e. for DOC of 1 and 2 mm, the data contained information on more than one wear event and tool wear form,

compared to those for DOC of 3 and 4 mm which contained information exclusively on nominally sharp tool state. Secondly, changes in DOC had a greater impact on the magnitudes of the process parameters than gradual tool wear events, and previous studies showed that neural network models responded more erratically to DOC changes than for the more discrete wear events. Thus, by aiming to predict the value of the DOC, the model's sensitivity to the input data fields could be explored.

A comparison of the network predicted DOC and the actual DOC values was carried out. An initial attempt was made to compute the true error of the predicted DOC and the desired DOC (as a percentage). This, it was hoped, would give an indication on how successful the prediction had been. However, it was difficult to relate the obtained error to the whole data range as it varied from <1% to >20% in some cases. The approach adopted was to convert the predicted values of the DOC and compare them to the actually implemented values. The actual integer values of the DOC were obtained by reverse normalisation of the network outputs (i.e. multiplying the predicted and target DOC by a normalising factor).

Inspection of the results show that, considering just the training data, only 2 of the data's DOC were wrongly predicted (98% correct predictions). The network under-predicted the DOC by one step (i.e. 2 instead of 3) in one case and then over-predicted by a single step ahead (4 instead of 3) for the other. When the model was presented with un-seen test data similar in content distribution to the training set, the network predicted 11 wrong DOC values out of the 110 data sets supplied (i.e. 90 % correct prediction). Further inspection of the individual wrongly predicted DOC values was performed. Out of the 11 mis-predicted cases, 7 were single step ahead predictions, one was a three-step ahead prediction and the remaining three were 1 step under-predicted.

Overall, the network model accurately predicted the DOC and if used in parallel with the tool wear identification model, represents a TCMS with a broad scope of application.

11.7 CONCLUSIONS

- Network training conditions (i.e. initial network weights, number of hidden nodes, MSE) determines the success of the network classification. In this investigation, it was found that depending on the specified MSE and number of hidden nodes, different classification rates were achieved for each paradigm.

- The neural networks' attempt to classify the tool data as simply worn/sharp can not be considered to satisfactorily fulfill the requirement for TCM. It was necessary to establish ANN's capability and suitability to perform total TCM as it was able to distinguish sharp, part worn, worn and fractured tools.

- The inclusion of the cutting conditions as independent input fields in developing the TCMS model with the sole aim of broadening its scope of applicability was not realised. The investigation conducted showed that the TCMS model was still sensitive to changes in the cutting conditions.

- The cutting conditions individually carry unique characteristics required by the model for knowledge acquisition. The most sensitive of these parameters appears to be the DOC and the least sensitive being the cutting speed.

- Normalisation of the data did not enable the application of the model independently of the cutting conditions but eliminated saturation of the neural network activation function.

Table 11.1: Results of cross-validation

	No. failed cases/Total No. of data	
Training Data (No.)	P15 Data ONLY	P25 Data ONLY
P15 Data ONLY	6/48 = 12.5%	13/68 = 18.1%
P25 Data ONLY	22/88 = 25%	2/2813/68 = 14.3%

Table 11.2: Percentage of tool wear classification success using multiple wear indicators

No. Hidden Nodes	Flank Wear	Nose Wear	Chipping/Fracture
5	95.7	89.9	94.2
20	97.7	94.2	91.3

Table 11.3: Summary of 'PREDICT' implementation

Data field	Transformations Performed	Variables Selected?
Cutting Speed	logical	No
Feed-rate	Linear	YES
	ln x/1-x	NO
	Rt^4	NO
DOC	CONSTANT	NO
x-Static Force	Linear	YES
	Inverse	YES
	Tanh	NO
y-Static Force	Linear	YES
	Inverse	YES
	Tanh	NO
z-Static Force	Linear	NO
	PWr^2	NO
	Tanh	NO
x-Dynamic Force	Linear	NO
	Inverse PWr^2	YES
	Tanh	YES
y-Dynamic Force	Linear	NO
	Inverse	YES
	Tanh	YES
z-Dynamic Force	Linear	YES
	PWr^2	NO
	Tanh	NO
x-Vibration	Linear	NO
	Rt^4	NO
	ln x/1-x	NO
y-Vibration	Linear	NO
	Rt^4	NO
	ln x/1-x	NO
z-Vibration	Linear	NO
	Log	NO
	ln x/1-x	YES

Table 11.4: Process parameter sensitivity to tool wear

Sensitivity Criteria	Static Force			Dynamic Forces			Vibration		
	x	y	z	x	y	z	x	y	z
Flank wear	3	3	2	2	2	3	2	2	3
Nose wear	2	3	1	2	3	2	2	3	3
Total Response	**5**	**6**	3	4	**5**	**5**	4	**5**	**6**

Table 11.5: Sensitivity of process parameters to cutting conditions

Cutting Conditions	Static Force			Dynamic Force			Vibration		
Components	x	y	z	x	y	z	x	y	z
Speed	1	1	1	1	2	3	3	1	2
Feed	2	1	3	1	2	3	3	1	2
DOC	2	1	3	2	2	3	3	1	3
Total Response	**5**	3	**7**	4	**6**	**9**	**9**	3	**7**

Table 11.6: Combined effect of cutting conditions and wear on measured signals

	Static Force			Dynamic Force			Vibration		
Components	x	y	z	x	y	z	x	y	z
Total Response	10	9	10	8	11	14	13	8	13

CHAPTER 12

CONCLUSIONS

12.0. Overview

In this thesis, the TCM problem has been addressed. Specifically, attention concentrated on the development of a modular TCMS implemented via the application of perceptron neural networks. In spite of the numerous works carried out, TCM remains an active field in engineering science with various methods and approaches having been attempted ranging from direct to indirect sensor detection, mathematical and neural network interpretation and identification of tool wear. However, no universally applicable TCMS has so far been developed. One of the main reasons lies in the fact that systems developed so far have inadequately utilised the cutting conditions and insufficiently explored the use of more than one sensor signals. The use of either supervised or unsupervised neural network paradigms for the sensor signal fusion does not seem to preclude the success of the TCMS. This research work sought to overcome this hindrance by utilising multivariate process parameters, simple neural network paradigms, and experimented over a broader range of cutting conditions. Conclusions reached in the study are outlined and novel aspects from the investigation highlighted.

12.1. Summary

The rapid increase in industrial automation over the past 20 years have led to considerable research efforts into instituting tool change during metal cutting due to tool wear and damage through adaptive inspection mechanisms. In determining the tool wear or damage, many on-line attempts based on traditional methods (heuristic rules and analytical based models) have been applied to relate the process parameters in the cutting environment to the ensuing state of the cutting tool. These methods have had very limited successes and applicability due

to the stochastic nature of the metal cutting process, and the reliance upon cutting process data and mathematical modelling.

Advanced knowledge systems such as ANN have rekindled interest in TCMS with the ANN used in formalising and mimicking human decision making during TCM. It was initially thought that the benefits of instituting tool change policies based on intelligent decision making systems and knowledge acquisition could lead to unmanned machining environments with the human operator relegated to a bystander. However, a literature survey centred on the application of neural networks to-date in TCM showed that a widely applicable automated TCMS was still lacking.

The application of ANNs in TCMSs have been unsuccessful mainly because the design of these systems did not consider the complex nature of the metal cutting process. Often, data employed in the development of the TCMS were acquired from experiments utilising only a single cutting condition and the resultant trend generalised.

In view of this shortfall, an experimental test rig was set-up, instrumented, and validated for use in providing analytical data for an MLP neural network to perform TCM. The study was designed to incorporate a broader scope of cutting conditions, and cutting tests were conducted to assess the correlation of the sensor signals behaviour to both cutting conditions and tool wear.

The acquired experimental data using plain-faced tool inserts (P10 and P40) were fed into a purposely designed and simulated neural network. Initially, experimentation with a linear neural network model, a single layer perceptron, was carried out and it showed that the nature of the cutting data was such that the SLP could not adequately deal with the data, i.e. separate the data into one of two tool classes (worn/sharp) with a 100% confidence level. The inability of the SLP to classify tool wear successfully, lead to the introduction of multiple layer

perceptrons whose topology was such that it could handle the complex nature of the cutting data.

The implementation of MLP neural networks for tool state classification was successfully accomplished. However, a critical examination of the results obtained showed that the network was sensitive to chip formation and breakage, because the dynamics of the cutting process was altered during such occurrences. A decision was made to control the chip and cutting tool contact by using tool inserts with chip breaker geometry, and therefore, focus on the tool state classification.

Further test cuts were conducted and the behaviour of the sensor signals to cutting conditions and tool wear assessed. The trends obtained were as expected except for the chip separation and lamination frequencies whose peak magnitudes were higher than the tool holder resonant frequency.

The acquired data from test cuts employing inserts with chip breaker geometry were used to perform TCM in three phases. Firstly, only flank wear was used as the tool wear indicator with the MLP required to classify the data into one of two tool states (worn/sharp). Next, flank and nose wear were both used as the tool wear indicators and the network task was still to classify the data into one of the two tool states above. Finally, the flank and nose wear mark values were expanded to include an intermediary value between the two classes; that of partly worn, and tool fracture/chipping represented as a separate tool state.

The implemented MLP configurations could satisfactorily classify flank, nose and chipped tool states with accuracies greater than 90% for all the classes investigated. The sometimes unequal distribution of membership class data for the tool states (often more sharp state data than for the worn tool state) meant that the results were biased in favour of sharp tool diagnosis.

A study was undertaken to investigate the underlying features in the data extracted by the neural network as its blue print for classification. The study was carried out through implementation of an automatic neural network model builder that utilises genetic algorithm in selecting data features. A comparison of the automatically generated model and the purposely designed and simulated MLP showed that the choice of input sensor signals had been well made. The input data fields did not seem to have any unreasonable amount of redundant fields and data points, with both models achieving approximately the same classification success rate.

An on-line validation though desirable was not performed due to time constraints. On-line testing involves extensive coding to interface the sampling set-up and the modular TCMS neural network model, with allowance made for real-time data analysis and normalisation, and finally the institution of an external relay mechanism to the operator. At this stage of the investigation, it suffices for the ability of the modular TCMS to recognising a change in cutting area as well as tooling material to be assessed. Results obtained from the implementation suggested that the TCMS was capable of successfully classifying data acquired with a tool insert of different material type (P15) though the training was performed exclusively on another (P25). However, by altering the area of cut, it transpired that the TCMS could not distinguish process parameter changes emanating from a change in the area of cut from those arising from changes due to tool wear. A separate neural network paradigm was suggested to be used in parallel with the TCMS model for detecting changes in the area of cut, and thus reduce the false alarm levels.

12.3. Conclusions

The findings of the thesis can be summarised as follows:

- The implemented MLP neural networks were capable of tool wear mark categorisation into three distinct classes: nominally sharp, part worn and

severely worn for both flank and nose wear. A fourth class, fracture, was independently represented. The investigation showed that tool states were classified with accuracies of up to 90% success rate.

- It is necessary to establish a confidence interval for each tool wear feature classification. This was primarily because some errors in the classification resulted overwhelmingly from data class overlap. Owing to the nature of the network used, the network could not distinguish the ensuing tool state with a high degree of certainty. When the network output values were rounded to either 0 or 1, the incorrect class might have be allocated. So long as the TCM problem was one of classification, there has to be distinct classes to which a data point can be associated, and classes are bound to overlap.

- The networks were better at tool state quantification than tool wear classification. This could be partly attributed to the fact that tool wear is rather a continuous process than intermittent as binary coding would seem to suggest. The obtained network output during testing, it could be argued, reflected wear mark values rather than the various coded classes.

- The neural network model could not successfully identify or classify nominally sharp and partly worn tools of different tooling material, when trained exclusively with data from a different tooling material. The TCMS found to be sensitive to the tooling material, but due to the limited amount of experimental data used, the nature of the model's sensitivity could not be determined.

- Though the network was sensitive to changes in the cutting conditions, results of its classification were nonetheless still within acceptable bounds. The TCMS was generally better at severely worn and chipped/fracture tool state identification.

12.4. Novelty Aspects

During the course of this study, analytical and interpretation methods have been employed that bore novel aspects especially in this field of engineering science.

The use of principal sensor signal components as opposed to selecting wear sensitive features from each component ensured that the neural network's knowledge of the machining operation was in the global neighbourhood of the optimal operating conditions, and therefore not severely affected by slight deviations emanating from workpiece material change, geometry of the cutting tool and the cutting conditions.

The signal processing method though not novel in its entirety, the correlation of the energy of the vibration and dynamic force signal represented a novelty. The energy content in the signal gave maximum separability between clusters (sharp, worn or chipped) and minimal intra class. To the best of the author's knowledge, such a correlation though alluded to in some published work has not been practically realised and applied extensively as this study has illustrated.

The neural network paradigm employed was simple in design and function. Most often, complicated functions are used in the activation level of the neural network with learning performed through an uncompromisingly complex method. These have been completely avoided in this study, as the emphasis was on a simple and yet robust MLP.

One of the main motivations for this work was the current lack of TCM studies based on utilising tool inserts with chip breaker geometry configurations, and the effects such control has on the sensor signals. Almost all existing methods to-date are primarily based on plane-faced tool geometry, but increasingly, chip breaker geometry inserts are becoming the most used insert types especially for CNC machines. This study, one believes, makes a substantial contribution to this field.

A comparative study of the results of the user defined MLP configuration and the self-selected configuration gave great insight into MLP designing for TCMS applications in terms of the topology selection criteria. The exercise showed that though most of the neural network input fields for TCM might show sensitivity to tool wear, in practical situations, not necessarily all the inputs were employed in network training and learning. In execution, however, results obtained were of the same magnitude regardless of whether all the inputs fields were used during learning or not.

By testing the developed modular TCMS's applicability, it was possible for realistic bounds to be set for its operation. Though system was shown to be sensitive to tooling material, it was nonetheless capable of reasonable tool state classification when tooling material was changed. It was not able to distinguish a change in area of cut from process changes emanating from the tool wear process. Above all, the method proposed is maintenance free, versatile, and simple and cost effective.

CHAPTER 13

FUTURE WORK SUGGESTIONS

Since the prediction of tool life is a difficult task as it has a wide and scattered distribution, it may be practically impossible to set-up the ideal tool change and tool monitoring policy. In order to improve the design and implementation of the TCMS discussed in this thesis that takes the complex and diverse nature of the metal cutting into consideration, the following factors need to be explored:

- The work undertaken demonstrates that neural network has some potential in tool wear state classification. Rather than introduce further tool state classes, attention could shift from tool wear classification to tool wear quantification.

- Further tests are required covering a broader range of cutting conditions especially for the worn tool state than have been investigated in this study, and as much data as time and material resources allows ought to be collected.

- In order to be able to identify tool wear as well as distinguish process parameter increments emanating from DOC changes (changed cutting area), a separate classifier ought to be used in parallel with that which identifies tool wear. Typically, both classifiers have to be designed to use the same process parameters for the TCM section as well as for the DOC identification. As the area of cut is directly proportional to the DOC, it could be used as the target and desired values in training and implementation. This would require the elimination of DOC as an input signal feature. Alternatively, the investigation can be broadened to include the identification of all three cutting conditions.

- There is also room to improve upon the signal processing procedures such as applying AR, ARMA and wavelet techniques in order to further verify wear sensitive features and their trend in terms of wear correlation.

- Though training time was not a problem in this investigation, the use of other types of ANN learning and training methods such as conjugate gradient optimisation, quasi-Newton (such as BFCS) and the Levenberg-Marquardt algorithms that are reputed to train faster with better convergence ought to be explored. It is also suggested that any results obtained be benchmark i.e. MLP vs. RBF vs. LVQ.

- The overlapping of tool state class membership can be eliminated through the introduction of probability density functions deduced from the salient characteristics of the principal sensor signals (e.g. mean, RMS, etc.) by relative location constraints (local or global) with possible threshold density.

- The use of two data sets in designing the TCMS is deemed inadequate. The data set ought to be split into three groups as follows: a design set consisting of a training and validation set, and a test set. This ensures that the neural network's output is unbiased.

- Consideration should be given to the possibility of sensor failure, missing data and the use of PCA, and the data set determined to be uniquely different and characterised from each other to be so through an appropriate method.

- It is possible to implement a pattern recognition system using the contour plots and the waterfall plots. This proposition needs to be investigation.

REFERENCES

AB Sandvik Coromant (1995) Metal Working Products Catalogue-Turning Tools

ACOST (1992) Artificial Neural Networks. HMSO London

Aleksander I. and Morton H. (1990) Neural Computing: An introduction to. Chapman and Hall

Barschdorff D. and Femmer U. (1994) Artificial neural networks for wear estimation. Postprint IFAC Intelligent Manufacturing Systems, Vienna, Austria, pp 151-155

Barschdorff D., Monostori L., Kottenstede T. Warnecke G. and Muller M. (1993a) Cutting tool monitoring in turning under varying cutting; an artificial neural network approach. Proc. 6th Int. Conf. on Industrial and Engineering Applications of AI & ES (IEA/AIE), Edinburgh, June 1-4, pp 353-359

Barschdorff D., Monostori L., Kottenstede T., Warnecke G. and Müller M. (1993b) Wear estimation and state classification of cutting tools in turning via artificial neural networks. Tooldiag'93, International Conference on Fault Diagnosis, Toulouse (France), April 5-7, pp 669-677

Beale R and Jackson T. (1990) Neural Computing: An Introduction. IOP Publishing Ltd.

Bishop C. M. (1994) Neural networks and their Applications. Rev. Sci. Instrum. Vol. 65, No. 6, pp 1803-1832

Blum T. and Inasaki I. (1990) A study on acoustic emission from the orthogonal cutting process. ASME Trans. J. of Eng. for Industry, Vol. 112, No. 3, pp 203-211

Boothroyd G. (1975) Fundamental of metal machining and machine tools. 1st Ed. Scrapta Book Company

Bressloff P. C. (1995) Stochastic dynamics of reinforcement learning. Network: Computation in Neural Systems, Vol. 6, No. 2, pp 289-309

Bruel and Kjaer (1977) Application of Bruel & Kjaer Equipment to Frequency Analysis

Bruel and Kjaer (1987) Piezoelectric Accelerometers and Vibration preamplifiers, Theory and Applications Handbook

Burke L. I. (1989) Automated identification of tool wear states in machining processes : an application of self-organising neural networks. PhD Thesis, Depart. of Ind. Eng. and Operations Research, UC at Berkeley, USA

Burke L. I. (1992) Competitive learning based approaches to tool-wear identification. IEEE Trans. Sys., Man and Cyber., Vol. 22, No. 3, pp 558-563

Burke L. I. (1993) An unsupervised neural network approach to tool wear identification. IIE Trans., Vol. 25, No. 1, pp 16-25

Burke L. I. and Rangwala S. (1991) Tool condition monitoring in metal cutting: a neural network approach. J. of Intelligent Manuf., Vol. 2, pp 269-280

Byrne G., Dornfeld D., Inasaki I., Ketteler G., König W. and Teti R. (1995) Tool Condition Monitoring Systems (TCMS) - the state of research and industrial application. Annals of CIRP, Vol. 44, No. 2, pp 541-567

Carling A. (1992) Introducing neural networks. Sigma Press

Carpenter G. A. and Grossberg S. (1987a) A massively parallel architecture for a self-organising neural pattern recognition machine. Computer Vision, Graphics and Image Processing, Vol. 37, pp 54-115

Carpenter G. A. and Grossberg S. (1987b) ART-2: Self-organisation of stable category recognition codes for analog input patterns. Applied optics, Vol. 26, No. 23, pp 4919-4930

Chen Y. and Du R. (1996) Artificial neural network architecture design using similarity measure with applications in engineering monitoring and diagnosis. J. Dynamic Systems, Measurement and Control, Vol 118, pp 635-639

Choi G. S., Wang Z. X. and Dornfeld D. A. (1991) Detection of tool wear using neural networks. Proc. 4th World Meeting on AE/1st Int. Conf. AE in Manufact, ASNT, Boston, pp 342-349

Choi G. S., Wang Z. X., Dornfeld D. A. and Tsujino K. (1990). Development of an intelligent on-line tool wear monitoring system for turning operations. Proc. USA-Japan Symposium on Flexible Automation, A Pacific Rim Conference ISCIE Kyoto, Japan, pp 683-690.

Chow J. G. and Wright P. K. (1988) On-line estimation of tool/chip interface temperatures for a turning operation. ASME Trans. J. of Eng. for Industry, Vol. 110, pp 56-64

Chryssolouris G. and Domroese M. (1988) Sensor integration for tool wear estimation in machining. ASME Sensors and Control for Manufacturing, PED Vol. 33, pp 115-123

Chryssolouris G. and Domroese M. (1989) An experimental study of strategies for integrating sensor information in machining. Annals CIRP, Vol. 38, No. 1, pp 425-428

Chryssolouris G. and Guillot M. (1990) A comparison of statistical and AI approaches to the selection of process parameters in intelligent machining. Trans. ASME, J. Eng. Ind., Vol. 112, pp 123-131

Chryssolouris G., Domroese M. and Beaulieu P. (1992) Sensor synthesis for control of manufacturing processes. Trans. ASME J. of Eng. Ind., Vol. 114, pp 158-174

Chung E. S., Chiou Y. S. and Liang S. Y. (1993) Tool wear and chatter detection in turning via time-series modelling and frequency band averaging. ASME PED-Vol. 64, Manufacturing Science and Engineering, pp 351-358

Clement W. I. (1993) Generalisation capabilities of back-propagation neural networks. Modelling and Simulation, Vol. 23, No. 5, pp 2435-2442

Colbaugh R. and Glass K. (1995) Real-time tool wear estimation using recurrent neural networks. IEEE Int. Symp. on Intelligent Control, Monteray, CA, USA, pp 357-62

Colgan J, Chin H, Danai K, and Hayashi S R (1994) On-line tool breakage detection in turning: a multi-sensor method. J. Eng. Ind. Vol. 116, pp 117-123

Connor F. R. (1972) Introductiory Topics in Electronics and Telecommunication Signals. Edward Arnold

Constantinides N. and Bennet S. (1987) An investigation of methods for on-line estimation of tool wear. Int. J. Mach. Tools Manufact., Vol. 27, N. 2, pp 225-237

Dan L. and Mathew J. (1990) Tool wear and failure monitoring techniques for turning - a review. Int. J. Mach. Tools Manufact., Vol. 30, No. 4, pp 579-598

Dayhoff J. E. (1990) Neural Network architectures: An introduction. Van Nostrand Reinhold

Dornfeld D. A. (1990) Neural network sensor fusion for tool condition monitoring. Annals CIRP, Vol. 39/1, pp 101-105

Dornfeld D. A. (1992) Application of acoustic emission techniques in manufacturing. NDT & E International, Vol. 25, No. 6, pp 259-269

Dornfeld D. A. (1994) In process recognition of cutting states. JSME Int. J., Series C: Dynamics Control, Vol. 37, No. 4, pp 638-650

DTI (1993) Neural Computing Technology Transfer Programme UK

Du R., Zhang B., Hungerford W. and Pryor T. (1993) Tool condition monitoring and compensation in finish turning using optical sensor. ASME DSC-Vol. 50/PED-Vol. 63, Symp. Mechatronics, pp 245-251

El Gomayel J. I. and Bregger K. D. (1986) On-line tool wear sensing for turning operations. Trans. ASME J. Eng. Industry, Vol. 108, pp 44-47

Elanayar S. and Shin Y. C. (1995) Robust tool wear estimation with radial basis function neural Networks. Trans. ASME J. Dynamic Systems, Measurement, and Control, Vol. 117, pp 459-467

Elanayar S. V. T., Shin Y. C. and Kumara S. (1990) Machining condition monitoring for automation using neural networks. ASME's Winter Annual Meeting, Monitoring and Control of Manufacturing Processes, PED Vol. 44, pp 85-100

Elanayar S., Shin Y. C. (1991) Tool wear estimation in turning operations based on Radial Basis Functions. Proc. Artificial Neural Networks in Engineering,(ANNIE) St. Louis MO, ASME Press, NY, USA, pp 685-692

Emel E. (1991) Tool wear detection by neural network based acoustic emission sensing. ASME DSC-Vol. 28/PED-Vol. 52, Control of Manufacturing Processes, pp 79-85

Emel E. and Kannatey-Asibu E. Jr. (1989) Acoustic Emission and Force Sensor Fusion for Monitoring the Cutting Process. Int. J. Mech. Sci., Vol. 31, No. 11/12, pp 795-809

Fausett L. (1994) Fundamentals of Neural Networks: Architecture, Algorithms and Applications. Pentice-Hall

Gere J. M. and Timoshenko S. P. (1991) Mechanics of Materials. Chapter 10, 3rd Edition, Chapman and Hall

Ghasempoor A., Moore T. N. and Jeswiet J. (1996) On-line flank wear estimation using neural networks. Proc. Advanced Manuf Processes Systems and Technologies Conference (AMPST '96) Bradford, UK, pp 173-181

Gomm J. B., Williams D. and Page G. F. (1993) Introduction to neural networks. In G. F. Page et al. (eds.): Application of neural networks to modelling and control, Chapman and Hall. pp 1-8

Gould L (1988) Sensing tool and drive element conditions in machine tools. Sensor, pp 5-13

Govekar E. and Grabec I. (1994) Self-organising neural network application to drill wear classification. Trans. ASME J. of the Eng. Ind., Vol. 116, pp 233-238

Govekar E., Grabec I. and Madsen H. O. (1991). Estimation of drill wear from AE signals using self-organising neural network. Proc. 4th World Meeting on AE and 1st Int. Conf. on AE in Manufacturing, ASNT, Boston, USA, pp 65-71

Grabec I. (1988) Chaotic dynamics of the cutting process. Int. J. Mach. Tools Manufact., Vol. 28, No. 1, pp 19-32

Grossberg S. (1987). Competitive learning: from interactive activation to adaptive resonance. Cognitive Science, Vol. 11, pp 23-63

Guillot M. and El Ouafi A. (1991). On-line identification of tool breakage in metal cutting processes by use of artificial neural networks. Proc. Artificial Neural Networks in Engineering (ANNIE) St Louis, MO USA, November 9-12, pp 701-709

Guinea D., Ruiz A. and Barrios L. J. (1991) Multi-sensor integration- An automatic feature selection and sate identification methodology for tool wear estimation. Computers in Industry, Vol. 17. pp 121-130

Harvey R. L. (1994) Neural Network Principles. Pentice-Hall

Hatschek R. L. (1978) Tiurning with inserts. American Machinist, pp. 101-116

Hecht-Nielsen R. (1990) Theory of the back-propagation Neural Network. Proc. Int. Joint Conf. on Neural Networks, Part-1 pp 1593-1605

Hertz J. I., Krogh A. and Palmer R. G. (1994) Introduction to the theory of Neural Computation. Eight Reprint, Addison-Wesley Publishing Company

Holmbom P, Pedersen O, Sandell B and Lauber A, (1989) Fusing sensor systems: promises and problems. Sensor Reviews, Vol. 9, No. 3, pp 143-152

Holmbom P, Pedersen O, Sandell B and Lauber A. (1989) Fusing Sensor Systems: Promises and Problems. Sensor Reviews, Vol. 9, No. 3, pp 143-152

Hong G. S., Rahman M. and Zhou Q. (1996) Using neural networks for tool condition monitoring based on wavelet decomposition. Int. J Mach. Tools Manufact., Vol. 36, No. 5, pp 551-566

ISO 3685 (1993) Tool-life testing with single-point turning tools. International Standard, Second Edition

Jammu V. B., Danai K. and Malkin S. (1993) Unsupervised neural network for tool breakage detection in turning. Annals CIRP, Vol. 42, No. 1, pp 67-70

Javed M. A., Hope, D. A. Adradi D., Smith G. T. and Rao B. K. N. (1996) On-line tool condition monitoring using artificial neural networks. Insight, Vol. 38, No. 5, pp 351-354

Jawahir I. S. and van Luttervelt C. A. (1993) Recent developments in chip control research and applications. Annals CIRP, Vol 42, No. 2 pp 659-685

Jetley S. K. and Gollajesse A. (1994) Measuring tool wear using magnitism. Japan-USA Symposium Flexible Automation- A Pacific Rim Conference, July 11-18, Kobe, Japan, pp 345-347

Jia K., Zheng L., Luo Z. and Zhang B. (1993) Information fusion of acoustic emission signals with neural network for tool condition monitoring. In V. Orpana and A. Lukka (eds): Production Research, Elsevier Science Publishers B. V.(North Holland), pp 145-147

Jiang C. Y., Zhang Y. Z. and Xu H. J. (1987) In-process monitoring of tool wear stage by the frequency band-energy method. Annals of the CIRP, Vol. 36, No. 1, pp 45-48

Kakade S. et al. (1995) Monitoring of tool status using intelligent acoustic emission sensing and decision based neural network. IEEE/IAS Int. Conf. on Industrial Automation & Control (IA C '95), Hyderabad, India, pp 25-9

Kakade S., Vijayaraghavan L. and Krishnamurthy R. (1994) In-process tool wear and chip-form monitoring in face milling operation using acoustic emission. J. Material Processing Technology, Vol. 44, pp 207-214

Kalpakjian S. (1991). Manufacturing Processes for Engineering Materials. 2nd Edition, Chapter 8, pp 473-581, Addison-Wesley Publication Company.

Kamarthi S. V., Sankar G. S., Cohen P. H. and Kumara S. R. T. (1991) On-line tool wear monitoring using a Kohonen Feature Map. Proc. Artificial Neural Networks in Engineering, (ANNIE), St. Louis MO, ASME Press, NY, USA, pp 639-644

Karmathi S. V. (1994) On-line tool wear estimation in turning through sensor data fusion and neural networks. Ph.D Thesis, Department of Industrial and Manufacturing Engineering, The Pennsylvania State University, USA

Khraisheh M. K., Pezeshki C. and Bayoumi A. E. (1995) Time series based analysis for primary chatter in metal cutting. J. of Sound and Vibration, Vol. 180, No. 1, pp 67-87

Kistler K-Shear® Accelerometers, Operating Instructions, Type 8730A Kistler Piezo-Instrumentation, Form 0.024 Ed.8., 1994

Kistler Quartz 3-Component Dynamometer Operating Instructions, Type 9257A Kistler Piezo-Instrumentation, Form 0.024 Ed.6., 1990

Kitagawa T., Maekawa K., Shirakashi T and Usui E. (1988) Analytical prediction of flank wear of carbide tools in turning plain carbon steels (Part 1). Bull. Japan Soc. of Prec. Engg., Vol. 22, No. 4, pp 263-269

Ko T. J. and Cho D. W. (1994) Cutting state monitoring in milling by a neural network. Int. J. Mach. Tools Manufact., Vol. 34, No. 5, pp 659-676

König W., Kutzner K. and Schehl U. (1992) Tool monitoring of small drills with acoustic emission. Int. J. Mach. Tools Manufact., Vol. 32, No. 4, pp 487-493

Kumudha S., Srinivasa Y. and Krishnamurthy R. (1994) Tool wear monitoring using an unsupervised artificial neural network. 3rd Int. Conf. on Automation, Robotics and Computer Vision (ICARCV '94), Singapore, Nov. 9-11, pp 1348-1352

Lee J. H., Kim D. E. and Lee S. J. (1996) Application of neural networks to flank wear prediction. Mechanical Systems and Signal Processing, Vol. 10, No. 3, pp 265-276

Lee K. S., Lee L. C. and Teo S. C. (1992) On-line tool wear monitoring using a PC. J. Material Process Technology, Vol. 29, pp 3-13

Lee L C, Lee K S, and Gan C S (1989) On the correlation between dynamic cutting force and tool wear. Int. J. Mach. Tools Manufact., Vol. 29, No. 3, pp 295-303

Lee L. C., Lam K. Y. and Liu X. D. (1994) Characterisation of tool wear and failure. J. Materials Processing Technology, Vol. 40, pp 143-153

Leem C. S.and Dreyfus S. E. (1992) Learning input feature selection for sensor fusion in tool wear monitoring. In Dagli, Burke and Shin (eds.): Intelligent Engineering Systems through Artificial Neural Networks (ANNIE '92), ASME Press, pp 814-820

Li X. Q., Wong Y. S. and Nee A. Y. C. (1996) Tool condition monitoring

using acoustic emission sensing and an integrated multi-ART 2 enural network. Proc. Advanced Manufacturing Processes Systems and Technologies Conference (AMPST '96) Bradford, UK, pp ?

Lin J. (1995) Inverse estimation of the tool-work interface temperature in end milling. Int. J. Mach. Tools Manufact., Vol. 35, No. 5, pp 751-760

Lin Z. C., Chang F. S. and Lin Y. T. (1987) The effect of tool flank wear on the temperature distribution of a machined workpiece. J. Chinese Inst. Eng., Vol. 10, No. 4, pp 353-362

Lippman R. P. (1987) An introduction to computing with neural nets. IEEE ASP Magazine, Vol. 4, pp 4-22

Lisboa P. J. G. (Ed) (1992) Neural Networks, Current Applications. Chapman and Hall

Lister P. M. (1993) On-line measurement of tool wear. Ph.D. Thesis, Manufacturing and Machine Tools Division, Depart. of Mech. Eng., UMIST, Manchester, England

Lister P. M. and Barrow G. (1986) Tool condition monitoring systems. Proc. 26th Machine Tool Design and Research Conference, Manchester, England, pp 271-288

Liu T. I. , Ko E. J. and Sha S. L. (1990) Intelligent monitoring of tapping tools, J. Mater. Shaping Technol., Vol. 8, pp 249-254

Liu T. I. , Ko E. J. and Sha S. L. (1991) Diagnosis of tapping operations using an AI approach, J. Mater. Shaping Technol., Vol. 9, pp 39-46

Liu T. I. and Anantharaman K. S. (1994) Intelligent classification and measurement of drill wear. Trans. ASME J. of Eng. Ind., Vol. 116, pp 392-397

Liu T. I. and Ko E. J. (1990) On-line recognition of drill wear via artificial neural networks. Winter Annual Meeting of the ASME, Monitoring and

Control for Manufact. Processes, PED-Vol. 44, Dallas USA, pp 101-110

Ly S. and Choi J. J. (1994) Drill condition monitoring using ART-1. IEEE Int. Conf. on Neural Networks, Orlando, FL, USA, Vol. 2, pp 1226-9

Markos S., Szalay T., Szollos, G. and Raifu A. W. (1993) Monitoring of milling processes based on artificial intelligence. Mechatronics Vol. 3, No. 2, pp 231-240

Marques M. J. M. and Mesquita R. M. D. (1991) Monitoring the wear of sintered high-speed steel tools. J. Material Process Technology, Vol. 25, pp 195-213

Martin K. F. (1994) A review by discussion of condition monitoring and fault diagnosis in machine tools. Int. J. Mach. Tools Manufact., Vol. 34, No. 4, pp 527-551

Martin K. F., Brandon J. A., Grosvenor R. I. and Owen A (1986) A comparison of in-process tool wear measurement methods in turning. Proc. 26th Machine Tool Design and Research Conference, Manchester, England, pp 289-296

Masory O. (1991) Detection of tool wear using multi-sensor readings defused by artificial neural network. Proc. SPIE - Int. Soc for Optical Eng. Vol. 1469, pt 2., pp 515-525

MathWorks (1994) User guide, Neural Network Toolbox for use with MATLAB, MathWorks Inc.

Minai A. A. and Williams R. D. (1990) Acceleration of the back-propagation through learning rate and momentum adaptation. Proc. Int. Joint Conf. on Neural Networks, Part-1, pp 1676-1679

Monostori L. (1988). New trends in machine tool monitoring and diagnostics. Robotics and Computer-Integrated Manufacturing. Vol. 4, No. 3/4, pp 457-464

Monostori L. (1993) A step towards intelligent manufacturing: modelling and monitoring of manufacturing processes through artificial neural networks. Annals CIRP, Vol. 42, No. 1, pp 485-488

Moore H. R. and Kibbey D. R. (1982). Manufacturing Materials and Processes, 3rd Edition, Grid Publishing Inc. Columbus OH, USA, Chapter 18, pp 439-472,

Moriwaki T. (1994) Intelligent machine tool; perspective and themes for future development. ASME J. Manuf. Sc. Eng., PED - Vol. 68-2, pp 841-849

Moriwaki T. and Hino R. (1991) Application of neural network to AE signal processing for automatic detection of cutting tool life. JSPE, Vol. 57, No. 7, pp 1259-1264

Moriwaki T. and Mori Y. (1993a) Sensor fusion for in-process identification of cutting process based on neural network approach. In Takamori T. and Tsuchiya K. (eds.): Robotics, Mechatronics and Manufacturing Systems, Elsevier Science Publishers B. V. (North Holland), pp 599-604

Moriwaki T. and Mori Y. (1993b) Recognition of cutting state based on neural network sensor fusion. JSPE, Vol. 59, Part 5, pp 779-784

Moriwaky T. and Tobito M. (1990) A new approach to automatic detection of life of coated tool based on acoustic emission measurement. ASME Trans. J. of Eng. for Industry, Vol. 112, No. 3, pp 212-218

Musgrove P. B. (1995) Lecture notes [CP3338] and personal communication, SCIT, University of Wolverhampton

Myers D. J., Nightingale C. and Linggard (Eds.) (1992) Neural Networks for Vision, Speech and Natural Language. BT Telecommunications Series, Chapman and Hall

Noori-Khajavi A. and Komanduri R. (1993) On multi-sensor approach to drill wear monitoring. Annals of the CIRP, Vol. 42, No. 1, pp 71-74

Noori-Khajavi A. and Komanduri R. (1995). Frequency and time domain analyses of sensor signals in drilling-II. Investigation on some problems associated with sensor integration. Int. J. Mach. Tool Manuf., Vol. 35, No. 6, pp 795-815

Noori-Khajavi A. and Komanduri R. (1995b). Frequency and time domain analyses of sensor signals in drilling-I. Correlation with drill wear. Int. J. Mach. Tool Manuf., Vol. 35, No. 6, pp 775-793

Novak A. and Wiklund H. (1992) Reliability of tool-wear monitoring. Annals CIRP, Vol. 42. No. 1, pp 63-66

Oguananam D. C. D., Raafat H. and Taboun S. M. (1994) A machine vision system for wear monitoring and breakage detection of single-point cutting tools. Computers in Industrial Engineering, Vol. 26, No. 3, pp 575-598

Oraby S E and Hayhurst D R. (1991) Development of models for tool wear force relationships in metal cutting. Int. J. Mach. Tools Manufact., Vol. 33, No. 2, pp 125-138

Osuri R. H., Chatterjee S. and Chandrashekhar S. (1991) On-line condition monitoring of tool wear in end milling using acoustic emission. Int. J. Prod. Res., Vol. 29, No. 7, pp 1339-1353

Parra L. Deco G. and Miesbach S. (1996) Statistical independence and novelty detection with information preserving non-linear maps. Neural Computation, Vol. 8, pp 260-269

Purushothaman S. and Srinivasa Y. G. (1994) A back-propagation algorithm applied to tool wear monitoring. Int. J. of Mach. Tools and Manufact. Vol. 34, No. 5, pp 625-631

Radford J. D. and Richardson D. B. (1974) Production Engineering Technology. The MacMilllan Press Ltd. London, Chapter 7, pp 119-155,

Radulescu R. and Kapoor S. G. (1994) An analytical model for prediction of

tool temperature fields during continuous and interrupted cutting. Trans. ASME J. Eng. Industry, Vol. 116, NO. 2, pp 135-143

Rahman M., Zhou Q. and Hong G. S. (1995a) Application of kohonen neural network for tool condition monitoring. SPIE Vol 2620, pp 422-8

Rahman M., Zhou Q. and Hong G. S. (1995b) On-line cutting state recognition in turning using a neural network. Int. J. Adv. Manuf. Technol., Vol. 10, pp 87-92

Raman S, Shaikh A and Cohen P. H. (1992) A mathematical model for tool temperature sensing. MD-Vol. 39/PED-Vol. 61, ASME Computational Methods in Materials Processing, pp 181-193

Rangwala S. (1988) Machining process characterisation and intelligent tool condition monitoring using acoustic emission signal analysis. PhD Thesis, Mechanical Eng. Depart., UC at Berkeley, USA

Rangwala S. and Dornfeld D. (1987) Integration of sensors via neural networks for detection of tool wear states. ASME PED, Vol. 25, pp 109-120

Rangwala S. and Dornfeld D. (1990) Sensor integration using neural networks for intelligent tool condition monitoring. Trans. ASME J. Eng. Ind. Vol. 112, No. 3, pp 219-228

Ravinder H V, Srinivasa Y G and Krishnamurthy R. (1993) Modelling of tool wear based on cutting forces in turning. Wear, Vol. 169, pp 25-32

Roget J., Souquet P. and Gsib N. (1988) Application of acoustic emission to the automatic monitoring of tool condition during machining. ASNDT Materials Evaluation, Vol. 46, pp 225-229

Rotberg J., Braun S. and Lenz E. (1987) Mechanical signature analysis in interrupted cutting. Annals of the CIRP, Vol. 36, No. 1, pp 249-252

Rotberg J., Braun S. and Lenz E. (1989) Vibration generation models for cutting tool monitoring. Diagnostics, Vehicle Dynamics and Special Topics - ASME Design Eng. Div., Vol. 18, Part 5, pp 1-6

Ruiz A., Guinea D., Barrios J. and Betancourt F. (1993) An empirical multi-sensor estimation of tool wear. Mech. Sys. and Signal Processing Vol. 7, No. 2, pp 105-119

Rumelhart D. and Zipser D. (1985) Feature discovery by competitive learning. Cognitive Science, Vol. 9, pp 75-112

Sarle W. S. (1994) Neural networks and statistical models. Proc. 19th Annual SAS Users Group International Conference, SAS Institute Inc., Cary, NC, USA, pp ?

Sarwar M, Li J, Penlington R and Ahmed W (1996) Development of thermal imaging systems for metal cutting applications. Proc. Advanced Manufacturing Processes Systems and Technologies Conference (AMPST '96) Bradford, UK, pp 361-369.

Schey J.A. (1987) Introduction to Manufacturing Processes. 2nd Edition, McGraw-Hill Book Company, Chapter 8, pp 441

Shaw M. C. (1984) Metal Cutting Principles. Clarendon Press, Oxford Chapter 3, pp 18-46

Shaw M. C. (1988) Temperature in Cutting. Proc. ASME Symp. on Thermal Aspects in Manufact., Vol. 30, pp 133-143

Shi T. and Ramalingam S. (1990) Real-time flank wear sensing. ASME Winter Annual Meeting, PED-Vol. 43, pp 157-170

Shiraishi M. (1988) Scopeof in-process measurement, monitoring and control techniques in machining processes- Part 1: In-process techniques for tools. Precision Engineering, Vol. 10, No. 4, pp 179-189

Stephenson D. A. and Ali A. (1990) Tool temperatures in interrupted metal cutting. Winter Annual Meeting of ASME (eds) Klamecki B. E. and Weinmann K. J., Dallas TX, Nov. 25-30, PED-Vol. 43, pp 261-281

Strenkowski J. S. and Moon K. J. (1990) Finite element prediction of chip geometry and tool/workpiece temperature distributions in orthogonal metal cutting. ASME Trans. J. of Eng. for Industry, Vol. 112, pp 313-318

Tanner R. and Loh N. K. (1994) A taxonomy of multi-sensor fusion. J. of Manufacturing Systems, Vol. 11, No. 5, pp 314-325

Tansel I. N. and McLaughlin C. (1991) On-line monitoring of tool breakage with unsupervised neural network. Trans. NAMRI/SME, pp 364-370

Tansel I. N. and McLaughling C. (1993) Detection of tool breakage in milling operations-II. The Neural Network Approach. Int. J. Mach. Tools Manufact., Vol. 33, No. 4, pp 545-558

Tansel I. N. and Rodriguez O. (1992) Automated monitoring of micro-drilling operations. Trans. NAMRI/SME, Vol. XX, pp 205-210

Tansel I. N., Mekdeci C. and McLaughlin C. (1993a) Detection of tool failure in end milling with wavelet transformations and neural networks (WT-NN). ASME PED-Vol. 64, Manufact. Science and Eng., pp 369-374

Tansel I. N., Mekdeci C., Rodriguez O. and Uragun B. (1993b) Monitoring drill conditions with wavelet based encoding and neural networks. Int. J. Mach. Tools Manufact., Vol. 33, No. 4, pp 559-575

Tansel I. N., Rodriguez O. and Mekdeci C. (1992) Detection of tool breakage in micro-drilling operation with RCE Neural networks. ASME PED-Vol. 47-1, Eng. Sys. Design and Analysis, pp 83-88

Tansel I. N., Wagiman A. and Tziranis A. (1991) Recognition of chatter with neural networks. Int. J. Mach. Tools Manufact., Vol. 31, No. 4, pp 539-552

Tarng Y. S., Hseih Y. W. and Hwang S. T. (1994) Sensing tool breakage in

face milling with a neural network. Int. J. Mach. Tools Manufact., Vol. 34, No. 3, pp 341-350

Taylor J. G. (1996) New avenues in neural networks. In Taylor J. G. (ed): Neural Networks and their applications. John Wiley, London, pp 277-287

Teshima T., T. Shibasaka T., Takuma M. and Yamamoto A. (1993) Estimation of cutting tool life by processing tool image data with neural network. Annals CIRP, Vol. 42, No. 1, pp 59-62

Trent E M (1977) Metal cutting. Butterworths

Turner J. D. (1988). Instrumentation for engineers, Macmillan Education

Venkatesh K., Zhou M. C. and Caudill R. (1994) Monotoring of tool wear using artificial neural networks. Proc. American Control Conf. Baltimore MD, pp 2585-2569

Wang Z. and Dornfeld D. A. (1992) In-process tool wear monitoring using neural networks, Japan/USA Symposium on flexible automation, ASME, Vol. 1, pp 263-270

Warnecke G., Jenewein A. and Reinfelder A. (1990) Tool monitoring based on process identification, monitoring and control for manufacturing processes. ASME Winter Annual Meeting, Dallas-TX, USA, pp 43-55

Wasserman P. D. (1989) Neural Computing: Theory and practice. Van Nostrand Reinhold

Weck M. (1984) Handbook of Machine Tools, Vol. 4: Metrological Analysis and Performance Tests. John Wiley and Sons

Weis W. (1994) Processing optical sensor data for tool monitoring with neural networks. Proc. IEEE WESCON 94 IDEA/Microelectronics, pp 351-355

White et al. (1992) Artificial Neural Networks: Approximation and learning theory. Blackwell

Winston P. H. (1992) Artificial Intelligence. Addison Wesley

Yan D. and El-Wardany T. I. and Elbestawi M. A. (1995) A multi-sensor strategy for tool failure detection in milling. Int. J. Mach. Tools Manufact., Vol. 35, No. 3, pp 383-398,

Yao Y. and Fang X. D. (1992) Modelling of multivariate time series for tool wear estimation in finish-turning. Int. J. Mach. Tools Manufact., Vol. 32, No. 4, pp 495-508

Yao Y. L. and Fang X. (1993) Assessment of chip forming patterns with tool wear progression in machining via neural networks. Int. J. Mach Tool and Manufact. Vol. 33, No. 1, pp 89-102

Yao Y., Fang X. D. and Arndt G. (1990) Comprehensive tool wear estimation in finish-machining via multivariate time-series analysis of 3-D cutting forces. Annals of the CIRP, Vol. 39, No. 1, pp 57-60

Yao Y., Fang X. D. and Arndt G. (1991) On-line estimation of groove wear in the minor cutting edge for finish machining. Annals CIRP, Vol. 40, No. 1, pp 41-44

Yen D. W. and Wright P. K. (1986) A remote temperature sensing technique for estimating the cutting interface distribution. ASME Trans. J. of Eng. for Industry, Vol. 108, pp 252-263

Zhang D., Dai S., Han Y. and Chen D. (1994) On-line monitoring of tool breakage using spindle current in milling. 1st Asia-Pacific & 2nd Japan-China Int. Conf. Progress of Cutting & Grinding, Shanghai, China, Sept., pp 270-6

Zheng S. X., McBride R., Barton J. S., Jones J. D. C., Hale K. F. and Jones B. E. (1992) Intrinsic optical fibre sensor for monitoring acoustic emission. Sensors and Actuators, A: Physical, Vol. 31, pp 110-114

Zhou J. M., Andersson M. and Ståhl J. E. (1995b) A system for monitoring cutting tool spontaneous failure based on stress estimation. J. Material Processing Technology, Vol. 48, pp 231-237

Zhou Q., Hong G. S. and Rahman M. (1995) A new tool wear criterion for tool condition monitoring using neural network. Engineering Application of Artificial Intelligence, Vol. 8, No. 5, pp 579-588

Zupan J. and Gasteiger J. (1993) Neural Networks for chemists: an introduction. VCH

PUBLICATIONS LIST

REFEREED JOURNAL PAPERS:

- Dimla, Jnr. et al., (1997) "Neural network solutions to the Tool Condition Monitoring problem - a critical review of methods", Int. J. of Machine Tools Manufact. Vol 37, No. 9, pp. 1219-1242

- Dimla, Jnr. D. E., Lister P. M. and Leighton N. J. (1998) "Automatic tool state identification in a metal turning operation using MLP neural networks and multivariate process parameters" Int. J. of Machine Tools and Manufacture, Vol. 38, No. 11, pp. 343-352

- Dimla, Jnr. D. E. (1998) "Application of perceptron neural networks to tool state classifcation in a metal turning operation", Submitted to Int. J. Eng. Applications of AI, Pergamon

REFEREED CONFERENCE PAPERS AND PRESENTATIONS:

- Dimla, Jnr. D. E., Lister P. M. and Leighton N. J. (1996a), "Using single layer perceptron neural networks in tool wear identification", IEE Colloquium on Modelling and Signal Processing for Fault Diagnosis, Leicester, England, Sept. 17-18, 1996, Digest Reference Number 1996/260 pp 3/1-3/4.

- Dimla, Jnr. D. E., Lister P. M. and Leighton N. J. (1996b), "Investigation of the sensitivity of single layer perceptron neural networks to tool wear inception during a metal turning operation", In C. H. Dagli et al. (eds.): Intelligent Engineering Systems Through Artificial Neural Networks, Vol. 6 (ANNIE '96), ASME Press New York, pp. 867-873

- Dimla, Jnr. D. E., Lister P. M. and Leighton N. J. (1997a) "A back-propagation neural network solution to Tool Condition Monitoring in a metal cutting process", IEE Colloquium on Fault Diagnosis in Process Systems, York University, York, England, 21st April, Digest No: 97/174, pp. 9/1-9/3

- Dimla, Jnr. D. E., Lister P. M. and Leighton N. J. (1997b) "A multi-sensor fusion method using multiple layered perceptron neural networks in a metal turning process", Proc. 5th IEE Int. Conf. on Artificial Neural Networks, 7-9 July, Cambridge, England, pp. 306-311

- Dimla, Jnr. D. E., Lister P. M. and Leighton N. J. (1997c)"Application of a back-propagation neural network to Tool Condition Monitoring in a metal turning process", Proc. 32nd International MATADOR Conf., 10-12 July, UMIST, Manchester, England, pp. 287-292

- Dimla, Jnr. D. E., Lister P. M. and Leighton N. J. (1997d) "Sensor fusion for cutting tool state identification in metal turning through application of perceptron neural networks", Proc. IFAC Symposium on Fault Detection, Supervision and Safety for Technical Processes- SAFEPROCESS '97, 9-11 August, Hull, England, Vol. 2, pp. 1144-1147

- Dimla, Jnr. D. E. (1998a) "Tool wear monitoring in a metal cutting operation using percetron neural networks and multivariate process parameters", To be presented at the Int. ICS/IFAC Symposium on Neural Computation, TU Vienna, September 23-25, 1998

- Dimla, Jnr. D. E. (1998b) "A modular tool wear monitoring system for metal cutting operations using MLP neural networks and multivariate process parameter", To be presented at the UKACC International Conference on CONTROL '98, University of Wales, Swansea, 1-4 September, 1998.

INVITED PRESENTATIONS:

- Dimla, Jnr. D. E.(1998) "Application of neural networks to cutting tool state classification in a metal turning process", NCAF Annual General Meeting, DERA Malvern, 21-22 Jan. 1998

APPENDICES

APPENDIX I

SIGNAL TECHNIQUES

I-1. Signal Classification

There are two basic types of signals: deterministic and random signals. Signals that can be explicitly described in mathematical terms are deterministic (e.g. a one degree of freedom fixed end vibrating cantilever system). The displacement of the cantilever can be deduced at any given instant when initial conditions and dynamics are known. Random signals tend to behave in a manner for which exact values cannot be predicted at any instant in time (e.g. ocean current induced structural vibration on an offshore oil platform). However, some random signals can appear deterministic, i.e. when corrupted with noise (distortion). Some random signals can be made to yield determinable data through the application of suitable methods of analysis.

Deterministic signals are either periodic or transient. Periodic signals can be analysed through the application of Fourier series whereas transients could be analysed by the application of Fourier Transforms. Spectra resulting from the former consist of discrete lines whereas those from the latter are continuous as an infinite number of frequency components exist in the transients.

Random signals can generally be analysed by determining their probabilistic or statistical variation, i.e. application of N separated time histories. Examples of such techniques include calculation of mean values ($\bar{x}$), mean square ($\bar{x}^2$).

The mean and mean square values can be obtained at time t_i over the period T as follows:

$$\bar{x} = \frac{1}{N}\sum_{i-1}^{N} x_i(t_i) \qquad [i]$$

$$\bar{x}^2 = \lim_{T\to\infty}\frac{1}{T}\int_0^T x^2(t)dt \qquad [ii]$$

Alternatively, the root mean square (RMS) value can be used.

The $\bar{x}$, $\bar{x}^2$ and RMS all give an indication of amplitude variation but not necessarily any descriptive information to aid explain such variable nature. For descriptive information, the probabilistic descriptions are needed.

The probability density series (PDS) describes the probability P_i of a signal amplitude lying in the range x to $x + \delta x$ when normalised with δx.

That is,

$$\bar{x}^2 = \lim_{T \to \infty} t_n | (T \delta x) \qquad \text{[iii]}$$

where n is the number of samples and T the preiodic time.

Extension of equation [iii] leads to the probability distribution function (PDF) illustrated in Figure I(a) and equation [iv].

$$P(x) = \int_{-\infty}^{\infty} P_i(x)\, dx \qquad \text{[iv]}$$

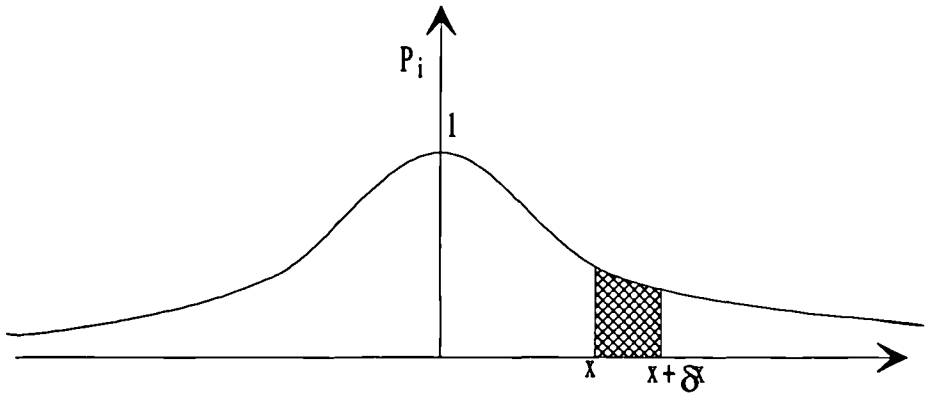

Figure I(a): Typical Probability Distribution Function

I.2. Sampling

Transmission of analogue signals usually is through an entire and continuous process. On closer examination, provided certain conditions are met, it is sufficient to transmit only "samples" of the signal at given time intervals, and this technique is what is commonly called Sampling.

Consider a pulse with repetitive frequency, f_r, period T, where $f_r=1/T$. An assumption is madethat the signal contains a frequency F_m as its highest frequency component.

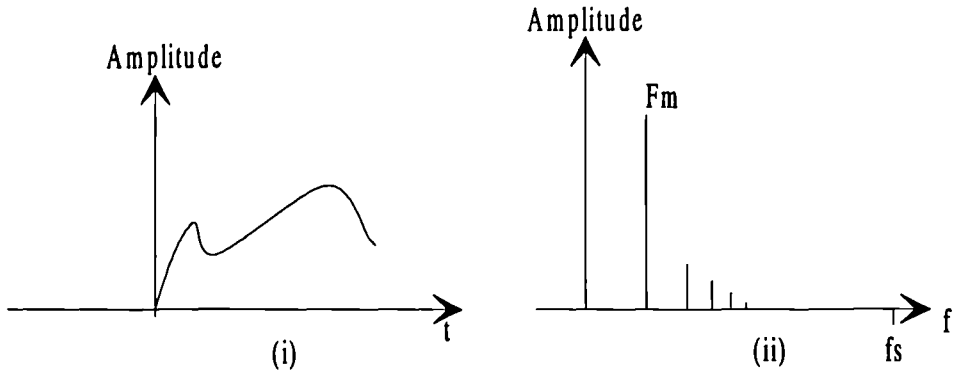

Figure I(b): Sampled signal (i) and its FFT (ii)

Through the application of Discrete Fourier Transformation, the frequency components are found to vary in factors of f_r (0, f_r, $2f_{r...}$). At the zero frequency (d.c.), only some frequencies are physically realisable and provided F_m and (f_r-F_m) do not overlap, it is possible to separate out the first group of frequencies at the receiving end. This is done by using a low pass filter with a cut off frequency $f_c=F_m$ and separated frequencies are precisely those of the analogue signal transmitted. This leads to a situation where the repetition frequency must be at least equal to twice the highest frequency component in the signal (equation [v]).

$$f_r - F_m \geq F_m \quad \text{or} \quad f_r \geq 2F_m \qquad [v]$$

This condition places on upper limit on F_m otherwise, f_r would be excessively high and the pulses extremely narrow. Therefore, this technique is only

applicable in systems where the bandwidth of sampled signal can be restricted to a maximum value of F_m without destroying the essential information in the signal. Band-limited signals are easily obtainable through the application of this technique which can be expressed more concisely in the Sampling Theorem (Connor, 1972) below:

"any function f(t) whose highest frequency is F_m Hz, can be completely determined by sampled amplitudes spaced at time intervals of 1/2 F_m apart".

However, if sampling is performed below twice the frequency of the input signal, a falsehood of low frequency variation appears. This is what is called *aliasing* and the false frequency is expressed by Shannon's Sampling Theorem. This theorem states that a sampled time signal must not contain components at frequencies above half the sampling rate - the Nyquist frequency. If the frequency of the input voltage, f_{in}, is greater than half the sample rate f_s, the spurious signal that results will appear to have a frequency f_{alias} given by

$$f_{alias} = f_s - f_{in} \qquad \text{[vi}$$

The requirement for correct measurement that the sample rate be faster than twice the highest frequency contained in the input signal is known as the Nyquist Criterion (Tanner and Loh, 1994).

I.3. Experimental Determination of Sampling Rate

The main focus was the determination of appropriate values for the sampling frequency (f_s), sampling time interval (Δt), and the number of data samples (N). It is only when appropriate values of these entities are employed in the data acquisition that any meaningful existence in their trend can genuinely be attributed to reflect underlying variation of the cutting process.

Normally, only two of these parameters need be defined, and the third calculated. Thus, if f_s and N are defined, Δt is calculated as follows-

Total sampling time, $T = N\Delta t$,

Frequency spacing, $\Delta f = \frac{1}{2N\Delta t} = \frac{1}{2T}$, therefore, $\frac{f_s}{N} = \Delta f \Rightarrow f_s = \frac{1}{2\Delta t}$

I.3.1. Procedure

A channel was selected on the DAC and set to the maximum throughput of the card (200 kHz). with the charge amplifier reset to clear residual charges, cutting was carried out at a cutting speed of 300 m/min, feed rate of 0.3778 mm/rev and depth of cut of 4.0 mm. A data sample was recorded after the tool had been engaged in cutting for some time, enough for the process to stabilise (about 10 seconds). Using the sampled data, its FFT was calculated and displayed alongside the time varying signal. The same procedure was repeated for one of each acceleration and force channels.

Inspection of obtained FFT plots showed that a single main frequency component and harmonics were identifiable in the sampled frequency range. On the accelerometer plot, no frequency component appeared beyond approximately 7 kHz, with the main component (largest amplitude) appearing around 3 - 4 kHz. The frequency spectra lines had wider bandwidths. The force plot was identical to the acceleration plot, but none of its frequency spectra went beyond 6 kHz. Thus, by observing the obtained spectra, if sampling is performed beyond 10 kHz, enough spectra will be covered. Applying the Nyquist Criterion, a sampling frequency of 20 kHz per channel was chosen.

I.3.2. Theoretical Interpretation

Normally, if the input signal frequency, f_{in}, is greater than 1/2 f_s, then a spurious signal spectra would result having a frequency, f_{alias} given by

$$f_{alias} = f_s - f_{in}$$

In such a case, the obtained spectrum would be of the form shown in Fig. I(c).

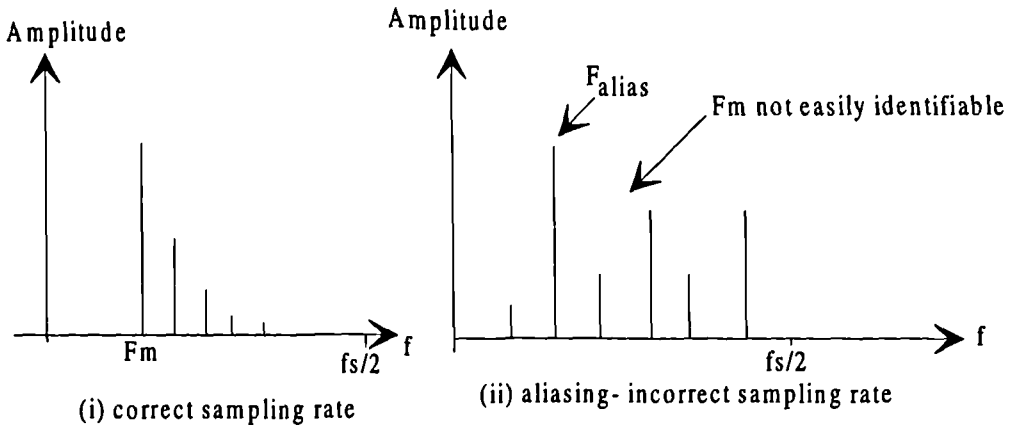

Figure I(c): Possible FFT spectra outcomes

For an incorrect sampling rate, the FFT outcome depicted in Fig. f(ii) would be obtained, requiring that frequencies higher than those of the frequency of interest would have to be filtered out. This is normally achieved through application of an RC circuit whose cut-off frequency (f_c) equals f_m, chosen so as to let F_m through.

This procedure has served to illustrate that the sampling range and available instrumentation were sufficient for the TCM task, and additional filter not required.

I.4. *Signal Analysis through Application of the Fourier Transform*

Consider a as signal shown in Figure I(d).

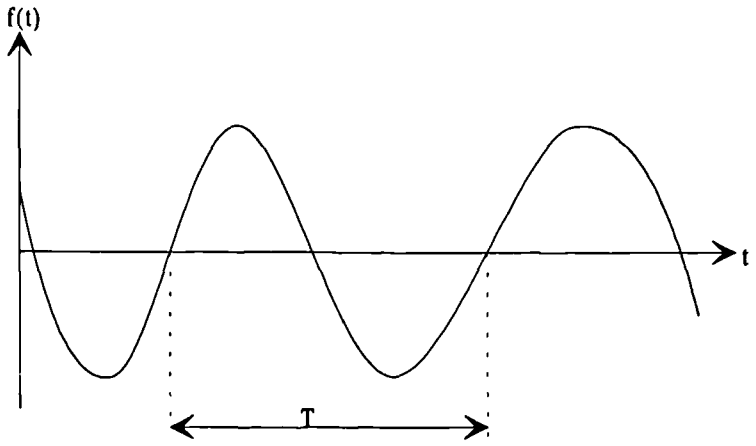

Figure I(d): Typical time base signal function

The signal is clearly repetitive and is a periodic function of time. Any such periodic function of time f(t) can be represented by the Fourier Series

$$f(t) = a_0 + \sum_{n=1}^{\infty} \{a_n \cos(n\omega t) + b_n \sin(n\omega t)\} \qquad \text{[vii]}$$

where T= period of time function f(t).

This basically is an infinite sum of weighted sine and cosine functions of the proper frequencies of the periodic function. In essence, it allows time domain functions to be interpreted by analysis of their frequency content.

The coefficients a_n and b_n can be evaluated and described by the following equations

$$a_n = \frac{2}{T} \int_{-\frac{T}{2}}^{+\frac{T}{2}} f(t)\cos(n\omega t)dt \qquad \text{[viii]}$$

$$b_n = \frac{2}{T} \int_{T}^{+\frac{T}{2}} f(t)\sin(n\omega t)dt \qquad \text{[ix]}$$

The d.c. component term, a_0 is given by averaging the value of f(t) over period T,

$$a_o = \frac{2}{T}\int_{-\frac{T}{2}}^{+\frac{T}{2}} f(t)dt \qquad [x]$$

Equation [x] could be viewed as describing exhaustively, the well known Fourier Theorem, whose restriction in application in this form is solely its dependency on the time signal being periodic. Re-evaluation of the Fourier Series to overcome this restriction to periodic functions pre-empts allowing T to increase infinitely, thus $T \rightarrow \infty$. The transformation of the Fourier Series through the boundaries described above is called Fourier Transform and is defined below.

Forward transform $$S\{f(t)\} = \int_{-\infty}^{+\infty} f(t)e^{-j n\omega t}dt \qquad [xi]$$

Reverse transform $$f(t) = \int_{-\infty}^{+\infty} S\{f(t)\}e^{+j n\omega t}d\,\mathrm{f(t)} \qquad [xii]$$

The S{f(t)} is the Fourier Transform of f(t) which contains amplitude and phase information for all the component frequencies of f(t). F(t) needn't be periodic for S{f(t)} to be determinable.

The solution from the above Fourier Transformations have four possibilities, all dependent on the nature of f(t).

- If f(t) = f(-t): function is even and symmetrical about 0. Only cosine terms are present and the dc term is optional.
- When f(t) = -f(-t): function is odd and only sine terms are present with the dc term optional.
- For f(t+T/2) = f(t): only even harmonics present.

- For f(t+T/2) = -f(t): only odd harmonics present.

The Fourier Transform is hardly applied as shown in either of the aforementioned equations, primarily because the time interval between the data points is infinitesimal, i.e. $\Delta t \rightarrow dt$. A summation is used instead viz.

$$S'\{f(t)\} = \Delta t \sum_{n=-\infty}^{\infty} x(n\Delta t) e^{-j2\pi f n \Delta t} \qquad \text{[xiv]}$$

where $x(n\Delta t)$= signal measured at sampling interval Δt.

In the form as shown in equation [xiv], the Fourier Transform can be calculated much more easily only if an infinite number of samples is supplied. Thus, given either two of the following, the data acquisition time T, number of data points N, and sampling interval Δt, the third is determinable as follows

$$N = \frac{T}{\Delta t} \qquad \text{[xv]}$$

By this restriction, the truncated version of the summation will not produce a continuous frequency spectrum and therefore, requires modifications, thus, a new Fourier Transform Algorithm, the Discrete Fourier Transform (DFT). The DFT can be written as follows:

$$S''\{m\Delta f\} = \Delta t \sum_{n-0}^{N-1} x(n\Delta t) e^{-j2\pi m \Delta f n \Delta t} \qquad \text{[xvi]}$$

where m = 0, 1, 2, 3, ..., N-1.

This expression, a Sampled Fourier Series with N real valued time domain data points, can easily be implemented on a computer. The most commonly used algorithm for this operation is the forward Fast Fourier Transform (FFT).

I.5. The Fast Fourier Transform (FFT)

The FFT is an algorithm that allows the user to efficiently and effortlessly obtain the DFT of a function with a smaller number of arithmetic operations than would normally be required with the direct approach. It operates on an array of N complex data points in one domain producing N/2 data points and redundancies. The only necessary condition for operation is that the number of samples be a power of two (2^9, 2^{10}, 2^{11}, etc.). The minimum number of input points data should be 2^9, otherwise the transformed data will be too widely spaced (low resolution). The normal output frequency range is from 0 (dc) to the Nyquist frequency which is independent of N (see Figure I(b)).

Some Definitions Associated with FFTs

a) The Frequency Range: Normally from zero (DC) to the Nyquist ($f_s/2$)

b). Resolution (R): Frequency interval between adjacent lines in the spectrum. Its is calculated as $R = \frac{f_s}{N}$.

c). Bandwidth (B_{eff}): Passband determined by the sample number and rate, the resolution and time window type applied to the data. For linearly weighted data, i.e. rectangular windowing, the bandwidth equals the resolution. For Hanning and Hamming window types, their bandwidths are usually noisy, thus, $B_{eff} = 1.5R$

d). Dynamic Range: Determined by the number of bits with which the input data is represented. 6 dB of dynamic range is obtained for every bit of the input data, thus, a total of 72 dB is obtained from analogue-to-digital conversion with 12 bits. This range is not affected by FFT calculations or transforms.

I.6. Time Windowing

It is never possible to take an infinite number of sampled data for the Fourier Transform. An implicit assumption of the record contained in the spectrum or sampled block has therefore to be adopted. This is repeatability of the record length throughout time. For transient signals, such an assumption works well as its repeats are smooth hence, minimum distortion is imposed on the spectrum.

For continuous and non-periodic signals, that principal and elementary requirement does not exist and the spectra difficult to obtain. If the spectra are somehow obtained, it is distorted and often leaks energy off one resolution line into another. This is because instead of taking FFT of an infinite time record, that of a finite one is taken. The leakage might be severe as to mask small signals, if close to the main frequency. A possible solution is to take the FFT of a time windowed signal instead. This technique allows the FFT to concentrate on the middle of the signal ignoring the ends, thus, giving correct single line spectra in the frequency domain.

A number of functions can be used to window data, but the most popular one is the Hanning or Cosine^2 window. It tails off the data at both ends in a Cosine^2 (bell) shape. Currently, Rectangular, Hanning, Hamming (Hanning on small rectangular pedestal) and Gaussian functions are the most commonly used windowing types.

APPENDIX II

POWER SPECTRUM ANALYSIS

Usually, signals are treated in terms of voltage amplitude but not always is the power associated with such signals known. With periodic signals, the mean power associated with a voltage f(t) across a resistance of 1 Ω could be calculated and the results extended.

The instantaneous power of a time dependent signal f(t) is $[f(t)]^2$ (an equivalent extension of $P=I^2R$ or V^2/R), hence its mean power over one period (applicable over other periods) is given by integrating the instantaneous value over one period and dividing by the periodic time. Thus, represented mathematically by the following equation:

$$P_{mean} = \frac{1}{T}\int_{-\frac{T}{2}}^{+\frac{T}{2}} f^2(t)\,dt \qquad \text{[xvi]}$$

$$f(t) = C_0 + \sum_{1}^{\infty} C_n e^{jn\omega t} + \sum_{-\infty}^{-1} C_n e^{jn\omega t}$$

$$= \sum_{-\infty}^{+\infty} C_n e^{jn\omega t} \qquad \text{[complex form of the PDS of f(t)]}$$

The dc component $C_o=0$.

When re-substituted into equation (p), the following equation results

$$P_{mean} = \sum_{-\infty}^{+\infty} C_n \cdot \frac{1}{T}\int_{-\frac{T}{2}}^{+\frac{T}{2}} f(t) \cdot \sum_{-\infty}^{+\infty} C_n e^{jn\omega t}\,dt \qquad \text{[xvii]}$$

$$= \sum_{\infty}^{+\infty} C_n \cdot C_n$$

$$\therefore P_{mean} = \sum_{-\infty}^{+\infty} |C_n|^2 \quad \underline{watts} \qquad \text{[xviii]}$$

where n = 0, 1, 2, ..., ∞

$P_{mean} \rightarrow 0$ because $1/T \rightarrow 0$ as $T \rightarrow \infty$. Hence it is much more meaningful to evaluate the total energy associated with a signal than its power. The energy is calculated as follows:

$$Energy,\ W = \int_{-\infty}^{+\infty} f^2(t)dt \qquad \text{[xix]}$$

but since $f(t) = \frac{1}{2\pi} \int_{-\infty}^{+\infty} g(w) e^{j\omega t} d\omega$

then, $W = f(t).\frac{1}{2\pi} \int_{-\infty}^{+\infty} g(w).e^{j\omega t} d\omega.dt$

which simplifies as follows:

$$W = \frac{d\omega}{2\pi}.g(\omega) \int_{-\infty}^{+\infty} f(t).e^{j\omega t}.dt$$

$$= \frac{1}{2\pi} \int_{-\infty}^{+\infty} g(\omega).g(-\omega).d\omega$$

$$= \frac{1}{2\pi} \int_{-\infty}^{+\infty} |g(\omega)|^2.d\omega$$

Finally,

$$W = \int_{-\infty}^{+\infty} |g(f)|^2.df \quad J / Hz \qquad \text{[xx]}$$

Equation (t) is known as Rayleigh's Theorem and the quantity $(g(f))^2$ is the energy spectral density (ESD).

APPENDIX III

A. The Signal Processing Algorithm

```
%Calculate the static and dynamic force components from the sampled force
%(TAB DELIMETERED ONLY), output and save ASCII FFT data from the
%calculations. Repeat for the vibration(acceleration) signal.
%
%By Dimla, Jnr. Version 2.0, 22/10/96
%Last Modified, 17-02-97
%
%       STEP ONE
%Calculate the static force components of the cutting force
%using the sampled force, and save as ASCII text in a file
%
      clear;
      load [data_file.txt];
      P=data_file;
      for i=1:3; for j=1:2048;
      A1(:,i)=mean(P(:,i));
      end;end;
%      STEP TWO
%Calculate the dynamic components of the cutting force
%using the sampled force and the static components.
      for i=1:3;for j=1:2048;
      static(1)=A1(:,1); static(2)=A1(:,2); static(3)=A1(:,3);
      damp(1)=1000; damp(2)=1000; damp(3)=1000;
%The damp constant represents the sensitivity of dynamometer
      y(j,i)=(P(j,i)-static(i)).*damp(i);
      end;end;
      L=[y P(:,4:6)];
%      STEP THREE & FOUR
%Now, Calculate sum of the FFT spectra
%with Hanning window and save as ascii text in a file
      t= (-pi/2:(pi/2047):pi/2);
      u= cos(t).^2';
      for j=1:2048;
      x0(j,:)=u(j).*L(j,:);
      x1(j,:)=100.*x0(j,4:6);
      LL=[[x0(:,1:3)] x1];
      end;
%The constant 100 represents the sensitivity of the accelerometers@10mv/g
%since recorded values are in Volts with GAIN set to 1
      x2= fft(LL,2048);
      x3=(1/2048).*sqrt(2.*x2.*conj(x2));
      for i=1:6;
```

```
        x4(:,i)=sum(x3((1:1024),i));
        B1=static(1)*1000;
        B2=static(2)*1000;
        B3=static(3)*1000;
        x5=[B1 B2 B3 x4];       %Record print-out, i.e. 9-component data
        save [experimental_data] x5 -ascii -tabs;
        end;
%
%       STEP FIVE
%Smoothen FFT data for spectra plots
        for i=4:2045;
        for j=1:6;                  %CHANGE j if file not 6 experimental data
collumns
        A1(i,j)=mean(x3(((i-3):1:(i+3)),j));
        end;
        end;
        C1=x3((1:3),:);
        C2=A1((4:2045),:);%This merely replaces middle of truncated matrix
        C3=x3((2045:2048),:);
        B=[C1; C2; C3];
        save [spectra_data] -ascii -tabs;    %save FFT DATA
```

B. The Back-propagation Algorithm

```
%Dimla MLP5
%Created  13/06/97
%12 inputs
%20 Hidden
%5 output
%Network trained with backpropagation (with momentum).
%
        clear;
        help back
        clf reset
        pausetime = 0.10;

% PROBLEM DEFINITION
%===================
        load [training_data.txt];
        load [target_data.txt];
        P = [training_data]';
        T = [target_data]';
        [R,Q] = size(P);
        S1=12;
        S2=20;
        [S3,Q] = size(T);
        [W1,B1]=nwlog(S1,R);
```

```
    [W2,B2]=nwlog(S2,S1);
    [W3,B3]=nwlog(S3,S2);
% TRAIN THE NETWORK
%==================
% TRAINING PARAMETERS
    disp_freq = 100;
    max_epoch = 500000;
    err_goal = 0.009;
    lr = 0.05;
    momentum=0.85;
    err_ratio=1.04;
    %lr_inc=1.05;
    %lr_dec=0.7;
    TP = [disp_freq,max_epoch,err_goal,lr,momentum,err_ratio];
    [W1,B1,W2,B2,W3,B3,epoch,errors]
    trainbpm(W1,B1,'logsig',W2,B2,'logsig',W3,B3,'logsig',P,T,TP);
    SSE = sumsqr(T-logsig(W3*logsig(W2*logsig(W1*P,B1),B2),B3));

%Present results
%===============
    fprintf('\nFINAL NETWORK VALUES:\n')
    W1;
    save W12 W1 -ascii -tabs
    W2;
    save W22 W2 -ascii -tabs
    W3;
    save W32 W3 -ascii -tabs
    B1;
    save B12 B1 -ascii -tabs
    B2;
    save B22 B2 -ascii -tabs
    B3;
    save B32 B3 -ascii -tabs
    %
    fprintf('Trained for %.0f epochs.\n',epoch)
    fprintf('Sum squared error goal was %g.\n',err_goal);
    fprintf('Final sum squared error is %g.\n',SSE);
    fprintf('Trained network operates: ');
    if SSE < err_goal
    disp('Adequately.')
    else
    disp('Inadequately.')
    end
```